ABSTRACT

Ageing infrastructure is a widespread problem, with potentially catastrophic consequences. Reliable structural integrity and remaining life assessment are essential for the resolution of the problem.

Ageing *railway bridges* is a particularly difficult subset of the ageing infrastructure problem. There is a complex array of issues that face integrity and remaining life assessment of railway bridges. The structural conditions of railway bridges may change from site to site, even where bridges are supposedly of the same design. Structural conditions may also change over the life of any particular bridge. Dynamic interaction, between railway vehicles and railway bridge structures, has a dramatic effect on structural response and therefore remaining life. This dynamic interaction often requires complex modelling techniques in integrity assessment. For assessment of railway bridges, different assumptions and different methods of assessment are often used, making repeatable and verifiable assessment difficult.

In this research, in order to work toward addressing the problem of ageing steel railway bridges, a clear, repeatable methodology for high-level structural assessment has been formulated. The method integrates state-of-the-art modelling, testing and fatigue code tools, and uses dynamic digital data for testing, modelling and assessment. The method is demonstrated by assessment of the steel girder approach spans of the Mullet Creek Railway Bridge, Dapto, NSW, Australia.

The method developed in this research begins with a finite element sensitivity model, that is a finite element model that permits variations in joint fixity and support

conditions. This model is tuned and validated, using transient digital data from the dynamic field-test response of a slow moving vehicle of known load, through a dynamic analytical model intermediate step. The dynamic field-test response of normal traffic is then recorded and axle loads are identified from the digitised measured response, using the dynamic analytical model as a transfer function. Identified loads are applied to the tuned finite element sensitivity model and the dynamic stress history generated for virtually any bridge component. Dynamic stress histories are then entered directly into a software system, which estimates remaining life via several international fatigue codes. After verification of the finite element sensitivity model against dynamic field-test results, loading and structural conditions may be adjusted and the integrity and remaining life of the structure evaluated for virtually any combination of structural and loading condition.

In the demonstration of the method, three components of the Mullet Creek Railway Bridge approach spans have been chosen for structural integrity and remaining life assessment. Structural conditions and applied loading conditions have been altered and the impact of the changes investigated. From the structural integrity and remaining life assessment, two locations have been identified as fatigue critical and recommendations have been made for structural changes and ongoing inspection.

The most significant contribution of this research is expected to be the complete methodology, its clarity and repeatability, its integration throughout and the way in which it deals with the difficult problem of true dynamic response. Other contributions have been made within individual steps of the methodology, where attempts have been made to extend current research. These contributions include: the development of a

technique for modelling the dynamic response of structures in finite element software; a dynamic analytical model for beams with rotationally stiffened supports subjected to moving distributed loads; extension of load identification theory to distributed loads on non-simply supported beams; and a comparative study of several key international fatigue codes.

ACKNOWLEDGEMENTS

The author wishes to gratefully acknowledge the following:

- Rail Infrastructure Corporation (RIC) and the Co-operative Research Centre for Welded Structures (CRC - WS), for their support for research on structural integrity assessment of railway bridges.

- Project leader and Ph.D. supervisor Michael West, for his excellent supervision, leadership and friendship.

- RIC project partners John Marcer, Ted Bain and Ben Chung for sharing their invaluable expertise and experience.

- University of Wollongong project partner and friend Brad Glass, who has worked together with me on this project since the beginning.

- University of Wollongong project partner and friend Ben Lake, and friend Jane Langridge, for their friendship and their work proof reading and editing this thesis.

- University of Wollongong technical staff Tony Kent, Keith Maywald, Peter Harding and Ron Young, for their technical excellence and willing assistance.

- My wife Erica, for her love, godliness, patience and support.

- My God and Saviour Jesus, to whom I owe everything.

TABLE OF CONTENTS

ABSTRACT i

ACKNOWLEDGEMENTS iv

NOMENCLATURE xi

LIST OF FIGURES AND TABLES xiv

CHAPTER 1 – INTRODUCTION

1.1 The Problem 1

1.2 Working Toward a Solution 3

1.3 Thesis Outline 5

1.4 An Iterative Process 9

CHAPTER 2 - THEORY

2.1 An Integrated Methodology for Stress-Based Fatigue Assessment of Steel Railway Bridges 10

2.1.1 Introduction and Literature Review 10

2.1.2 An Integrated Methodology for Stress-Based Fatigue Assessment of Steel Railway Bridges 14

2.2 Modelling the Dynamic Response of Structures in Finite Element Software 17

2.2.1 Introduction and Literature Review 17

2.2.2 Modelling Moving Loads in Finite Element Software 22

2.2.3 Comparison of Finite Element and Analytical Solutions 28

2.2.4 Application to Structural Assessment 34

2.3 Dynamic Field Testing Techniques for Model Validation and Load Identification **37**

2.3.1 Introduction and Literature Review 37

2.3.2 Dynamic Field-Test Validation of a Finite Element Model 41

2.3.3 Load Identification from Dynamic Field-Test Results 43

2.4 An Analytical Model for Euler-Bernoulli Beams with Rotational Stiffness at Supports Subjected to Multiple Moving Uniformly Distributed Loads **45**

2.4.1 Introduction and Literature Review 45

2.4.2 An Analytical Model for Euler-Bernoulli Beams with Rotational Stiffness at Supports Subjected to a Single Moving Concentrated Load 46

2.4.3 An Analytical Model for Euler-Bernoulli Beams with Rotational Stiffness at Supports Subjected to Multiple Moving Concentrated Loads 51

2.4.4 An Analytical Model for Euler-Bernoulli Beams with Rotational Stiffness at Supports Subjected to a Single Moving Uniformly Distributed Load 55

2.4.5 An Analytical Model for Euler-Bernoulli Beams with Rotational Stiffness at Supports Subjected to Multiple Moving Uniformly Distributed Loads 70

2.4.6 Application to Structural Assessment 71

2.4.7 Validation of the Analytical Model 71

2.4.7.1 Comparison against the Concentrated Load Solution 72

2.4.7.2 Comparison against the Quasi-Static Uniformly Distributed Load Solution 75

2.4.7.3 Comparison against the Heaviside Approximation of a Uniformly Distributed Load and Field Test Results 76

2.5 Load Identification of Uniformly Distributed Loads on Euler-Bernoulli Beams with Rotational Stiffness at Supports **80**

2.5.1 Introduction and Literature Review 80

2.5.2 Review of Load Identification Theory 85

2.5.3 Load Identification of Uniformly Distributed Loads on Euler-Bernoulli Beams with Rotational Stiffness at Supports 92

2.5.4 An Approximate Method for Load Identification of Multiple Moving Loads 98

2.6 Duty Cycle Loading Schedule Development **105**

2.6.1 Introduction 105

2.6.2 Identify Potential Sources of Loading 105

2.6.3 Identify Loading History from Those Sources 106

2.6.4 Simplify Loading into Representative Units 107

2.6.5 Clearly Document Loading History, Reference Information Sources and Outline Assumptions and Uncertainties 107

2.7 Fatigue Assessment Software System and Comparative Study of Stress-Based Structural Fatigue Codes **109**

2.7.1 Introduction and Literature Review 109

2.7.2 Fatigue Assessment Software System 112

2.7.3 Comparative Study of Stress-Based Structural Fatigue Codes 114

2.7.3.1 Qualitative Study 115

2.7.3.2 Quantitative Study 119

2.7.3.3 Discussion 129

2.7.3.4 Conclusions 131

CHAPTER 3 - DEMONSTRATION

3.1 The Mullet Creek Railway Bridge 133

3.1.1 The Mullet Creek Railway Bridge 133

3.1.2 The Mullet Creek Railway Bridge Approach Spans 134

3.1.3 The Significance of Some Design Aspects on Remaining Life and Structural Integrity 137

3.2 Finite Element Models of the Mullet Creek Railway Bridge 139

3.2.1 Finite Element Sensitivity Model 139

3.2.2 Stress Data Recovery from Beam Element Sensitivity Models 141

3.2.3 High-Detail Finite Element Model 142

3.2.4 Plate Element Sub-Model 143

3.3 Field Testing 145

3.3.1 Field Test Program 145

3.3.2 Test Equipment 145

3.3.3 2000 Field Testing 146

3.3.4 2001 Field Testing 152

3.4 Validation of Finite Element Models 154

3.4.1 Variation of Field Test Results from Predicted Response 154

3.4.2 Finite Tuning of Analytical Model Response to Field Test Results 155

3.4.3 Fine Tuning of Finite Element Sensitivity Model Response 157

3.4.4 The Significance of the Variation from the Simply Supported Assumption 159

3.5 Load Identification from Structural Response 161
3.5.1 Identification of 'Noisy' and 'Quiet' Response Signals from Test Data 161
3.5.2 Identification of Loads from 'Noisy' and 'Quiet' Response Signals 165

3.6 Duty Cycle Development 171
3.6.1 Duty Cycle Development 171
3.6.2 Potential Sources of Loading 171
3.6.3 Load History 172
3.6.4 Load History Simplified into Representative Units 180
3.6.5 Information Sources, Assumptions and Uncertainties 183

3.7 Stress Recovery from Identified Loads and Duty Cycle Data 188
3.7.1 Stress Recovery 188
3.7.2 Comparison of the Finite Element Response with Analytical and Field Test Results 189
3.7.3 Manipulation of Applied Loads 191
3.7.4 Manipulation of Structural Conditions 193

3.8 Structural Integrity and Remaining Life Assessment 195
3.8.1 Structural Integrity and Remaining Life 195
3.8.1.1 Broad Flange Beam at Mid Span and Fixed Bearing Component 195
3.8.1.2 Broad Flange Beam Web-Stiffener Component 198
3.8.2 Effect of Manipulating Applied Loads 201
3.8.3 Effect of Manipulating Structural Conditions 202

CHAPTER 4 – DISCUSSION

4.1 Review 203

4.2 Implications and Recommendations 208

4.3 Implications and Recommendations for the Mullet Creek Railway Bridge 210

CHAPTER 5 – CONCLUSION

5.1 Aims of the Research Fulfilled 211

5.2 Overall Importance of the Research 214

REFERENCES 216

BIBLIOGRAPHY 226

APPENDICES

A Mode Shape Function for Euler-Bernoulli Beams with Rotational Stiffness at Supports 228

B Quasi-Static Analytical Model for Euler-Bernoulli Beams with Rotational Stiffness at Supports Subjected to Multiple Moving Uniformly Distributed Loads 234

C Acceleration Response for Euler-Bernoulli Beams with Rotational Stiffness at Supports Subjected to Multiple Moving Uniformly Distributed Loads 245

D Example Output from Fatigue Assessment Software 253

E Fatigue Assessment Software Source Code 258

F Engineering Drawings of Mullet Creek Railway Bridge Approach Spans 313

G Dynamic Stress Data Recovery from Strand7 Beam Element Sensitivity Models 315

H Catalogue of Field Test Results 320

I Analogue to Digital Conversion Software Source Code 325

J Simplified Traffic Data 329

K Remaining Life Calculations 331

NOMENCLATURE

Specific symbols not included in the nomenclature here are defined as they come up in the text

A	distance from first load
A	cross sectional area
C	damping
D	location of bending moment measurement
E	modulus of elasticity
F	force
I	Second moment of area
J	equivalent torsional constant
K	stiffness
L	length of beam
M	moment
M	mass
P	load
Q	first moment of area
R_0	vertical reaction force at x = 0
R_L	vertical reaction force at x = L
S	total length of distributed load
T	torque
U	initial velocity
V	velocity

a	acceleration
$\bar{c}$	distributed damping
d	distance of location of bending moment measurement from origin
k	rotational stiffness
k_0	rotational stiffness at x = 0
k_L	rotational stiffness at x = L
l	length of element
m	modal mass
$\bar{m}$	distributed mass
q	distributed load
s	length of distributed load on beam
t	time
t	plate thickness
v(x,t)	displacement
x	distance from origin
y	perpendicular distance from neutral axis
$\Omega = V\lambda^{\frac{1}{4}}$	velocity dependent frequency
α	mode shape factor
β	mode shape factor
ϕ	mode shape function
γ	modal normalising constant
λ	eigenvalue of the mode shape equation

θ	angle of rotation
σ	normal stress
σ_B	normal stress due to bending
τ	dimensionless time
τ	shear stress
ω	modal frequency
ω_D	damped modal frequency
ξ	modal displacement
$\dot{\xi}$	modal velocity
$\ddot{\xi}$	modal acceleration
ξ_P	particular solution modal displacement
ζ	modal damping ratio
Δ	mode shape factor

LIST OF FIGURES AND TABLES

Figures

Figure 2.1.1.	An integrated methodology for stress-based fatigue assessment of steel railway bridges.	16
Figure 2.2.1.	(a) Ten-element beam with a rectangular impulse load applied at node 5. (b) Force time history for node 5. (c) Displacement response of a ten element beam at mid-span to applied loading modelled as rectangular impulses.	20
Figure 2.2.2.	(a) Beam with concentrated load of constant magnitude and velocity. (b) Force time histories for nodes 3 and 4.	24
Figure 2.2.3.	Single moving concentrated load of variable magnitude and constant acceleration on an elastic beam.	25
Figure 2.2.4.	Magnitude of (a) load and (b) velocity for a single concentrated load of randomly varying magnitude moving with variable velocity.	26
Figure 2.2.5.	Loads applied at nodes (a) 2 and (b) 3 for simulation of the load of figure 2.2.2.	27
Figure 2.2.6.	Case 1: constant load, constant velocity.	31
Figure 2.2.7.	Case 2: sinusoidal varying load, constant velocity.	31
Figure 2.2.8.	Case 3: constant load with rectangular impulses, constant velocity.	32
Figure 2.2.9.	Case 4: random load, constant velocity.	32
Figure 2.2.10.	Case 5: random load, constant acceleration.	33
Figure 2.2.11.	Rendered approach span beam model.	34
Figure 2.2.12.	Symmetrical high detail finite element model of a steel girder bridge.	36

Figure 2.3.1. Analytical model, with tuneable structural properties, subjected to moving distributed loads of variable magnitude. 42

Figure 2.3.2. Example of the tuning of the analytical model response to the measured bridge response from field-testing. 42

Figure 2.4.1. A single moving concentrated load on a Euler-Bernoulli beam, with rotational stiffness at supports. 46

Figure 2.4.2. Two moving concentrated loads on a Euler-Bernoulli beam, with rotational stiffness at supports. 51

Figure 2.4.3. A single moving uniformly distributed load on a Euler-Bernoulli beam, with rotational stiffness at supports. 55

Figure 2.4.4. A single moving uniformly distributed load entering a Euler-Bernoulli beam, with rotational stiffness at supports. 58

Figure 2.4.5. A single moving uniformly distributed load completely on a Euler-Bernoulli beam, with rotational stiffness at supports. 63

Figure 2.4.6. A single moving uniformly distributed load leaving a Euler-Bernoulli beam, with rotational stiffness at supports. 67

Figure 2.4.7. Multiple moving uniformly distributed loads on a Euler-Bernoulli beam, with rotational stiffness at supports. 70

Figure 2.4.8. Comparison of the bending stress response of the model developed in this section (equation (2.4.26), (2.4.29) and (2.4.31)) with 3 distributed loads of length 0.001m, with the solution for 3 concentrated loads (equation (2.4.17)). 74

Figure 2.4.9. Comparison of the bending stress response of the model developed in this section (equation (2.4.26), (2.4.29) and (2.4.31)) with 3 distributed loads of length 1m, with the quasi-static solution of Appendix B. 75

Figure 2.4.10.	Comparison of the modal displacement response of the model developed in this section with the response from the Heaviside approximation, for a single moving load, and a relatively high damping ratio (ζ=0.1).	78
Figure 2.4.11.	Comparison of the modal displacement response of the model developed in this section with the response from the Heaviside approximation,for a single moving load, and a relatively low damping ratio (ζ=0.005).	78
Figure 2.4.12.	A typical acceleration response of (a) the Heaviside approximation and (b) the model developed in this section, under the passage of a single moving constant magnitude and velocity load.	79
Figure 2.4.13.	The acceleration response of a four-bogie (two-carriage) passenger train from field-testing.	79
Figure 2.5.1.	Concentrated load on a Euler-Bernoulli beam, with simply supported end conditions.	85
Figure 2.5.2.	Displacement response curve generated under the conditions described in Table 2.5.1.	90
Figure 2.5.3.	Comparison of applied load and identified load.	90
Figure 2.5.4.	A single moving uniformly distributed load on a Euler-Bernoulli beam, with rotational stiffness at supports.	92
Figure 2.5.5.	A schematic representation of the lower triangular matrix represented as f in Section 2.5.2, showing the arrangement of Equations (2.5.12), (2.5.13) and (2.5.14) within the matrix.	95
Figure 2.5.6.	Displacement response curve generated under the conditions described in Table 2.5.2.	96
Figure 2.5.7.	Comparison of applied load and identified load.	96

Figure 2.5.8.	Displacement response curve generated under the conditions described in Table 2.5.3.	101
Figure 2.5.9.	Comparison of applied load and identified load.	102
Figure 2.5.10.	Comparison of original displacement curve with the response reproduced using identified loads.	103
Figure 2.7.1.	Uncorrected S-N curves for (a) non-welded sections, (b) longitudinally welded joints, (c) transverse welded joints, (d) butt-welded joints and (e) cover plate details.	122
Figure 2.7.2.	Longitudinally welded joint class.	123
Figure 2.7.3.	Remaining life for a longitudinally welded joint for the prescribed two load cases.	123
Figure 2.7.4.	Remaining life for a cover plate detail for load series 1 and 2.	126
Figure 2.7.5.	Fatigue life for a longitudinally welded joint to stresses of varying mean stress. (a) welded, (b) welded and stress relieved	127
Figure 2.7.6.	Fatigue life for a longitudinally welded joint including correction and safety	128
Figure 2.7.7.	Comparison of the effect of using a stress spectrum.	129
Figure 3.1.1.	Mullet Creek Railway Bridge.	133
Figure 3.1.2.	Typical Mullet Creek Railway Bridge approach span.	133
Figure 3.1.3.	Mullet Creek Railway Bridge main span.	134
Figure 3.1.4.	Typical stress history at the mid-span of a short approach spans (a) and the long main span (b) under the passage of two locomotives and two carriages with axle spacing shown in (c).	135
Figure 3.1.5.	Broad Flange Beam with web-stiffeners welded on the top flange and web.	136

Figure 3.1.6.	Cross girder and sway bracing connections.	136
Figure 3.1.7.	Expansion and fixed bearing details.	137
Figure 3.1.8.	Eccentric loading causing the transoms to load the inside edge of the top flange.	138
Figure 3.2.1.	Rendered approach span beam element sensitivity model.	139
Figure 3.2.2.	Transom-broad flange beam connection.	141
Figure 3.2.3.	High detail finite element model.	142
Figure 3.2.4.	High detail finite element model identifying critical locations of high localised stresses in the top flange due to transom bending.	143
Figure 3.2.5.	Preliminary web-stiffener plate element sub-model.	144
Figure 3.3.1.	Equipment used during testing.	146
Figure 3.3.2.	Approach span chosen for the first round of testing.	147
Figure 3.3.3.	Strain gauge located on the top flange of the Broad Flange Beams above one of the web-stiffeners.	148
Figure 3.3.4.	High level FEA identifying locations of high localised stresses.	148
Figure 3.3.5.	Strain gauge set-up and Wheatstone bridge for relative axle load measurement.	149
Figure 3.3.6.	Strain gauge set-up for relative axle load measurement.	149
Figure 3.3.7.	Accelerometers at one of the fixed bearings.	150
Figure 3.3.8.	Schematic of test set up.	150
Figure 3.3.9.	Locomotive stopped at mid span for equipment calibration.	151
Figure 3.3.10.	Sample of digitised test data.	152

Figure 3.4.1. Bending stress (MPa) versus time results from field-testing and the predicted bending stress results assuming simply supported conditions. 154

Figure 3.4.2. Analytical model with tuneable load distribution length, rotational stiffness at supports and overall stiffness. 155

Figure 3.4.3. Bending stress (MPa) versus time results from field-testing and the bending stress results from the tuned model. 156

Figure 3.4.4. Bending stress distribution of the approach span under a static locomotive load. 158

Figure 3.4.5. Cracking at the fixed bearings of consecutive spans of a similar bridge in Richmond, NSW [Rail Infrastructure Corporation]. 159

Figure 3.4.6. Damage at the pier beneath the fixed bearing at one of the Mullet Creek Railway Bridge approach spans. 160

Figure 3.5.1. The measured strain versus time response for a series of Manildra wagons (tape 2, event 10). 162

Figure 3.5.2. The measured strain versus time response for a series of BHP wagons (tape 2, event 31). 162

Figure 3.5.3. The measured strain versus time response for a series of BHP wagons (tape 2, event 24). 163

Figure 3.5.4. The measured strain versus time response for a Tangara train (tape 2, event 21). 163

Figure 3.5.5. The measured strain versus time response for a City Rail Electric train (tape 2, event 20). 163

Figure 3.5.6. Load identification for the 'noisy' 81 Class Loco of tape 1, event 6. (a) Raw identified loads (in kN); (b) Corrected identified loads (in kN) with a lower bound of 100 kN and an upper bound of 150 kN; (c) Comparison of forward solution using corrected loads and test response (in MPa). 167

Figure 3.5.7. Load identification for the 'noisy' diesel passenger train of tape 2, event 6. (a) Raw identified loads (in kN); (b) Corrected identified loads (in kN) with a lower bound of 60 kN and an upper bound of 100 kN; (c) Comparison of forward solution using corrected loads and test response (in MPa). 168

Figure 3.5.8. Load identification for the 'noisy' Tangara passenger train of tape 2, event 21. (a) Raw identified loads (in kN); (b) Corrected identified loads (in kN) with a lower bound of 40 kN and an upper bound of 100 kN; (c) Comparison of forward solution using corrected loads and test response (in MPa). 169

Figure 3.5.9. Load identification for the 'noisy' electric passenger train of tape 2, event 27. (a) Raw identified loads (in kN); (b) Corrected identified loads (in kN) with a lower bound of 70 kN and an upper bound of 130 kN; (c) Comparison of forward solution using corrected loads and test response (in MPa). 170

Figure 3.6.1. Locomotives which have crossed the Mullet Creek Railway Bridge. (a) D34 Locomotive, (b) 44 Class Locomotive, (c) 442 Class Locomotive, (d) 45 Class Locomotive, (e) 48 Class Locomotive and (f) 81 Class Locomotive. 177

Figure 3.6.2. 620 Class driver motor railcar with luggage area. 178

Figure 3.6.3. V Set driver motor carriage (intercity services). 178

Figure 3.6.4. V Set trailer carriage (intercity services). 178

Figure 3.6.5. TE Endeavour driver motor railcar with toilet. 178

Figure 3.6.6. LE Endeavour driver motor railcar with luggage area. 178

Figure 3.6.7. G Set (Tangara) driver trailer (intercity and suburban services). 179

Figure 3.6.8. G Set (Tangara) motor carriage (intercity and suburban services). 179

Figure 3.6.9. G Set (Tangara) motor carriage with toilet (intercity suburban services). 179

Figure 3.7.1. Comparison of the predicted bending stress versus time response (in MPa) from the tuned finite element model with the analytical model response for the representative duty cycle 'noisy' electric passenger train. 189

Figure 3.7.2. Comparison of the predicted bending stress versus time response (in MPa) from the tuned finite element model with the analytical model response for the representative duty cycle 'noisy' 81 Class locomotive. 189

Figure 3.7.3. Comparison of the predicted bending stress versus time response (in MPa) from the tuned finite element model with the measured field-test response for the representative duty cycle 'noisy' electric passenger train. 190

Figure 3.7.4. Comparison of the predicted bending stress versus time response (in MPa) from the tuned finite element model with the measured field-test response for the representative duty cycle 'noisy' 81 Class locomotive. 190

Figure 3.7.5. Comparison of the predicted bending stress versus time response (in MPa) from the web-stiffener connection plate element model with the measured field-test response for the representative duty cycle 'noisy' 81 Class locomotive. 191

Figure 3.7.6.	The complete finite element bending stress versus time response (in MPa) at mid-span for the 'noisy' duty cycle Manildra train.	192
Figure 3.7.7.	The complete finite element shear stress versus time response (in MPa) at the fixed bearing for the 'noisy' duty cycle Manildra train.	192
Figure 3.7.8.	The complete finite element bending stress versus time response (in MPa) at mid-span for the 'noisy' duty cycle six carriage electric passenger train.	192
Figure 3.7.9.	The complete finite element shear stress versus time response (in MPa) at the fixed bearing for the 'noisy' duty cycle six carriage electric passenger train.	192
Figure 3.7.10.	The complete finite element bending stress versus time response (in MPa) at mid span and the shear stress response at the fixed bearing for the 'noisy' duty cycle two carriage diesel passenger train.	193
Figure 3.7.11	The effect of reducing the longitudinal stiffness of the modelled pandrol clip connection on the bending stress versus time response (in MPa) at quarter span intervals for a 'noisy' duty cycle bogie of an electric passenger train.	193
Figure 3.7.12	Figure 3.7.12. The effect on the bending stress versus time response in the compression flange above the web-stiffener (in MPa) of moving the point of application of the loads from a position above the inner edge of the BFB compression flange to directly above the beam axis.	194
Figure 3.8.1	a) Rolled non-welded section of the BFB at mid-span, (b) Weld loaded in shear of the fixed bearing connection.	196
Figure 3.8.2	Transverse fillet welded section of the web stiffener connection.	200

Tables

Table 2.4.1.	Assumed beam structural properties for comparison against known solutions.	74
Table 2.5.1.	Conditions under which the curve shown in Figure 2.5.3 was generated.	90
Table 2.5.2.	Conditions under which the curve shown in Figure 2.5.6 was generated.	96
Table 2.5.3.	Conditions under which the curve shown in Figure 2.5.8 was generated.	101
Table 2.7.1.	Stress indicators used in the codes.	115
Table 2.7.2.	S-N data and curves.	117
Table 2.7.3.	Safety factor recommendations.	118
Table 2.7.4.	Guidance on stress spectrum compilation.	119
Table 2.7.5.	List of joint classes considered	120
Table 2.7.6.	Number of repetitions to failure for a non-welded section for each of the five prescribed load series (to three sig. fig.).	124
Table 2.7.7.	Number of repetitions to failure for a longitudinally welded joint for each of the five prescribed load series (to three sig. fig.).	125
Table 2.7.8.	Number of repetitions to failure for a transverse welded joint for each of the five prescribed load series (to three sig. fig.).	125
Table 2.7.9.	Number of repetitions to failure for a butt-welded joint for each of the five prescribed load series (to three sig. fig.).	125
Table 2.7.10.	Number of repetitions to failure for a cover plate detail for each of the five prescribed load series (to three sig. fig.).	126

Table 3.4.1.	Final properties of the tuned analytical model.	156
Table 3.5.1	The complete set of test data categorised into 'noisy' or 'quiet' response.	165
Table 3.5.2	Recorded events chosen for load identification.	166
Table 3.6.1.	Raw data from the 1968 NSW Department of Railways Working Timetable.	173
Table 3.6.2.	Raw data from the 1979 Public Transport Commission of NSW Working Timetable.	174
Table 3.6.3.	Raw data from the 1985 State Rail Authority of NSW Working Timetable.	174
Table 3.6.4.	Raw data from the 2000 State Rail Authority of NSW Working Timetable.	175
Table 3.6.5	Raw data from the some of the Illawarra's local industries.	176
Table 3.6.6	Representative passenger traffic (1965 – 2000).	180
Table 3.6.7	Representative passenger traffic wheel load specifications.	180
Table 3.6.8	Representative passenger traffic axle spacing specifications.	181
Table 3.6.9	Representative freight traffic (1965 – 2000).	181
Table 3.6.10	Representative freight traffic wheel load specifications.	181
Table 3.6.11	Representative freight traffic axle spacing specifications.	182
Table 3.6.12	Representative passenger traffic (current annual).	182
Table 3.6.13	Representative freight traffic (current annual).	182

Table 3.8.1.	Detail categories of the mid-span and fixed bearing components.	197
Table 3.8.2.	Remaining life estimates for the mid-span and fixed bearing components.	198
Table 3.8.3.	Detail categories for the transverse fillet web-stiffener connection.	200
Table 3.8.4.	Remaining life estimates for the transverse fillet web-stiffener connection.	201
Table 3.8.5.	Remaining life estimates for the non-welded BFB at mid-span after manipulation of applied loads.	201

1. INTRODUCTION

1.1 The Problem

Australian railway bridges, like all structures the world over, are ageing. Many Australian railway bridges are approaching, or have even passed, their design life. The problem of ageing infrastructure will, for obvious reasons, only worsen and may have potentially catastrophic consequences. Reflection on history shows the consequences of the failure of structures, such as railway bridges has, in many cases, been catastrophic. Great works of engineering infrastructure have been destroyed and, at times, a great many lives lost. Three useful surveys of the history of structural failure are:

- Volume five of Liebowitz [1], in which a number of highly publicised catastrophic structural failures are described;
- Hayes [2], which is a useful survey of the failure of five large welded structures including the Belgium Hasselt Bridge and the Australian Kings Bridge;
- *Fatigue and Fracture in Steel Bridges* [3], by Fischer, which details twenty-two case studies of bridges that have undergone cracking and failure.

Not only are the consequences of the problem of ageing infrastructure potentially severe, the problem is also widespread. For evidence on how widespread the problem of ageing infrastructure is, one needs only to survey current literature and note the constant call for increased investment of resources into ageing infrastructure. In 2000, Jackson [4], reviewing the draft report of the Australian inquiry into rail reform [5], noted that a focus on infrastructure investment is regarded by the rail industry as more important to the longer-term viability of railways than the economic and commercial aspects of rail operation. In that article, Associate Professor Phillip Laird, the chairman

of the Institution of Engineers Australia Railway Technical Society of Australasia, said, "Infrastructure investment needs to be increased on all lines linking the major population centres." A number of similar infrastructure report cards have been developed by professional associations, major infrastructure providers and representatives of professional associations around the world [6-9]. Invariably demands for increased investment, as well as more integrated approaches, of a higher standard, to structural assessment are made in each report. Yates and Jackson [10], present an article on the launch of the most recent Australian report, the 2001 Australasian Infrastructure Report Card [11]. The main finding of that report was Australia's infrastructure needs urgent attention to ensure it meets its current demands as well as future needs. At the launch John Boshier, IEAust Chief Executive observed, "100 years after federation, the development and maintenance of our infrastructure assets suffers from a lack of integration and co-ordination." He also notes, "we cannot manage what we cannot measure. In compiling this Report Card, one of the difficulties encountered was the lack of timely, consistent and complete data. If the community, business and government want confidence that their investments are being looked after, we need this information and it should be publicly accessible." Discussing the need for 100% reliability both for large 'majestic' bridge structures as well as 'insignificant' utilitarian structures, West [12] notes the need for a sure focus on the future and the remaining life of societies' infrastructure. In his discussion, West focuses on structural integrity and remaining life, highlighting the urgent need for the investment of resources, both human and fiscal.

The problem of ageing railway bridges is a particularly difficult one. There is a complex array of issues that face integrity and remaining life assessment of railway

bridges [12-14]. The structural conditions of railway bridges may change from site to site, even where bridges are supposedly of the same design. The conditions for any particular bridge often change over the life of the bridge; with degradation of piers, supports and structure. The dynamic interaction between rolling stock and structure, due to normal vehicle and structural dynamics, and defects such as wheel flats, out of round wheels and structural degradation, has a dramatic effect on structural response [15-20]. The dynamic interaction between vehicle and structure often requires complex modelling techniques [21-26] and is therefore often neglected in assessment. Current railway bridge fatigue assessments in Australia are at times unreliable since different methods and assumptions are used from one assessment to the next, with varying understanding of the issues of railway bridge assessment. This is true not only in Australia but also around the world [27-28].

1.2 Working Toward a Solution

The aim of this research is to work toward addressing the problem of ageing steel railway bridges by formulating a clear, repeatable, top-down methodology for high-level structural assessment. The method aims to integrate the state-of-the-art in modelling, testing and fatigue code tools and use transient digital data for testing, modelling and assessment. Responding to the demands made in the infrastructure report cards reviewed earlier, a methodology has been developed which is integrated throughout, that is each step of the method flows into the next. An effort has been made to produce a method whose application is simple enough to be useful to the structural engineers for whom it is intended, while remaining sophisticated and state-of-the-art. Assumptions and data used in assessment are clearly presented, so as to

yield a procedure which is transparent and therefore repeatable and verifiable. In order to demonstrate the methodology, the steel girder approach spans of the Mullet Creek Railway Bridge at Dapto, NSW, have been assessed.

As the literature review beginning Section 2.1 indicates, most modern bridge assessments fall into two groups. The first conducts assessment using *measured dynamic response* from field-testing only [29, 30]. This ensures that significant dynamic effects are included in the assessment, although relies on the assumption that the particular test conditions and measured responses are a sufficient representation of all loading and structural conditions; past, present and future. Using test data only also assumes that the only components of interest are those measured. The second group conducts assessment using *verified structural models*. The use of structural models allows variation in loading and structural conditions to simulate known or predicted changes in both applied loads and structural conditions. Theoretically it also allows all components of the structure to be economically investigated. Most assessments carried out using structural models, however, tend to use only static response from structural models and therefore neglect the highly significant dynamic effects [31, 32], or else deal with dynamic effects by including a single amplification factor [33, 34].

In the method developed in this research, structural models are used so that changes in loading and structural conditions may be modelled and potentially all components of a bridge investigated. Structural models in this work, however, are used to predict the complete dynamic response of the structure. In order to use structural models to predict the complete dynamic response, efficient methods for modelling moving loads in finite element software have been developed. Efficient methods of tuning models to

measured dynamic response, and methods for identifying the time varying magnitude of moving loads are also used. For railway bridge assessment this has required the development of an analytical model for beams with rotational stiffness at the supports subjected to multiple uniformly distributed loads.

The most significant contribution of this research is expected to be the complete methodology, its clarity and repeatability, its integration throughout and the way in which it attempts to deal with the difficult problem of true dynamic response. Contributions are also anticipated in some individual steps of the methodology where attempts have been made to extend current research.

1.3 Thesis Outline

This thesis begins with the present introduction (Chapter 1). The proposed method and theory are presented in Chapter 2 and demonstrated in Chapter 3. The theory of Chapter 2 is divided into six sections. Due to the broad scope of the work, summaries of previous and current research are presented at the beginning of the relevant theory sections, rather than in a single literature review.

The opening section of the theory chapter (Section 2.1) begins with a review of reported bridge assessment methods. These demonstrate the need, already highlighted in the present introductory chapter, for an integrated method that accounts for the true dynamic response of structures under transient load. The methodology developed in this research, which aims to address that need, is then outlined.

One of the most significant requirements for the success of the method, described in Section 2.1, is an efficient method for modelling moving loads, with time-varying magnitudes, using finite element analysis software. An efficient method has been developed and is presented in Section 2.2. The literature review, at the beginning of this section, highlights that over the last 150 years a great deal of research has been carried out into structures, particularly beams, subjected to moving loads. Although finite element methods have gained popularity, they have been considered, by some, too cumbersome and impractical for moving loads analysis. Some researchers have sought to overcome this difficulty, by developing efficient methods for applying moving loads as nodal forces and moments at the nodes of elements on which the load is acting. Generally these methods have been developed and demonstrated for loads of constant magnitude, with nodal forces defined by applied loads and the shape function of the elements on which they are applied. The method presented in Section 2.2 does not rely on the shape functions of elements. It is suitable for multiple loads, of varying magnitude and may be efficiently used in finite element analysis software. Theoretical results for the method are compared to those from analytical techniques, in this section. In Chapter 3 the theory is compared against field test results. After the method presented in Section 2.2 was developed, but before any attempt had been made to publish, an almost identical method for the modelling of the dynamic response of gantry cranes was published by Wu, Whittaker and Cartmell in *Computers and Structures* [35]. No experimental verification was provided at that time.

In this research dynamic field testing techniques have been used for finite element model validation and load identification from structural response. A short review of field test techniques, used in bridge assessment, is presented in Section 2.3 and those

techniques suitable for dynamic testing are identified. The methods used in this research are outlined in general terms.

Often in the design and analysis of bridges subjected to moving loads two simplifications are made; moving loads are considered to be concentrated point loads, and bridges are considered to be simply supported. For assessment of railway bridges these simplifications are not always appropriate. Railway bridges may not be simply supported, and loads, which are applied to the structures, may be distributed rather than point loads. This is significant both for model validation, from dynamic field-testing, and for load identification, from structural response (that is identification of the time-varying magnitude of moving loads from measured structural response). For model validation and load identification for railway bridges, an analytical model has been developed for Euler-Bernoulli beams, with rotational stiffness at supports, subjected to multiple distributed loads. The analytical model, presented in Section 2.4, is the solution of the uncoupled equations of motion for the beam. The response from the analytical model is compared to other known solutions, the Heaviside unit function approximation of a uniformly distributed load and field test results.

Section 2.5 presents methods used to identify the magnitude of moving loads from measured structural response. In a literature review, beginning the section, the motivation for identifying moving loads from structural response is presented. Over the last 20 years a great deal of progress has been made in identifying the magnitude of loads from structural response. Research has generally focussed on simply supported beam structures subjected to moving point loads. The research presented in Section 2.5 considers, using the analytical model of Section 2.4, load identification for moving

loads with a uniformly distributed contact patch on Euler-Bernoulli beams with rotational stiffness at supports.

Section 2.6 details the method used in this research for the development of the duty cycle loading schedule, that is, the method used to develop a complete history of loading for the bridge.

Section 2.7 begins with a brief review of fatigue assessment methods and an explanation of why stress based fatigue assessment methods have been chosen for the present research. Details are given for a software system, developed and used in the methodology, which estimates remaining life from digital stress histories according to several international fatigue codes. According to the literature reviewed in this section, stress-based fatigue codes remain the most popular tools used to predict remaining life. There are, however, many codes, with differing methods, which often yield significantly different results. There is a need, therefore, to critically compare key international fatigue codes. The bulk of this section is devoted to a comparative study of several international structural fatigue codes.

In the demonstration of the method, presented in Chapter 3, details of the Mullet Creek Railway Bridge are given and the finite element model built for analysis is described. In that chapter structural integrity and remaining life assessment is carried out for the steel girder approach spans of the Mullet Creek Railway Bridges, following the methodology outlined in Chapter 2, focussing on three significant components of the bridge.

Chapter 4 presents a discussion of the theory, presented in Chapter 2, and the results, presented in Chapter 3. Also included in Chapter 4 are general implications of the research and recommendations for future work, as well as specific implications and recommendations for the Mullet Creek Railway Bridge. Chapter 5 summarises what aims were fulfilled, summarises the results of the research and what they mean and comments on the overall importance of the work.

1.4 An Iterative Process

The process of developing the method, proposed in this thesis, has been largely iterative. The proposed method has evolved as a result of reviews of the literature, initial development of theory, significant testing and then redevelopment of theory. Field-testing was carried out a number of times, for example. On each occasion field-test results lead to development of the theory, while advances in the theory informed future field-testing. Similarly, as one step in the theory was developed, or the literature further reviewed, other parts of the method were developed further.

For the sake of clarity, only the final method is presented in this thesis, rather than a complete history of every development and redevelopment. Note that the structure of Chapters 2 and 3 follow the order of the final method, even though in some instances the later steps were developed before the former.

2. THEORY

2.1 An Integrated Methodology for Stress-Based Fatigue Assessment of Steel Railway Bridges

2.1.1 Introduction and Literature Review

A number of methods are reported in the literature for fatigue assessment of road and rail bridges.

In 1987 Grundy, Deutch, Hardcastle and Park [33] carried out fatigue assessment on the then 98-year-old Melton Railway Bridge in Victoria, Australia. The method employed was:

1. Identify the most highly stressed connection.
2. Develop a stress history, from a scrutiny of traffic records, old timetables, and records of rolling stock and locomotives.
3. From the stress history establish a characteristic freight and passenger train.
4. Develop a simple history for the passage of characteristic trains.
5. Add an impact factor to theoretical stresses.
6. Manually rain flow cycle count the stress history and estimate remaining life from Australian and Swiss codes of practice.
7. Verify fatigue assessment with field-testing.

In 1993 Chung [34] presented a method for the fatigue assessment of rail underbridges, more or less as per BS5400 guidelines. Their procedure follows.

1. Develop a duty cycle, from historical data.
2. Determine peak stresses, from field-test verified numerical models and stress concentration factors.
3. Apply a 'blanket' amplification factor to stresses.
4. Choose an appropriate S-N curve, from BS5400 for the joint detail in question.
5. Cycle count, using the Reservoir or Rainflow cycle counting methods and sum damage using the Palmgren-Miner damage summation rule.

In 1995 Marcer and Bhavnagri [31, 32] carried out assessment on an old lattice girder bridge. Their method follows.

1. Develop a structural model and verify by strain gauge testing.
2. Generate a stress history, by obtaining influence lines for static unit loads in different locations along the bridge. Compare these to dynamic strain gauge results.
3. Develop a historic duty cycle loading schedule and condense into a few typical 'fatigue trains' over appropriate periods.
4. Develop numerical stress history response for fatigue trains using static influence lines.
5. Conduct fatigue assessment via BS5400.

Marcer and Bhavnagri note in the papers that the purpose of strain gauging is not to assess stress ranges directly, but to verify structural models. It is also noted that the

influence line method of generating numerical stress histories does not account for the true dynamic behaviour of the bridge and the interaction of the load and structure.

Yamada, Kato, Ishiguro and Uemura [29] present field-test stress measurements and the subsequent fatigue life estimation, for a Japanese plate-girder road bridge. The method for fatigue assessment presented in their paper is:

1. Strain gauge the bridge.
2. Record the stress response for 24 hours of normal traffic at various members.
3. Divide stresses into a stress spectrum with an interval size of 2.5 MPa.
4. Rain flow cycle count stresses.
5. Calculate fatigue life via ECCS Fatigue Design Recommendations using two different S-N curves.

Korondi, Szittner, Kally and Kristy [30] in 1998 use static load tests with loads positioned at successive locations, to verify calculated stress histories for a riveted railway bridge.

1. Record the stress histories of 100 trains, using strain gauges and extrapolate to represent the annual traffic loads for fifty years.
2. Increase the measured stress values by 50%, to account for stress concentration effects.
3. Carry out fatigue assessment for the bridge, using Hungarian codes of practice.

In the literature reviewed above, various methods are used for fatigue assessment of bridges. Where structural models or calculated stresses are used, either the dynamic interaction between vehicles and the structure is ignored [31, 32], or it is accounted for

by a single dynamic amplification factor applied to the entire stress history [33, 34]. Where the true dynamic behaviour of the bridge is included in assessment, measured stresses only are used [29, 30]. Static modelling is often verified using dynamic test results [35, 31, 32]. Most fatigue assessment appears to be conducted using manual application of various codes.

A number of elements common to many of the methods described are used in the method presented here. Duty cycle data is used. Testing is conducted using strain gauges. Final fatigue assessment is conducted using coded methods. In the method developed in this project, structural models are used, taking advantage of the fact that by utilising verified structural models stresses may be found at more locations on the structure and for a greater number of loading and structural conditions than were tested. The models used in this project, however, do not ignore true dynamic behaviour or use single blanket amplification factors, but instead model the complete dynamic behaviour of the bridge under load. ***Dynamic*** modelling is verified against ***dynamic*** testing and ***dynamic*** results are used in final fatigue assessment. Fatigue assessment software is used so that assessments from a number of codes may be compared. The procedure developed here is integrated throughout due to the consistent use of dynamic methods, and software for stress analysis and fatigue assessment.

2.1.2 An Integrated Methodology for Stress-Based Fatigue Assessment of Steel Railway Bridges

The method developed in this project is outlined below and in Figure 2.1.1.

1. The first step in the method is to build a reliable preliminary finite element sensitivity model (that is a finite element model which permits variations in joint fixity and support conditions) and an analytical model of the bridge. Models are built from both structural drawings and, recognising that built structures often vary from design and that structural conditions change over time, from site inspections. The finite element model is built using beam or plate elements so that it may be suitable for dynamic modelling. Section 2.2 outlines the method used for dynamic modelling of moving loads.
2. Field-testing is carried out by strain gauging the structure and measuring the response under the passage of a locomotive, or other rolling stock of known load, at crawl speed. Further details of the test set-up are given in Section 2.3.
3. The known loads of the vehicle used during testing are applied to an analytical model (described in Section 2.4). The analytical model parameters are tuned, so that the response from it matches the dynamic response measured during testing.
4. The finite element sensitivity model is now tuned to the test results, using the tuned analytical model as an intermediate step, to guide how the finite element model is to be tuned. The finite element model is tuned under the same dynamic loading conditions used to tune the analytical model from dynamic test results.
5. Further dynamic field-testing is carried out for normal traffic, using the same test set-up as was used for model validation.
6. Using an inverted structural matrix (transfer function), taken from the tuned analytical model, and the test data, recorded from dynamic testing of the structure

under normal traffic, actual axle or wheel loads are identified, using the method outlined in Section 2.5.

7. A historic duty cycle loading schedule of bridge traffic is compiled, from available records and archive data.
8. Load tables are developed, from duty cycle data and identified loads.
9. Load tables are applied to the finite element sensitivity model, developing dynamic stress histories for any component of the bridge using the method of Section 2.2.
10. Finally, dynamic stress histories are entered directly into a software system, described in Section 2.6, which estimates remaining life via several international fatigue codes.

Loading and structural conditions may be adjusted at this point and the integrity and remaining life of the structure evaluated for virtually any combination of structural and loading condition.

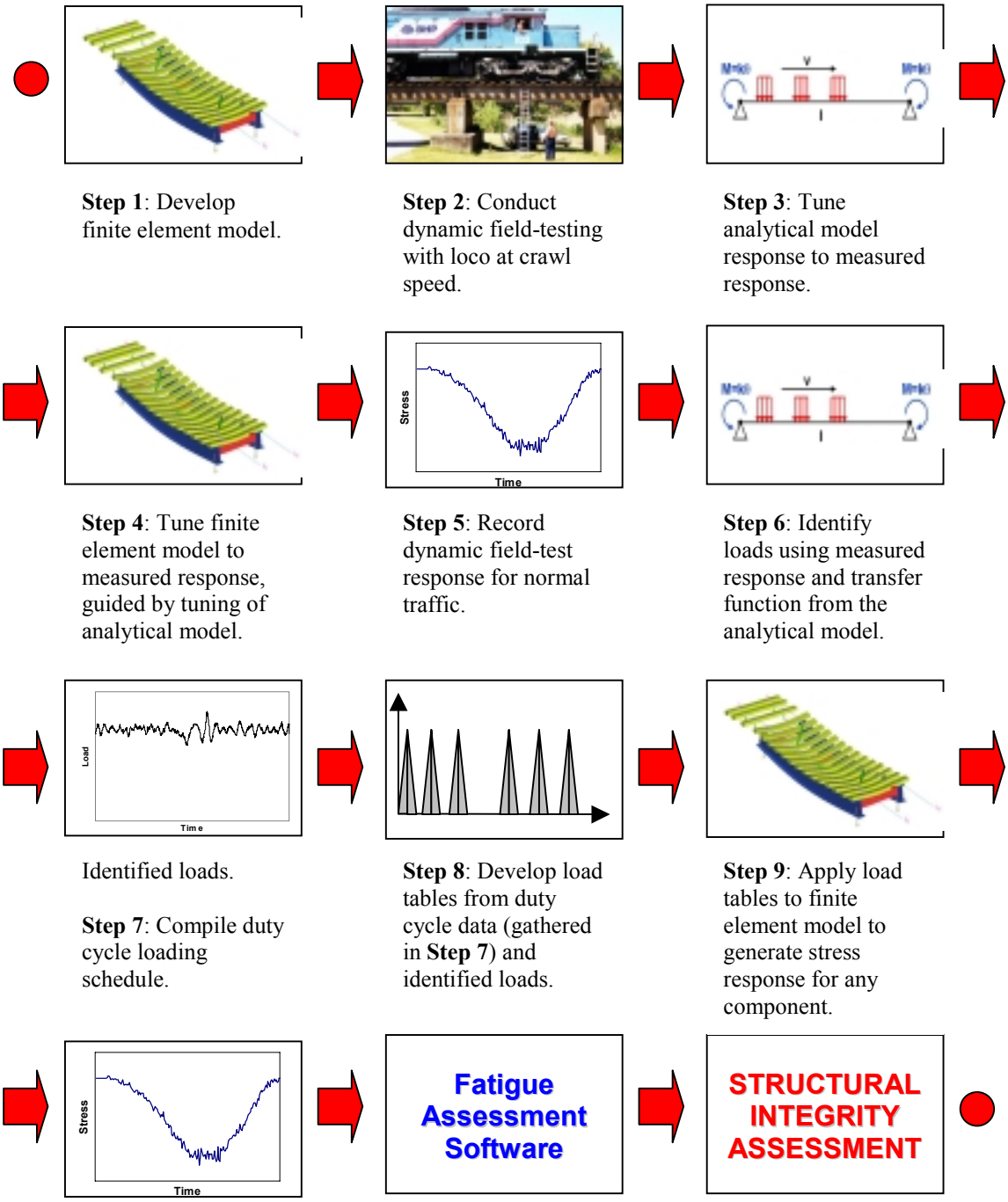

Step 1: Develop finite element model.

Step 2: Conduct dynamic field-testing with loco at crawl speed.

Step 3: Tune analytical model response to measured response.

Step 4: Tune finite element model to measured response, guided by tuning of analytical model.

Step 5: Record dynamic field-test response for normal traffic.

Step 6: Identify loads using measured response and transfer function from the analytical model.

Identified loads.

Step 7: Compile duty cycle loading schedule.

Step 8: Develop load tables from duty cycle data (gathered in **Step 7**) and identified loads.

Step 9: Apply load tables to finite element model to generate stress response for any component.

Stress response from finite element model.

Step 10: Determine remaining life, using generated stress histories and fatigue assessment software.

Final structural assessment.

Figure 2.1.1. An integrated methodology for stress-based fatigue assessment of steel railway bridges.

2.2 Modelling the Dynamic Response of Structures in Finite Element Software

2.2.1 Introduction and Literature Review

The study of beams, subjected to moving loads, has received a great deal of attention for many years. Interest in the problem has its origin in civil engineering, particularly in the design and assessment of railroad and highway bridges. The problem of a mass-less beam traversed by a non-sprung mass was considered first by Willis in 1849 [36]. Later Stokes [37] showed the solution for a beam of uniform mass traversed by a force moving at constant velocity. In 1922 Timonshenko [15] presented a short article, providing mathematical formulae for the hammer blows resulting from the imperfect balance of locomotive driving wheels. Ingliss [16], in 1934, presented a mathematical treatise on vibrations in railway bridges. Ingliss notes that the calculation of static stresses "hardly admits any further advance" and yet calculation of stresses under dynamic load still relies heavily on empirically derived amplification factors. Using empirically derived amplification factors, he argues, is unsatisfactory, and he presents mathematical methods for the calculation of dynamic stresses, particularly for stresses resulting from oscillations due to the hammer blows of locomotive driving wheels, as Timonsheko had before him. Important contributions have been made by many others, including Ayre, Ford and Jacobsen [38] who consider a moving constant force travelling along a 2 span simply supported beam, comparing analytical results to measured results from a test model. Ayre, Jacobsen and Hsu [39] use similar experiment apparatus, for a 2 span simply supported beam considering a mass load, concluding that inertia forces are significant for relatively high velocities. A great deal of research has followed the early work of these pioneers of the field. A thorough review of the history of the study of the moving loads problem is provided by Fryba

[40] in his text *Vibration of Solids and Structures under Moving Loads*. See also *Dynamics of Railway Bridges* [41], by the same author.

The study of beams subjected to moving loads is not only of interest in bridge design and assessment. Lin and Trethewey [42] note that the problem of moving loads on elastic structures also arises in many modern machining operations. Karaolides and Kounadis [43] consider the dynamic response of a two-member frame subjected to a constant force moving across its girder. Wu, Whittaker and Cartmell [35], investigate the response of mobile gantry cranes, by simplifying the problem into four moving point loads on a static frame.

The classic solution method, and arguably the most popular method for the study of the dynamic response of simple or continuous beams subjected to moving loads, is the mode-superposition technique where the uncoupled equations of motion of a system are solved. An outline of this method is presented in Section 2.4 of this thesis as well as many texts including those by Biggs [44] and Clough and Penzien [45]. Mode-superposition theory continues to be published in many papers. Yang, Yau and Hsu [46] use mode-superposition in their analytical approach to the vibration of simple beams due to the passage of trains moving at high speeds. Law, Chan and Zeng [47] use mode-superposition to identify and reconstruct vertical dynamic interaction forces from measured structural responses. Chen and Li [48] study the dynamic response of an elevated railway, at the preliminary design stage, by the mode-superposition method. Wu and Dai [49] use mode superposition to analyse the dynamic response of a non-uniform multispan beam. Where the technique is not used directly as an analysis technique, it is inevitably used as the benchmark by which new methods are judged.

A number of papers have been written modelling moving loads using the finite element method including those written by Olsson [50] (using a general bridge-vehicle element for railway bridges), Hino, Yoshimura and Ananthanarayana [51], Lin and Trethewey [42], Fryba, Nakagiri and Yoshikawa [52] and Thambiratnam and Zhuge [53]. These papers make use of the finite element method in terms of numerical method. That is, the moving load problem is dealt with using matrix methods and mathematical theory, rather than using the application of commercial finite element software into which the finite element method is built. Henchi, Fafard, Dhatt and Talbot [54] and Wang [55] note that the finite element method may be both cumbersome and impractical and provide alternative methods based on modal techniques.

Lin and Trethewey [42], studying elastic beams with general end conditions, and Thambiratnam and Zhuge [53], studying beams on an elastic foundation, greatly simplify the finite element analysis of moving loads on beams. Both sets of authors model single dimension moving loads, with constant magnitude, as nodal forces and moments. Nodal forces are given a magnitude of zero for all nodes, except for nodes of those elements on which the load is acting. The magnitude of the applied load and the shape function of the element, on which the load is applied, define the nodal forces applied to the elements.

Saadeghvaziri [56] presents a potentially practical approach to modelling moving loads, using the finite element method. He suggests that general-purpose finite element packages may be used to model the dynamic effect of moving loads by modelling loads as a series of rectangular impulses. He notes, however, that modelling moving loads in this way means the mesh size is not left up to the modeller's discretion, but is instead

defined by the applied loading. In practice this means that the mesh must be relatively fine, so the impact effect of the rectangular impulse application of the loads is reduced. To demonstrate this, the response of a ten-element simply supported beam model, with a moving load applied in this way, is presented in Figure 2.2.1(c). (Figure 2.2.1(a) shows the applied load at node 5. Figure 2.2.1(b) show the force-time history at node 5.) Comparing the finite element response against the analytical, a significant and unacceptable effect due to the impact application of the load is observed.

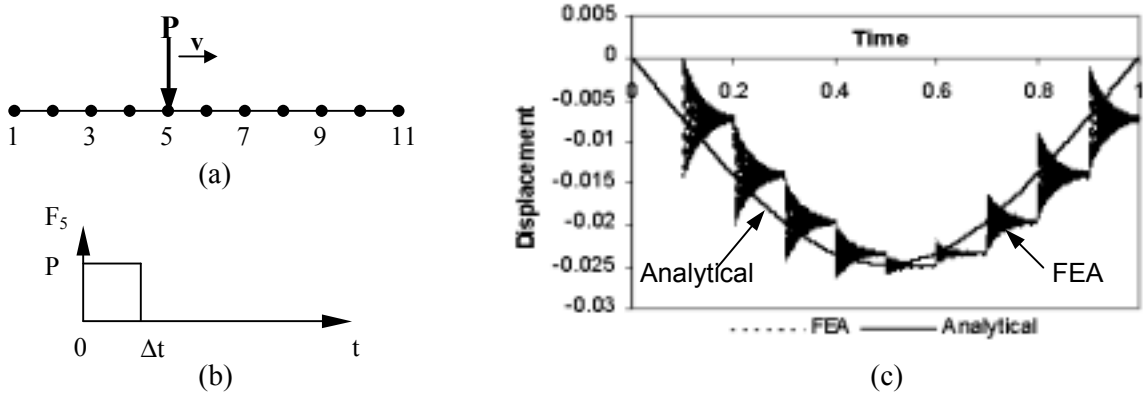

Figure 2.2.1. (a) Ten-element beam with a rectangular impulse load applied at node 5. (b) Force time history for node 5. (c) Displacement response of a ten element beam at mid-span to applied loading modelled as rectangular impulses.

A great deal of the foregoing research on moving loads analysis has focussed on single constant magnitude loads, rather than multiple loads with time varying magnitude. Some methods have been relatively inaccessible due to their complexity, while others, although accessible, have been shown to be of insufficient accuracy. The contribution of the research made in this section of the thesis is the development of a simple, yet relatively accurate, method for modelling multiple moving time varying loads.

After the method presented here was developed, but before any attempt had been made to publish, an almost identical method for the modelling of the dynamic response of

gantry cranes was published. The authors of that work are Wu, Whittaker and Cartmell [35]. Wu, Whittaker and Cartmell use finite element software techniques to simplify the dynamic modelling of mobile gantry cranes, as a static frame-work and four moving time-variant point loads representing the moving substructure. Three techniques are presented in their research, all of which are compared against analytical solutions. Two of the techniques yield results that match analytical results. Both of these methods use load-versus-time tables, developed for all nodes, and are termed the 'full' method and the 'simple' method. The 'full' method uses force-versus-time and moment-versus-time tables, which, like methods already discussed by Lin and Trethewey [42] and Thambiratnam and Zhuge [53], are based on the applied load and the shape function of the elements on which they are applied. The contribution made by Wu et al. is the fact that methods are presented for multiple time varying loads in more than one dimension, rather than single, constant magnitude loads. The second method is named the 'simple' method and is of most interest here. The 'simple' method presented by Wu et al. ignores the shape functions of elements and ignores external moments applied at the end of elements. In this method loads are applied only as force-versus-time tables. Wu and Dai [49] used the same technique for applying loads in 1987, although they used the transfer matrix method rather than the finite element method. The magnitude of loads is found by linearly interpolating forces, as loads move from one node of an element to the next. This method is a significant simplification on methods presented to date and, like the 'full' method, is capable of efficiently modelling multiple time-varying loads in more than one dimension in finite element analysis software. Wu et al. do not provide experimental verification of their techniques and point out that experimental validation is essential in order to have full confidence in the techniques.

The method developed in this research is almost identical to the 'simple' method of Wu et al., although the application of the method differs. The method developed here has been validated against field test results.

In this section, the dynamic response, to various loading conditions, is presented against analytical and numerical solutions of the modal equations of motion of a simply supported Euler-Bernoulli beam using the mode-superposition technique. Comparisons are made, using vertical reaction forces, at the supports, and displacement response, at the mid-span of the beam. Bending stress response is not compared in this section. Of course bending stress is equivalent to constant Beam Section values multiplied by the second derivative of displacement. Therefore, if the method may be validated against displacement response, it is also applicable for bending stress response. The theory is further validated using stress response against field test results, in the demonstration presented in Chapter 3.

2.2.2 Modelling Moving Loads in Finite Element Software

In the development of the presented technique, a number of attempts were made to model moving loads on structures in finite element software. Simply supported beam models were used for development of the technique, due to the ease of verifying solutions against analytical models. In early attempts, point loads were modelled as rectangular impulses at nodes. Although the trend of the response compared well with analytical solutions, large spikes were introduced because of the nature of the impact loading, similar to that shown in Figure 2.2.1. The impact response of the finite element modelled loads was minimised by using a very fine mesh, although this proved

inefficient and expensive in resources. This method of modelling moving loads is similar to the technique presented by Saadeghvaziri [56].

Further attempts were made modelling loads, not as point loads, but as distributed loads, in order to model the elliptical rail-wheel contact area. Finite element representation of distributed loads was achieved by modelling time varying loads, with load magnitudes dependent on the assumed load distribution, at all nodes within the contact area, in a manner similar to that used for point applied loads. Again, the trend of the response of the finite element model compared well with the analytical solution, although spikes were again introduced due to the impact nature of the applied loading. From these attempts the method presented herein evolved.

In the method developed in this research, the value of externally applied nodal forces are zero at all nodes, except for those nodes of the element on which the load is acting. The magnitude of the nodal force is found by a simple linear interpolation of the forces. Consider the simplest case shown in Figure 2.2.2 (a), i.e. a concentrated load of constant magnitude and velocity, and the force-time histories in Figure 2.2.2 (b). The force on node 3 is a maximum, when the moving concentrated load is directly above it, at $t = 0$. This force linearly decreases to zero, as the load moves along the element at constant velocity to node 4. Similarly, the force on node 4 begins with a magnitude of zero, linearly increasing to maximum value, as the concentrated load moves along the element from node 3 to node 4, at $t = \Delta t$. This method is, of course, analogous to elementary formulae that describe the vertical reaction forces of a beam subject to a moving load.

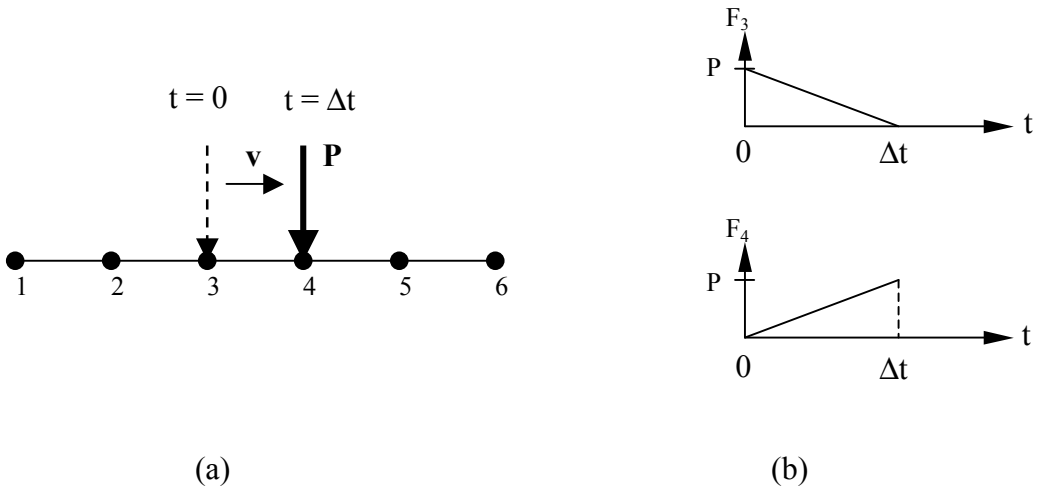

Figure 2.2.2. (a) Beam with concentrated load of constant magnitude and velocity.

(b) Force time histories for nodes 3 and 4.

For multiple point loads, the same simple principal of discrete linearly varying loading may be applied. Although a seemingly simplistic method (note that consideration of element shape functions is not required and loads only are applied without accompanying moments), the results, presented in Section 2.2.3, show close conformance with analytical solutions under identical conditions. The results of Wu et al. [35] also support the application of externally applied nodal forces without accompanying moments or consideration of the element shape functions. For the purpose of explanation, loads of constant magnitude and velocity have been considered, although loads of variable magnitude and velocity, or even variable acceleration, may be similarly applied, as is later demonstrated, in section 2.2.3.

Equation (2.2.1) gives the general equation that defines the force at each node for a single moving concentrated load of variable magnitude and constant acceleration, on an elastic beam. See also Figure 2.2.3. Note that the equation is simply the value of the

applied load, of time dependent magnitude, multiplied by a factor, which is the linear interpolation of the position of the load on the element.

$$F(t)_i = \frac{\left(V_{i-1}(t_i - t_{i-1}) + \frac{1}{2}a(t_i - t_{i-1})^2\right)}{l_{i-1}} P(t) \qquad \text{for } t_{i-1} \le t \le t_i$$

$$= \frac{\left(l_i - \left(V_i(t_{i+1} - t_i) + \frac{1}{2}a(t_{i+1} - t_i)^2\right)\right)}{l_i} P(t) \qquad \text{for } t_i \le t \le t_{i+1} \qquad (2.2.1)$$

for $1 \le i \le n$

where n = number of nodes.

P(t) = applied transient load.

$F(t)_i$ = transient force at ith node.

V_i = velocity at ith node.

t_i = time at ith node.

l_i = length of ith element.

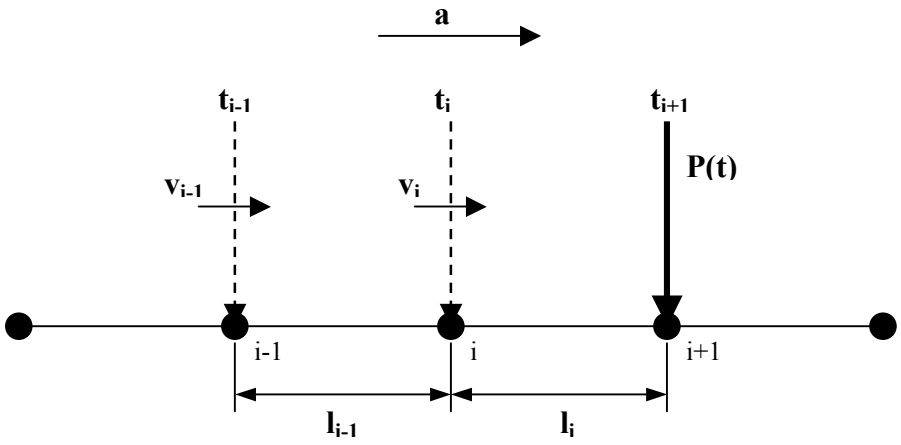

Figure 2.2.3. Single moving concentrated load of variable magnitude and constant acceleration on an elastic beam.

It is a relatively simple task to extend the theory further to include variable acceleration, by including an expression, either analytical or numerical, to define the location of the load on the beam if need be. For this project, consideration of variable acceleration has been considered unnecessary, since trains should neither accelerate nor brake on railway bridges.

For the load of variable magnitude and velocity of Figure 2.2.4, the loads applied at the second and third nodes of a ten element simply supported beam of span 0.5 m, may be found using equation (2.2.1). The time variant applied loads at nodes 2 and 3 are shown in Figure 2.2.5

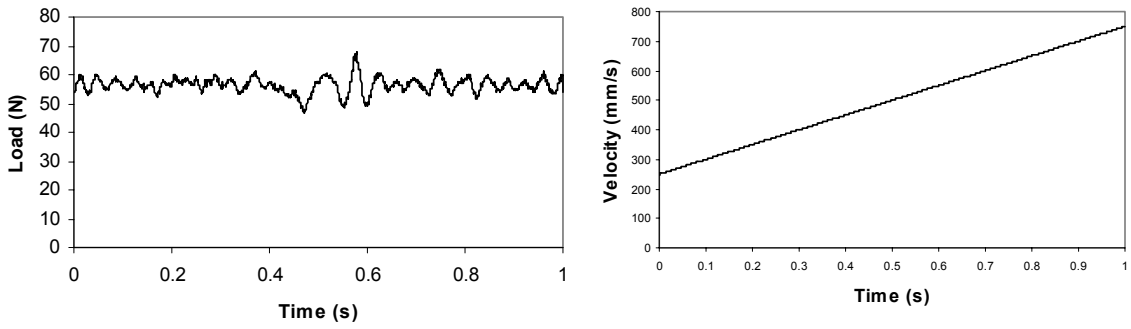

(a) **(b)**

Figure 2.2.4. Magnitude of (a) load and (b) velocity for a single concentrated load of randomly varying magnitude moving with variable velocity.

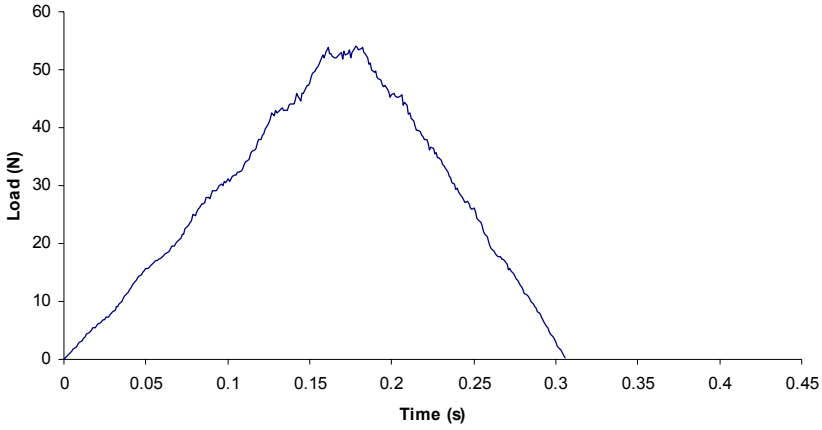

(a)

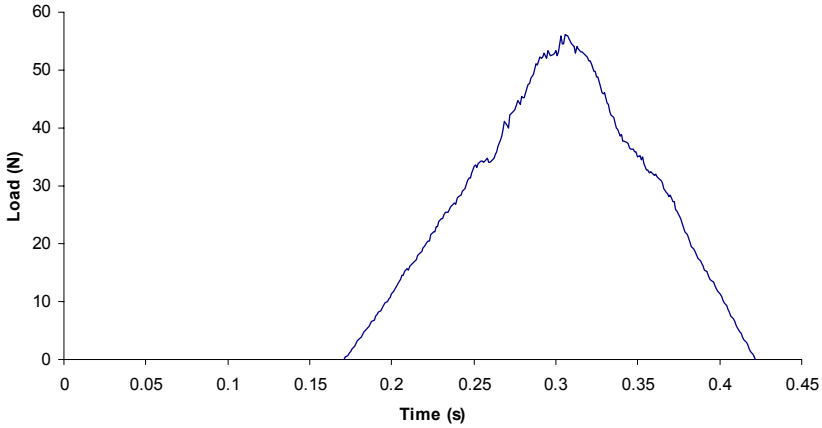

(b)

Figure 2.2.5. Loads applied at nodes (a) 2 and (b) 3

for simulation of the load of figure 2.2.2.

The complete response for this load case, as well as several others, in terms of displacement at mid-span and vertical reaction force at supports, is presented in Section 2.2.3, for a simple ten element beam, using equation (2.2.1) to define the external force at each node. Although the external time variant force applied at each node appears to vary only slightly from a linear triangular form, the variation has a dramatic effect on the dynamic response, as will be seen in Section 2.2.3.

2.2.3 Comparison of Finite Element and Analytical Solutions

For the following comparisons, a rectangular simply supported steel beam is assumed, with a mass density of 7810 $kg.m^{-3}$, an area of 250 mm^2 (height of 50 mm and a width of 5 mm), a length of 500 mm and with damping 10% of critical damping. The dynamic response is determined using finite element software and is compared to analytical solutions.

For finite element analysis, the beam is divided into ten beam elements of equal length. The responses shown are from the G+D Computing, Strand7, finite element package, although identical results have been obtained using MSC NASTRAN and are obtainable in principle from any conventional finite element package. The analytical response is found using the mode-superposition method, solving the modal equations of motion.

Five load cases are considered (see Figures 2.2.6 to 2.2.10):

1. A single concentrated load of 100 N in magnitude, moving at a constant velocity of 500 $mm.s^{-1}$.
2. A single concentrated sinusoidally varying magnitude load with a mean of 100 N, an amplitude of 20 N and a period of 0.1 seconds, moving at a constant velocity of 500 $mm.s^{-1}$.
3. A single concentrated load of 100 N in magnitude, with two rectangular impulse loads of 100 N, lasting 0.2 seconds moving at a constant velocity of 500 $mm.s^{-1}$.
4. A single concentrated load, of randomly varying magnitude, moving at a constant velocity of 500 $mm.s^{-1}$.

5. A single concentrated load, of randomly varying magnitude, moving at a constant acceleration of 500 mm.s^{-2}, with an initial velocity of 250 mm.s^{-1}

The loading cases listed above are not chosen arbitrarily, but with the overall project in mind. For example, for case 3, the magnitude of the load at impact is assumed twice that of the perfect rolling load, i.e. a 100% increase in load at impact. An increase in load of this order of magnitude, while highly dependent on exact structural conditions, speed of vehicle etc., is reasonable for wheel impact loads on railway bridges, according to the literature [17-19].

For the simple cases of a constant load and a sinusoidally varying load the analytical response is found by solving the equations of motion directly, using the first three modes in the plane of bending. For the more complex loading of cases 3 to 5, the analytical response is found using the central finite difference method, with a 10^{-4} second time step, for the first two modes in the plane of bending. For case 4 the analytical response is found both by the central finite difference method and by direct solution of the equations of motion where, for a single moving load at each time step j, the modal force is;

for constant velocity, and

$$F_j(t) = P_j(t)\sin\left(\pi\left(\frac{Vt}{l}\right)\right), \tag{2.2.2}$$

for constant acceleration.

$$F_j(t) = P_j(t)\sin\left(\pi\left(\frac{Ut + \frac{1}{2}at^2}{l}\right)\right) \tag{2.2.3}$$

Figures 2.2.6 to 2.2.10 compare the finite element and analytical responses. For all cases, the magnitude of the load applied to the beam, the magnitude of the vertical displacement response at mid-span and the magnitude of the vertical reaction force response at the beam-ends is presented. For the constant acceleration case (case 5, Figure 2.2.10) the same random load is used from the previous case (case 4 and Figure 2.2.9) and the velocity profile of the moving load is presented in its place.

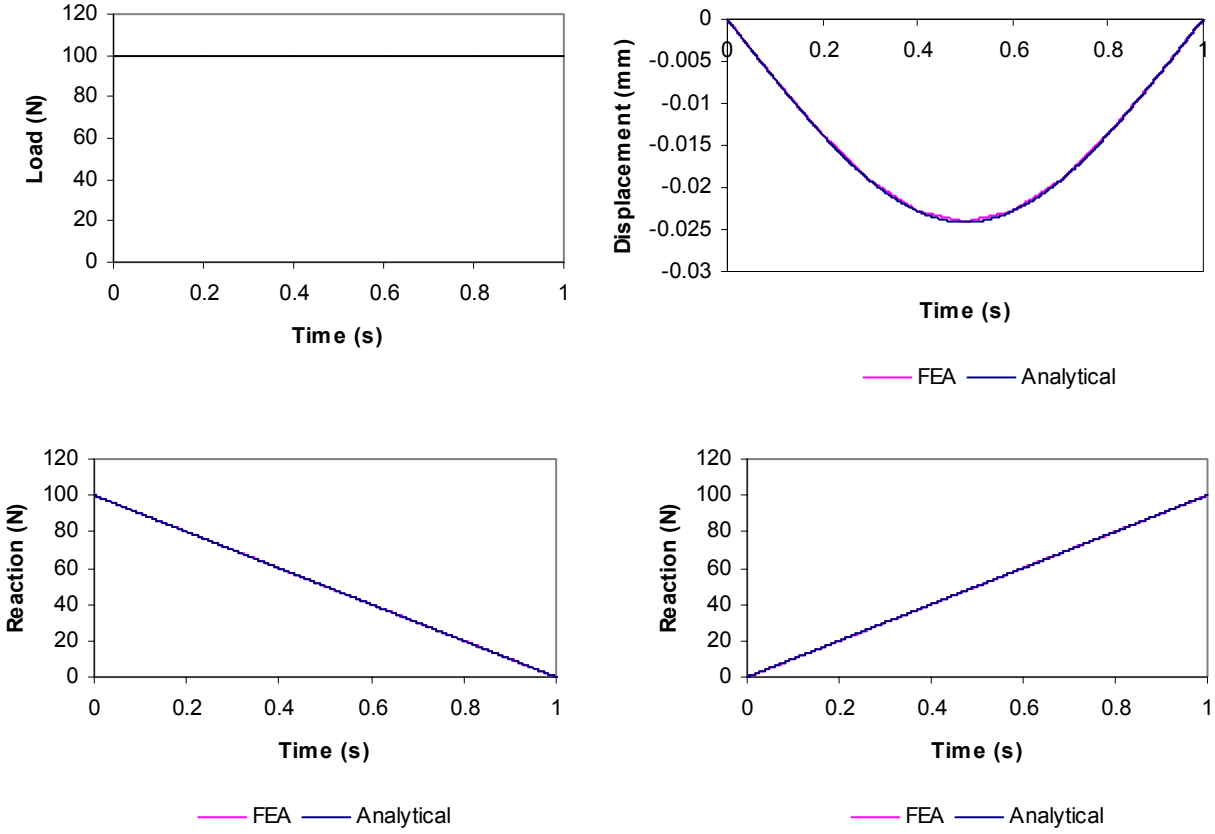

Figure 2.2.6. Case 1: constant load, constant velocity.

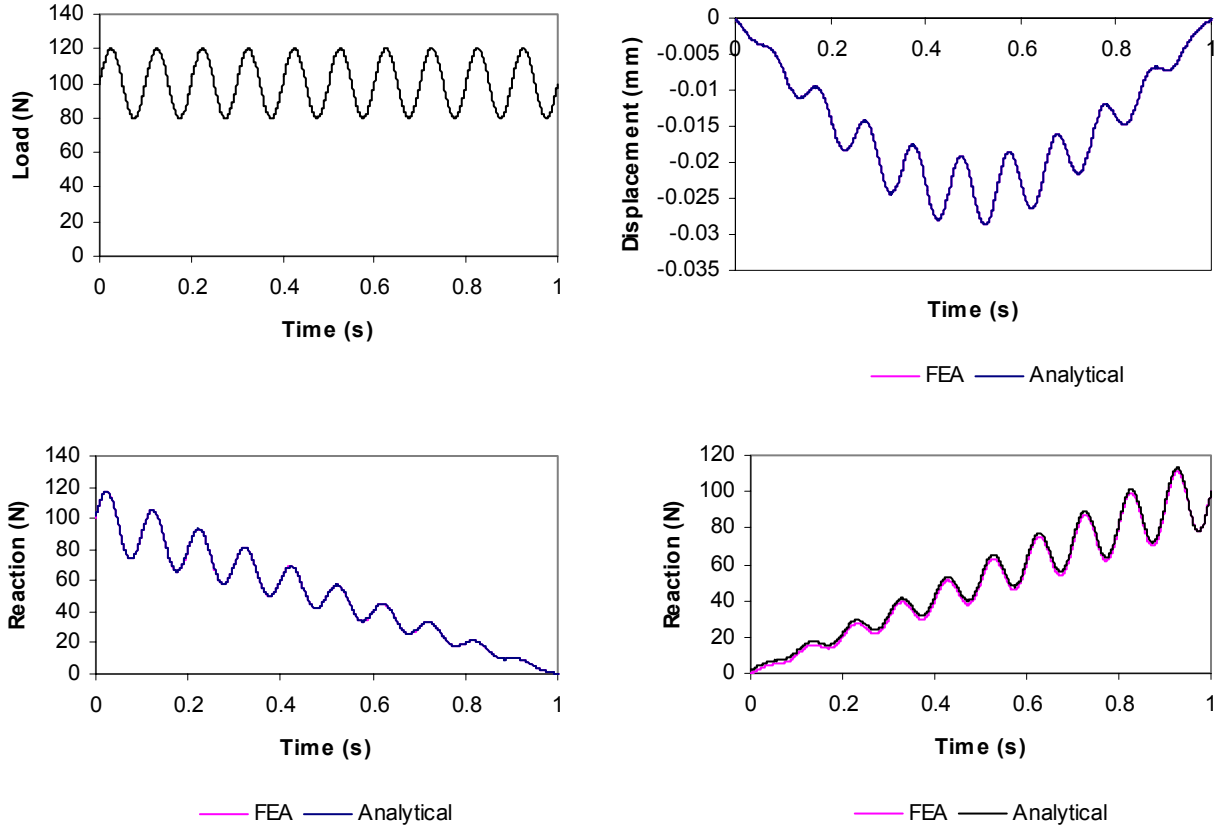

Figure 2.2.7. Case 2: sinusoidal varying load, constant velocity.

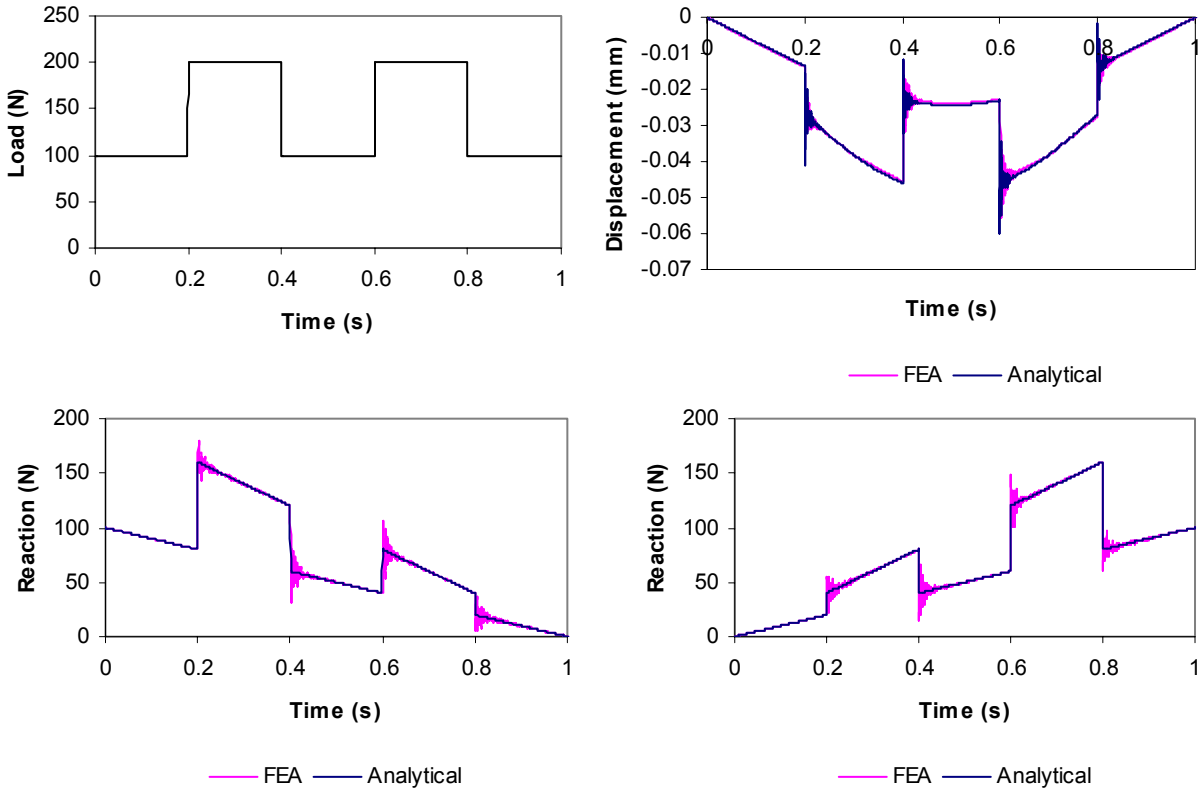

Figure 2.2.8. Case 3: constant load with rectangular impulses, constant velocity.

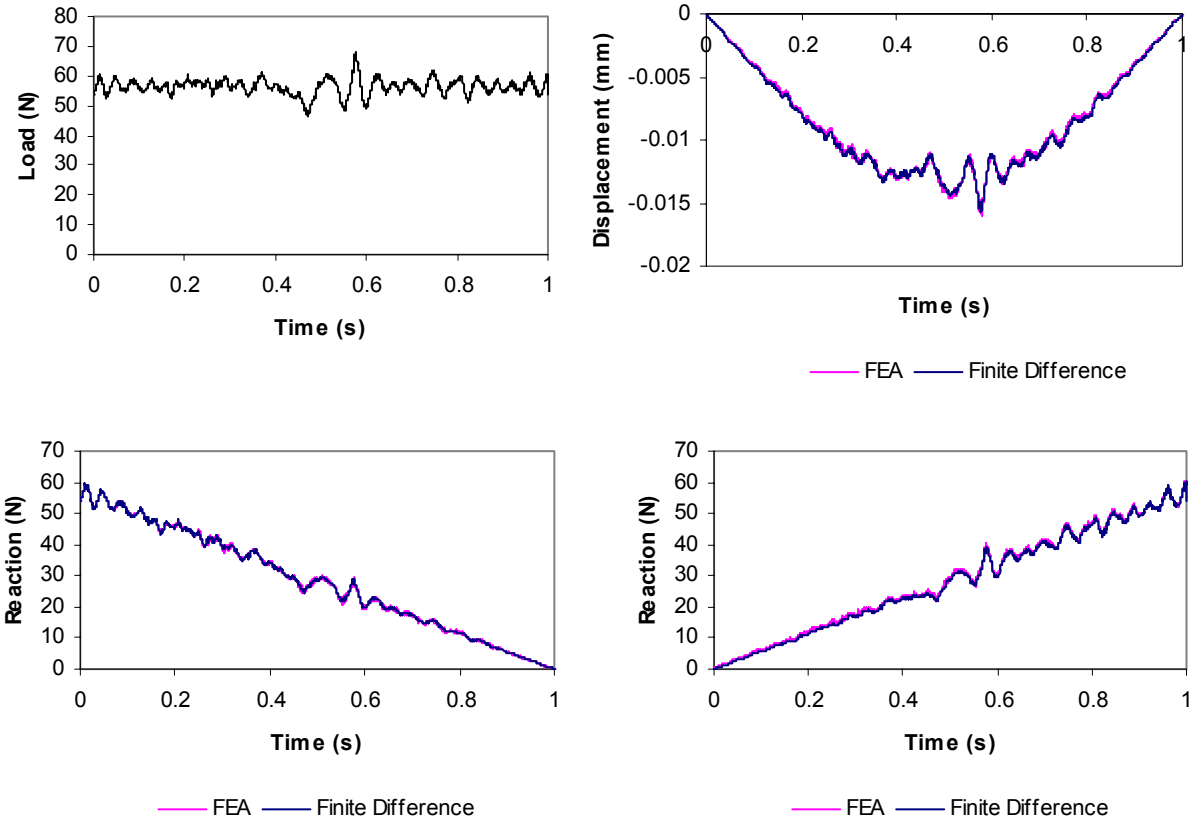

Figure 2.2.9. Case 4: random load, constant velocity.

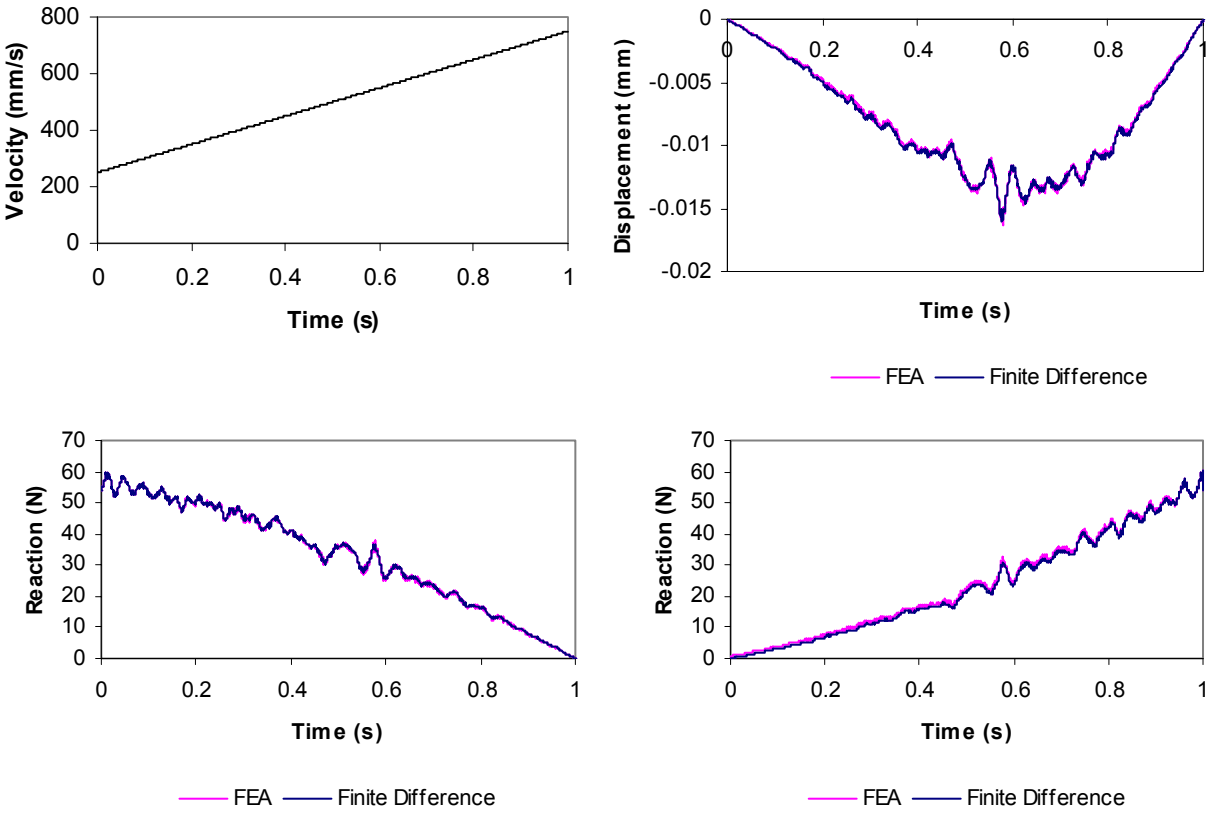

Figure 2.2.10. Case 5: random load, constant acceleration.

For all load cases chosen, the analytical response is, for all intents and purposes, identical to the finite element response using the method proposed in this thesis. The beam used in analysis is assumed simply supported for the purpose of a relatively easy comparison to analytical data. This need not be the case. The method should, in principal, also hold true for all beams, continuous or single span, regardless of the support conditions.

2.2.4 Application to Structural Assessment

The above method for applying moving loads may be easily and efficiently used for structural assessment in finite element software. This is particularly true for railway bridge assessment, which has been considered in this project, where spatially simple external loads are applied along rails. In this research, most modelling has been carried out using beam element models. These are described in some detail in Chapter 3; a rendered approach span beam model is shown in Figure 2.2.11.

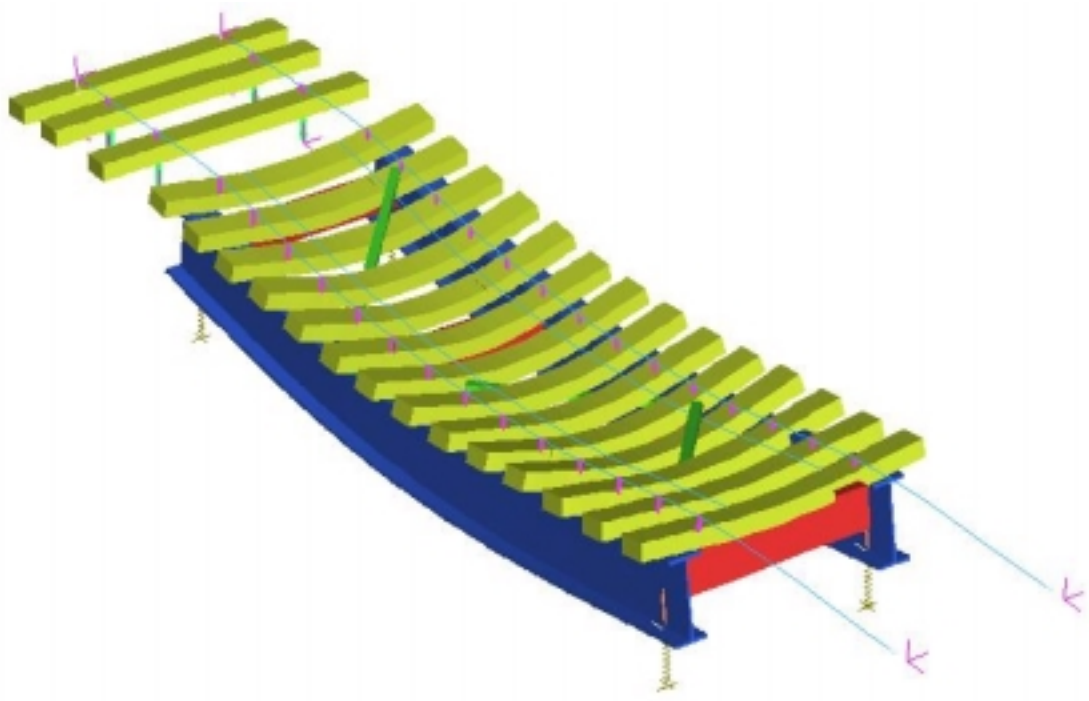

Figure 2.2.11. Rendered approach span beam model.

A simple program has been written which generates nodal force tables using equation (2.2.1) for all nodes, on the two rails, for any number of time dependent loads at any axle spacing. Load tables may be generated, therefore, for any rolling stock, or locomotive, and then imported directly into the finite element package for structural assessment.

In the case used in this research, just thirty-six load tables were required for full dynamic simulation of a locomotive and rolling stock loads. Loads have been modelled at an intermediate node between transoms to account for the effect of bending in the rail. (Note that 'transom' is the name given to a sleeper when on a bridge structure). However, if it were assumed that the rail transmits vertical forces only into transoms (i.e. the rail-transom connections possess no rotational or longitudinal stiffness), applied loads may be modelled at the nodes above the transom connections only. This would of course further simplify dynamic analysis. In this project rolling stock loads have been assumed to act vertically only. For fatigue and structural assessment on straight track this is considered an appropriate simplification. However, if longitudinal or lateral loads are known with confidence, they too may be modelled using the same method.

Perhaps the most useful output from the finite element model and the dynamic simulation, is the stress history during loading. Once a finite element model has been validated with field-testing, simulated loads may be applied to the model and stress histories generated at any point on the structure. These histories may then be treated using normal fatigue assessment methodology; data may be cycle counted, screened, and then filtered data applied to assessment codes. Alternatively the stress histories may be used to investigate the stress peaks and dynamic amplification, for different loading or structural conditions.

A full demonstration of the method, validated against field test results, is provided in Chapter 3.

As has been noted earlier in this section, beam element models have been predominately used for analysis in this research. Of course structural modelling using beam elements is not a prerequisite for using the method presented here. The complete structure could, in principal, be modelled using continuum elements. Since, in this research, the stresses in the rails are of little interest and, instead, of most interest is the supporting bridge structure, in theory the model may be simplified by modelling the rails using beam elements (Fig 2.2.12), allowing identical application of the method presented above. Modelling the entire bridge structure using continuum elements would be significantly more expensive, in terms of resource use, however.

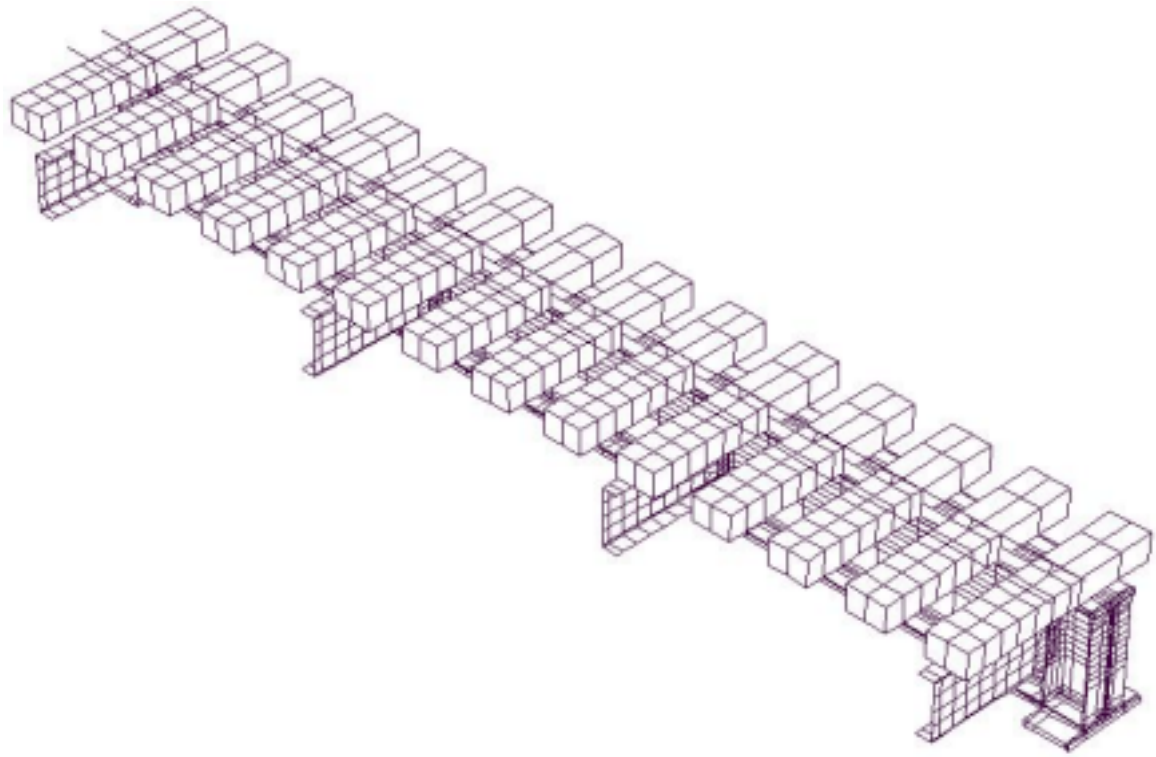

Figure 2.2.12. Symmetrical high detail finite element model of a steel girder bridge.

2.3 Dynamic Field-Testing Techniques for Model Validation and Load Identification

2.3.1 Introduction and Literature Review

Grundy [57], in his comparison of impact factors in Railway Bridge loading codes, notes that it is difficult, or impossible, to determine dynamic response of railway bridges using only code formulations. He concludes that field-testing is essential for confidence in dynamic structural analysis.

There are a number of techniques for field-testing of bridge structures. These include photogrammetry and acoustic emission techniques. Jackson [58] describes the use of photogrammetry to monitor Australian railway viaducts. Olaskez [59] presents a method based on the photogrammetry method called the computer-vision method. It works on the same principle as the photogrammetry method, that is, photographing a structure from several sites and plotting the three dimensional co-ordinates of selected points on the structure, viewing the system with an additional reference frame. Olaskez's method samples at a video rate of 25 frames per second, although may sample at up to 100Hz. With some similarities to photogrammetry techniques is the "Thermovision" method. Pasternak and Horvath [60] describe this technique, where emitted infrared radiation is measured by a sensitive infrared camera. The sum of principal stresses are derived from the temperature change in the material. For the separation of principal stresses, further calculations are necessary. The method, unlike strain gauging (according to the authors), is suitable where plastic deformations are present. Acoustic emissions and signal analysis techniques have been used to monitor railway bridge structures [61, 62]. Acoustic emissions are transient, elastic waves generated by the rapid release of energy from a material subjected to an external stress.

Most dynamic processes in metal release insufficient energy to be detected audibly, therefore, sensitive electronic equipment such as transducers, amplifiers and totalisers are required to detect these processes. Elliot and Quarrie [63] have developed methods for using acoustic emissions to monitor high strength steel wire in post-tensioned, cable-stayed and suspension bridges. While the authors note that global monitoring of steel bridges using the acoustic emissions techniques does not appear cost effective, and is therefore of little interest in this project, the methods of data recovery are very exciting. Elliot and Quarrie use internet delivery of data, to proprietary software at a home base, allowing one technician to monitor many structures from conceivably great distances. Triggers have been set up using acoustic sensors to begin data acquisition, begin video surveillance and send email alerts to an operator at the occurrence of a significant event.

Proof testing in order to gain a load rating for bridges is a method gaining popularity amongst some asset managers. Faber, Val and Stewart [64] use proof load testing to demonstrate the resistance of a bridge. They suggest diagnostic tests may be used to verify or refine analytical or predictive structural models; whilst proof load testing is used to assess the actual load carrying capacity of a bridge. Deterministic approaches, they assert, are not efficient for decisions taken under uncertainty, since such decisions tend to be conservative and based on 'prudent pessimism' or 'worst case' scenarios. By Faber, Val and Stewart's own admission the proof test method appears unsuitable for fatigue assessment or model validation. Barker [65] uses strain gauges in field-testing to test the response of a three span steel girder bridge. His research also deals with load rating, rather than fatigue testing or assessment for remaining life.

In many cases, finite element or mathematical modelling is used in conjunction with field-testing to assess bridge structures. Often field-tests are used to verify finite element or mathematical models, so that values of stress may be taken with relative confidence from models. Haritos and Abu-Aisheh [66] and Ventura [67] use modal analysis via field-testing, using accelerometers, to verify finite element models of road bridges. Casas [68] validates mathematical and wind tunnel models, using accelerometer measurement. Idriss, White, Woodward and Jauregui [69], on the other hand, have used finite element modelling for initial safety considerations and to determine where to place strain gauges only. Having placed strain gauges on the structure, all results are obtained from the gauges in both static and dynamic tests.

Mohammad and Mahmud [70] use strain gauges at bearings and strain gauges, dial gauges and linear deflection transducers at mid-span, in their study of Malaysian bridges built soon after World War II. The project they report on was one in which a simple and reliable methodology to determine load capacity was to be designed. All testing is static, with no indication that testing is used to verify finite element models or that fatigue assessment is carried out. The testing method approaches proof load testing in its methodology. The authors suggest that load testing is an expensive and complex operation and therefore should be considered a last resort.

A decision was made early in the present research that full-scale dynamic field-testing techniques were most appropriate for the methodology developed here. Dynamic techniques were expected to best integrate into the overall method and were expected to best measure the true dynamic response required for reliable railway bridge assessment. There are various methods of carrying out full scale dynamic testing of structures.

Salawu and Williams [71] provide an excellent review of these methods with some seventy three references. The types of testing are classified into groups based on the degree of control over the input excitation. Ambient excitation, i.e. where there is no control over the excitation input, is the most common method and assumes the response data alone may be used to estimate vibration parameters.

The two main purposes for the field-testing carried out in the present research are:

1. dynamic model validation and refinement, and
2. gathering of structural response data for load identification.

It is possible to achieve model validation and refinement using static field-testing techniques, although the task of model validation was made significantly easier due to the dynamic technique used in this research. Load identification, however, must be conducted using data acquired from dynamic testing, if the important effects of vehicle-structure interaction are to be reliably measured. From the very brief review above, the ability to use photogrammetry without site access makes it very useful for some applications. It would appear less suitable, however, for model verification or for dynamic data acquisition where a high sampling rate, say several kHz, is required. The Thermovision method also allows testing without site access, however, appears unsuitable for dynamic analysis of stresses in the elastic range. Proof testing, apart from the fact that it is generally static in nature, contradicts the very theory of fatigue failure - that a structure may fail at some stress well below the expected failure stress (or greatest resistance to load), where the load is applied many times.

While both strain gauge and accelerometer techniques are suitable for dynamic testing and model verification, strain gauges are simpler to use for load identification, according to the literature reviewed and discussed later in section 2.5, and have been used in this research. Having said that, however, low frequency accelerometers show great promise for load identification and model validation and are discussed further in the plans for further work discussed in Chapter 4.

2.3.2 Dynamic Field-Test Validation of a Finite Element Sensitivity Model

The procedure for the validation of the finite element models used in this research, via dynamic field-test results, is outlined below in general terms. This is further detailed in the demonstration of Chapter 3 and has been published in Sorrenson and West [72].

1. The first step is the strain gauge installation. Strain gauges are placed along the bottom flanges of the main girders. These are used initially for global model validation and later for load identification. Strain gauges are also set up on crucial components. These are used to test parts of the structure whose response may be difficult to capture from only global results.
2. Dynamic field-testing is carried out with a locomotive, or other rolling stock of known loads, at crawl speed. The vehicle travels at crawl speed, so dynamic impact effects from vehicle-structure interaction and from vehicle and structural defects, which are often greater at higher speeds, are minimised. The data recorded from strain gauges is not merely the free vibration response of the structure but is the forced response under normal load.
3. The same locomotive or rolling stock loads are then modelled in an analytical model (Figure 2.3.1). The analytical model has end conditions that may be tuned along with other structural properties, and moving distributed loads whose

distribution length may be tuned. The analytical model is presented in detail in Section 2.4. Effectively the process is one of matching response curves at a number of locations on the structure. The response curve from the analytical model, through a process of tuning various parameters, is matched to the measured bridge response (Figure 2.3.2). This analytical model is used as an efficient intermediate step for the tuning of the finite element sensitivity model. The process of tuning the analytical model guides how and where the finite element model is to be tuned.

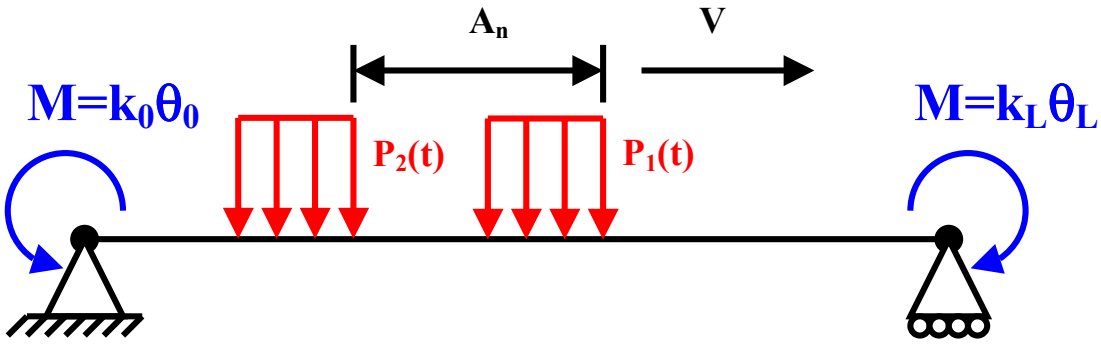

Figure 2.3.1. Analytical model, with tuneable structural properties, subjected to moving distributed loads of variable magnitude.

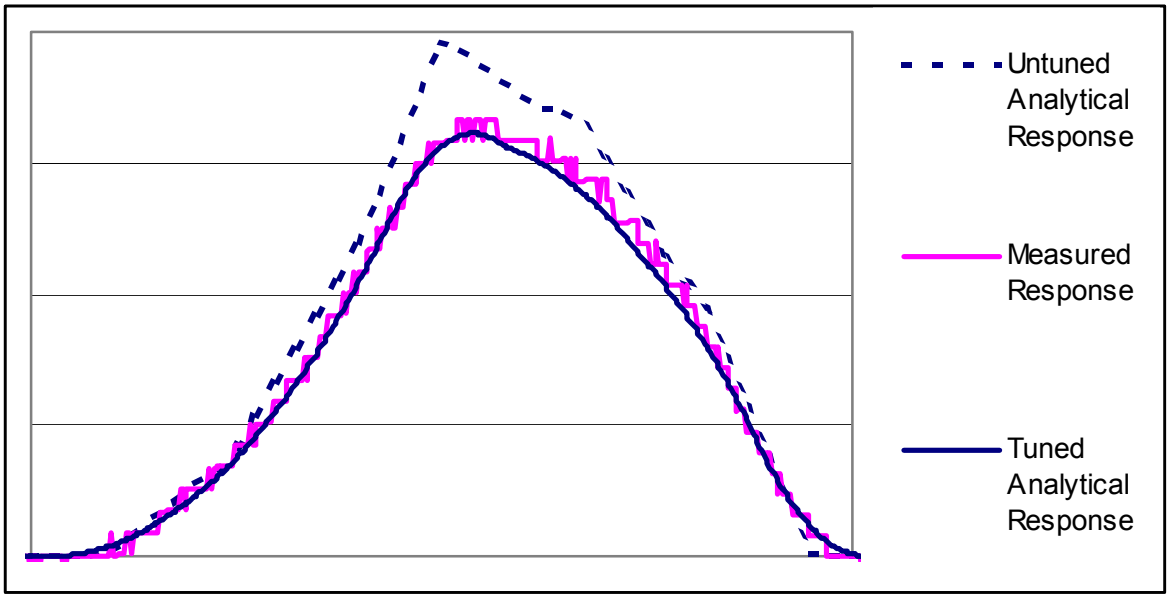

Figure 2.3.2. Example of the tuning of the analytical model response to the measured bridge response from field-testing.

4. The finite element sensitivity model is now tuned to the actual bridge, using dynamic test results and the analytical model intermediate step. The use of the analytical model may seem superfluous for the tuning of the finite element model and perhaps would be if the bridges always behaved in an ideal manner. This is unlikely and certainly was not the case in this research. The Mullet Creek Bridge behaved as a non-simply supported structure and varied greatly from preliminary models, where simply supported behaviour and point applied loads were assumed. Reconciling the finite element model response to the test response would have been very difficult, were it not for the analytical model intermediate step.

A comment made in the reviewed literature was that site testing is often an expensive and complex operation and therefore should be considered a last resort. Dynamic testing, as performed in this research, minimises possession times of the structure being tested, since traffic flow is uninterrupted during testing, and so the cost may be reduced. Dynamic testing procedures may also lend themselves to use of low frequency accelerometers, which would greatly reduce set-up time and therefore cost. This is discussed more in the proposals for the direction of future work at the end of this thesis (Chapter 4).

2.3.3 Load Identification from Dynamic Field-Test Results

Once the analytical and finite element models are tuned to measured results, dynamic field-testing is carried out for normal (ambient) traffic, using the same test set-up as was used for model validation, and the results recorded for use in load identification. The recorded structural response, along with an inverted structural matrix, or transfer

function, from the analytical model are used to identify moving loads of variable magnitude. This is discussed further in Section 2.5.

2.4 An Analytical Model for Euler-Bernoulli Beams with Rotational Stiffness at Supports Subjected to Multiple Moving Uniformly Distributed Loads

2.4.1 Introduction and Literature Review

Often in the analysis of bridges subjected to moving loads, moving loads are simplified to concentrated point loads and bridges to simply supported beams [15, 16, 23, 26, 37, 39, 42, 46, 47, 56]. For assessment of railway bridges these simplifications are not always appropriate. Railway bridges may behave according to non-simply supported end conditions (due to interactions at bearings and between the rails, transoms and structure) and loads as distributed rather than point loads (due to the distribution of loads through rails and transoms) [32, 34]. This is significant both for model validation from dynamic field testing (Section 2.3) and for load identification from structural response (Section 2.5). An analytical model is developed in this section for Euler-Bernoulli beams with rotational stiffness at supports subjected to multiple distributed loads.

A complete train is modelled as a single distributed load by Fryba [40] and others using the Heaviside unit function. A comparison of the method presented here is made with the Heaviside approximation at the end of this section.

2.4.2 An Analytical Model for Euler-Bernoulli Beams with Rotational Stiffness at Supports Subjected to a Single Moving Concentrated Load

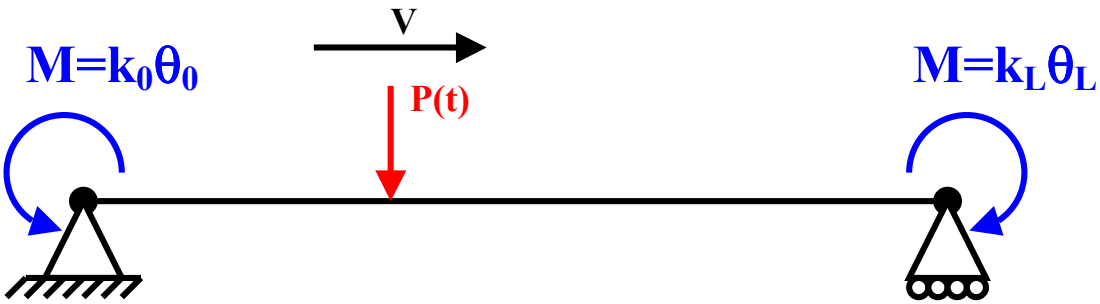

Figure 2.4.1. A single moving concentrated load on a Euler-Bernoulli beam, with rotational stiffness at supports.

The dynamic equations of motion for a beam may be written,

$$\overline{m}\frac{\partial^2 v(x,t)}{\partial t^2}+\overline{c}\frac{\partial v(x,t)}{\partial t}+EI\frac{\partial v^4(x,t)}{\partial x^4}=p(t) \qquad (2.4.1)$$

where $v(x,t)=$ bending deflection

Equation (2.4.1) is solved with $\overline{c}=0$ using separation of variables, and eigenvalues are determined. The solution leads to a series of uncoupled single degree of freedom ordinary differential equations, which are correct for an undamped system. A damping term is then added to each equation, and these approximate modal equations (Equation (2.4.2)) are then solved.

$$\ddot{\xi}_i+2\zeta_i\omega_i\dot{\xi}_i+\omega_i{}^2\xi=\frac{1}{m_i}p_i \qquad i=1,2,... \qquad (2.4.2)$$

Using modal superposition, the dynamic deflection $v(x,t)$ may be written,

$$v(x,t)=\sum_{i=1}^{\infty}\xi_i(t)\phi_i(x) \qquad (2.4.3)$$

The mode shape function for the beam in Figure 2.4.1 is derived in Appendix A and is

$$\phi(x)=\gamma\left\{\left(\cos\left(x\lambda^{\frac{1}{4}}\right)-\cosh\left(x\lambda^{\frac{1}{4}}\right)\right)-\alpha\left(\sin\left(x\lambda^{\frac{1}{4}}\right)+\beta.\sinh\left(x\lambda^{\frac{1}{4}}\right)\right)\right\} \tag{2.4.4}$$

where

$$\alpha=\frac{\cos\left(L\lambda^{\frac{1}{4}}\right)-\cosh\left(L\lambda^{\frac{1}{4}}\right)}{\sin\left(L\lambda^{\frac{1}{4}}\right)-\Delta\sinh\left(L\lambda^{\frac{1}{4}}\right)},$$

$$\beta=\frac{\cos\left(L\lambda^{\frac{1}{4}}\right)-\cosh\left(L\lambda^{\frac{1}{4}}\right)}{\sin\left(L\lambda^{\frac{1}{4}}\right)-\Delta\sinh\left(L\lambda^{\frac{1}{4}}\right)}\Delta,$$

γ = modal normalising constant,

$$\Delta=\left\{\frac{\frac{k_0}{2\lambda^{\frac{1}{4}}EI}\left[\cosh\left(L\lambda^{\frac{1}{4}}\right)-\cos\left(L\lambda^{\frac{1}{4}}\right)\right]+\sin\left(L\lambda^{\frac{1}{4}}\right)}{\frac{k_0}{2\lambda^{\frac{1}{4}}EI}\left[\cosh\left(L\lambda^{\frac{1}{4}}\right)-\cos\left(L\lambda^{\frac{1}{4}}\right)\right]+\sinh\left(L\lambda^{\frac{1}{4}}\right)}\right\},$$

and λ is found by iterating equation (2.4.5).

$$\begin{aligned}0=&\,4\lambda^{\frac{1}{2}}\sin\left(L\lambda^{\frac{1}{4}}\right)\sinh\left(L\lambda^{\frac{1}{4}}\right)+\left(2-2\cos\left(L\lambda^{\frac{1}{4}}\right)\cosh\left(L\lambda^{\frac{1}{4}}\right)\right)\frac{k_0.k_L}{(EI)^2}\\&+2\lambda^{\frac{1}{4}}\left(\cosh\left(L\lambda^{\frac{1}{4}}\right)\sin\left(L\lambda^{\frac{1}{4}}\right)-\sinh\left(L\lambda^{\frac{1}{4}}\right)\cos\left(L\lambda^{\frac{1}{4}}\right)\right)\frac{(k_0+k_L)}{EI}\end{aligned} \tag{2.4.5}$$

Assuming the beam in Figure 2.4.1 has constant cross section, the modal mass is,

$$m_i = \int_0^L \phi_i{}^2 \overline{m}(x)\,dx$$

$$= \overline{m}\int_0^L \left(\gamma\left\{\left(\cos\left(x\lambda^{\frac{1}{4}}\right) - \cosh\left(x\lambda^{\frac{1}{4}}\right)\right) - \alpha\left(\sin\left(x\lambda^{\frac{1}{4}}\right) + \beta\sinh\left(x\lambda^{\frac{1}{4}}\right)\right)\right\}\right)^2 dx$$

$$= \gamma^2\overline{m}\int_0^L \left(\cos^2\left(x\lambda^{\frac{1}{4}}\right) + \cosh^2\left(x\lambda^{\frac{1}{4}}\right) + \alpha^2\sin^2\left(x\lambda^{\frac{1}{4}}\right) + \beta^2\sinh^2\left(x\lambda^{\frac{1}{4}}\right)\right.$$
$$- 2\cos\left(x\lambda^{\frac{1}{4}}\right)\cosh\left(x\lambda^{\frac{1}{4}}\right) - 2\alpha\sin\left(x\lambda^{\frac{1}{4}}\right)\cos\left(x\lambda^{\frac{1}{4}}\right) + 2\beta\sinh\left(x\lambda^{\frac{1}{4}}\right)\cos\left(x\lambda^{\frac{1}{4}}\right)$$
$$\left. - 2\alpha\beta\sin\left(x\lambda^{\frac{1}{4}}\right)\sinh\left(x\lambda^{\frac{1}{4}}\right) - 2\beta\cosh\left(x\lambda^{\frac{1}{4}}\right)\sinh\left(x\lambda^{\frac{1}{4}}\right) + 2\alpha\sin\left(x\lambda^{\frac{1}{4}}\right)\cosh\left(x\lambda^{\frac{1}{4}}\right)\right) dx$$

$$= \gamma^2\overline{m}\left[\frac{x}{2}\left(2+\alpha^2-\beta^2\right) + \frac{1}{4\lambda^{\frac{1}{4}}}\left(1-\alpha^2\right)\sin\left(2.x.\lambda^{\frac{1}{4}}\right) + \frac{1}{4\lambda^{\frac{1}{4}}}\left(1+\beta^2\right)\sinh\left(2x\lambda^{\frac{1}{4}}\right)\right.$$
$$+ \frac{\alpha}{2\lambda^{\frac{1}{4}}}\cos\left(2x\lambda^{\frac{1}{4}}\right) - \frac{\beta}{2\lambda^{\frac{1}{4}}}\cosh\left(2x\lambda^{\frac{1}{4}}\right) - \frac{1}{2\lambda^{\frac{1}{4}}}e^{x\lambda^{\frac{1}{4}}}\cos\left(x\lambda^{\frac{1}{4}}\right)(1-\beta)(1+\alpha)$$
$$- \frac{1}{2\lambda^{\frac{1}{4}}}e^{x\lambda^{\frac{1}{4}}}\sin\left(x\lambda^{\frac{1}{4}}\right)(1-\beta)(1-\alpha) + \frac{1}{2\lambda^{\frac{1}{4}}}e^{-x\lambda^{\frac{1}{4}}}\cos\left(x.\lambda^{\frac{1}{4}}\right)(1+\beta)(1-\alpha)$$
$$\left. - \frac{1}{2\lambda^{\frac{1}{4}}}e^{-x\lambda^{\frac{1}{4}}}\sin\left(x\lambda^{\frac{1}{4}}\right)(1+\beta)(1+\alpha)\right]_0^L$$

$$m_i = \gamma^2\overline{m}\left[\frac{L}{2}\left(2+\alpha^2-\beta^2\right) + \frac{1}{4\lambda^{\frac{1}{4}}}\left(1-\alpha^2\right)\sin\left(2L\lambda^{\frac{1}{4}}\right) + \frac{1}{4\lambda^{\frac{1}{4}}}\left(1+\beta^2\right)\sinh\left(2L\lambda^{\frac{1}{4}}\right)\right.$$
$$+ \frac{\alpha}{2\lambda^{\frac{1}{4}}}\cos\left(2L\lambda^{\frac{1}{4}}\right) - \frac{\beta}{2\lambda^{\frac{1}{4}}}\cosh\left(2L\lambda^{\frac{1}{4}}\right) - \frac{1}{2\lambda^{\frac{1}{4}}}e^{L\lambda^{\frac{1}{4}}}\cos\left(L\lambda^{\frac{1}{4}}\right)(1-\beta)(1+\alpha)$$
$$- \frac{1}{2\lambda^{\frac{1}{4}}}e^{L\lambda^{\frac{1}{4}}}\sin\left(L\lambda^{\frac{1}{4}}\right)(1-\beta)(1-\alpha) + \frac{1}{2\lambda^{\frac{1}{4}}}e^{-L\lambda^{\frac{1}{4}}}\cos\left(L.\lambda^{\frac{1}{4}}\right)(1+\beta)(1-\alpha)$$
$$\left. - \frac{1}{2\lambda^{\frac{1}{4}}}e^{-L\lambda^{\frac{1}{4}}}\sin\left(L\lambda^{\frac{1}{4}}\right)(1+\beta)(1+\alpha) + \frac{1}{2\lambda^{\frac{1}{4}}}(\alpha-\beta)\right] \qquad (2.4.6)$$

For a moving concentrated load of uniform velocity V, utilising the Dirac-delta function, the ith modal force becomes

$$\begin{aligned} p_i &= \int_0^l f(x,t)\phi_i dx \\ &= \int_0^l -P\delta(x-Vt)\gamma\left(\cos\left(x\lambda^{\frac{1}{4}}\right)-\cosh\left(x\lambda^{\frac{1}{4}}\right)-\alpha\sin\left(x\lambda^{\frac{1}{4}}\right)+\beta\sinh\left(x\lambda^{\frac{1}{4}}\right)\right)dx \\ &= -P\gamma\left(\cos\left(Vt\lambda^{\frac{1}{4}}\right)-\cosh\left(Vt\lambda^{\frac{1}{4}}\right)-\alpha\sin\left(Vt\lambda^{\frac{1}{4}}\right)+\beta\sinh\left(Vt\lambda^{\frac{1}{4}}\right)\right) \\ &= -P\gamma\left(\cos(\Omega t)-\cosh(\Omega t)-\alpha\sin(\Omega t)+\beta\sinh(\Omega t)\right) \end{aligned} \quad (2.4.7)$$

where,

$$\Omega = \left(V\lambda^{\frac{1}{4}}\right)$$

After substitution, the uncoupled SDOF equations of motion may be written,

$$\{\ddot{\xi}_i\}+2\zeta_i\omega_i\{\dot{\xi}_i\}+\omega_i^{\,2}\{\xi_i\}=-\frac{P}{m_i}\gamma\left(\cos(\Omega t)-\cosh(\Omega t)-\alpha\sin(\Omega t)+\beta\sinh(\Omega t)\right) \quad (2.4.8)$$

This equation may be solved using the Duhamel or convolution integral. The Duhamel integral for equation (2.4.8) is written,

$$\xi_i = -\frac{P}{m_i\omega_{iD}}\int_0^t e^{-\zeta_i\omega_i(t-\tau)}\sin[\omega_{iD}(t-\tau)]\gamma\left(\cos(\Omega\tau)-\cosh(\Omega\tau)-\alpha\sin(\Omega\tau)+\beta\sinh(\Omega\tau)\right)d\tau \quad (2.4.9)$$

Upon solving, the particular solution becomes

$$\begin{aligned}\xi_{iP} = &-\frac{P\gamma\left[\left(\omega_i{}^2-\Omega^2\right)+\alpha(2\zeta_i\omega_i\Omega)\right]\left[\cos(\Omega t)-e^{-\zeta_i\omega_i t}\left(\left(\frac{\zeta_i\omega_i}{\omega_{iD}}\right)\sin(\omega_{iD}t)+\cos(\omega_{iD}t)\right)\right]}{m_i\left(\left(\omega_i{}^2-\Omega^2\right)^2+(2\zeta_i\omega_i\Omega)^2\right)}\\ &+\frac{P\gamma\left[\alpha\left(\omega_i{}^2-\Omega^2\right)-(2\zeta_i\omega_i\Omega)\right]\left[\sin(\Omega t)-e^{-\zeta_i\omega_i t}\left(\frac{\Omega}{\omega_{iD}}\right)\sin(\omega_{iD}t)\right]}{m_i\left(\left(\omega_i{}^2-\Omega^2\right)^2+(2\zeta_i\omega_i\Omega)^2\right)}\\ &+\frac{P\gamma\left[\left(\omega_i{}^2+\Omega^2\right)+\beta(2\zeta_i\omega_i\Omega)\right]\left[\cosh(\Omega t)-e^{-\zeta_i\omega_i t}\left(\left(\frac{\zeta_i\omega_i}{\omega_{iD}}\right)\sin(\omega_{iD}t)+\cos(\omega_{iD}t)\right)\right]}{m_i\left(\left(\omega_i{}^2+\Omega^2\right)^2-(2\zeta_i\omega_i\Omega)^2\right)}\\ &-\frac{P\gamma\left[\beta\left(\omega_i{}^2+\Omega^2\right)+(2\zeta_i\omega_i\Omega)\right]\left[\sinh(\Omega t)-e^{-\zeta_i\omega_i t}\left(\frac{\Omega}{\omega_{iD}}\right)\sin(\omega_{iD}t)\right]}{m_i\left(\left(\omega_i{}^2+\Omega^2\right)^2-(2\zeta_i\omega_i\Omega)^2\right)}\end{aligned} \tag{2.4.10}$$

which combined with the homogeneous solution gives a complete modal solution:

$$\xi_i = e^{-\zeta_i\omega_i t}\left(A_i\sin(\omega_{iD}t)+B_i\cos(\omega_{iD}t)\right)+\xi_{iP} \tag{2.4.11}$$

where

$$\omega_{iD} = \omega_i\sqrt{\left(1-\zeta_i{}^2\right)}$$

With initial conditions of zero displacement and velocity the equation for the modal displacement is

$$\xi_i = -\frac{P\gamma\left[\left(\omega_i{}^2-\Omega^2\right)+\alpha(2\zeta_i\omega_i\Omega)\right]\left[\cos(\Omega t)-e^{-\zeta_i\omega_i t}\left(\left(\frac{\zeta_i\omega_i}{\omega_{iD}}\right)\sin(\omega_{iD}t)+\cos(\omega_{iD}t)\right)\right]}{m_i\left(\left(\omega_i{}^2-\Omega^2\right)^2+(2\zeta_i\omega_i\Omega)^2\right)}$$
$$+\frac{P\gamma\left[\alpha\left(\omega_i{}^2-\Omega^2\right)-(2\zeta_i\omega_i\Omega)\right]\left[\sin(\Omega t)-e^{-\zeta_i\omega_i t}\left(\frac{\Omega}{\omega_{iD}}\right)\sin(\omega_{iD}t)\right]}{m_i\left(\left(\omega_i{}^2-\Omega^2\right)^2+(2\zeta_i\omega_i\Omega)^2\right)}$$
$$+\frac{P\gamma\left[\left(\omega_i{}^2+\Omega^2\right)+\beta(2\zeta_i\omega_i\Omega)\right]\left[\cosh(\Omega t)-e^{-\zeta_i\omega_i t}\left(\left(\frac{\zeta_i\omega_i}{\omega_{iD}}\right)\sin(\omega_{iD}t)+\cos(\omega_{iD}t)\right)\right]}{m_i\left(\left(\omega_i{}^2+\Omega^2\right)^2-(2\zeta_i\omega_i\Omega)^2\right)}$$
$$-\frac{P\gamma\left[\beta\left(\omega_i{}^2+\Omega^2\right)+(2\zeta_i\omega_i\Omega)\right]\left[\sinh(\Omega t)-e^{-\zeta_i\omega_i t}\left(\frac{\Omega}{\omega_{iD}}\right)\sin(\omega_{iD}t)\right]}{m_i\left(\left(\omega_i{}^2+\Omega^2\right)^2-(2\zeta_i\omega_i\Omega)^2\right)} \qquad (2.4.12)$$

2.4.3 An Analytical Model for Euler-Bernoulli Beams with Rotational Stiffness at Supports Subjected to Multiple Moving Concentrated Loads

The response of the system to a second load, a distance A behind the first (Figure 2.4.2), also travelling at a velocity V, may be found by replacing Vt with Vt-A in the Dirac-delta function.

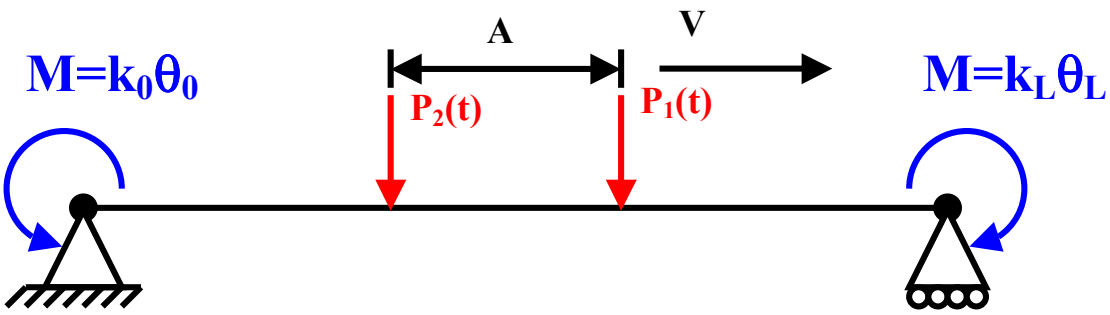

Figure 2.4.2. Two moving concentrated loads on a Euler-Bernoulli beam, with rotational stiffness at supports.

The modal force becomes

$$\begin{aligned} p_i &= \int_0^l f(x,t)\phi_i dx \\ &= \int_0^l -P\delta(x-(Vt-A))\gamma\left(\cos\left(x\lambda^{\frac{1}{4}}\right)-\cosh\left(x\lambda^{\frac{1}{4}}\right)-\alpha\sin\left(x\lambda^{\frac{1}{4}}\right)+\beta\sinh\left(x\lambda^{\frac{1}{4}}\right)\right)dx \\ &= -P\gamma\left(\cos\left((Vt-A)\lambda^{\frac{1}{4}}\right)-\cosh\left((Vt-A)\lambda^{\frac{1}{4}}\right)-\alpha\sin\left((Vt-A)\lambda^{\frac{1}{4}}\right)+\beta\sinh\left((Vt-A)\lambda^{\frac{1}{4}}\right)\right) \\ &= -P\gamma\left(C_1(A)\cos(\Omega t)-C_2(A)\cosh(\Omega t)-C_3(A)\sin(\Omega t)+C_4(A)\sinh(\Omega t)\right) \end{aligned} \quad (2.4.13)$$

where $C_1(A), C_2(A), C_3(A)$ and $C_4(A)$ are constant functions of the distance between the applied loads, A:

$$C_1(A) = \cos\left(A\lambda^{\frac{1}{4}}\right)+\alpha\sin\left(A\lambda^{\frac{1}{4}}\right)$$

$$C_2(A) = \cosh\left(A\lambda^{\frac{1}{4}}\right)+\beta\sinh\left(A\lambda^{\frac{1}{4}}\right)$$

$$C_3(A) = -\sin\left(A\lambda^{\frac{1}{4}}\right)+\alpha\cos\left(A\lambda^{\frac{1}{4}}\right)$$

$$C_4(A) = \sinh\left(A\lambda^{\frac{1}{4}}\right)+\beta\cosh\left(A\lambda^{\frac{1}{4}}\right)$$

$$\Omega = \left(V\lambda^{\frac{1}{4}}\right)$$

Again solving using the Duhamel Integral the particular solution becomes,

$$\begin{aligned} \xi_i = &-\frac{P\gamma\left[C_1(A)\left(\omega_i{}^2-\Omega^2\right)+C_3(A)(2\zeta_i\omega_i\Omega)\right]\left[\cos(\Omega t)-e^{-\zeta_i\omega_i t}\left(\left(\frac{\zeta_i\omega_i}{\omega_{iD}}\right)\sin(\omega_{iD}t)+\cos(\omega_{iD}t)\right)\right]}{m_i\left(\left(\omega_i{}^2-\Omega^2\right)^2+(2\zeta_i\omega_i\Omega)^2\right)} \\ &+\frac{P\gamma\left[C_3(A)\left(\omega_i{}^2-\Omega^2\right)-C_1(A)(2\zeta_i\omega_i\Omega)\right]\left[\sin(\Omega t)-e^{-\zeta_i\omega_i t}\left(\frac{\Omega}{\omega_{iD}}\right)\sin(\omega_{iD}t)\right]}{m_i\left(\left(\omega_i{}^2-\Omega^2\right)^2+(2\zeta_i\omega_i\Omega)^2\right)} \\ &+\frac{P\gamma\left[C_2(A)\left(\omega_i{}^2+\Omega^2\right)+C_4(A)(2\zeta_i\omega_i\Omega)\right]\left[\cosh(\Omega t)-e^{-\zeta_i\omega_i t}\left(\left(\frac{\zeta_i\omega_i}{\omega_{iD}}\right)\sin(\omega_{iD}t)+\cos(\omega_{iD}t)\right)\right]}{m_i\left(\left(\omega_i{}^2+\Omega^2\right)^2-(2\zeta_i\omega_i\Omega)^2\right)} \\ &-\frac{P\gamma\left[C_4(A)\left(\omega_i{}^2+\Omega^2\right)+C_2(A)(2\zeta_i\omega_i\Omega)\right]\left[\sinh(\Omega t)-e^{-\zeta_i\omega_i t}\left(\frac{\Omega}{\omega_{iD}}\right)\sin(\omega_{iD}t)\right]}{m_i\left(\left(\omega_i{}^2+\Omega^2\right)^2-(2\zeta_i\omega_i\Omega)^2\right)} \end{aligned} \quad (2.4.14)$$

Assuming small deflections, the total response may be solved by superposition of the response of each load.

Combining the homogeneous and particular solutions and solving for the initial conditions of the second load, $\xi\left(\frac{A}{V}\right)=0, \dot{\xi}\left(\frac{A}{V}\right)=0$, yields a complete modal displacement solution of,

$$\begin{aligned}\xi_i = &-\frac{P\gamma\left[C_1(A)\left(\omega_i{}^2-\Omega^2\right)+C_3(A)(2\zeta_i\omega_i\Omega)\right]\left[\cos\left(\Omega\left(t-\frac{A}{V}\right)\right)-e^{-\zeta_i\omega_i\left(t-\frac{A}{V}\right)}\left(\left(\frac{\zeta_i\omega_i}{\omega_{iD}}\right)\sin\left(\omega_{iD}\left(t-\frac{A}{V}\right)\right)+\cos\left(\omega_{iD}\left(t-\frac{A}{V}\right)\right)\right)\right]}{m_i\left(\left(\omega_i{}^2-\Omega^2\right)^2+(2\zeta_i\omega_i\Omega)^2\right)}\\ &+\frac{P\gamma\left[C_3(A)\left(\omega_i{}^2-\Omega^2\right)-C_1(A)(2\zeta_i\omega_i\Omega)\right]\left[\sin\left(\Omega\left(t-\frac{A}{V}\right)\right)-e^{-\zeta_i\omega_i\left(t-\frac{A}{V}\right)}\left(\frac{\Omega}{\omega_{iD}}\right)\sin\left(\omega_{iD}\left(t-\frac{A}{V}\right)\right)\right]}{m_i\left(\left(\omega_i{}^2-\Omega^2\right)^2+(2\zeta_i\omega_i\Omega)^2\right)}\\ &+\frac{P\gamma\left[C_2(A)\left(\omega_i{}^2+\Omega^2\right)+C_4(A)(2\zeta_i\omega_i\Omega)\right]\left[\cosh\left(\Omega\left(t-\frac{A}{V}\right)\right)-e^{-\zeta_i\omega_i\left(t-\frac{A}{V}\right)}\left(\left(\frac{\zeta_i\omega_i}{\omega_{iD}}\right)\sin\left(\omega_{iD}\left(t-\frac{A}{V}\right)\right)+\cos\left(\omega_{iD}\left(t-\frac{A}{V}\right)\right)\right)\right]}{m_i\left(\left(\omega_i{}^2+\Omega^2\right)^2-(2\zeta_i\omega_i\Omega)^2\right)}\\ &-\frac{P\gamma\left[C_4(A)\left(\omega_i{}^2+\Omega^2\right)+C_2(A)(2\zeta_i\omega_i\Omega)\right]\left[\sinh\left(\Omega\left(t-\frac{A}{V}\right)\right)-e^{-\zeta_i\omega_i\left(t-\frac{A}{V}\right)}\left(\frac{\Omega}{\omega_{iD}}\right)\sin\left(\omega_{iD}\left(t-\frac{A}{V}\right)\right)\right]}{m_i\left(\left(\omega_i{}^2+\Omega^2\right)^2-(2\zeta_i\omega_i\Omega)^2\right)}\end{aligned} \tag{2.4.15}$$

Note that the response for any point load may be written,

$$\begin{aligned}\xi_{in} = &-\frac{P_n\gamma\left[C_1(A)\left(\omega_i{}^2-\Omega^2\right)+C_3(A)(2\zeta_i\omega_i\Omega)\right]\left[\cos\left(\Omega\left(t-\frac{A_n}{V}\right)\right)-e^{-\zeta_i\omega_i\left(t-\frac{A_n}{V}\right)}\left(\left(\frac{\zeta_i.\omega_i}{\omega_{iD}}\right)\sin\left(\omega_{iD}\left(t-\frac{A_n}{V}\right)\right)+\cos\left(\omega_{iD}\left(t-\frac{A_n}{V}\right)\right)\right)\right]}{m_i\left(\left(\omega_i{}^2-\Omega^2\right)^2+(2\zeta_i\omega_i\Omega)^2\right)}\\ &+\frac{P_n\gamma\left[C_3(A)\left(\omega_i{}^2-\Omega^2\right)-C_1(A)(2\zeta_i\omega_i\Omega)\right]\left[\sin\left(\Omega\left(t-\frac{A_n}{V}\right)\right)-e^{-\zeta_i\omega_i\left(t-\frac{A_n}{V}\right)}\left(\frac{\Omega}{\omega_{iD}}\right)\sin\left(\omega_{iD}\left(t-\frac{A_n}{V}\right)\right)\right]}{m_i\left(\left(\omega_i{}^2-\Omega^2\right)^2+(2\zeta_i\omega_i\Omega)^2\right)}\\ &+\frac{P_n\gamma\left[C_2(A)\left(\omega_i{}^2+\Omega^2\right)+C_4(A)(2\zeta_i\omega_i\Omega)\right]\left[\cosh\left(\Omega.\left(t-\frac{A_n}{V}\right)\right)-e^{-\zeta_i\omega_i\left(t-\frac{A_n}{V}\right)}\left(\left(\frac{\zeta_i.\omega_i}{\omega_{iD}}\right)\sin\left(\omega_{iD}\left(t-\frac{A_n}{V}\right)\right)+\cos\left(\omega_{iD}\left(t-\frac{A_n}{V}\right)\right)\right)\right]}{m_i\left(\left(\omega_i{}^2+\Omega^2\right)^2-(2\zeta_i\omega_i\Omega)^2\right)}\\ &-\frac{P_n\gamma\left[C_4(A)\left(\omega_i{}^2+\Omega^2\right)+C_2(A)(2\zeta_i\omega_i\Omega)\right]\left[\sinh\left(\Omega\left(t-\frac{A_n}{V}\right)\right)-e^{-\zeta_i\omega_i\left(t-\frac{A_n}{V}\right)}\left(\frac{\Omega}{\omega_{iD}}\right)\sin\left(\omega_{iD}\left(t-\frac{A_n}{V}\right)\right)\right]}{m_i\left(\left(\omega_i{}^2+\Omega^2\right)^2-(2\zeta_i\omega_i\Omega)^2\right)}\end{aligned} \tag{2.4.16}$$

where

P_n = the magnitude of the nth load.

and

A_n = the distance between the nth and first loads.

For the first load, $A_n = 0$ and the equation for the response due to the single moving load is identical to the response derived in the previous section for a beam subjected to a single moving load, Equation (2.4.12).

The complete modal response for a number of loads may then be written,

$$\xi_{in} = \sum_{n=1} \left\{ - \frac{P_n \gamma \left[C_1(A)\left(\omega_i^2 - \Omega^2\right) + C_3(A)(2\zeta_i \omega_i \Omega) \right] \left[\cos\left(\Omega\left(t - \frac{A_n}{V} \right) \right) - e^{-\zeta_i \omega_i \left(t - \frac{A_n}{V} \right)} \left(\left(\frac{\zeta_i \omega_i}{\omega_{iD}} \right) \sin\left(\omega_{iD}\left(t - \frac{A_n}{V} \right) \right) + \cos\left(\omega_{iD}\left(t - \frac{A_n}{V} \right) \right) \right) \right]}{m_i \left(\left(\omega_i^2 - \Omega^2 \right)^2 + (2\zeta_i \omega_i \Omega)^2 \right)} \right.$$

$$+ \frac{P_n \gamma \left[C_3(A)\left(\omega_i^2 - \Omega^2\right) - C_1(A)(2\zeta_i \omega_i \Omega) \right] \left[\sin\left(\Omega\left(t - \frac{A_n}{V} \right) \right) - e^{-\zeta_i \omega_i \left(t - \frac{A_n}{V} \right)} \left(\frac{\Omega}{\omega_{iD}} \right) \sin\left(\omega_{iD}\left(t - \frac{A_n}{V} \right) \right) \right]}{m_i \left(\left(\omega_i^2 - \Omega^2 \right)^2 + (2\zeta_i \omega_i \Omega)^2 \right)}$$

$$+ \frac{P_n \gamma \left[C_2(A)\left(\omega_i^2 + \Omega^2\right) + C_4(A)(2\zeta_i \omega_i \Omega) \right] \left[\cosh\left(\Omega\left(t - \frac{A_n}{V} \right) \right) - e^{-\zeta_i \omega_i \left(t - \frac{A_n}{V} \right)} \left(\left(\frac{\zeta_i \omega_i}{\omega_{iD}} \right) \sin\left(\omega_{iD}\left(t - \frac{A_n}{V} \right) \right) + \cos\left(\omega_{iD}\left(t - \frac{A_n}{V} \right) \right) \right) \right]}{m_i \left(\left(\omega_i^2 + \Omega^2 \right)^2 - (2\zeta_i \omega_i \Omega)^2 \right)}$$

$$\left. - \frac{P_n \gamma \left[C_4(A)\left(\omega_i^2 + \Omega^2\right) + C_2(A)(2\zeta_i \omega_i \Omega) \right] \left[\sinh\left(\Omega\left(t - \frac{A_n}{V} \right) \right) - e^{-\zeta_i \omega_i \left(t - \frac{A_n}{V} \right)} \left(\frac{\Omega}{\omega_{iD}} \right) \sin\left(\omega_{iD}\left(t - \frac{A_n}{V} \right) \right) \right]}{m_i \left(\left(\omega_i^2 + \Omega^2 \right)^2 - (2\zeta_i \omega_i \Omega)^2 \right)} \right\} \tag{2.4.17}$$

The complete response of the system is found by summing the response of each load for each mode.

$$v_{total}(x,t) = v_1(x,t) + v_2(x,t) \tag{2.4.18}$$

where

$$v(x,t) = \sum_{i=1}^{\infty} \xi_{in}(t) \phi_i(x)$$

2.4.4 An Analytical Model for Euler-Bernoulli Beams with Rotational Stiffness at Supports Subjected to a Single Moving Uniformly Distributed Load

For the response of a single uniformly distributed load (Figure 2.4.3), the distributed load is approximated as a series of concentrated loads, equally spaced over the load distribution. The magnitude of each load may be approximated as the total load divided by the number of divisions.

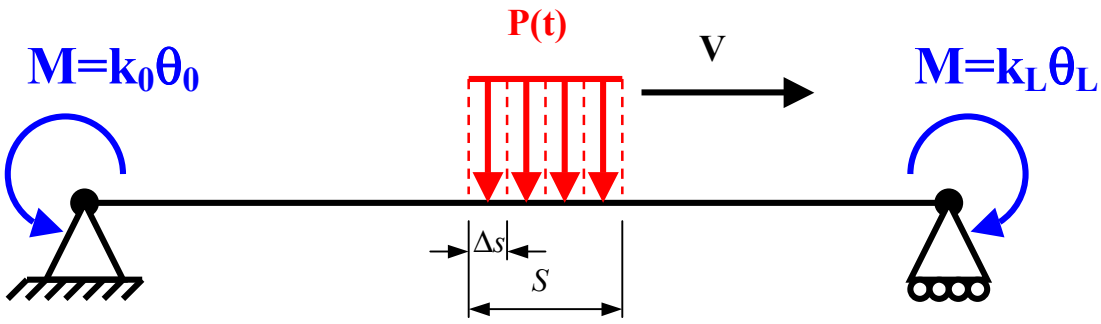

Figure 2.4.3. A single moving uniformly distributed load on a Euler-Bernoulli beam, with rotational stiffness at supports.

The number of divisions may be written,

$$n = \frac{S}{\Delta s} \tag{2.4.19}$$

while the magnitude of each load is

$$\begin{aligned} P_n &= \frac{P}{n} \\ &= \frac{P\Delta s}{S} \end{aligned} \tag{2.4.20}$$

In a manner similar to modelling multiple moving concentrated loads, replacing the distance from the first load, A_n, with s, which varies along the length of the distributed load from 0 to S, and the magnitude of the load P_n with $\frac{P\Delta s}{S}$, the modal force may be written

$$
\begin{aligned}
p_i &= \int_0^l f(x,t)\phi_i .dx \\
&= \int_0^l -\frac{P\Delta s}{S}\delta(x-(Vt-s))\gamma\left(\cos\left(x\lambda^{\frac{1}{4}}\right)-\cosh\left(x\lambda^{\frac{1}{4}}\right)-\alpha\sin\left(x\lambda^{\frac{1}{4}}\right)+\beta\sinh\left(x\lambda^{\frac{1}{4}}\right)\right)dx \\
&= -\frac{P\Delta s}{S}\gamma\left(C_1(s)\cos(\Omega t)-C_2(s)\cosh(\Omega t)-C_3(s)\sin(\Omega t)+C_4(s)\sinh(\Omega t)\right)
\end{aligned}
\tag{2.4.21}
$$

Where $C_1(s), C_2(s), C_3(s)$ and $C_4(s)$ are functions of the distance along the distributed load, s:

$$C_1(s) = \cos\left(s\lambda^{\frac{1}{4}}\right)+\alpha\sin\left(s\lambda^{\frac{1}{4}}\right)$$

$$C_2(s) = \cosh\left(s\lambda^{\frac{1}{4}}\right)+\beta\sinh\left(s\lambda^{\frac{1}{4}}\right)$$

$$C_3(s) = -\sin\left(s\lambda^{\frac{1}{4}}\right)+\alpha\cos\left(s\lambda^{\frac{1}{4}}\right)$$

$$C_4(s) = \sinh\left(s\lambda^{\frac{1}{4}}\right)+\beta\cosh\left(s\lambda^{\frac{1}{4}}\right)$$

$$\Omega = \left(V\lambda^{\frac{1}{4}}\right)$$

Solving again using the Duhamel integral the particular solution becomes,

$$
\begin{aligned}
\xi_{iP} = &-\frac{P\Delta s\gamma\left[C_1(s)\left(\omega_i{}^2-\Omega^2\right)+C_3(s)(2\zeta_i\omega_i\Omega)\right]\left[\cos(\Omega t)-e^{-\zeta_i\omega_i t}\left(\left(\frac{\zeta_i\omega_i}{\omega_{iD}}\right)\sin(\omega_{iD}t)+\cos(\omega_{iD}t)\right)\right]}{Sm_i\left(\left(\omega_i{}^2-\Omega^2\right)^2+(2\zeta_i\omega_i\Omega)^2\right)} \\
&+\frac{P\Delta s\gamma\left[C_3(s)\left(\omega_i{}^2-\Omega^2\right)-C_1(s)(2\zeta_i\omega_i\Omega)\right]\left[\sin(\Omega t)-e^{-\zeta_i\omega_i t}\left(\frac{\Omega}{\omega_{iD}}\right)\sin(\omega_{iD}t)\right]}{Sm_i\left(\left(\omega_i{}^2-\Omega^2\right)^2+(2\zeta_i\omega_i\Omega)^2\right)} \\
&+\frac{P\Delta s\gamma\left[C_2(s)\left(\omega_i{}^2+\Omega^2\right)+C_4(s)(2\zeta_i\omega_i\Omega)\right]\left[\cosh(\Omega t)-e^{-\zeta_i\omega_i t}\left(\left(\frac{\zeta_i\omega_i}{\omega_{iD}}\right)\sin(\omega_{iD}t)+\cos(\omega_{iD}t)\right)\right]}{Sm_i\left(\left(\omega_i{}^2+\Omega^2\right)^2-(2\zeta_i\omega_i\Omega)^2\right)} \\
&-\frac{P\Delta s\gamma\left[C_4(s)\left(\omega_i{}^2+\Omega^2\right)+C_2(s)(2\zeta_i\omega_i\Omega)\right]\left[\sinh(\Omega t)-e^{-\zeta_i\omega_i t}\left(\frac{\Omega}{\omega_{iD}}\right)\sin(\omega_{iD}t)\right]}{Sm_i\left(\left(\omega_i{}^2+\Omega^2\right)^2-(2\zeta_i\omega_i\Omega)^2\right)}
\end{aligned}
\tag{2.4.22}
$$

Approximating the total response of a distributed load as the sum of a series of concentrated loads, the particular solution for a distributed load becomes,

$$\xi_{iP} = \sum_{m=1}^{n=\frac{S}{\Delta s}} \left\{ - \frac{P\Delta s\gamma\left[C_1(s)\left(\omega_i{}^2 - \Omega^2\right) + C_3(s)(2\zeta_i\omega_i\Omega)\right]\left[\cos(\Omega t) - e^{-\zeta_i\omega_i t}\left(\left(\frac{\zeta_i\omega_i}{\omega_{iD}}\right)\sin(\omega_{iD}t) + \cos(\omega_{iD}t)\right)\right]}{Sm_i\left(\left(\omega_i{}^2 - \Omega^2\right)^2 + (2\zeta_i\omega_i\Omega)^2\right)} \right.$$

$$+ \frac{P\Delta s\gamma\left[C_3(s)\left(\omega_i{}^2 - \Omega^2\right) - C_1(s)(2\zeta_i\omega_i\Omega)\right]\left[\sin(\Omega t) - e^{-\zeta_i\omega_i t}\left(\frac{\Omega}{\omega_{iD}}\right)\sin(\omega_{iD}t)\right]}{Sm_i\left(\left(\omega_i{}^2 - \Omega^2\right)^2 + (2\zeta_i\omega_i\Omega)^2\right)}$$

$$+ \frac{P\Delta s\gamma\left[C_2(s)\left(\omega_i{}^2 + \Omega^2\right) + C_4(s)(2\zeta_i\omega_i\Omega)\right]\left[\cosh(\Omega t) - e^{-\zeta_i\omega_i t}\left(\left(\frac{\zeta_i\omega_i}{\omega_{iD}}\right)\sin(\omega_{iD}t) + \cos(\omega_{iD}t)\right)\right]}{Sm_i\left(\left(\omega_i{}^2 + \Omega^2\right)^2 - (2\zeta_i\omega_i\Omega)^2\right)}$$

$$\left. - \frac{P\Delta s\gamma\left[C_4(s)\left(\omega_i{}^2 + \Omega^2\right) + C_2(s)(2\zeta_i\omega_i\Omega)\right]\left[\sinh(\Omega t) - e^{-\zeta_i\omega_i t}\left(\frac{\Omega}{\omega_{iD}}\right)\sin(\omega_{iD}t)\right]}{Sm_i\left(\left(\omega_i{}^2 + \Omega^2\right)^2 - (2\zeta_i\omega_i\Omega)^2\right)} \right\} \quad (2.4.23)$$

Assuming $\Delta s \to 0$, the summation, Σ, may be replaced with $\int$ and Δs with ds.

$$\xi_{iP} = \int \left\{ - \frac{P\gamma\left[C_1(s)\left(\omega_i{}^2 - \Omega^2\right) + C_3(s)(2\zeta_i\omega_i\Omega)\right]\left[\cos(\Omega t) - e^{-\zeta_i\omega_i t}\left(\left(\frac{\zeta_i\omega_i}{\omega_{iD}}\right)\sin(\omega_{iD}t) + \cos(\omega_{iD}t)\right)\right]}{Sm_i\left(\left(\omega_i{}^2 - \Omega^2\right)^2 + (2\zeta_i\omega_i\Omega)^2\right)} \right.$$

$$+ \frac{P\gamma\left[C_3(s)\left(\omega_i{}^2 - \Omega^2\right) - C_1(s)(2\zeta_i\omega_i\Omega)\right]\left[\sin(\Omega t) - e^{-\zeta_i\omega_i t}\left(\frac{\Omega}{\omega_{iD}}\right)\sin(\omega_{iD}t)\right]}{Sm_i\left(\left(\omega_i{}^2 - \Omega^2\right)^2 + (2\zeta_i\omega_i\Omega)^2\right)}$$

$$+ \frac{P\gamma\left[C_2(s)\left(\omega_i{}^2 + \Omega^2\right) + C_4(s)(2\zeta_i\omega_i\Omega)\right]\left[\cosh(\Omega t) - e^{-\zeta_i\omega_i t}\left(\left(\frac{\zeta_i\omega_i}{\omega_{iD}}\right)\sin(\omega_{iD}t) + \cos(\omega_{iD}t)\right)\right]}{Sm_i\left(\left(\omega_i{}^2 + \Omega^2\right)^2 - (2\zeta_i\omega_i\Omega)^2\right)}$$

$$\left. - \frac{P\gamma\left[C_4(s)\left(\omega_i{}^2 + \Omega^2\right) + C_2(s)(2\zeta_i\omega_i\Omega)\right]\left[\sinh(\Omega t) - e^{-\zeta_i\omega_i t}\left(\frac{\Omega}{\omega_{iD}}\right)\sin(\omega_{iD}t)\right]}{Sm_i\left(\left(\omega_i{}^2 + \Omega^2\right)^2 - (2\zeta_i\omega_i\Omega)^2\right)} \right\} ds \quad (2.4.24)$$

Note that upon integration of Equation (2.4.24), along the length of the distributed load, the only terms affected by the integration (i.e. containing the integrated term s) are the coefficients $C_1(s), C_2(s), C(s)_3$ & $C_4(s)$.

For the total response Equation (2.4.24) is combined with homogeneous equations with appropriate initial conditions.

For the response of Euler-Bernoulli Beams with rotational stiffness at supports, subjected to a single moving uniformly distributed load, the solution is treated in three stages. First for the period where the distributed load enters the span, second for the period where the distributed load is fully on the span and finally for the period where the distributed load leaves the span.

The load enters the span during the period $0 \le t \le \frac{S}{V}$. Assuming constant velocity, the length of the distributed load on the span during that time interval varies from 0 to the total length S, according to $s = Vt$. See Figure 2.4.4.

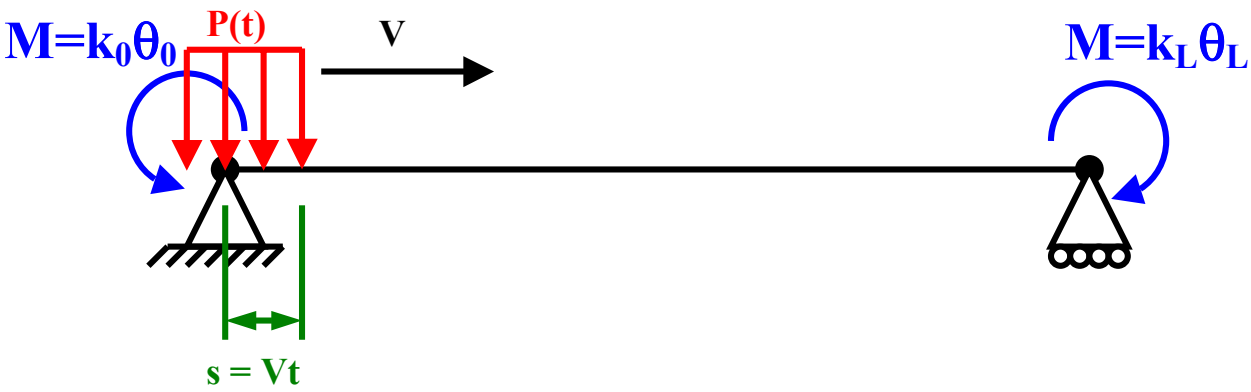

Figure 2.4.4. A single moving uniformly distributed load entering a Euler-Bernoulli beam, with rotational stiffness at supports.

The integration for the particular solution, Equation (2.4.24), is carried out from 0 to Vt. The particular solution becomes

$$\xi_{iP} = -\frac{P\gamma\left[C_1(t)\left(\omega_i{}^2-\Omega^2\right)+C_3(t)(2\zeta_i\omega_i\Omega)\right]\left[\cos(\Omega t)-e^{-\zeta_i\omega_i t}\left(\left(\frac{\zeta_i\omega_i}{\omega_{iD}}\right)\sin(\omega_{iD}t)+\cos(\omega_{iD}t)\right)\right]}{m_i\left(\left(\omega_i{}^2-\Omega^2\right)^2+(2\zeta_i\omega_i\Omega)^2\right)}$$
$$+\frac{P\gamma\left[C_3(t)\left(\omega_i{}^2-\Omega^2\right)-C_1(t)(2\zeta_i\omega_i\Omega)\right]\left[\sin(\Omega t)-e^{-\zeta_i\omega_i t}\left(\frac{\Omega}{\omega_{iD}}\right)\sin(\omega_{iD}t)\right]}{m_i\left(\left(\omega_i{}^2-\Omega^2\right)^2+(2\zeta_i\omega_i\Omega)^2\right)}$$
$$+\frac{P\gamma\left[C_2(t)\left(\omega_i{}^2+\Omega^2\right)+C_4(t)(2\zeta_i\omega_i\Omega)\right]\left[\cosh(\Omega t)-e^{-\zeta_i\omega_i t}\left(\left(\frac{\zeta_i\omega_i}{\omega_{iD}}\right)\sin(\omega_{iD}t)+\cos(\omega_{iD}t)\right)\right]}{m_i\left(\left(\omega_i{}^2+\Omega^2\right)^2-(2\zeta_i\omega_i\Omega)^2\right)}$$
$$-\frac{P\gamma\left[C_4(t)\left(\omega_i{}^2+\Omega^2\right)+C_2(t)(2\zeta_i\omega_i\Omega)\right]\left[\sinh(\Omega t)-e^{-\zeta_i\omega_i t}\left(\frac{\Omega}{\omega_{iD}}\right)\sin(\omega_{iD}t)\right]}{m_i\left(\left(\omega_i{}^2+\Omega^2\right)^2-(2\zeta_i\omega_i\Omega)^2\right)} \qquad (2.4.25)$$

where $C_1(t), C_2(t), C_3(t)$ and $C_4(t)$ are functions of time, since $s = Vt$:

$$C_1(t) = \frac{1}{S\lambda^{\frac{1}{4}}}\left(\sin(\Omega t)-\alpha\cos(\Omega t)+\alpha\right)$$
$$C_2(t) = \frac{1}{S\lambda^{\frac{1}{4}}}\left(\sinh(\Omega t)+\beta\cosh(\Omega t)-\beta\right)$$
$$C_3(t) = \frac{1}{S\lambda^{\frac{1}{4}}}\left(\alpha\sin(\Omega t)+\cos(\Omega t)-1\right)$$
$$C_4(t) = \frac{1}{S\lambda^{\frac{1}{4}}}\left(\beta\sinh(\Omega t)+\cosh(\Omega t)-1\right)$$

Upon combination with the homogeneous equation and initial conditions of zero displacement and velocity the modal displacement equation remains unchanged and is

$$\xi_i = -\frac{P\gamma\left[C_1(t)\left(\omega_i{}^2-\Omega^2\right)+C_3(t)(2\zeta_i\omega_i\Omega)\right]\left[\cos(\Omega t)-e^{-\zeta_i\omega_i t}\left(\left(\frac{\zeta_i\omega_i}{\omega_{iD}}\right)\sin(\omega_{iD}t)+\cos(\omega_{iD}t)\right)\right]}{m_i\left(\left(\omega_i{}^2-\Omega^2\right)^2+(2\zeta_i\omega_i\Omega)^2\right)}$$
$$+\frac{P\gamma\left[C_3(t)\left(\omega_i{}^2-\Omega^2\right)-C_1(t)(2\zeta_i\omega_i\Omega)\right]\left[\sin(\Omega t)-e^{-\zeta_i\omega_i t}\left(\frac{\Omega}{\omega_{iD}}\right)\sin(\omega_{iD}t)\right]}{m_i\left(\left(\omega_i{}^2-\Omega^2\right)^2+(2\zeta_i\omega_i\Omega)^2\right)}$$
$$+\frac{P\gamma\left[C_2(t)\left(\omega_i{}^2+\Omega^2\right)+C_4(t)(2\zeta_i\omega_i\Omega)\right]\left[\cosh(\Omega t)-e^{-\zeta_i\omega_i t}\left(\left(\frac{\zeta_i\omega_i}{\omega_{iD}}\right)\sin(\omega_{iD}t)+\cos(\omega_{iD}t)\right)\right]}{m_i\left(\left(\omega_i{}^2+\Omega^2\right)^2-(2\zeta_i\omega_i\Omega)^2\right)}$$
$$-\frac{P\gamma\left[C_4(t)\left(\omega_i{}^2+\Omega^2\right)+C_2(t)(2\zeta_i\omega_i\Omega)\right]\left[\sinh(\Omega t)-e^{-\zeta_i\omega_i t}\left(\frac{\Omega}{\omega_{iD}}\right)\sin(\omega_{iD}t)\right]}{m_i\left(\left(\omega_i{}^2+\Omega^2\right)^2-(2\zeta_i\omega_i\Omega)^2\right)} \qquad (2.4.26)$$

The solution for the modal velocity is

$$
\begin{aligned}
\dot{\xi}_i = & -P\gamma \Big/ \left[m_i \left(\left(\omega_i{}^2 - \Omega^2 \right)^2 + (2\zeta_i \omega_i \Omega)^2 \right) \right] \\
& \bullet \Big\{ \left[C_1(t)\left(\omega_i{}^2 - \Omega^2 \right) + C_3(t)(2\zeta_i \omega_i \Omega) \right] \\
& \bullet \left[-\Omega \sin(\Omega t) + \zeta_i \omega_i e^{-\zeta_i \omega_i t} \left(\left(\frac{\zeta_i \omega_i}{\omega_{iD}} \right) \sin(\omega_{iD} t) + \cos(\omega_{iD} t) \right) - \omega_{iD} e^{-\zeta_i \omega_i t} \left(\left(\frac{\zeta_i \omega_i}{\omega_{iD}} \right) \cos(\omega_{iD} t) - \sin(\omega_{iD} t) \right) \right] \\
& + \left[\dot{C}_1(t)\left(\omega_i{}^2 - \Omega^2 \right) + \dot{C}_3(t)(2\zeta_i \omega_i \Omega) \right] \times \left[\cos(\Omega t) - e^{-\zeta_i \omega_i t} \left(\left(\frac{\zeta_i \omega_i}{\omega_{iD}} \right) \sin(\omega_{iD} t) + \cos(\omega_{iD} t) \right) \right] \\
& - \left[C_3(t)\left(\omega_i{}^2 - \Omega^2 \right) - C_1(t)(2\zeta_i \omega_i \Omega) \right] \times \left[\Omega \cos(\Omega t) + e^{-\zeta_i \omega_i t} \left(\frac{\zeta_i \omega_i \Omega}{\omega_{iD}} \right) \sin(\omega_{iD} t) - e^{-\zeta_i \omega_i t} \Omega \cos(\omega_{iD} t) \right] \\
& - \left[\dot{C}_3(t)\left(\omega_i{}^2 - \Omega^2 \right) - \dot{C}_1(t)(2\zeta_i \omega_i \Omega) \right] \times \left[\sin(\Omega t) - e^{-\zeta_i \omega_i t} \left(\frac{\Omega}{\omega_{iD}} \right) \sin(\omega_{iD} t) \right] \Big\} \\
& + P\gamma \Big/ \left[m_i \left(\left(\omega_i{}^2 + \Omega^2 \right)^2 - (2\zeta_i \omega_i \Omega)^2 \right) \right] \\
& \bullet \Big\{ \left[C_2(t)\left(\omega_i{}^2 + \Omega^2 \right) + C_4(t)(2\zeta_i \omega_i \Omega) \right] \\
& \bullet \left[\Omega \sinh(\Omega t) + \zeta_i \omega_i e^{-\zeta_i \omega_i t} \left(\left(\frac{\zeta_i \omega_i}{\omega_{iD}} \right) \sin(\omega_{iD} t) + \cos(\omega_{iD} t) \right) - \omega_{iD} e^{-\zeta_i \omega_i t} \left(\left(\frac{\zeta_i \omega_i}{\omega_{iD}} \right) \cos(\omega_{iD} t) - \sin(\omega_{iD} t) \right) \right] \\
& + \left[\dot{C}_2(t)\left(\omega_i{}^2 + \Omega^2 \right) + \dot{C}_4(t)(2\zeta_i \omega_i \Omega) \right] \times \left[\cosh(\Omega t) - e^{-\zeta_i \omega_i t} \left(\left(\frac{\zeta_i \omega_i}{\omega_{iD}} \right) \sin(\omega_{iD} t) + \cos(\omega_{iD} t) \right) \right] \\
& - \left[C_2(t)\left(\omega_i{}^2 + \Omega^2 \right) + C_4(t)(2\zeta_i \omega_i \Omega) \right] \times \left[\Omega \cosh(\Omega t) + e^{-\zeta_i \omega_i t} \left(\frac{\zeta_i \omega_i \Omega}{\omega_{iD}} \right) \sin(\omega_{iD} t) - e^{-\zeta_i \omega_i t} \Omega \cos(\omega_{iD} t) \right] \\
& - \left[\dot{C}_2(t)\left(\omega_i{}^2 + \Omega^2 \right) + \dot{C}_4(t)(2\zeta_i \omega_i \Omega) \right] \times \left[\sinh(\Omega t) - e^{-\zeta_i \omega_i t} \left(\frac{\Omega}{\omega_{iD}} \right) \sin(\omega_{iD} t) \right] \Big\}
\end{aligned}
\qquad (2.4.27)
$$

Where $C_1(t), C_2(t), C_3(t)$ and $C_4(t)$ are functions of time:

$$C_1(t) = \frac{1}{S\lambda^{\frac{1}{4}}}\left(\sin(\Omega t) - \alpha\cos(\Omega t) + \alpha\right)$$

$$C_2(t) = \frac{1}{S\lambda^{\frac{1}{4}}}\left(\sinh(\Omega.t) + \beta\cosh(\Omega t) - \beta\right)$$

$$C_3(t) = \frac{1}{S\lambda^{\frac{1}{4}}}\left(\alpha\sin(\Omega t) + \cos(\Omega t) - 1\right)$$

$$C_4(t) = \frac{1}{S\lambda^{\frac{1}{4}}}\left(\beta\sinh(\Omega t) + \cosh(\Omega t) - 1\right)$$

$$\dot{C}_1(t) = \frac{\Omega}{S\lambda^{\frac{1}{4}}}\left(\cos(\Omega t) + \alpha\sin(\Omega t)\right)$$

$$\dot{C}_2(t) = \frac{\Omega}{S\lambda^{\frac{1}{4}}}\left(\cosh(\Omega t) + \beta\sinh(\Omega t)\right)$$

$$\dot{C}_3(t) = \frac{\Omega}{S\lambda^{\frac{1}{4}}}\left(\alpha\cos(\Omega t) - \sin(\Omega t)\right)$$

$$\dot{C}_4(t) = \frac{\Omega}{S\lambda^{\frac{1}{4}}}\left(\beta\cosh(\Omega t) + \sinh(\Omega t)\right)$$

While the distributed load is completely on the span, i.e. during the period $\frac{S}{V} \le t \le \frac{L}{V}$, the length of the distributed load remains constant and is equal to the total distributed load length, S. See Figure 2.4.5.

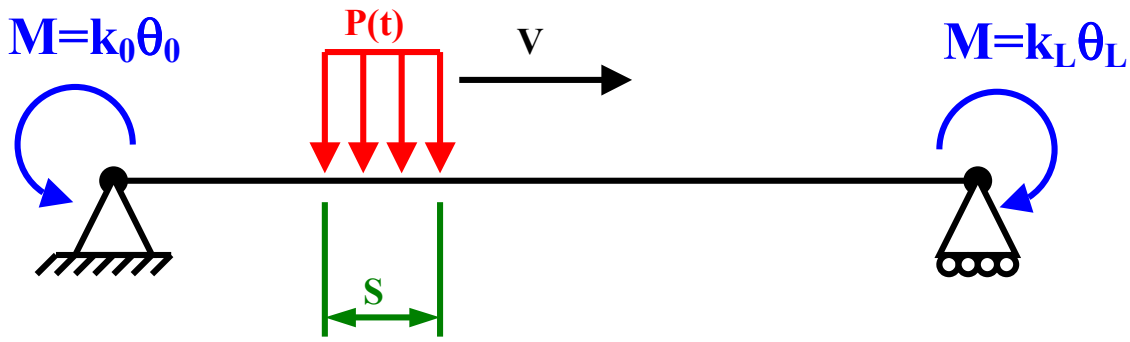

Figure 2.4.5. A single moving uniformly distributed load completely on a Euler-Bernoulli beam, with rotational stiffness at supports.

The integration for the particular solution is carried out from 0 to S. The particular solution becomes,

$$\begin{aligned}\xi_{iP} = &-\frac{P\gamma\left[C_1(S)\left(\omega_i{}^2-\Omega^2\right)+C_3(S)(2\zeta_i\omega_i\Omega)\right]\left[\cos(\Omega t)-e^{-\zeta_i\omega_i t}\left(\left(\frac{\zeta_i\omega_i}{\omega_{iD}}\right)\sin(\omega_{iD}t)+\cos(\omega_{iD}t)\right)\right]}{m_i\left(\left(\omega_i{}^2-\Omega^2\right)^2+(2\zeta_i\omega_i\Omega)^2\right)}\\ &+\frac{P\gamma\left[C_3(S)\left(\omega_i{}^2-\Omega^2\right)-C_1(S)(2\zeta_i\omega_i\Omega)\right]\left[\sin(\Omega t)-e^{-\zeta_i\omega_i t}\left(\frac{\Omega}{\omega_{iD}}\right)\sin(\omega_{iD}t)\right]}{m_i\left(\left(\omega_i{}^2-\Omega^2\right)^2+(2\zeta_i\omega_i\Omega)^2\right)}\\ &+\frac{P\gamma\left[C_2(S)\left(\omega_i{}^2+\Omega^2\right)+C_4(S)(2\zeta_i\omega_i\Omega)\right]\left[\cosh(\Omega t)-e^{-\zeta_i\omega_i t}\left(\left(\frac{\zeta_i\omega_i}{\omega_{iD}}\right)\sin(\omega_{iD}t)+\cos(\omega_{iD}t)\right)\right]}{m_i\left(\left(\omega_i{}^2+\Omega^2\right)^2-(2\zeta_i\omega_i\Omega)^2\right)}\\ &-\frac{P\gamma\left[C_4(S)\left(\omega_i{}^2+\Omega^2\right)+C_2(S)(2\zeta_i\omega_i\Omega)\right]\left[\sinh(\Omega t)-e^{-\zeta_i\omega_i t}\left(\frac{\Omega}{\omega_{iD}}\right)\sin(\omega_{iD}t)\right]}{m_i\left(\left(\omega_i{}^2+\Omega^2\right)^2-(2\zeta_i\omega_i\Omega)^2\right)}\end{aligned} \qquad (2.4.28)$$

Where $C_1(S), C_2(S), C_3(S)$ and $C_4(S)$ are constant functions of the total length of the distributed load, S:

$$C_1(S) = \frac{1}{S\lambda^{\frac{1}{4}}}\left(\sin\left(S\lambda^{\frac{1}{4}}\right) - \alpha\cos\left(S\lambda^{\frac{1}{4}}\right) + \alpha\right)$$

$$C_2(S) = \frac{1}{S\lambda^{\frac{1}{4}}}\left(\sinh\left(S\lambda^{\frac{1}{4}}\right) + \beta\cosh\left(S\lambda^{\frac{1}{4}}\right) - \beta\right)$$

$$C_3(S) = \frac{1}{S\lambda^{\frac{1}{4}}}\left(\alpha\sin\left(S\lambda^{\frac{1}{4}}\right) + \cos\left(S\lambda^{\frac{1}{4}}\right) - 1\right)$$

$$C_4(S) = \frac{1}{S\lambda^{\frac{1}{4}}}\left(\beta\sinh\left(S\lambda^{\frac{1}{4}}\right) + \cosh\left(S\lambda^{\frac{1}{4}}\right) - 1\right)$$

The initial conditions for the solution for the modal displacement and velocity for a distributed load completely on the span are at $t = \frac{S}{V}$, and are non-zero, found from Equations (2.4.26) and (2.4.27) above. Upon combination with the homogeneous equation the modal displacement equation during the period $\frac{S}{V} \le t \le \frac{L}{V}$ is,

$$\begin{aligned}
\xi_i = &-\frac{P\gamma\left[C_1(S)\left(\omega_i{}^2 - \Omega^2\right) + C_3(S)(2\zeta_i\omega_i\Omega)\right]\left[\cos(\Omega t) - e^{-\zeta_i\omega_i t}\left(\left(\frac{\zeta_i\omega_i}{\omega_{iD}}\right)\sin(\omega_{iD}t) + \cos(\omega_{iD}t)\right)\right]}{m_i\left(\left(\omega_i{}^2 - \Omega^2\right)^2 + (2\zeta_i\omega_i\Omega)^2\right)} \\
&+\frac{P\gamma\left[C_3(S)\left(\omega_i{}^2 - \Omega^2\right) - C_1(S)(2\zeta_i\omega_i\Omega)\right]\left[\sin(\Omega t) - e^{-\zeta_i\omega_i t}\left(\frac{\Omega}{\omega_{iD}}\right)\sin(\omega_{iD}t)\right]}{m_i\left(\left(\omega_i{}^2 - \Omega^2\right)^2 + (2\zeta_i\omega_i\Omega)^2\right)} \\
&+\frac{P\gamma\left[C_2(S)\left(\omega_i{}^2 + \Omega^2\right) + C_4(S)(2\zeta_i\omega_i\Omega)\right]\left[\cosh(\Omega t) - e^{-\zeta_i\omega_i t}\left(\left(\frac{\zeta_i\omega_i}{\omega_{iD}}\right)\sin(\omega_{iD}t) + \cos(\omega_{iD}t)\right)\right]}{m_i\left(\left(\omega_i{}^2 + \Omega^2\right)^2 - (2\zeta_i\omega_i\Omega)^2\right)} \\
&-\frac{P\gamma\left[C_4(S)\left(\omega_i{}^2 + \Omega^2\right) + C_2(S)(2\zeta_i\omega_i\Omega)\right]\left[\sinh(\Omega t) - e^{-\zeta_i\omega_i t}\left(\frac{\Omega}{\omega_{iD}}\right)\sin(\omega_{iD}t)\right]}{m_i\left(\left(\omega_i{}^2 + \Omega^2\right)^2 - (2\zeta_i\omega_i\Omega)^2\right)}
\end{aligned} \tag{2.4.29}$$

The solution for the modal velocity is,

$$
\begin{aligned}
\dot{\xi}_i = & -P\gamma \Big/ \left[m_i \left(\left(\omega_i{}^2 - \Omega^2 \right)^2 + (2\zeta_i \omega_i \Omega)^2 \right) \right] \\
& \bullet \Big\{ \left[C_1(S) \left(\omega_i{}^2 - \Omega^2 \right) + C_3(S)(2\zeta_i \omega_i \Omega) \right] \\
& \bullet \left[-\Omega \sin(\Omega t) + \zeta_i \omega_i e^{-\zeta_i \omega_i t} \left(\left(\frac{\zeta_i \omega_i}{\omega_{iD}} \right) \sin(\omega_{iD} t) + \cos(\omega_{iD} t) \right) - \omega_{iD} e^{-\zeta_i \omega_i t} \left(\left(\frac{\zeta_i \omega_i}{\omega_{iD}} \right) \cos(\omega_{iD} t) - \sin(\omega_{iD} t) \right) \right] \\
& + \left[\dot{C}_1(S) \left(\omega_i{}^2 - \Omega^2 \right) + \dot{C}_3(S)(2\zeta_i \omega_i \Omega) \right] \times \left[\cos(\Omega t) - e^{-\zeta_i \omega_i t} \left(\left(\frac{\zeta_i \omega_i}{\omega_{iD}} \right) \sin(\omega_{iD} t) + \cos(\omega_{iD} t) \right) \right] \\
& - \left[C_3(S) \left(\omega_i{}^2 - \Omega^2 \right) - C_1(S)(2\zeta_i \omega_i \Omega) \right] \times \left[\Omega \cos(\Omega t) + e^{-\zeta_i \omega_i t} \left(\frac{\zeta_i \omega_i \Omega}{\omega_{iD}} \right) \sin(\omega_{iD} t) - e^{-\zeta_i \omega_i t} \Omega \cos(\omega_{iD} t) \right] \\
& - \left[\dot{C}_3(S) \left(\omega_i{}^2 - \Omega^2 \right) - \dot{C}_1(S)(2\zeta_i \omega_i \Omega) \right] \times \left[\sin(\Omega t) - e^{-\zeta_i \omega_i t} \left(\frac{\Omega}{\omega_{iD}} \right) \sin(\omega_{iD} t) \right] \Big\} \\
& + P\gamma \Big/ \left[m_i \left(\left(\omega_i{}^2 + \Omega^2 \right)^2 - (2\zeta_i \omega_i \Omega)^2 \right) \right] \\
& \bullet \Big\{ \left[C_2(S) \left(\omega_i{}^2 + \Omega^2 \right) + C_4(S)(2\zeta_i \omega_i \Omega) \right] \\
& \bullet \left[\Omega \sinh(\Omega t) + \zeta_i \omega_i e^{-\zeta_i \omega_i t} \left(\left(\frac{\zeta_i \omega_i}{\omega_{iD}} \right) \sin(\omega_{iD} t) + \cos(\omega_{iD} t) \right) - \omega_{iD} e^{-\zeta_i \omega_i t} \left(\left(\frac{\zeta_i \omega_i}{\omega_{iD}} \right) \cos(\omega_{iD} t) - \sin(\omega_{iD} t) \right) \right] \\
& + \left[\dot{C}_2(S) \left(\omega_i{}^2 + \Omega^2 \right) + \dot{C}_4(S)(2\zeta_i \omega_i \Omega) \right] \times \left[\cosh(\Omega t) - e^{-\zeta_i \omega_i t} \left(\left(\frac{\zeta_i \omega_i}{\omega_{iD}} \right) \sin(\omega_{iD} t) + \cos(\omega_{iD} t) \right) \right] \\
& - \left[C_2(S) \left(\omega_i{}^2 + \Omega^2 \right) + C_4(S)(2\zeta_i \omega_i \Omega) \right] \times \left[\Omega \cosh(\Omega t) + e^{-\zeta_i \omega_i t} \left(\frac{\zeta_i \omega_i \Omega}{\omega_{iD}} \right) \sin(\omega_{iD} t) - e^{-\zeta_i \omega_i t} \Omega \cos(\omega_{iD} t) \right] \\
& - \left[\dot{C}_2(S) \left(\omega_i{}^2 + \Omega^2 \right) + \dot{C}_4(S)(2\zeta_i \omega_i \Omega) \right] \times \left[\sinh(\Omega t) - e^{-\zeta_i \omega_i t} \left(\frac{\Omega}{\omega_{iD}} \right) \sin(\omega_{iD} t) \right] \Big\} \qquad (2.4.30)
\end{aligned}
$$

Where $C_1(S), C_2(S), C_3(S)$ and $C_4(S)$ are constant functions of the total length of the distributed load, S, and are equal to the functions $C_1(t), C_2(t), C_3(t)$ and $C_4(t)$ at $t = \frac{S}{V}$:

$$C_1(S) = \frac{1}{S\lambda^{\frac{1}{4}}}\left(\sin\left(S\lambda^{\frac{1}{4}}\right) - \alpha\cos\left(S\lambda^{\frac{1}{4}}\right) + \alpha\right)$$

$$C_2(S) = \frac{1}{S\lambda^{\frac{1}{4}}}\left(\sinh\left(S\lambda^{\frac{1}{4}}\right) + \beta\cosh\left(S\lambda^{\frac{1}{4}}\right) - \beta\right)$$

$$C_3(S) = \frac{1}{S\lambda^{\frac{1}{4}}}\left(\alpha\sin\left(S\lambda^{\frac{1}{4}}\right) + \cos\left(S\lambda^{\frac{1}{4}}\right) - 1\right)$$

$$C_4(S) = \frac{1}{S\lambda^{\frac{1}{4}}}\left(\beta\sinh\left(S\lambda^{\frac{1}{4}}\right) + \cosh\left(S\lambda^{\frac{1}{4}}\right) - 1\right)$$

And $\dot{C}_1(S), \dot{C}_2(S), \dot{C}_3(S)$ and $\dot{C}_4(S)$ are constant functions of the total length of the distributed load, S, and are equal to the functions $\dot{C}_1(t), \dot{C}_2(t), \dot{C}_3(t)$ and $\dot{C}_4(t)$ at $t = \frac{S}{V}$:

$$\dot{C}_1(S) = \frac{\Omega}{S\lambda^{\frac{1}{4}}}\left(\cos\left(S\lambda^{\frac{1}{4}}\right) + \alpha\sin\left(S\lambda^{\frac{1}{4}}\right)\right)$$

$$\dot{C}_2(S) = \frac{\Omega}{S\lambda^{\frac{1}{4}}}\left(\cosh\left(S\lambda^{\frac{1}{4}}\right) + \beta\sinh\left(S\lambda^{\frac{1}{4}}\right)\right)$$

$$\dot{C}_3(S) = \frac{\Omega}{S\lambda^{\frac{1}{4}}}\left(\alpha\cos\left(S\lambda^{\frac{1}{4}}\right) - \sin\left(S\lambda^{\frac{1}{4}}\right)\right)$$

$$\dot{C}_4(S) = \frac{\Omega}{S\lambda^{\frac{1}{4}}}\left(\beta\cosh\left(S\lambda^{\frac{1}{4}}\right) + \sinh\left(S\lambda^{\frac{1}{4}}\right)\right)$$

The load leaves the span during the period $\frac{L}{V} \le t \le \frac{L+S}{V}$. Assuming constant velocity, the length of the distributed load on the span during that time interval varies from the total length, S, to 0. See Figure 2.4.6.

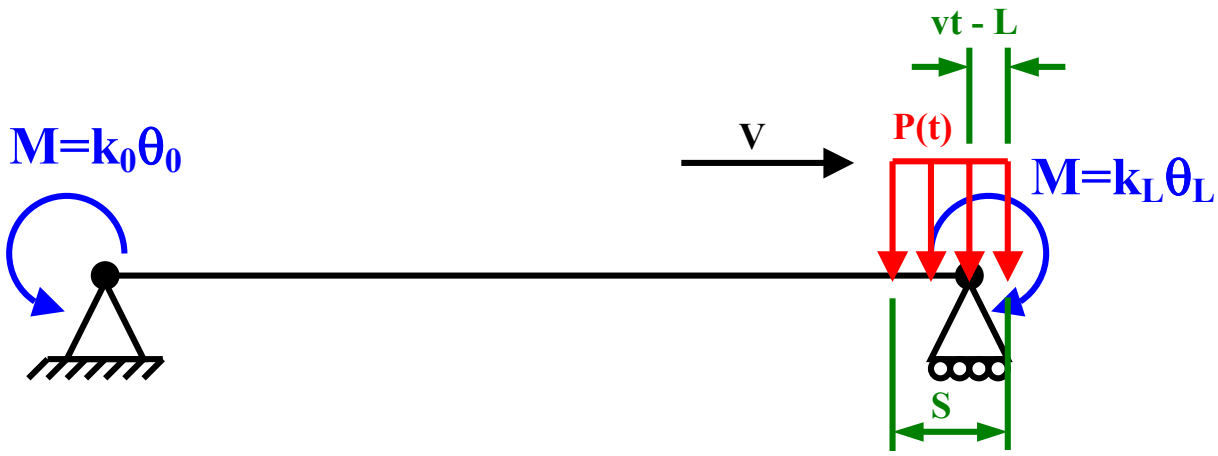

Figure 2.4.6. A single moving uniformly distributed load leaving a Euler-Bernoulli beam, with rotational stiffness at supports.

The integration of the particular solution is carried out from $Vt-L$ to S. Once again the particular solution is of the same form as Equations (2.4.25) and (2.4.28) where only the coefficients C_1 – C_4 vary. For the particular solution for the period $\frac{L}{V} \le t \le \frac{L+S}{V}$, $C_1(t), C_2(t), C_3(t)$ and $C_4(t)$ are functions of time and are:

$$C_1(t) = \frac{1}{S\lambda^{\frac{1}{4}}}\left(-\sin\left(\Omega t - L\lambda^{\frac{1}{4}}\right) + \alpha\cos\left(\Omega t - L\lambda^{\frac{1}{4}}\right) + \sin\left(S\lambda^{\frac{1}{4}}\right) - \alpha\cos\left(S\lambda^{\frac{1}{4}}\right)\right)$$

$$C_2(t) = \frac{1}{S\lambda^{\frac{1}{4}}}\left(-\sinh\left(\Omega t - L\lambda^{\frac{1}{4}}\right) - \beta\cosh\left(\Omega t - L\lambda^{\frac{1}{4}}\right) + \sinh\left(S\lambda^{\frac{1}{4}}\right) + \beta\cosh\left(S\lambda^{\frac{1}{4}}\right)\right)$$

$$C_3(t) = \frac{1}{S\lambda^{\frac{1}{4}}}\left(-\alpha\sin\left(\Omega t - L\lambda^{\frac{1}{4}}\right) - \cos\left(\Omega t - L\lambda^{\frac{1}{4}}\right) + \alpha\sin\left(S\lambda^{\frac{1}{4}}\right) + \cos\left(S\lambda^{\frac{1}{4}}\right)\right)$$

$$C_4(t) = \frac{1}{S\lambda^{\frac{1}{4}}}\left(-\beta\sinh\left(\Omega t - L\lambda^{\frac{1}{4}}\right) - \cosh\left(\Omega t - L\lambda^{\frac{1}{4}}\right) + \beta\sinh\left(S\lambda^{\frac{1}{4}}\right) + \cosh\left(S\lambda^{\frac{1}{4}}\right)\right)$$

After solving, the particular solution is combined with the homogeneous solution at initial conditions $t = \frac{L}{V}$, which are non-zero, found from equations (2.4.29) and

(2.4.30) above. The modal displacement equation during the period $\frac{L}{V} \le t \le \frac{L+S}{V}$ then is,

$$
\begin{aligned}
\xi_i = & -P\gamma / \left[S m_i \left(\left({\omega_i}^2 - \Omega^2 \right)^2 + \left(2\zeta_i \omega_i \Omega \right)^2 \right) \right] \\
& \bullet \left\{ \left[\frac{1}{\lambda^{\frac{1}{4}}} \left(\sin\left(S\lambda^{\frac{1}{4}} \right) - \alpha \cos\left(S\lambda^{\frac{1}{4}} \right) \right) \left({\omega_i}^2 - \Omega^2 \right) + \frac{1}{\lambda^{\frac{1}{4}}} \left(\alpha \sin\left(S\lambda^{\frac{1}{4}} \right) + \cos\left(S\lambda^{\frac{1}{4}} \right) \right) \left(2\zeta_i \omega_i \Omega \right) \right] \right. \\
& \bullet \left[\cos(\Omega t) - e^{-\zeta_i \omega_i t} \left(\left(\frac{\zeta_i \omega_i}{\omega_{iD}} \right) \sin(\omega_{iD} t) + \cos(\omega_{iD} t) \right) \right] \\
& - \left[\frac{1}{\lambda^{\frac{1}{4}}} \left(\alpha \sin\left(S\lambda^{\frac{1}{4}} \right) + \cos\left(S\lambda^{\frac{1}{4}} \right) \right) \left({\omega_i}^2 - \Omega^2 \right) - \frac{1}{\lambda^{\frac{1}{4}}} \left(\sin\left(S\lambda^{\frac{1}{4}} \right) + \alpha \cos\left(S\lambda^{\frac{1}{4}} \right) \right) \left(2\zeta_i \omega_i \Omega \right) \right] \\
& \bullet \left[\sin(\Omega t) - e^{-\zeta_i \omega_i t} \left(\frac{\Omega}{\omega_{iD}} \right) \sin(\omega_{iD} t) \right] \\
& + \left[\frac{\Omega}{\lambda^{\frac{1}{4}}} \left(\cos\left(S\lambda^{\frac{1}{4}} \right) + \alpha \sin\left(S\lambda^{\frac{1}{4}} \right) \right) \left({\omega_i}^2 - \Omega^2 \right) + \frac{\Omega}{\lambda^{\frac{1}{4}}} \left(\alpha \cos\left(S\lambda^{\frac{1}{4}} \right) - \sin\left(S\lambda^{\frac{1}{4}} \right) \right) \left(2\zeta_i \omega_i \Omega \right) \right] \\
& \bullet \frac{1}{\omega_{iD}} e^{-\zeta_i \omega_i \left(t - \frac{S}{v} \right)} \sin\left(\omega_{iD} \left[t - \frac{S}{v} \right] \right) \left[\cos\left(S\lambda^{\frac{1}{4}} \right) - e^{-\zeta_i \omega_i \frac{S}{v}} \left(\left(\frac{\zeta_i \omega_i}{\omega_{iD}} \right) \sin\left(\omega_{iD} \frac{S}{v} \right) + \cos\left(\omega_{iD} \frac{S}{v} \right) \right) \right] \\
& - \left[\frac{\Omega}{\lambda^{\frac{1}{4}}} \left(\alpha \cos\left(S\lambda^{\frac{1}{4}} \right) - \sin\left(S\lambda^{\frac{1}{4}} \right) \right) \left({\omega_i}^2 - \Omega^2 \right) - \frac{\Omega}{\lambda^{\frac{1}{4}}} \left(\cos\left(S\lambda^{\frac{1}{4}} \right) + \alpha \sin\left(S\lambda^{\frac{1}{4}} \right) \right) \left(2\zeta_i \omega_i \Omega \right) \right] \\
& \bullet \frac{1}{\omega_{iD}} e^{-\zeta_i \omega_i \left(t - \frac{S}{v} \right)} \sin\left(\omega_{iD} \left[t - \frac{S}{v} \right] \right) \left[\sin\left(S\lambda^{\frac{1}{4}} \right) - e^{-\zeta_i \omega_i \frac{S}{v}} \left(\frac{\Omega}{\omega_{iD}} \right) \sin\left(\omega_{iD} \frac{S}{v} \right) \right] \\
& + \frac{1}{\lambda^{\frac{1}{4}}} \left[\alpha \left({\omega_i}^2 - \Omega^2 \right) + (-1)\left(2\zeta_i \omega_i \Omega \right) \right] \times \left[\cos\left(L\lambda^{\frac{1}{4}} \right) - e^{-\zeta_i \omega_i t} \left(\left(\frac{\zeta_i . \omega_i}{\omega_{iD}} \right) \sin(\omega_{iD} t) + \cos(\omega_{iD} t) \right) \right. \\
& \left. - \sin\left(L\lambda^{\frac{1}{4}} \right) e^{-\zeta_i \omega_i \left(t - \frac{L}{v} \right)} \left(\frac{\Omega}{\omega_{iD}} \right) \sin\left(\omega_{iD} \left[t - \frac{L}{v} \right] \right) \right] \\
& - \frac{1}{\lambda^{\frac{1}{4}}} \left[(-1)\left({\omega_i}^2 - \Omega^2 \right) - \alpha \left(2\zeta_i \omega_i \Omega \right) \right] \times \left[\sin\left(L\lambda^{\frac{1}{4}} \right) - e^{-\zeta_i \omega_i t} \left(\left(\frac{\zeta_i \omega_i}{\omega_{iD}} \right) \sin(\omega_{iD} t) + \cos(\omega_{iD} t) \right) \right. \\
& \left. \left. + \cos\left(L\lambda^{\frac{1}{4}} \right) e^{-\zeta_i \omega_i \left(t - \frac{L}{v} \right)} \left(\frac{\Omega}{\omega_{iD}} \right) \sin\left(\omega_{iD} \left[t - \frac{L}{v} \right] \right) \right] \right\}
\end{aligned}
$$

(continued over the page…)

$$+P\gamma/\left[S\,m_i\left(\left(\omega_i{}^2+\Omega^2\right)^2-(2\zeta_i\omega_i\Omega)^2\right)\right]$$

$$\bullet\left\{\left[\frac{1}{\lambda^{\frac{1}{4}}}\left(\sinh\left(S\lambda^{\frac{1}{4}}\right)+\beta\cosh\left(S\lambda^{\frac{1}{4}}\right)\right)\left(\omega_i{}^2+\Omega^2\right)+\frac{1}{\lambda^{\frac{1}{4}}}\left(\beta\sinh\left(S\lambda^{\frac{1}{4}}\right)+\cosh\left(S\lambda^{\frac{1}{4}}\right)\right)(2\zeta_i\omega_i\Omega)\right]\right.$$

$$\bullet\left[\cosh(\Omega t)-e^{-\zeta_i\omega_i t}\left(\left(\frac{\zeta_i\omega_i}{\omega_{iD}}\right)\sin(\omega_{iD}t)+\cos(\omega_{iD}t)\right)\right]$$

$$-\left[\frac{1}{\lambda^{\frac{1}{4}}}\left(\beta\sinh\left(S\lambda^{\frac{1}{4}}\right)+\cosh\left(S\lambda^{\frac{1}{4}}\right)\right)\left(\omega_i{}^2+\Omega^2\right)+\frac{1}{\lambda^{\frac{1}{4}}}\left(\sinh\left(S\lambda^{\frac{1}{4}}\right)+\beta\cosh\left(S\lambda^{\frac{1}{4}}\right)\right)(2\zeta_i\omega_i\Omega)\right]$$

$$\bullet\left[\sinh(\Omega t)-e^{-\zeta_i\omega_i t}\left(\frac{\Omega}{\omega_{iD}}\right)\sin(\omega_{iD}t)\right]$$

$$+\left[\frac{\Omega}{\lambda^{\frac{1}{4}}}\left(\cosh\left(S\lambda^{\frac{1}{4}}\right)+\beta\sinh\left(S\lambda^{\frac{1}{4}}\right)\right)\left(\omega_i{}^2+\Omega^2\right)+\frac{\Omega}{\lambda^{\frac{1}{4}}}\left(\beta\cosh\left(S\lambda^{\frac{1}{4}}\right)+\sinh\left(S\lambda^{\frac{1}{4}}\right)\right)(2\zeta_i\omega_i\Omega)\right]$$

$$\bullet\frac{1}{\omega_{iD}}e^{-\zeta_i\omega_i\left(t-\frac{S}{v}\right)}\sin\left(\omega_{iD}\left[t-\frac{S}{v}\right]\right)\left[\cosh\left(S\lambda^{\frac{1}{4}}\right)-e^{-\zeta_i\omega_i\frac{S}{v}}\left(\left(\frac{\zeta_i.\omega_i}{\omega_{iD}}\right)\sin\left(\omega_{iD}\frac{S}{v}\right)+\cos\left(\omega_{iD}\frac{S}{v}\right)\right)\right]$$

$$-\left[\frac{\Omega}{\lambda^{\frac{1}{4}}}\left(\beta\cosh\left(S\lambda^{\frac{1}{4}}\right)+\sinh\left(S\lambda^{\frac{1}{4}}\right)\right)\left(\omega_i{}^2+\Omega^2\right)+\frac{\Omega}{\lambda^{\frac{1}{4}}}\left(\cosh\left(S\lambda^{\frac{1}{4}}\right)+\beta\sin\left(S\lambda^{\frac{1}{4}}\right)\right)(2\zeta_i\omega_i\Omega)\right]$$

$$\bullet\frac{1}{\omega_{iD}}e^{-\zeta_i\omega_i\left(t-\frac{S}{v}\right)}\sin\left(\omega_{iD}\left[t-\frac{S}{v}\right]\right)\left[\sinh\left(S\lambda^{\frac{1}{4}}\right)-e^{-\zeta_i\omega_i\frac{S}{v}}\left(\frac{\Omega}{\omega_{iD}}\right)\sin\left(\omega_{iD}\frac{S}{v}\right)\right]$$

$$+\frac{1}{\lambda^{\frac{1}{4}}}\left[(-\beta)\left(\omega_i{}^2+\Omega^2\right)+(-1)(2\zeta_i\omega_i\Omega)\right]\times\left[\cosh\left(L\lambda^{\frac{1}{4}}\right)-e^{-\zeta_i\omega_i t}\left(\left(\frac{\zeta_i\omega_i}{\omega_{iD}}\right)\sin(\omega_{iD}t)+\cos(\omega_{iD}t)\right)\right.$$

$$\left.+\sinh\left(L\lambda^{\frac{1}{4}}\right)e^{-\zeta_i\omega_i\left(t-\frac{L}{v}\right)}\left(\frac{\Omega}{\omega_{iD}}\right)\sin\left(\omega_{iD}\left[t-\frac{L}{v}\right]\right)\right]$$

$$-\frac{1}{\lambda^{\frac{1}{4}}}\left[(-1)\left(\omega_i{}^2+\Omega^2\right)+(-\beta)(2\zeta_i\omega_i\Omega)\right]\times\left[\sinh\left(L\lambda^{\frac{1}{4}}\right)-e^{-\zeta_i\omega_i t}\left(\left(\frac{\zeta_i\omega_i}{\omega_{iD}}\right)\sin(\omega_{iD}t)+\cos(\omega_{iD}t)\right)\right.$$

$$\left.\left.+\cosh\left(L\lambda^{\frac{1}{4}}\right)e^{-\zeta_i\omega_i\left(t-\frac{L}{v}\right)}\left(\frac{\Omega}{\omega_{iD}}\right)\sin\left(\omega_{iD}\left[t-\frac{L}{v}\right]\right)\right]\right\} \qquad (2.4.31)$$

2.4.5 An Analytical Model for Euler-Bernoulli Beams with Rotational Stiffness at Supports Subjected to Multiple Moving Uniformly Distributed Loads

In order to find the displacement response to multiple moving uniformly distributed loads, recalling that small deflections are assumed, the time term, t, in Equations (2.4.26), (2.4.29) and (2.4.31) is simply replaced with $t-\frac{A_n}{V}$. Where 'A_n' is the distance from the start of the first distributed load to the start of the nth distributed load and 'V' is the speed of the loads. See Figure 2.4.7.

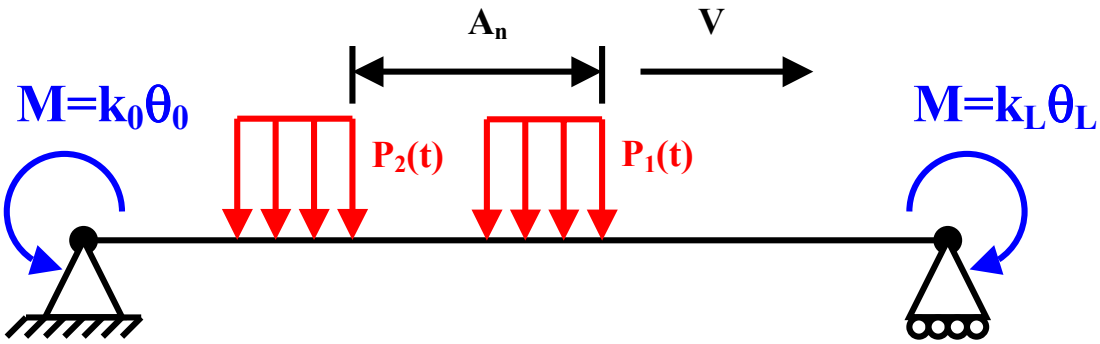

Figure 2.4.7. Multiple moving uniformly distributed loads on a Euler-Bernoulli beam, with rotational stiffness at supports.

Equation (2.4.32) is the bending moment response from the modal displacement and the second derivative of the mode shape function, with respect to x:

$$M(x,t)=\sum_{i=1}^{\infty}\xi_i(t)\frac{d^2\phi_i}{dx^2}EI \qquad (2.4.32)$$

From the equation for the dynamic bending moment the step to bending stress is of course straightforward by substituting equation (2.4.32) into equation (2.4.33).

$$\sigma_B=\frac{My}{I} \qquad (2.4.33)$$

2.4.6 Application to Structural Assessment

The analytical model developed above is used in structural assessment for model validation and refinement from dynamic field testing (Section 2.3), and for load identification from structural response (Section 2.5). For model validation and refinement (Section 2.3) the rotational stiffness at the supports and the length of the load distribution are tuned, so the response of the analytical model matches the response from field-testing with a vehicle at crawl speed. Each time structural properties, including the rotational stiffness of the supports, the length of the distributed load, the moment of inertia etc. are varied, the mode shape function, Equation (2.4.4), must be recalculated and λ iterated for a suitable number of modes. If a large number of modes are used the iteration process can take some time. To speed up the tuning process, a quasi-static model has been developed for the derivation of structural properties at slow vehicle speeds. The response from the quasi-static model is, in essence, simply an influence line for a given point, in the time domain. Since dynamic effects are minimal at slow speeds, the simple and computationally faster quasi-static model is considered sufficient for model validation at slow speeds. Once found, structural properties can be used in the dynamic analytical model. The solution for the quasi-static model is presented in Appendix B.

2.4.7 Validation of the Analytical Model

To validate the distributed load model presented above, the response for multiple distributed loads, with a very small distributed load length, is compared with the response of multiple concentrated loads from the concentrated load model. The response of slow moving multiple distributed loads, with a significant distributed load length, is then compared against the quasi-static solution for equivalent loads. Finally

the solution presented here is compared against the Heaviside approximation and field test results.

2.4.7.1 Comparison against the Concentrated Load Solution

For geometric comparison of the solution presented here for distributed loads against the concentrated load solution, consider a very small distributed load length. In fact assume the contact patch S approaches 0 in length. The only period of the distributed load solution to consider is the period $\frac{S}{v} \le t \le \frac{L}{V}$, Equation (2.4.29), which when S approaches 0 becomes $0 \le t \le \frac{L}{V}$. The coefficients $C_1(S)$ to $C_4(S)$ may be rewritten,

$$C_1(S) = \frac{\sin\left(S\lambda^{\frac{1}{4}}\right)}{S\lambda^{\frac{1}{4}}} - \frac{\alpha\left[\cos\left(S\lambda^{\frac{1}{4}}\right)+1\right]}{S\lambda^{\frac{1}{4}}}$$

$$C_2(S) = \frac{\sinh\left(S.\lambda^{\frac{1}{4}}\right)}{S\lambda^{\frac{1}{4}}} + \frac{\beta\left[\cosh\left(S.\lambda^{\frac{1}{4}}\right)-1\right]}{S\lambda^{\frac{1}{4}}}$$

$$C_3(S) = \alpha\frac{\sin\left(S\lambda^{\frac{1}{4}}\right)}{S\lambda^{\frac{1}{4}}} + \frac{\cos\left(S\lambda^{\frac{1}{4}}\right)-1}{S\lambda^{\frac{1}{4}}}$$

$$C_4(S) = \beta\frac{\sinh\left(S\lambda^{\frac{1}{4}}\right)}{S\lambda^{\frac{1}{4}}} + \frac{\cosh\left(S\lambda^{\frac{1}{4}}\right)-1}{S\lambda^{\frac{1}{4}}}$$

As S $\to$ 0, $S\lambda^{\frac{1}{4}} \approx \sin\left(S\lambda^{\frac{1}{4}}\right) \approx \sinh\left(S\lambda^{\frac{1}{4}}\right)$

and $\cos\left(S\lambda^{\frac{1}{4}}\right) \approx \cosh\left(S\lambda^{\frac{1}{4}}\right) \approx 1$

therefore,

$$\frac{\sin\left(S\lambda^{\frac{1}{4}}\right)}{S\lambda^{\frac{1}{4}}} \approx \frac{\sinh\left(S\lambda^{\frac{1}{4}}\right)}{S\lambda^{\frac{1}{4}}} \approx 1 \text{ and}$$

$$\cos\left(S\lambda^{\frac{1}{4}}\right) - 1 \approx \cosh\left(S\lambda^{\frac{1}{4}}\right) - 1 \approx 0$$

therefore the coefficients $C_1(S) - C_4(S)$ become,

$$C_1(\mathrm{S}) = 1$$
$$C_2(\mathrm{S}) = 1$$
$$C_3(\mathrm{S}) = \alpha$$
$$C_4(\mathrm{S}) = \beta$$

Substituting these into the equation for the dynamic modal displacement response of a distributed load, Equation (2.4.29), the equation becomes equivalent to the equation for the dynamic modal displacement response of a concentrated load, Equation (2.4.12).

It may be concluded, therefore, that the distributed load analytical model developed in this thesis is geometrically equivalent to the known concentrated load solution for a very small distributed load length (i.e. one which approaches zero in length).

For graphical comparison, the bending stress response of a beam subjected to multiple concentrated loads, Equation (2.4.17), is compared against the bending stress response of the dynamic distributed load model, with a very small load distribution (0.001 m). The comparison is presented in Figure 2.4.8. Three loads, at 2 metre spacings, with

magnitudes of 100 kN, travelling at 5 metres per second are used. The assumed structural properties of the beams are listed below in Table 2.4.1.

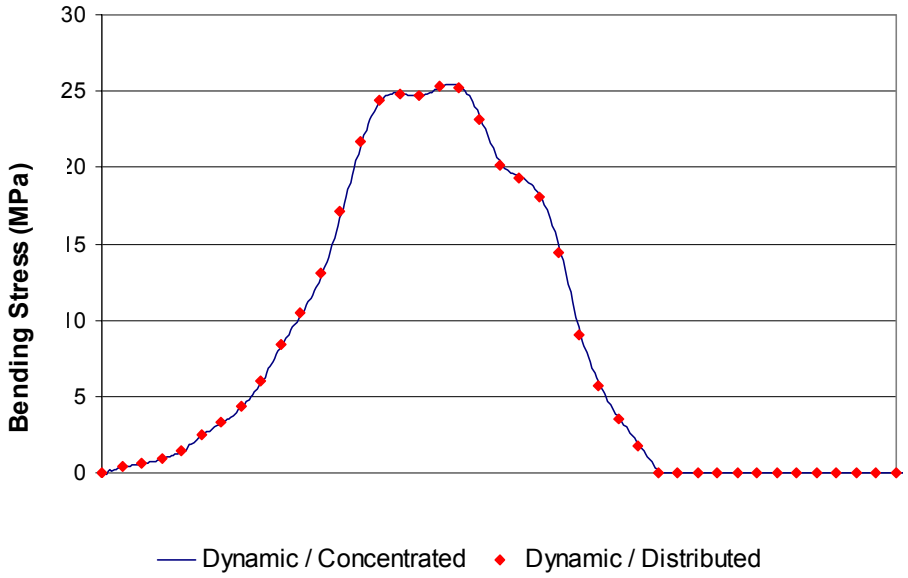

Figure 2.4.8. Comparison of the bending stress response of the model developed in this section, Equation (2.4.26), (2.4.29) and (2.4.31), with 3 distributed loads of length 0.001m, with the solution for 3 concentrated loads, Equation (2.4.17).

Properties Relevant to All Models		**Properties Relevant to Dynamic Models Only**	
Length	10 m	Mass Density	7850 kg m^{-3}
Modulus of Elasticity	207 GPa	Cross Sectional Area	0.5 m^2
Moment of Inertia	.003 m^4	Critical Damping (all modes)	1 %
Rotational Stiffness at First Support	0 N m rad^{-1}		
Rotational Stiffness at Second Support	$5x10^8$ N m rad^{-1}		

Table 2.4.1. Assumed beam structural properties for comparison against known solutions.

The distributed load analytical model developed in this thesis has been shown to be geometrically equivalent to the known concentrated load solution for a very small distributed load length. As expected therefore, when compared graphically, the bending stress response of the model developed in this section and the bending stress response of the concentrated loads solution, for a very small distributed load length, show close conformance.

2.4.7.2 Comparison against the Quasi-Static Uniformly Distributed Load Solution

The model is also compared graphically against the quasi-static model of Appendix B, for a distributed load with a load distribution of 1 metre (Figure 2.4.9). Again three loads, at 2 metre spacings, with magnitudes of 100 kN, travelling at 5 metres per second are used. The assumed structural properties of the beams are those listed in Table 2.4.1.

When compared graphically, the bending stress response of the model developed in this section and the bending stress response of the quasi-static model of Appendix B, for a distributed load with a load distribution length of 1 metre, show close conformance.

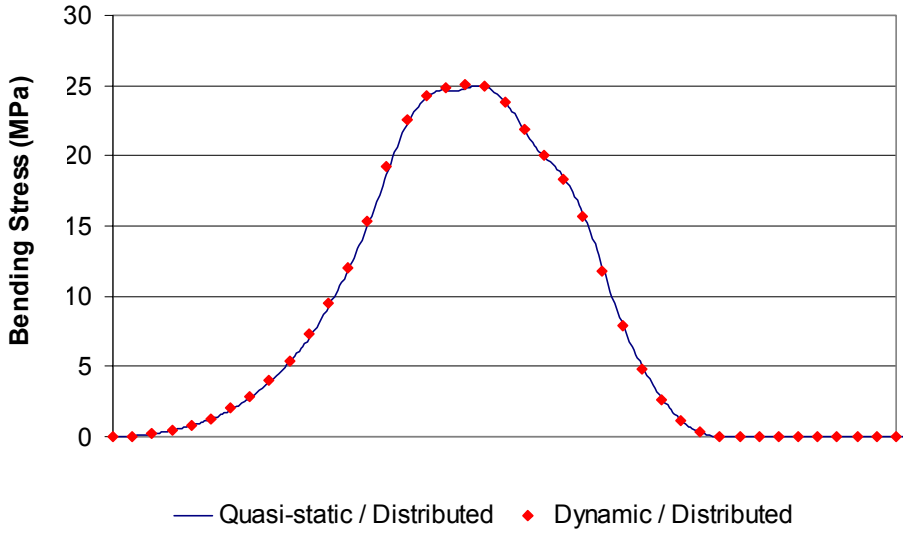

Figure 2.4.9. Comparison of the bending stress response of the model developed in this section Equation (2.4.26), (2.4.29) and (2.4.31), with 3 distributed loads of length 1m, with the quasi-static solution of Appendix B.

2.4.7.3 Comparison against the Heaviside Approximation of a Uniformly Distributed Load and Field Test Results

As was noted in the introduction to this section, Fryba [40] and others have modelled the passage of an entire train as a uniformly distributed load using the Heaviside unit function. The method outlined here for modelling the response of a uniformly distributed load differs somewhat from the Heaviside function method, particularly for the period when the load arrives on and departs from the beam.

In the method outlined in this thesis the integration step is carried out ***after*** the particular solution for a single moving load has been found. This is because the method here is based on the assumption that a moving distributed load may be approximated as the sum of infinitely many concentrated loads infinitely closely spaced (Section 2.4.4). Therefore the response for one load is found and then infinitely many loads summed by integration. The use of the Heaviside function for the arrival and departure of a continuous load on a beam is equivalent to integrating the modal force ***before*** the particular solution is found. For example using the Heaviside unit function for the period $0 \le t \le \frac{S}{V}$ the modal force becomes,

$$
\begin{aligned}
p_i &= \int_0^{vt}\int_0^{l} f(x,t)\phi_i \, dx\, ds \\
&= \int_0^{vt}\int_0^{l} -\frac{P}{S}\delta(x-(Vt-s))\gamma\left(\cos\left(x\lambda^{\frac{1}{4}}\right)-\cosh\left(x\lambda^{\frac{1}{4}}\right)-\alpha\sin\left(x\lambda^{\frac{1}{4}}\right)+\beta\sinh\left(x\lambda^{\frac{1}{4}}\right)\right)dx\, ds \\
&= \int_0^{vt} -\frac{P}{S}\gamma\left(C_1\cos(\Omega t)-C_2\cosh(\Omega t)-C_3\sin(\Omega t)+C_4\sinh(\Omega t)\right)ds \\
&= -\frac{P}{\lambda^{\frac{1}{4}}S}\gamma\left(\alpha\cos(\Omega t)+\beta\cosh(\Omega t)+\sin(\Omega t)-\sinh(\Omega t)-(\alpha+\beta)\right) \qquad (2.4.34)
\end{aligned}
$$

The total solution is found by solving the particular solution for the above using the Duhamel integral and summing with the homogeneous solution with appropriate initial conditions, most likely zero initial displacement and velocity. The total modal displacement, using the Heaviside function, becomes,

$$\begin{aligned}
\xi_i = &-\frac{P\gamma\left[\alpha\left(\omega_i{}^2-\Omega^2\right)-\left(2\zeta_i\omega_i\Omega\right)\right]\left[\cos(\Omega t)-e^{-\zeta_i\omega_i t}\left(\left(\frac{\zeta_i\omega_i}{\omega_{iD}}\right)\sin(\omega_{iD}t)+\cos(\omega_{iD}t)\right)\right]}{S\lambda^{\frac{1}{4}}m_i\left(\left(\omega_i{}^2-\Omega^2\right)^2+\left(2\zeta_i\omega_i\Omega\right)^2\right)} \\
&+\frac{P\gamma\left[-\left(\omega_i{}^2-\Omega^2\right)-\alpha\left(2\zeta_i\omega_i\Omega\right)\right]\left[\sin(\Omega t)-e^{-\zeta_i\omega_i t}\left(\frac{\Omega}{\omega_{iD}}\right)\sin(\omega_{iD}t)\right]}{S\lambda^{\frac{1}{4}}m_i\left(\left(\omega_i{}^2-\Omega^2\right)^2+\left(2\zeta_i\omega_i\Omega\right)^2\right)} \\
&+\frac{P\gamma\left[-\beta\left(\omega_i{}^2+\Omega^2\right)-\left(2\zeta_i\omega_i\Omega\right)\right]\left[\cosh(\Omega t)-e^{-\zeta_i\omega_i t}\left(\left(\frac{\zeta_i\omega_i}{\omega_{iD}}\right)\sin(\omega_{iD}t)+\cos(\omega_{iD}t)\right)\right]}{S\lambda^{\frac{1}{4}}m_i\left(\left(\omega_i{}^2+\Omega^2\right)^2-\left(2\zeta_i\omega_i\Omega\right)^2\right)} \\
&-\frac{P\gamma\left[-\left(\omega_i{}^2+\Omega^2\right)-\beta\left(2\zeta_i\omega_i\Omega\right)\right]\left[\sinh(\Omega t)-e^{-\zeta_i\omega_i t}\left(\frac{\Omega}{\omega_{iD}}\right)\sin(\omega_{iD}t)\right]}{S\lambda^{\frac{1}{4}}m_i\left(\left(\omega_i{}^2+\Omega^2\right)^2-\left(2\zeta_i\omega_i\Omega\right)^2\right)} \\
&+\frac{P\gamma}{S\lambda^{\frac{1}{4}}m_i\omega^2}\left(\alpha+\beta\right)\left[1-e^{-\zeta_i\omega_i t}\left(\left(\frac{\zeta_i\omega_i}{\omega_{iD}}\right)\sin(\omega_{iD}t)+\cos(\omega_{iD}t)\right)\right]
\end{aligned} \tag{2.4.35}$$

This differs from the total modal displacement response using the method outlined in this thesis, Equation (2.4.26). Comparing the solution presented in this thesis with the Heaviside approximation graphically, there is a practically no observable difference between the displacement response of the two solutions for relatively high damping, Figure 2.4.10. For lower damping ratios the displacement response using the method presented in this thesis tends to oscillate around the Heaviside approximation response, Figure 2.4.11. The damping ratio for the response shown in Figure 2.4.10 was 10% of critical damping (relatively high damping ratio) and the damping ratio for the response shown in Figure 2.4.11 was 0.5% of critical damping (relatively low damping ratio).

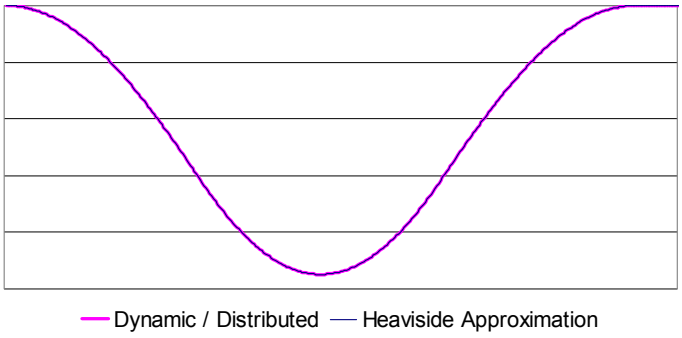

Figure 2.4.10. Comparison of the modal displacement response of the model developed in this section with the response from the Heaviside approximation, for a single moving load, and a relatively high damping ratio (ζ=0.1).

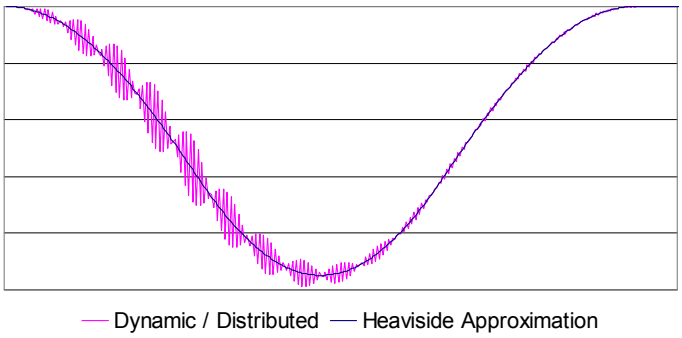

Figure 2.4.11. Comparison of the modal displacement response of the model developed in this section with the response from the Heaviside approximation, for a single moving load, and a relatively low damping ratio (ζ=0.005).

The difference between the two solutions is further highlighted in the acceleration response, which is, of course, the second derivative of the displacement response. The solution for the acceleration response for the model developed in this section is presented in Appendix C. A typical acceleration response from both the Heaviside approximation and the solution presented in this thesis is presented in Figure 2.4.12. The validity of either solution may be confirmed via laboratory testing or field-testing. The field test results of a four-bogie passenger train are shown in Figure 2.4.13.

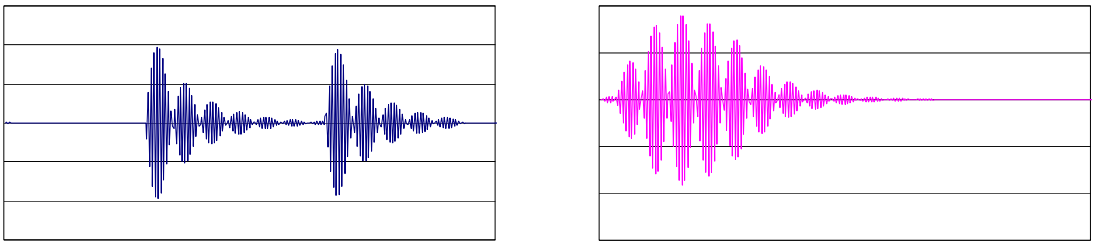

(a) **(b)**

Figure 2.4.12. A typical acceleration response of (a) the Heaviside approximation and (b) the model developed in this section, under the passage of a single moving constant magnitude and velocity load.

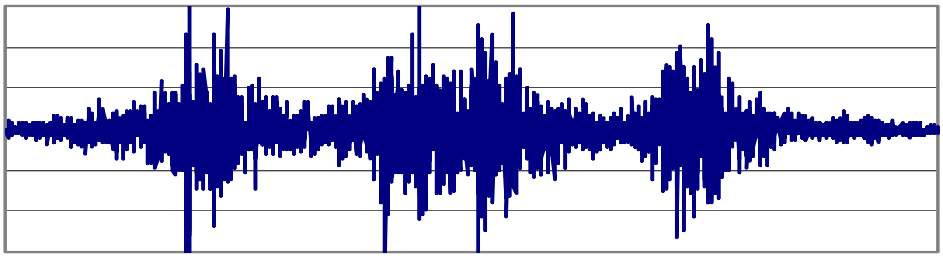

Figure 2.4.13. The acceleration response of a four-bogie (two-carriage) passenger train from field-testing.

These results suggest that the solution presented in this thesis appears to conform more closely with the test results than the Heaviside approximation does. Further testing is required, however, to confirm this observation.

2.5 Load Identification of Uniformly Distributed Loads on Euler-Bernoulli Beams with Rotational Stiffness at Supports

2.5.1 Introduction and Literature Review

Often the problem of modelling moving vehicular mass is approximated as a moving force problem. The moving force problem is an appropriate approximation to the moving mass problem, under certain conditions [73]. One of the major shortcomings of modelling moving vehicles on structures as moving forces, though, is that often local impacts and interaction forces between the vehicle and the structure are neglected, and the magnitude of the moving load is assumed to be constant [74]. In order to account for dynamic effects, normal practice has been to apply a single dynamic amplification factor to the complete response, so that *peak* theoretical stresses match measured stresses. Clearly this is a gross oversimplification. As early as 1934, Ingliss [16] noted that simply multiplying static loads by a single dynamic amplification factor is unsatisfactory. Ayre, Ford and Jacobsen [38], in 1950, argued that large dynamic stresses due to velocity alone, (such as those resulting at resonance) are generally not to be expected for structures under normal conditions. Others, since, have also suggested that a single overall amplification of dynamic response, from increased speed for example, is generally not to be expected [20, 32, 53]. Instead, large dynamic stresses are more likely to arise from local impacts. In order to overcome the simplification of a single amplification factor, attempts are often made to instead model both the moving vehicle and the structure, so the significant effects of interaction between the vehicle and structure are included, although this greatly increases the difficulty of the problem. A number of attempts have been made to resolve the difficult interaction problem by modelling both the structure and the vehicle dynamic model. Hino, Yoshimura, Konishi and Ananthanarayana [21] use the finite element technique to model the interaction

between a vehicle and a concrete bridge across the River Brahmaputra in India. Wang, Huang, Shahawy and Huang [22], Green and Cebon [23] and Fafard, Laflamme, Savadr and Bennur [24] model the interaction between highway bridges and vehicles, while Zhai and Cai [25] and Delgado and Santos [26] model the interaction between vehicles and rail, and vehicles and railway bridges.

A potential alternative to the use of a single dynamic amplification factor or the use of complicated vehicle-structure interaction models, is to use measured or identified transient interaction forces in loads modelling. A number of methods for identifying equivalent static axle loads from measured bridge response have been developed [75-81], however equivalent static axle loads from measured response again tend to neglect the dynamic component of the applied loads. A better method is to measure the complete transient load, which fully represents the dynamic nature of the applied load and its interaction with the structure. Theoretically, one option for measuring the transient forces applied to a structure is to measure the forces at the moving source. In the case of railway bridge structures, this would mean measuring the interaction forces at the wheels or axles of many or all types of rolling stock, which cross a particular bridge. This may be an expensive and impractical solution. Another option is to measure the response of the structure and to identify the applied loads of many or all types of rolling stock from the structure itself. In the last twenty years a good deal of work has been undertaken and presented for the identification of dynamic loads from the structural response of beams and bridges.

In 1984 Doyle [82] identified force histories from strain measurements in the time domain for a slender beam. Force histories were not generated by a moving load but,

instead, by a load of varying magnitude at a fixed location. In that same year Doyle [83] identified force histories in the frequency domain. Again in 1984, Hillary and Ewins [84] carried out force identification on a uniform cantilever beam, using strain gauges and accelerometers, noting that strain gauges gave more suitable results. In 1987 Stevens [85] published a very helpful overview of the force identification problem. He described a system as its own force sensor, i.e. that forces may be identified from system response. In theory, the usual procedure, where response is predicted from a known load, is simply reversed and instead an unknown load is found from a known (or measured) response. The force identification problem may be considered, then, the 'inverse' of the more traditional problem, where an unknown response is found from known loads, although in order to identify the magnitudes of loads from structural response a complete knowledge of the system is necessary. Stevens noted in his research that force identification for distributed loads has received little attention. In 1987 Hoshiya and Maruyama [86] published a technique to identify the dynamic parameters of both a beam and running load, for a simply supported beam. The technique was based largely on the modal superposition of the solution of the equations of motion for a simply supported beam. Solutions were presented for both smooth and rough surfaced beams, subjected to both a running static load and a single degree of freedom, damped spring-mass system. The paper ended with the hope that the procedure may be able to be developed for continuous systems under traffic load. In 1988 O'Connor and Chan [87, 88] published two papers investigating the identification of wheel loads from bridge strains. One of these papers outlined laboratory tests whereby loads of known transient magnitudes were applied at four fixed locations on a simply support beam. Loads were applied via two hydraulic actuators; each fitted with a simply supported spreader beam. O'Connor and Chan

noted that errors in the identified loads were great where the loads were near the supports. They also noted that strain response was better than displacement response, in terms of matching measured loads to known applied loads. In conclusion they suggest that by using bridge measurements, reasonable estimates of dynamic wheel loads during the passage of service vehicles should be obtainable. The other of the two papers published by these authors in 1988 set out to study bridge measurements to determine the static component of a moving load and the dynamic variation around the static component of that load. They concluded that load identification and measurement should be possible from structural response. In 1997 Law, Chan and Zeng [47] developed the theory of moving force identification in the time domain further. They used the superposition method to identify forces in the time domain for a simply supported beam. Accelerations and/or bending moments were used for beam response on this occasion. The theory was demonstrated for up to two moving loads, noting that the sensitivity to noise is greater where more than one load is identified. Curve fitting was used to match mode shapes of theoretical models, used in load identification, to measured mode shapes. Only the first three mode shapes were used in the modal superposition with the conclusion that it is possible to use measured structural response to identify moving forces in the time domain. In the concluding remarks of their paper, they suggested that the technique would be computationally expensive for multiple loads.

Force identification from the response of prestressed concrete bridges is the topic of more recent research using this approach [89]. For prestressed concrete bridges the equations of motion for a simply supported beam are summed with an axial compressive force in order to include prestressing forces. It is suggested that the mode

shapes are not significantly affected by the prestressing forces, with reference to work by Saiidi [90]; speed of the moving loads does not affect the accuracy of the force identification and just the first two modes are considered. Only the middle 80% of the measured response was used, due to the problem of large load spikes when any axle enters or leaves the span. This is the same problem identified earlier in the work of O'Connor and Chan [87]. The conclusion of work on prestressed concrete bridges is that input forces can be exactly recovered from simulated bridge response where no noise, either internal (instrument) or external (e.g. radio wave), is present. Chan, Law and Yung continued work on moving load identification on prestressed concrete bridges in 2000 [91]. A series of load identification methods are reviewed in their research, with the time domain method, used in almost all papers referenced above, deemed the best method for moving load identification. An existing prestressed concrete bridge was tested using thirty-five strain gauges on five parallel longitudinal concrete girders; seven on each girder. Seven sets of five strain gauges were set up in parallel, to measure the total bending moment at seven positions on the span. Only the middle 60% of the identified loading was used, with at least one test failing due to variable speed in the input load.

As a rule, the research carried out to date on load identification has focused on simply supported beam structures subjected to moving point loads. An exception to that rule is the most recent work by Chan et al. [89,91] who, while still studying beams subject to moving point loads, studied a beam which varies from simply supported conditions in that it includes a prestressing component. It was noted in the literature review above that load identification of distributed loads has received little attention. An attempt is made in the research presented herein, using the analytical model of Section 2.4, to

identify loads for many moving loads with a uniformly distributed contact patch on non-simply supported beam structures.

2.5.2 Review of Load Identification Theory

The following review of load identification theory is essentially a summary and explanation of the work presented by Law, Chan and Zeng, for identification of concentrated loads from simply supported structural response [47].

Consider the simply supported Euler-Bernoulli beam, subjected to a concentrated load of variable magnitude, travelling at constant velocity, shown in Figure 2.5.1.

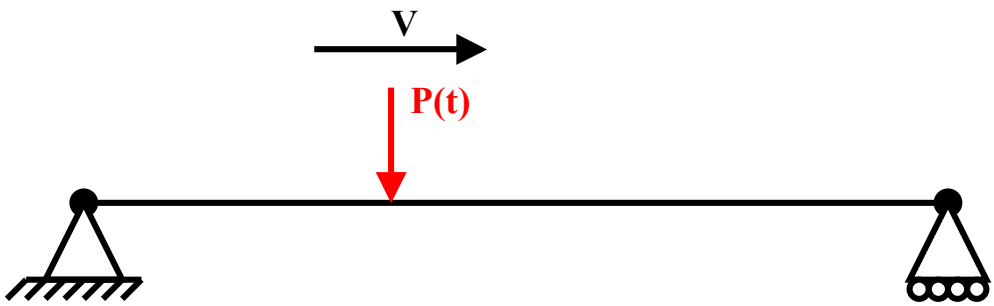

Figure 2.5.1. Concentrated load on a Euler-Bernoulli beam, with simply supported end conditions.

The dynamic equations of motion for that beam may be written,

$$\overline{m}\frac{\partial^2 v(x,t)}{\partial t^2} + \overline{c}\frac{\partial v(x,t)}{\partial t} + EI\frac{\partial v^4(x,t)}{\partial x^4} = p(t) \qquad (2.5.1)$$

After uncoupling the equations by modal decomposition, the equations of motion of the system may be written as a set of uncoupled single degree of freedom systems; as shown in Equation (2.5.2).

$$\ddot{\xi}_i + 2\zeta_i \omega_i \dot{\xi}_i + \omega_i^2 \xi_i = \frac{1}{m_i} p_i(t) \tag{2.5.2}$$

Using modal superposition, the dynamic deflection $v(x,t)$ may be written,

$$v(x,t) = \sum_{i=1}^{\infty} \xi_i(t)\phi_i(x) \tag{2.5.3}$$

where $\phi_i(x)$ is the mode shape function, $\sin\left(\frac{i\pi x}{l}\right)$ for a simple supported beam, and $\xi_i(t)$ is the modal displacement.

$\xi_i(t)$ may be found via the Duhamel integral,

$$\xi_i(t) = \frac{1}{m_i \omega_{iD}} \int_0^t e^{-\zeta_i \omega_i (t-\tau)} \sin[\omega_{iD}(t-\tau)]\sin(\Omega\tau) P(\tau) d\tau \tag{2.5.4}$$

For identification of a load of varying magnitude, the Duhamel integral is discretised and the concentrated load $P(t)$ is assumed to be a step function in a small time interval, Δt, that is, an impulse load of magnitude $P(t)$, for duration of Δt. Following the method proposed by Law et al [47], the equation is rewritten in discrete terms as

$$\xi_{ik}(t) = \frac{1}{m_i \omega_{iD}} \sum_{j=0}^{k} e^{-\zeta_i \omega_i (k-j)\Delta t} \sin\left[\omega_{iD}(k-j)\Delta t\right] \sin(\Omega j \Delta t) P(j) \Delta t \qquad (2.5.5)$$

$$k = 0, 1, 2, ..., N$$

where N+1 is the number of sample points,

j is the number of each time step included in the summation, which ranges from 0 to k, and

k is the number of the running time step.

At time $k\Delta t$, i.e. at the kth time step, the modal displacement response is found from the Equation (2.5.5) summation. The velocity dependent term is, of course, Ω where:

$$\Omega = V\lambda^{\frac{1}{4}}$$
$$= \frac{i\pi V}{L} \qquad \text{for a simply supported beam.}$$

Substituting Equation (2.5.5) into Equation (2.5.3) yields

$$v(x,t) = \sum_{i=1}^{\infty} \frac{\sin\left(\frac{i\pi x}{l}\right)}{m_i \omega_{iD}} \sum_{j=0}^{k} e^{-\zeta_i \omega_i (k-j)\Delta t} \sin\left[\omega_{iD}(k-j)\Delta t\right] \sin(\Omega j \Delta t) P(j) \Delta t \qquad (2.5.6)$$

The dynamic moment may be easily found from Equation (2.5.7).

$$M(x,t) = -EI \frac{\partial^2 v(x,t)}{\partial x^2} \qquad (2.5.7)$$

and is

$$M(x,t) = EI \sum_{i=1}^{\infty} \left(\frac{i\pi}{l}\right)^2 \frac{\sin\left(\frac{i\pi x}{l}\right)}{m_i \omega_{iD}} \sum_{j=0}^{k} e^{-\zeta_i \omega_i (k-j)\Delta t} \sin\left[\omega_{iD}(k-j)\Delta t\right] \sin(\Omega j \Delta t) P(j) \Delta t \qquad (2.5.8)$$

From the equation for the dynamic moment, the step to bending stress is of course straightforward by substituting Equation (2.5.8) into Equation (2.5.9).

$$\sigma_B = \frac{My}{I} \tag{2.5.9}$$

For a single moving load, if the system characteristics are completely known and the bending stresses known from measured response, the magnitude of the applied load may be found for the complete time history by $[\sigma] = [f] \times [P]$, where, for simplicity, f represents the complete function that is multiplied by the applied load to generate stress, i.e.,

$$\begin{bmatrix} \sigma_B(x,0) \\ \text{M} \\ \text{M} \\ \text{M} \\ \sigma_B(x,N) \end{bmatrix} = Ey \sum_{i=0}^{\infty} \left(\frac{i\pi}{l}\right)^2 \sin\left(\frac{i\pi x}{l}\right)\left(\frac{\Delta t}{\omega_{iD}}\right)$$

$$\times \begin{bmatrix} 0 & 0 & \Lambda & \Lambda & 0 \\ 0 & 0 & \Lambda & \Lambda & 0 \\ 0 & \sin(\Omega\Delta t(1))e^{-\zeta\omega\Delta t(1)}.\sin(\omega_{iD}\Delta t(1)) & 0 & \Lambda & 0 \\ \text{M} & \text{M} & \text{M} & \text{M} & \text{M} \\ 0 & \sin(\Omega\Delta t(1))e^{-\zeta\omega\Delta t(N-1)}\sin(\omega_{iD}\Delta t(N-1)) & \Lambda & \Lambda & \sin(\Omega\Delta t(N))e^{-\zeta\omega\Delta t(N-N)}\sin(\omega_{iD}\Delta t(N-N)) \end{bmatrix}$$

$$\times \begin{bmatrix} P(0) \\ \text{M} \\ \text{M} \\ \text{M} \\ P(N) \end{bmatrix}$$

(2.5.10)

This may be rewritten $[P]=[f]^{-1}\times[\sigma]$, i.e.,

$$\begin{bmatrix} P(0) \\ \text{M} \\ \text{M} \\ \text{M} \\ P(N) \end{bmatrix} = Ey\sum_{i=1}^{\infty}\left(\frac{i\pi}{l}\right)^2 \sin\left(\frac{i\pi x}{l}\right)\left(\frac{\Delta t}{\omega_{iD}}\right)$$

$$\times\begin{bmatrix} 0 & 0 & \Lambda & \Lambda & 0 \\ 0 & 0 & \Lambda & \Lambda & 0 \\ 0 & \sin(\Omega\Delta t(1))e^{-\zeta\omega\Delta t(1)}\sin(\omega_{iD}\Delta t(1)) & 0 & \Lambda & 0 \\ \text{M} & \text{M} & \text{M} & \text{M} & \text{M} \\ 0 & \sin(\Omega\Delta t(1))e^{-\zeta\omega\Delta t(N-1)}\sin(\omega_{iD}\Delta t(N-1)) & \Lambda & \Lambda & \sin(\Omega\Delta t(N))e^{-\zeta\omega\Delta t(N-N)}\sin(\omega_{iD}\Delta t(N-N)) \end{bmatrix}^{-1}$$

$$\times\begin{bmatrix} \sigma_B(x,0) \\ \text{M} \\ \text{M} \\ \text{M} \\ \sigma_B(x,N) \end{bmatrix} \qquad (2.5.11)$$

Equation (2.5.11) is condensed, removing the rows and column made up of entirely zeros, before solving.

In this project, the method proposed by Law, Chan and Zheng [47] was verified by identifying the magnitude of a single, moving, concentrated load of variable magnitude, travelling at constant velocity on a simply supported beam. A modal displacement response curve was generated for a known variable magnitude load using the central finite difference method for the first mode of the beam. The magnitude of the load was then identified using the method proposed by Law et al and the identified load compared to the known applied load. The conditions under which the curve was generated are given in Table 2.5.1; the displacement response curve is shown in Figure 2.5.2. The time varying magnitude of the identified load is compared to the time varying magnitude of the applied load in Figure 2.5.3.

Area	3.33×10^{-02} m^2
Mass density	7.85×10^{03} kg m^3
Length	5 m
Position of Measurement	2.5 m
Damping Ratio	0.1
Velocity	5 m s^{-1}
Circular Frequency	28.760 rad s^{-1}
Damped Frequency	28.616 rad s^{-1}
Modal Mass	6.54×10^{02} kg
Time step	5.00×10^{-03} s

Table 2.5.1. Conditions under which the curve shown in Figure 2.5.3 was generated.

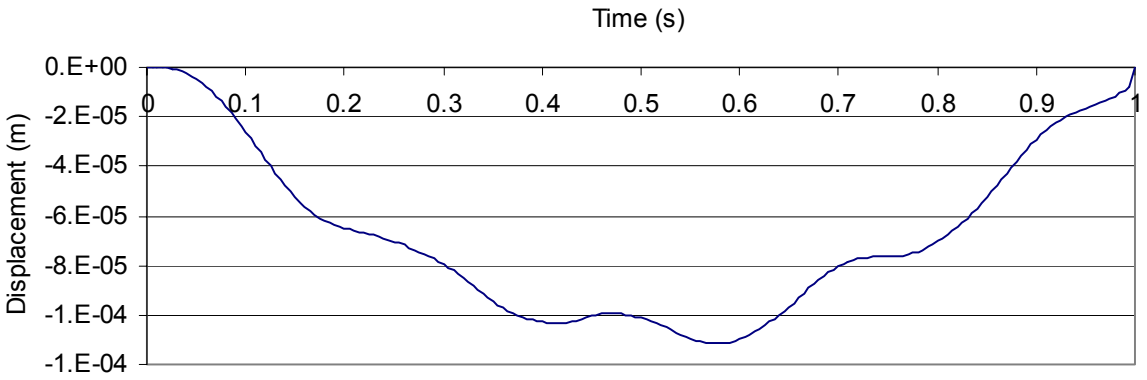

Figure 2.5.2. Displacement response curve generated under the conditions described in Table 2.5.1.

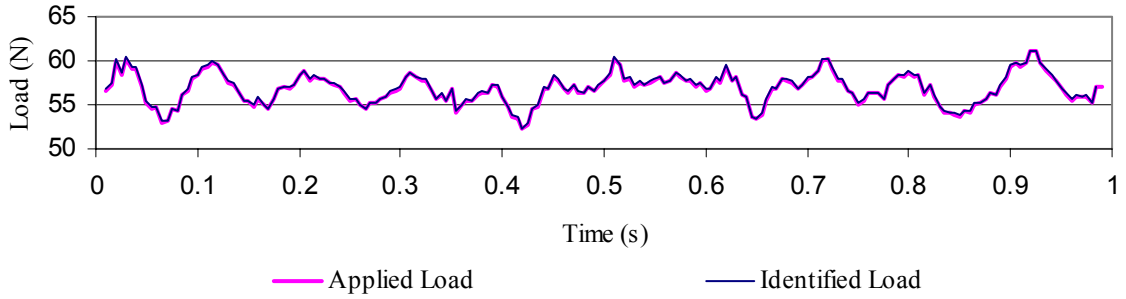

Figure 2.5.3. Comparison of applied load and identified load.

From Figure 2.5.3, for the modal displacement response curve shown in Figure 2.5.2, for the conditions described in Table 2.5.1, the time varying magnitude of the identified load is identical to the time varying magnitude of the applied load.

Using the method outlined above, loads are assumed to act in a vertical direction. This assumption appears appropriate for the purposes of the present research.

In practice, for load identification to be reliable, there must be at least as many equations as there are unknowns, i.e. at least as many measurement sources (strain gauges in the case of this research) as there are applied loads (wheel loads).

2.5.3 Load Identification of Uniformly Distributed Loads on Euler-Bernoulli Beams with Rotational Stiffness at Supports

In theory, the extension of the above work to the identification of uniformly distributed loads (rather than concentrated loads), on Euler-Bernoulli beams with rotational stiffness at supports (rather than simply supported end conditions), is relatively straightforward, given the work presented in Section 2.4 of this thesis. Load identification of uniformly distributed loads on beams with general end conditions (Figure 2.5.4), follows the same theory as simply supported beams subjected to concentrated loads, with the exception that the mode shape function and the equation for the modal displacement vary.

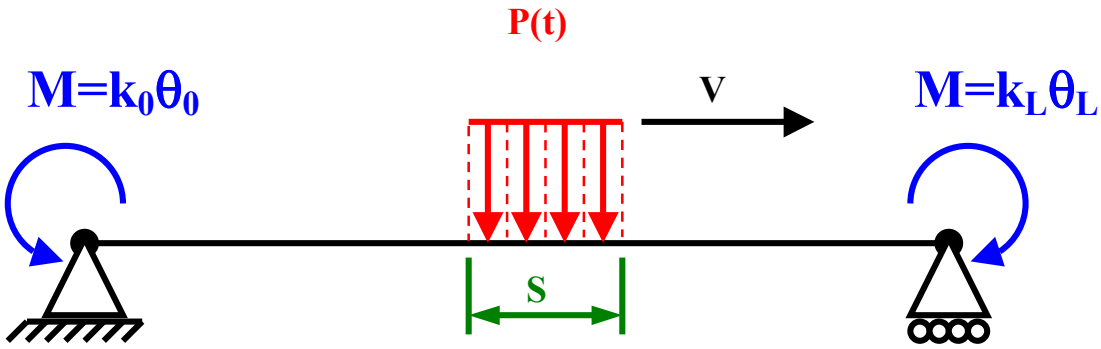

Figure 2.5.4. A single moving uniformly distributed load on a Euler-Bernoulli beam, with rotational stiffness at supports.

For a Euler-Bernoulli beam with rotational stiffness at supports, subjected to moving uniformly distributed loads, the Duhamel Integral, from Section 2.4, is,

$$\xi_i = \frac{1}{m_i \omega_{iD}} \int_0^t \int_0^{Vt} e^{-\zeta_i \omega_i (t-\tau)} \sin[\omega_{iD}(t-\tau)] P(\tau) \bullet \gamma\left(C_1(s)\cos(\Omega\tau) - C_2(s)\cosh(\Omega\tau) - C_3(s)\sin(\Omega\tau) + C_4(s)\sinh(\Omega\tau)\right) ds\, d\tau \tag{2.5.12}$$

for $0 \le t \le \frac{S}{V}$,

$$\xi_i = \frac{1}{m_i \omega_{iD}} \int_0^t \int_0^{S} e^{-\zeta_i \omega_i (t-\tau)} \sin[\omega_{iD}(t-\tau)] P(\tau) \bullet \gamma\left(C_1(s)\cos(\Omega\tau) - C_2(s)\cosh(\Omega\tau) - C_3(s)\sin(\Omega\tau) + C_4(s)\sinh(\Omega\tau)\right) ds\, d\tau \tag{2.5.13}$$

for $\frac{S}{V} \le t \le \frac{L}{V}$,

$$\xi_i = \frac{1}{m_i \omega_{iD}} \int_0^t \int_{Vt-L}^{S} e^{-\zeta_i \omega_i (t-\tau)} \sin[\omega_{iD}(t-\tau)] P(\tau) \bullet \gamma\left(C_1(s)\cos(\Omega\tau) - C_2(s)\cosh(\Omega\tau) - C_3(s)\sin(\Omega\tau) + C_4(s)\sinh(\Omega\tau)\right) ds\, d\tau \tag{2.5.14}$$

for $\frac{L}{V} \le t \le \frac{L+S}{V}$,

where $C_1(s), C_2(s), C_3(s)$ and $C_4(s)$ are functions of the distance along the distributed load, s:

$$C_1(s) = \cos\left(s\lambda^{\frac{1}{4}}\right) + \alpha \sin\left(s\lambda^{\frac{1}{4}}\right)$$

$$C_2(s) = \cosh\left(s\lambda^{\frac{1}{4}}\right) + \beta \sinh\left(s\lambda^{\frac{1}{4}}\right)$$

$$C_3(s) = -\sin\left(s\lambda^{\frac{1}{4}}\right) + \alpha \cos\left(s\lambda^{\frac{1}{4}}\right)$$

$$C_4(s) = \sinh\left(s\lambda^{\frac{1}{4}}\right) + \beta \cosh\left(s\lambda^{\frac{1}{4}}\right)$$

$$\Omega = \left(V\lambda^{\frac{1}{4}}\right)$$

In order to use the method proposed by Law et al, for load identification of the time varying magnitude of a variable magnitude distributed load on a beam with rotational stiffness at supports, the modal force must be integrated before the Duhamel Integral is discretised.

The time varying magnitude of a variable magnitude distributed load, on a beam with rotational stiffness at supports, is identified using the same method as was used for concentrated loads, in Equation (2.5.11). The only changes from Equation (2.5.11), for a distributed load on a beam with rotational stiffness at supports, are in the mode shape equation and the modal displacement equation. For a distributed load on a beam with rotational stiffness at supports, Equation (2.4.4) defines the mode shape and Equations (2.5.12), (2.5.13) and (2.5.14) define the modal displacement. Figure 2.5.5 presents a schematic representation of the lower triangular matrix represented as f in Section 2.5.2, showing the arrangement of Equations (2.5.12), (2.5.13) and (2.5.14) within the matrix.

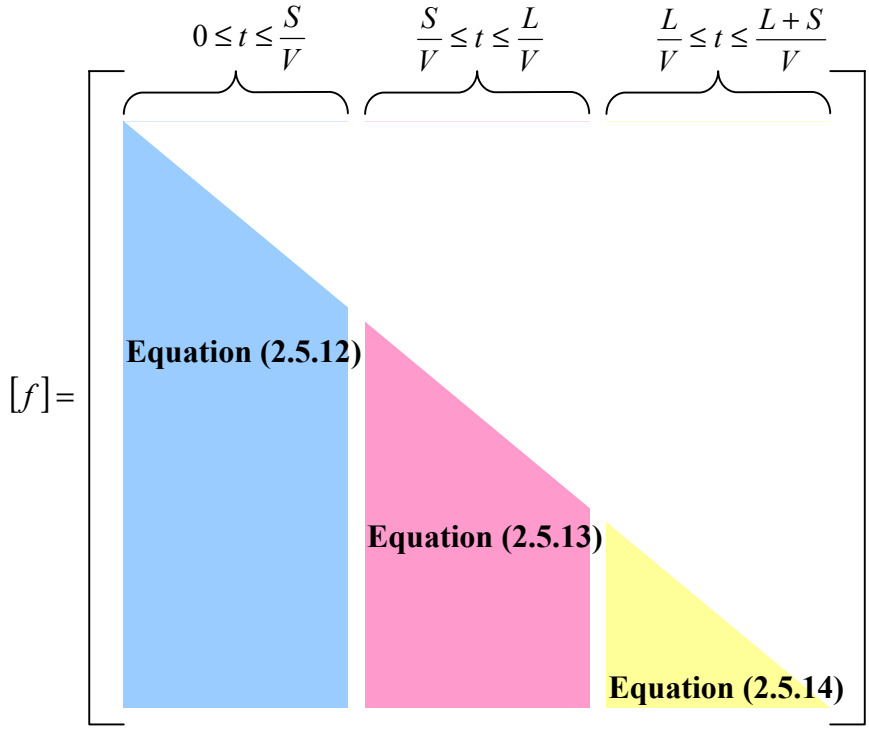

Figure 2.5.5. A schematic representation of the lower triangular matrix represented as *f* in Section 2.5.2, showing the arrangement of Equations (2.5.12), (2.5.13) and (2.5.14) within the matrix.

The extension of the method proposed by Law et al was verified by identifying the magnitude of a single, moving, distributed load of variable magnitude, travelling at constant velocity on a beam with rotational stiffness at supports. A modal displacement response curve was generated for a known variable magnitude load using the central finite difference method for the first mode of the beam. The magnitude of the load was then identified using the extension of Law et al's work outlined above and the identified load was compared to the known applied load. The conditions under which the curve was generated are given in Table 2.5.2; the displacement response curve is shown in Figure 2.5.6. The time varying magnitude of the identified load is compared with the time varying magnitude of the applied load in Figure 2.5.7.

Area	3.33×10^{-02} m^2
Mass density	7.85×10^{03} kg m^3
Length	6.81 m
Position of Measurement	1.75 m
Damping Ratio	0.1
Velocity	8.50 m s^{-1}
Circular Frequency	50 rad s^{-1}
Damped Vibration Frequency	49.7 rad s^{-1}
Contact Patch Length	1.70 m
γ	7.35×10^{-102}
α	-1.34×10^{101}
β	7.60×10^{98}
Time Step	5.00×10^{-03} s
Modal Mass	8.85×10^{02} kg

Table 2.5.2. Conditions under which the curve shown in Figure 2.5.6 was generated.

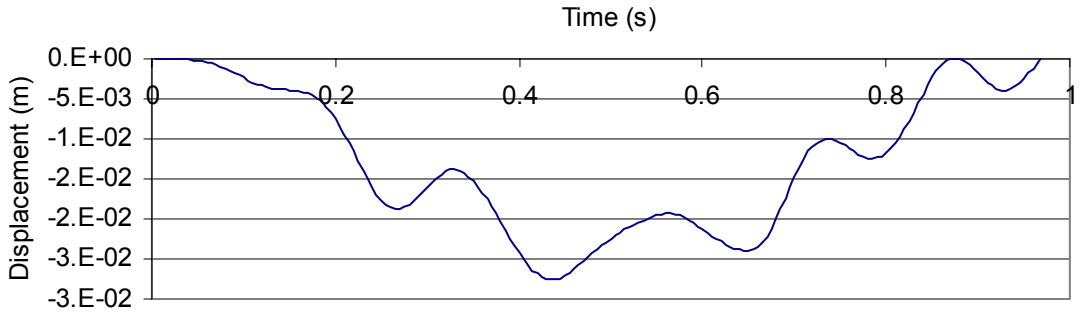

Figure 2.5.6. Displacement response curve generated under the conditions described in Table 2.5.2.

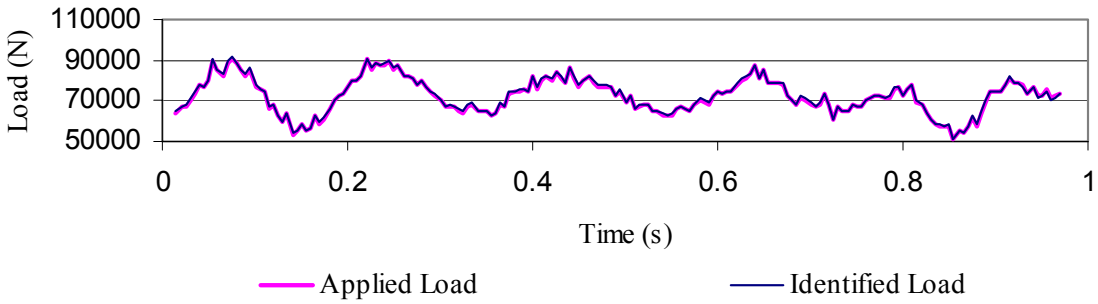

Figure 2.5.7. Comparison of applied load and identified load.

From Figure 2.5.7, for the modal displacement response curve shown in Figure 2.5.6 for the conditions described in Table 2.5.2, the time varying magnitude of the identified load is identical to the time varying magnitude of the applied load.

The theory may be extended further for multiple loads, using the linear superposition principal. This is outlined, for concentrated loads on a simply supported beam, in [47].

Again it is a simple extension to solve for multiple uniformly distributed loads on beams with rotational stiffness at supports, by using the mode shape function and modal displacement equation derived in Section 2.4. As was noted in the literature review however, the identification of multiple loads becomes computationally expensive. For the identification of the magnitude of a *single* moving time varying load, using the method described in Section 2.5.2 and 2.5.3, the matrix denoted *f* must be inverted and multiplied by the measured response, for each mode. The size of this square matrix is equal to the number of time steps required for accurate load identification. This matrix has the potential to be very large. For multiple loads, the matrix size is larger again, to account for the distance between the loads.

2.5.4 An Approximate Method for Load Identification of Multiple Moving Loads

Despite the significant work carried out over the last 20 years the use of load identification theory in practice, for multiple moving loads, remains difficult. As was identified in the literature review of Section 2.5.1, and noted above in Section 2.5.3, the identification of multiple loads is computationally expensive. For a bridge traversed by rolling stock, with many axles, load identification using the theory presented in Section 2.5.2 and 2.5.3, is unfeasible. To overcome this, a simplified approximate method has been used in this project, with the acknowledgement that more research is needed. Details for the simplified approximate method are given below.

As was noted in the literature review, a thorough knowledge of the system is required if load identification is to be successful and reliable [85]. System parameters are found for simply supported beams by correcting system parameters through curve fitting analytical response to measured response [47]. So too in this research and the method presented here for uniformly distributed loads on beams with general end conditions, system parameters, which are first estimated from structural drawings and site inspections, are corrected by curve fitting to measured response. The process of correcting to measured response has already been outlined in Section 2.2. In order to correct system parameters the usual 'forward' problem is solved. That is, traffic of known load travel across the span at a slow speed, to minimise dynamic interaction. The structural response is measured at a number of locations and the system parameters of the analytical solution are 'tuned' until the predicted response to known quasi-static loads matches the measured response. Once the system parameters are defined, loads may be identified from the measured structural response of the bridge subjected to normal traffic by solving the 'inverse' problem.

In the simplified approximate method proposed here, the measured response is discretised, replacing the time domain with a series of points, at an appropriate time step. The equivalent *static* load that would cause the measured displacement is then identified, at each time step, j. This is relatively straight forward, since for a static load the magnitude of the applied load may be separated from the remainder of the modal displacement equation (see modal displacement equations in Section 2.4) and may then be represented by Equation (2.5.15).

$$\xi_i(t)_j = P_j\, h_i(t)_j \tag{2.5.15}$$

For a single moving load, the equivalent *static* load that would cause the measured displacement at each time step, j, is easily identified from Equation (2.5.16).

$$P_j = \frac{v(x,t)_j}{\sum_{i=1}^{\infty} \phi_i(x)\, h_i(t)_j} \tag{2.5.16}$$

Equation (2.5.17) is solved at each time step in order to identify the magnitude of multiple moving loads, using the method proposed here.

$$\left[P(t)_1 \quad \Lambda \quad P(t)_n\right]_j = \sum_{i=1}^{\infty} \phi_i(x) \times \begin{bmatrix} h_i(t)_{11} & \Lambda & h_i(t)_{1n} \\ \mathrm{M} & & \mathrm{M} \\ h_i(t)_{m1} & \Lambda & h_i(t)_{mn} \end{bmatrix}_j^{-1} \times \left[v(x,t)_1 \quad \Lambda \quad v(x,t)_m\right]_j \tag{2.5.17}$$

where i = mode number,

j = number of each time step,

m = number of measurement sources, and

n = number of applied loads.

Note again that in practice, for load identification to be reliable, there must be at least as many equations as there are unknowns, i.e. at least as many measurement sources (strain gauges in the case of this research) as there are applied loads (wheel loads). In other words,

$$m \geq n$$

For the identification of multiple loads using the simplified approximate method proposed here, the largest matrix size required is square, with dimensions equal only to the number of applied loads to be identified. This requires much less computational expense than the method outlined in Sections 2.5.2 and 2.5.3 and is, therefore, more feasible for use with multiple moving loads

The proposed simplified approximate method is demonstrated below for a single, moving, distributed load of variable magnitude, travelling at constant velocity on a beam with rotational stiffness at supports. A modal displacement response curve was generated for a known variable magnitude load using the central finite difference method for the first mode of the beam. The magnitude of the load was then identified using the method proposed here and the identified load compared to the known applied load. The conditions under which the curve was generated are given in Table 2.5.3; the displacement response curve is shown in Figure 2.5.8. The time varying magnitude of the identified load is compared to the time varying magnitude of the applied load in Figure 2.5.9.

Area	3.33×10^{-02} m^2
Mass density	7.85×10^{03} kg m^3
Length	6.81 m
Position of Measurement	1.75 m
Damping Ratio	0.1
Velocity	8.50 m s^{-1}
Circular Frequency	345.000 rad s^{-1}
Damped Vibration Frequency	343.271 rad s^{-1}
Contact Patch Length	1.70 m
γ	7.35×10^{-102}
α	-1.34×10^{101}
β	7.60×10^{98}
Time Step	5.00×10^{-03} s
Modal Mass	8.85×10^{02} kg

Table 2.5.3. Conditions under which the curve shown in Figure 2.5.8 was generated.

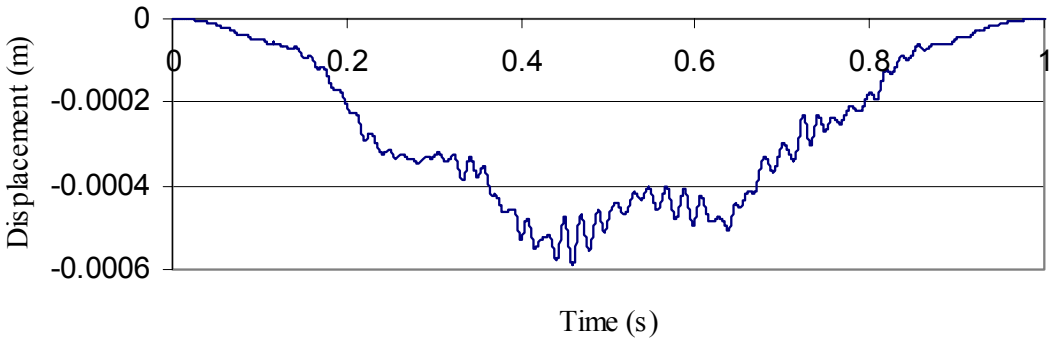

Figure 2.5.8. Displacement response curve generated under the conditions described in Table 2.5.3.

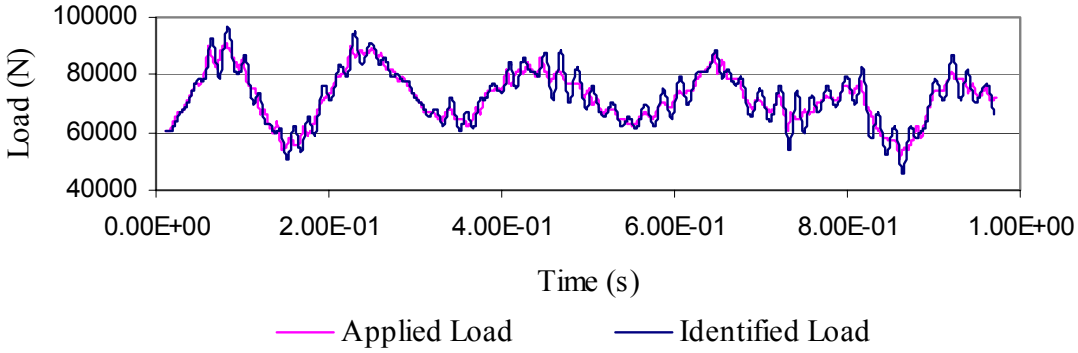

Figure 2.5.9. Comparison of applied load and identified load.

From Figure 2.5.9, for the modal displacement response curve shown in Figure 2.5.8, for the conditions described in Table 2.5.3, the time varying magnitude of the identified load is similar to the time varying magnitude of the applied load, though not identical. The identified load tends to over estimate the magnitude of identified load spikes. This is expected, since the dynamic amplification factor is ignored, using the simplified approximate method proposed here, and the equivalent *static* load that would cause the measured displacement is identified at each time step.

Since, in this project, the goal is to reproduce a measured response rather than to identify loads for the sake of load identification itself, this is not of great concern. Measured responses may be reliably reproduced, using loads identified from the method proposed here, if the damping of the structure, on which the identified loads are applied, is increased to account for the effect of the over estimated load spikes. This is demonstrated in Figure 2.5.10. Figure 2.5.10 compares the original modal displacement curve with damping 10% of critical, shown in Figure 2.5.8, with a modal displacement response curve with damping 50% of critical, generated from the

identified loads shown in Figure 2.5.9. Both response curves are generated using the central finite difference method for the first mode of the beam.

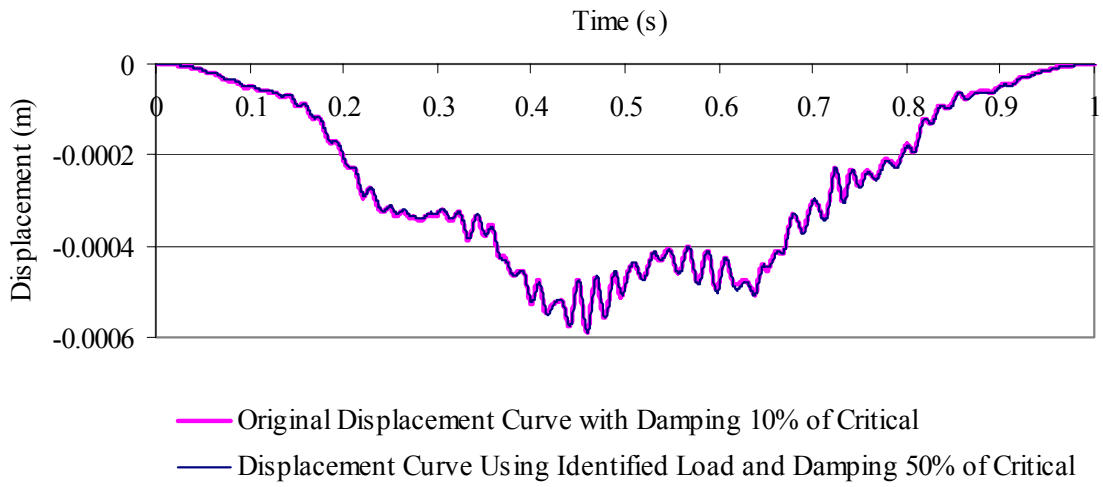

Figure 2.5.10. Comparison of original displacement curve with the response reproduced using identified loads.

From Figure 2.5.10, the modal displacement response curve with damping 50% of critical, generated from the identified loads is identical to the original modal displacement curve with damping 10% of critical.

A second difficulty encountered in load identification occurs when loads are applied near beam or bridge supports. In almost the entire recent research, large unrealistic load spikes are identified near supports. This is due to the fact that near supports both noise, and the smallest discrepancy between corrected system parameters and the actual system, can have enormous effects on the values of identified loads. Away from the supports, noise and small discrepancies have a less significant or an insignificant effect on identified loads. To overcome this Chan and others use only the middle 80%, or even 60%, of identified loads [87,89] in their research into load identification on road bridges, and relatively few loads so that loads are not entering or leaving the span, and

therefore not near supports, during measurement. This is not possible in railway bridge assessment. Loads are inevitably and constantly entering or leaving the span. In order to overcome this, a lower and upper bound is used in the method proposed in this thesis to correct identified loads. The error, from correction of the identified loads, is assessed by using the corrected load values in a 'forward' solution, generating a structural response, which is compared against the measured response. If the stress history, from the forward solution using the corrected identified load, closely matches the measured response, the corrected identified load is considered sufficiently accurate. If the error is deemed too great, the upper and lower bounds are adjusted and the response is checked again. Section 3.5 demonstrates the method for loads identified from measured response. Since, in this project, the goal is to reproduce a measured stress rather than to identify loads for the sake of load identification itself, using an upper and lower bound on identified loads appears suitable.

While the method proposed here is not ideal and, as was acknowledged earlier, more research is needed, the comparison of Figure 2.5.10 and the results shown later in Chapter 3 demonstrate that the simplified approximate method gives reasonably accurate results.

2.6 Duty Cycle Loading Schedule Development

2.6.1 Introduction

In this section, the principles for developing duty cycle loading schedules for fatigue assessment are outlined. A detailed case study load schedule is presented in Section 3.6.

Gathering data for the development of a duty cycle loading schedule is a difficult and time-consuming task. However, accurate assumptions of loading history are essential for the reliable estimation of remaining life. Typical techniques for developing duty cycle loading schedules are presented in a number of papers, some of the best of these include papers by Grundy [92] and Bruestle and Prucz [93]. In this research a somewhat traditional approach, essentially equivalent to that used by Grundy [92] and Bruestle and Prucz [93], has been followed, for the development the loading history for the Mullet Creek Railway Bridge.

1. Identify Potential Sources of Loading
2. Identify Loading History from those Sources
3. Simplify Loading into Representative Units
4. Clearly Document Loading History, Reference Information Sources and Outline Assumptions and Uncertainties

2.6.2 Identify Potential Sources of Loading

Development of a duty cycle for a given structure requires an understanding of the history of not only the structure itself, but also of the industry and development of the region around it. Historical information may be gathered from usual archival sources,

such as local and state libraries and state archives. Literature searches should be broad enough to include government and private reports and papers, such as environmental impact statements etc., which give a good indication as to the growth and development of the region. Old maps are a good way to identify potential sources of loading, since these may identify industries which have operated, often for considerable periods contributing greatly to loading, but which have since closed down.

Local knowledge is invaluable and potentially the best source of historical information. The current trend is for both commercial and government organisations to be particularly guarded regarding the sharing of information and, in some cases, to destroy all records after a given period, for example, seven years. Historical societies and the contacts they are able to provide to individuals who may be employed or have had previous employment in various industries, can provide some of the best historical data. This is particularly useful where the industry has since closed down.

2.6.3 Identify Loading History from Those Sources

With potential sources of loading identified, the challenge of developing a loading history from those sources begins. Historical societies may offer a great deal of information, but in the experience of this project, the best source of information are contacts within the various industries. Often where one company is unwilling or unable to divulge information regarding its activities, a representative of a competitor company or service company may. The Internet offers a wealth of information and it is generally easily accessible. The challenge when using information from the Internet is not so much accessing information as determining which information is reliable and

useful. Many Internet sites were explored during this project, the most useful are listed in Chapter 3.

Eventually, after an arduous process of searching, communication and diplomacy, a reliable estimate of the loading history from the various identified sources may be developed. This will include a number of assumptions, which should be faithfully recorded. The loading history is best defined in terms of loading (axle loading and spacing for this case) and frequency (number of passes over the bridge). Representative speeds and directions of travel are also important.

2.6.4 Simplify Loading into Representative Units

By now a vast amount of information will have been gathered. Loading will be made up of countless configurations of locomotives, freight wagons and passenger trains and carriages. For a useful loading history, this information needs to be sorted into a set of representative units. The decision of how many representative units should be used and how information may best be sorted, will be based a great deal on experience and judgement. Given that the decision is to some extent arbitrary it is very important that assumptions are clearly documented.

2.6.5 Clearly Document Loading History, Reference Information Sources and Outline Assumptions and Uncertainties

As noted above, clear documentation is very important. The development of a historical duty cycle loading schedule, as we know it, is largely subjective. It is based on the recollection of those who provide information, the faithfulness of those who have documented data over the years, and it relies on the assumptions the engineer

compiling the duty cycle loading schedule makes. People's perceptions therefore have the potential to impact greatly the assumed loading history that makes up the basis of fatigue assessment. Clarity in referencing sources used, transparency in the assumptions made and honesty in citing identified uncertainties, will provide a platform to an assessment which others may have confidence in. In fatigue assessment confidence is vital.

2.7 Fatigue Assessment Software System and Comparative Study of Stress-Based Structural Fatigue Codes

2.7.1 Introduction and Literature Review

Stress-based fatigue assessment remains the most appropriate method of carrying out assessment on many existing structures, including railway bridges. Indeed, according to Tang and Zhao [94], in a paper presenting a method of relating stress-based fatigue life to reliability, "for fatigue life analysis, the stress-life approach is the most important method to be used in the real world, especially for high cycle fatigue". Fracture mechanics is widely accepted and widely reported in the literature for applications in aerospace, offshore structures and nuclear industries. It is generally not appropriate, though, for assessment of many existing structures, where structural function and loading are generally not knowable with the certainty required for the fracture mechanics philosophy to be useful. Byers et al [27, 28] support this in a two-part review paper on fatigue reliability reassessment applications. In the second volume of their work, fatigue assessment methods for railroad bridges, highway bridges and offshore structures are discussed. For offshore structures, fracture mechanics models are used, while for railroad and highway bridges, stress-based fatigue life predictions relying on assumed loading histories are used.

Although fracture mechanics is often not suitable for structures such as railroad bridges, stressed-based assessment is by no means the only alternative for fatigue assessment. Probability based methods are reported in the literature for the assessment of fatigue reliability of steel bridges [95, 96] using statistical parameters based on available test results. It has been reported that fatigue based reliability may be determined even when the loading of a component is unknown [97], using the

probability approach. This seems to rely heavily on homogeneous conditions for all components, both in terms of structural condition and loading, and assumes failed components both exist and may be removed from service for testing. An integrated approach for determining risk of fatigue is reported by Maragakis and Sandis [98] using probabilistic methods and Monte Carlo simulations. Singh and Koenke [99] also provide a framework for risk assessment in terms of allowable risk and inspection intervals. Work continues on probabilistic risk based approaches for assessment of ageing road bridges based on Weight in Motion data [100]. These methods for fatigue assessment, while useful, tend to be on the fringe in terms of acceptance for use in practice. This is reflected in the fact that most structural fatigue codes and standards tend to use stress-based fatigue assessment.

That stress-based methods remain popular does not mean they are without contention. Almost every step in the stress-based approach has received attention in the literature. Colombi and Dolinski [101] compare cycle counting algorithms for determination of the fatigue lifetime of welded joints under random loading. They argue against the use of the rain flow cycle counting method (which is the most commonly used cycle counting regime in stress-based assessment), in favour of using the cycle sequence counting method, which, according to the authors, takes into account the sequence effect of cycles explicitly. Jones and Hudd [102] consider an alternate (and the authors claim advantageous) method for generating stress-strain curves using a random sequence of cyclic strains, with a pause at each strain reversal. Jones and Hudd don't appear to advocate a change from stress-based codes of practice, but rather use of more accurate stress-strain information in codes. Still considering stress-strain curves, there are recommendations in the literature for the elimination of the fatigue limit in codes of

practice [103], as well as papers by authors who claim to have validated the existence of a fatigue threshold [104]. Miner's rule for damage accumulation is considered non-conservative by Agerskov [105] and Agerskov and Nielson [106]. Liou, et al [107] discuss a number of damage accumulation rules and argue for the use of Morrow's plastic work interaction damage rule, also claiming Miner's rule to be non-conservative. For a relatively thorough survey of cumulative fatigue damage and life prediction theories see the excellent paper by Fatemi and Yang [108].

In much of the literature published reporting the fatigue assessment of existing steel structures using stress-based techniques, almost inevitably, all roads lead to codes and standards. Far more often than not, international fatigue codes are employed to determine remaining life. In many cases codes of practice are adhered to completely for fatigue assessment, once the stress history has been developed from modelling and field testing [30, 31, 32, 34]. On other occasions coded methods are used after S-N curves have been verified by testing. Two interesting examples in the literature are papers by Fryba and Gajdo [109] and Caramelli and Croce [110]. In both papers, real-scale bridge girder specimens are tested in order to verify which S-N curve, taken from Eurocode 3, is suitable for use in fatigue assessment. Despite the significant testing carried out on real-scale specimens, coded procedures are still relied upon for fatigue assessment.

In the present research, whose principal aim is to develop an integrated method for integrity and remaining life assessment of railway bridges, stress-based fatigue assessment methods have been chosen. In keeping with a significant proportion of the reported research, international fatigue code assessment methods have been used.

2.7.2 Fatigue Assessment Software System

A software system has been developed; it is capable of carrying out fatigue assessment via a number of international fatigue codes. The software conducts assessment on digital stress histories and so may be integrated neatly into the overall assessment method developed here. The following codes have been included in the software:

1. British Standard codes BS7608 [111] and
2. BS5400 [112],
3. the English version of the Japanese Society of Steel Construction Fatigue Design Recommendations for Steel Structures code [113],
4. the Association of American Railroads (AAR) code for Fatigue Design of New Freight Cars [114],
5. the American Welding Society (AWS) Structural Welding Code [115],
6. Eurocode (ENV 1993-1-1) [116], and
7. the Austroads Australian Bridge Design Code [117].

A generic assessment method is also included which uses the modified Goodman equation and a user defined S-N curve.

The software is written in C++ and is capable of filtering, cycle counting and sorting a digitised single time varying normal stress history into a user defined stress spectrum. The software carries out assessment on both raw cycles and stress spectrum-adjusted cycles, by each of the eight assessment methods listed above simultaneously, including correction and safety factors at the user's discretion.

To use the software, the user nominates a file from which the digitised stress history is to be read. In this research the intention is that the digitised stress history is generated

in finite element software, although this of course is not a prerequisite for using the software. The user then defines stress spectrum details, such as upper and lower bound and number of intervals, should a stress spectrum be desired. One, some or all of the eight assessment methods are then chosen and the relevant data required by each code is entered. Entered data includes S-N curve details, safety factors, thickness correction factors etc.

Software output options, sent either to disk or screen, include the following,

- a summary of user entered data,
- a list of the filtered stress history which is ultimately used in assessment,
- a presentation of both raw and normalised stress spectra, and
- a numerical value of the number of repetitions to failure for both raw and stress spectra adjusted stress cycles for each assessment method.

An example of the software output, for a short fictitious stress history, is presented in Appendix D.

The software described here has been verified against a series of hand worked solutions.

The source code for the fatigue assessment software system is included as Appendix E.

2.7.3 Comparative Study of Stress-Based Structural Fatigue Codes

According to the reviewed literature, stress-based fatigue codes remain the most popular tools used to predict remaining life. There are however many codes, with differing methods, which often yield significantly different results. There is a need therefore to critically compare key international fatigue codes. At the request of the industry sponsors of this research, a comparative study has been carried out for the seven international codes listed above. This is made up of two parts: a qualitative study (Section 2.7.3.1), which compares the written procedures of each code, as well as a quantitative study (Section 2.7.3.2), which compares numerical fatigue life estimates from each of the codes using a range of stress and structural conditions. The software system detailed in this section has facilitated a numerical comparison of the sensitivity of each of the codes to various parameters, and allowed trends of the relative conservatism of the codes to be identified. In effect the qualitative study considers the theory of the codes and the quantitative study the results of the theory under various conditions. A discussion of the results and some generalised conclusions follow.

This work is not expected to solve all mysteries of stress-based fatigue assessment and declare one method of coded assessment right and all others wrong. It does aim however to compare some of the more popular codes of practice for fatigue assessment that many engineers rely upon. It is anticipated that this will be helpful since "knowledge is the key to reliability" [118]. As a result of the work presented in this thesis a number of comments and changes were recommended to the 2001 Australian Standards Subcommittee whose role it was to discuss and amend the draft Australian Bridge Design Code. These recommendations were made in a private communication made by the author of this thesis to John Marcer of Rail Infrastructure Corporation on

Saturday, May 5, 2001. All recommendations were adopted. A summary of the results of the comparative study of stress-based structural fatigue codes is presented below.

2.7.3.1 Qualitative Study

For qualitative assessment, the entire method of each fatigue code is broken into units to simplify comparison. These units are:

- choice of stress indicator
- S-N curves, stress factors and methods used for converting stresses to fully reversed cycles
- safety factor recommendations
- cycle counting and stress spectrum compilation.

Choice of Stress Indicator

A summary of the variation in code recommendations for the type of stress indicator that should be used, is presented in Table 2.7.1.

BS7608 / BS5400	Japanese	AAR	AWS	Eurocode	Austroads
Principal Stress (dependant on the direction of the principal plane).	Shear stresses only, normal stresses only or maximum principal stress where normal and shear act together and shear is significant. Neglect shear stress if the ratio of shear to normal stress is less than 0.15.	Uni-axial normal stresses or combination of principal stresses if shear stress is significant.	No guidance given.	Shear and normal stresses added within Miner's rule where shear component exceeds 15% otherwise normal stress only. Maximum principal stress if shear and normal stresses vary simultaneously and principal plane doesn't vary significantly.	Principal stresses when normal and shear stresses occur simultaneously and at the same location. Otherwise shear and normal stresses added within Miner's rule.

Table 2.7.1. Stress indicators used in the codes.

S-N Data and Curves

The method used to convert stresses to fully reversed stress cycles, in preparation for use with S-N curves, varies, so do the curves themselves in form and in location of critical points such as the endurance limit etc. The use of stress correction factors for thickness and factors relating to weld enhancement also varies from code to code. Each of these, particularly the form of the S-N curve and the use of factors relating to weld enhancement, has the potential to significantly affect estimates of remaining life. Table 2.7.2 presents a summary of the variations.

Code	S-N Data				
	Stress Conversion	***Typical Curve Form (variable amplitude loading)***	***Thickness Effect***	***Weld Enhancement***	***Further Mods***
BS7608	Non-welded or stress relieved: 60% of comp. portion + tens. portion. No fatigue damage for fully comp. stresses in non-welded details. Welded: Entire range.	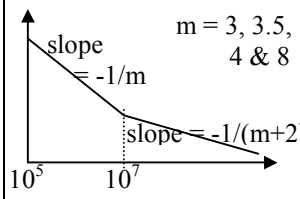	Factor strength by $\sqrt[4]{16/t}$ t in mm.	Factor strength by 1.3 for machining or grinding of weld toe.	Factor strength by ½, entire slope -⅓ in seawater.
BS5400			No guidance given.	Special Testing to prove enhancement.	No
Jap.	Factor by $C_R = 1$ for $R \geq -1$ $C_R = \frac{1.3(1-R)}{(1.6-R)}$ for $R \leq -1$ $C_R = 1.3$ for $R \leq -\infty$ (i.e. both min and max stresses compressive) where R is stress ratio.	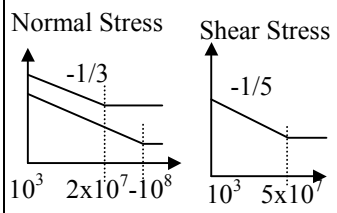	Factor strength by $\sqrt[4]{25/t}$ t in mm.	No guidance given.	No
AAR	Modified Goodman	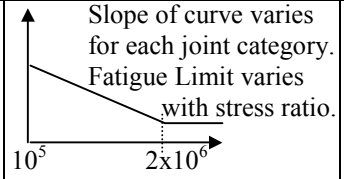	No guidance given.	No guidance given.	No
AWS	No guidance given.	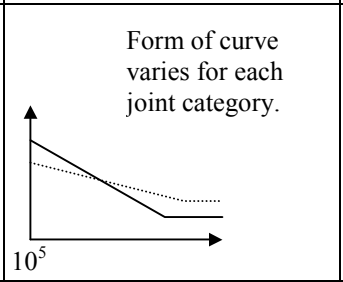	No guidance given.	Factor strength by 1.3 for toe grinding, hammer peening or TIG dressing. Factor strength by 1.5 for toe grinding + hammer peening. Improvement factor not to exceed highest design category.	No
Euro.	Non-welded or stress-relieved: 60% of compressive portion + tensile portion. Welded: entire range.	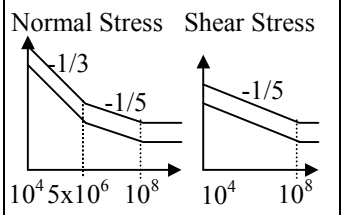	Factor strength by $\sqrt[4]{25/t}$ t in mm.	No guidance given.	No
Aust.	Entire range.	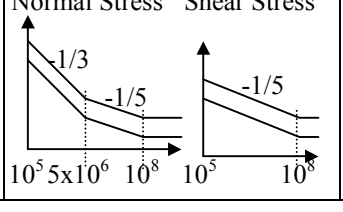	Factor strength by $\sqrt[4]{25/t}$ t in mm.	No guidance given.	No

Table 2.7.2. S-N data and curves.

Safety Factors

Safety factors are applied in different ways and at different steps of the fatigue assessment procedure. The safety factors of the Japanese code are applied at the Miner's summation step, while in the Eurocode factors are applied to both fatigue loading and strength (i.e. to the measured or predicted stress and the S-N curve stress). The AWS code provides a type of safety factor by providing different S-N curves for redundant and non-redundant structures. Safety factors are not explicitly mentioned in other codes, although in some cases are included within assessment in S-N curves or joint details. The British codes for example take S-N curves two standard deviations below the mean, recommending that this probability of failure could be increased for non-critical situations and decreased for critical ones. No specific guidance is given as to how to treat this in terms of factors of safety however, so it has not been included in the study of safety factors presented below in Table 2.7.3.

BS7608 / BS5400	Japanese	AAR	AWS	Eurocode	Austroads
None	Partial safety factors (redundancy, importance and inspection factors) used within Miner's rule for fatigue assessment	None	Different S-N Curves for redundant and non-redundant structures	Partial safety factors for fatigue loading and strength used in calculation of the number of cycles at a given stress range to cause failure.	Limit State capacity factor used in design only.

Table 2.7.3. Safety factor recommendations.

Cycle Counting and Stress Spectrum Compilation

The method of cycle counting employed by each of the compared codes is equivalent. The "rain flow" method is quoted in some codes while the "reservoir" method is in others. Both of these are simply different descriptions of the same algorithm and yield identical results.

The level of guidance for the use of stress spectra in fatigue assessment varies from code to code. The use of stress spectra has an inherent safety factor associated with it. Raw stress cycles are adjusted such that the minimum and maximum stress of the raw stress cycle becomes equivalent to the minimum and maximum stress of the bin the cycle is placed in, in the stress spectra. The variations in the guidance given for the use of spectra in fatigue assessment are summarised in Table 2.7.4.

BS7608 / BS5400	**Japanese**	**AAR**	**AWS**	**Eurocode**	**Austroads**
Yes, 40 intervals.	Yes, interval size less than 1/20 of maximum stress range	Yes, 20 intervals	No guidance given.	Yes, no guidance on interval size.	No guidance given.

Table 2.7.4. Guidance on stress spectrum compilation.

2.7.3.2 Quantitative Study

Estimates for remaining life are made for various joint classes and various stress conditions, using the software system described in Section 2.7.2. Often the stresses used in the examples have constant amplitudes, to facilitate sufficient control over the comparisons. The effects of the variation in S-N curves used, the variation in the treatment of mean stress, the variation in the guidance given for the use of stress spectra and the effect of correction and safety factors are investigated.

Two assumptions are made in order to provide some level of control within comparisons. It is assumed that: either shear stresses present during loading are insignificant and may therefore be ignored in analysis, or that shear stresses fluctuate simultaneously with normal stresses and the direction of the principal stresses do not

rotate significantly during loading. Based on either of these assumptions, the stress history used in all codes may be assumed to be the same single time varying principal stress history. If shear stresses are significant or if they do not fluctuate simultaneously with normal stress, then the stress history is not applied identically in each code. Where shear stresses are significant or fluctuate separately from normal stresses, some codes use separate S-N curves for shear and normal stresses (such as the Japanese code, Eurocode and the Austroads code). Others use equivalent uni-axial stresses based on principle stresses (such as the AAR code) and others use principal stresses, dependent on the direction of the principal plane (such as the British Standard codes). Ignoring the effect of shear stresses greatly simplifies the study. A further study including the effect of significant shear stresses in analysis would likely expose further variation between the codes in their estimation of remaining life.

Five joint classes are considered in this study. These are listed in table 2.7.5, along with the detail categories assigned to these joints in the codes.

Joint Class	**Detail Category**					
	BS5400/BS7608	**Japanese**	**AAR**	**AWS**	**Eurocode**	**Austroads**
non-welded	B	B	1.1.2	A	160	160
longitudinal weld	D	D	3.2.1	B	100	100
transverse weld	F2	E	3.1.7	C	71	71
butt weld	D	D	2.1.1	B	112	112
cover plate	G	G	3.1.5.1	E	50	50

Table 2.7.5. List of joint classes considered

The uncorrected S-N curves corresponding to the joint classes listed in table 2.7.5 are presented in Figure 2.7.1. The uncorrected S-N curve refers to the S-N curve before correction factors for plate thickness, weld enhancement etc. are applied.

For the Japanese and the Association of American Railways codes, where the S-N curve is dependent on the stress ratio (ratio of minimum to maximum stress), the stress ratio is assumed to be zero. For the AWS code the S-N curves presented are for non-redundant structures.

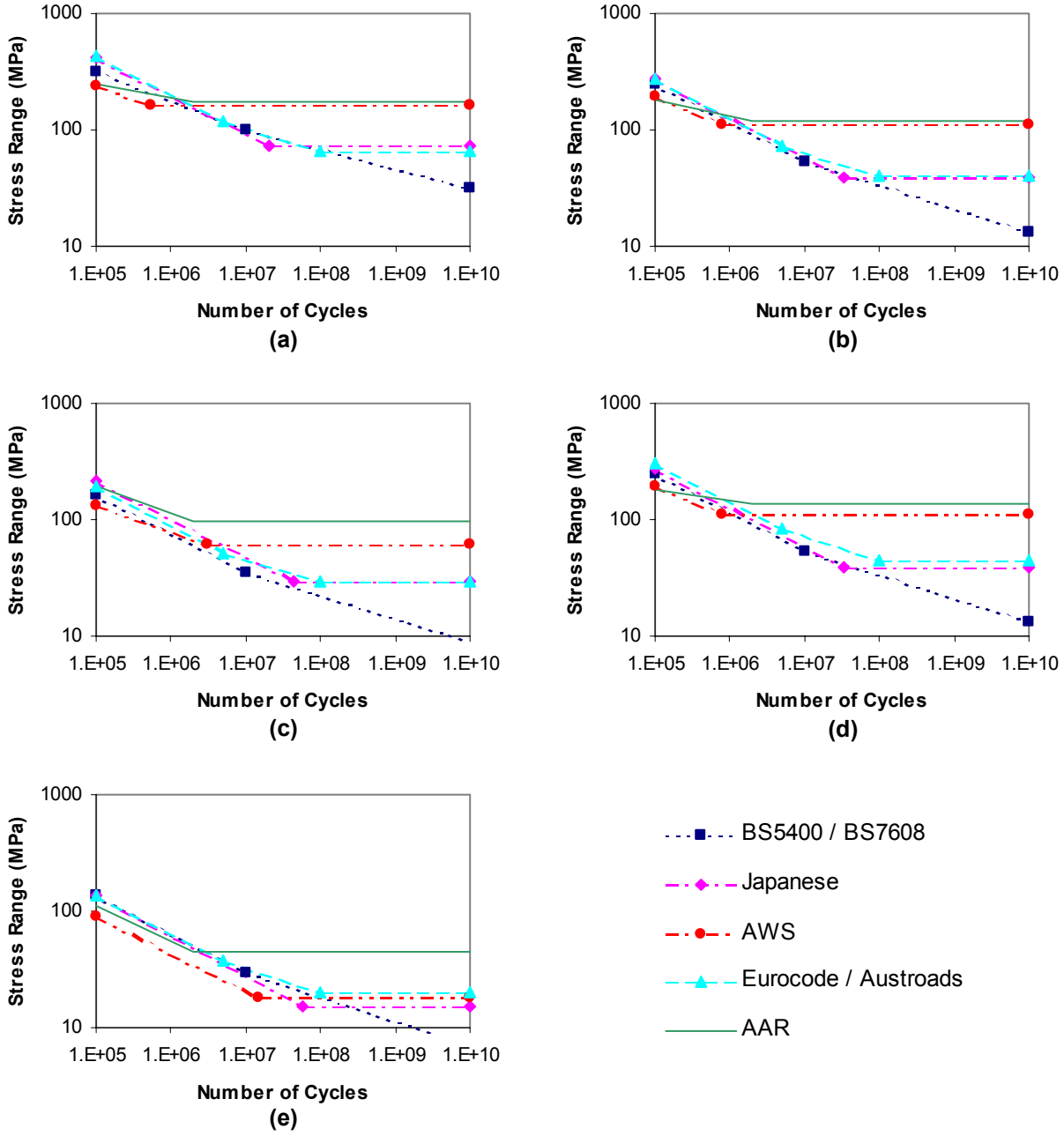

Figure 2.7.1. Uncorrected S-N curves for

(a) non-welded sections, (b) longitudinally welded joints,

(c) transverse welded joints, (d) butt-welded joints and (e) cover plate details.

Effect of Uncorrected S-N Curves

To investigate the effect the variation in the codes, for uncorrected S-N curves, has on predicting remaining life, two controlled stress histories are applied to a longitudinally welded joint detail (Figure 2.7.2). This detail is chosen since, by observation of Figure 2.7.1, this joint class has the least variation between the S-N curves so is expected to provide the most conservative comparison. The first case is a stress cycle ranging from 0 to 85 MPa and the second a repeating unit of one cycle ranging from 0 to 85 MPa and two hundred cycles ranging from 0 to 35 MPa. The estimated remaining life from each code is presented in Figure 2.7.3. The remaining life estimated by both the American codes is infinite, since the range of the stress cycles chosen fall below the fatigue limit.

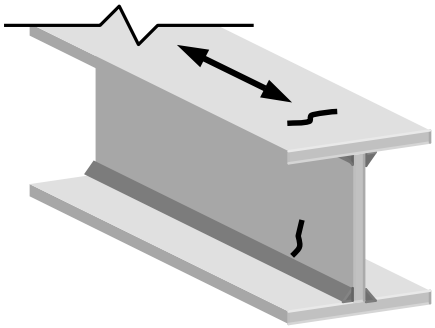

Figure 2.7.2. Longitudinally welded joint class.

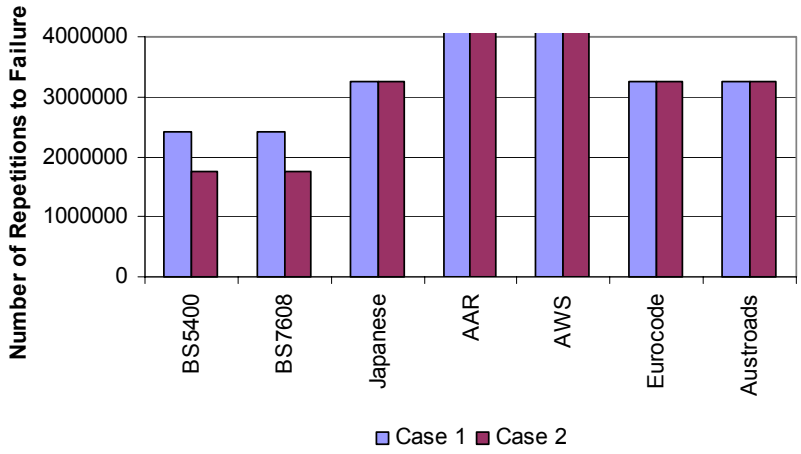

Figure 2.7.3. Remaining life for a longitudinally welded joint for the prescribed two load cases.

Investigating the effect of variation in the uncorrected S-N curves used in the codes further, five loading cycles of randomly varying amplitude are applied to the uncorrected S-N curves of the five joint details listed in Table 2.7.5. The first series of randomly generated load cycles falls between lower and upper stress range limits of 0 MPa and 100 MPa, the second series between 20 MPa and 80 MPa, the third –20 MPa and 60 MPa, the fourth –30 MPa and 30 MPa and the fifth –100 MPa and –20 MPa. The comparison on this occasion is shown in Tables 2.7.6 – 2.7.10. The trend for the first four joint classes (Tables 2.7.6 – 2.7.9) is generally the same as that shown in Figure 2.7.3, for all five loading series. For the cover plate detail (Table 2.7.10) the trend differs, with the remaining life estimated using the American codes being lower than the estimates made using the other codes. Figure 2.7.4 presents the remaining life estimates for the cover plate detail for the first and second randomly generated load series.

Code	**Series**				
	1	**2**	**3**	**4**	**5**
BS5400	418000	3800000	2920000	32200000	(infinite)
BS7608	418000	3800000	2920000	32200000	(infinite)
Japanese	247000	(infinite)	1190000	(infinite)	826000
AAR	(infinite)	(infinite)	(infinite)	(infinite)	(infinite)
AWS	(infinite)	(infinite)	(infinite)	(infinite)	(infinite)
Eurocode	439000	6530000	4720000	(infinite)	(infinite)
Austroads	439000	6530000	1870000	(infinite)	1920000

Table 2.7.6. Number of repetitions to failure for a non-welded section for each of the five prescribed load series (to three significant figures).

Code	Series				
	1	2	3	4	5
BS5400	38200	125000	76900	201000	80800
BS7608	51300	165000	101000	279000	221000
Japanese	(infinite)	(infinite)	(infinite)	(infinite)	(infinite)
AAR	(infinite)	(infinite)	(infinite)	(infinite)	(infinite)
AWS	55100	257000	132000	521000	136000
Eurocode	55100	257000	132000	521000	136000
Austroads	55100	257000	132000	521000	136000

Table 2.7.7. Number of repetitions to failure for a longitudinally welded joint for each of the five prescribed load series (to three significant figures).

Code	Series				
	1	2	3	4	5
BS5400	10700	32700	20700	48600	21900
BS7608	10700	32700	20700	48600	21900
Japanese	25700	79200	49600	124000	113000
AAR	88800	(infinite)	(infinite)	(infinite)	(infinite)
AWS	11900	114000	44400	(infinite)	44000
Eurocode	18400	60400	36900	96900	38800
Austroads	18400	60400	36900	96900	38800

Table 2.7.8. Number of repetitions to failure for a transverse welded joint for each of the five prescribed load series (to three significant figures).

Code	Series				
	1	2	3	4	5
BS5400	38200	125000	76900	201000	80800
BS7608	38200	125000	76900	201000	80800
Japanese	51300	165000	101000	279000	221000
AAR	(infinite)	(infinite)	(infinite)	(infinite)	(infinite)
AWS	(infinite)	(infinite)	(infinite)	(infinite)	(infinite)
Eurocode	81900	474000	232000	1000000	236000
Austroads	81900	474000	232000	1000000	236000

Table 2.7.9. Number of repetitions to failure for a butt-welded joint for each of the five prescribed load series (to three significant figures).

Code	Series				
	1	2	3	4	5
BS5400	6110	18400	11700	27000	12300
BS7608	6110	18400	11700	27000	12300
Japanese	6250	18700	11900	28500	27700
AAR	3710	13500	8000	22800	8210
AWS	1850	5780	3650	8600	3840
Eurocode	6290	19200	12100	28600	12800
Austroads	6290	19200	12100	28600	12800

Table 2.7.10. Number of repetitions to failure for a cover plate detail for each of the five prescribed load series (three significant figures).

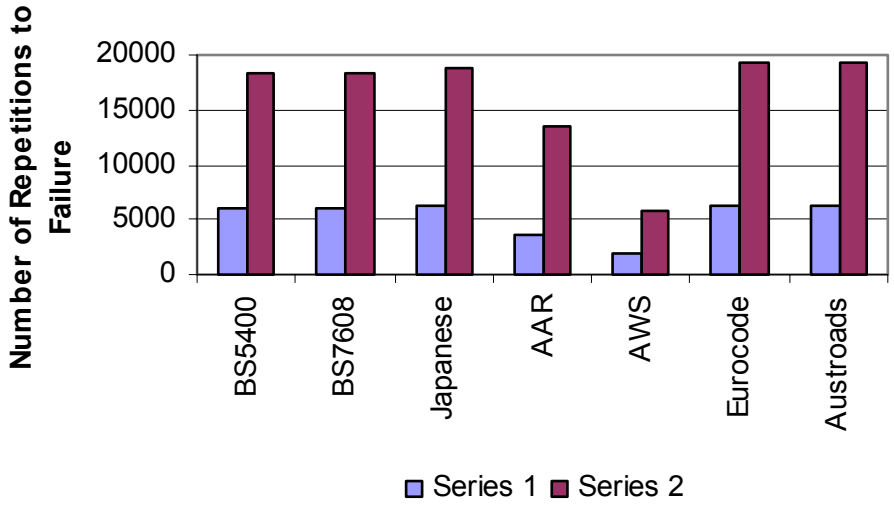

Figure 2.7.4. Remaining life for a cover plate detail for load series 1 and 2.

Effect of Mean Stress

Evaluating the effect of mean stress, four stress histories with various mean stresses are applied again to the longitudinal welded joint class. Each stress history has a repeating unit of one stress cycle with a range of 150 MPa and ten stress cycles with a range of 100 MPa. In the first history all stress cycles have a mean stress of 125 MPa, in the second, 75 MPa, in the third 0 MPa and in the fourth –75 MPa. The estimated

remaining lives are presented in Figure 2.7.5 for both welded and welded and stress-relieved conditions.

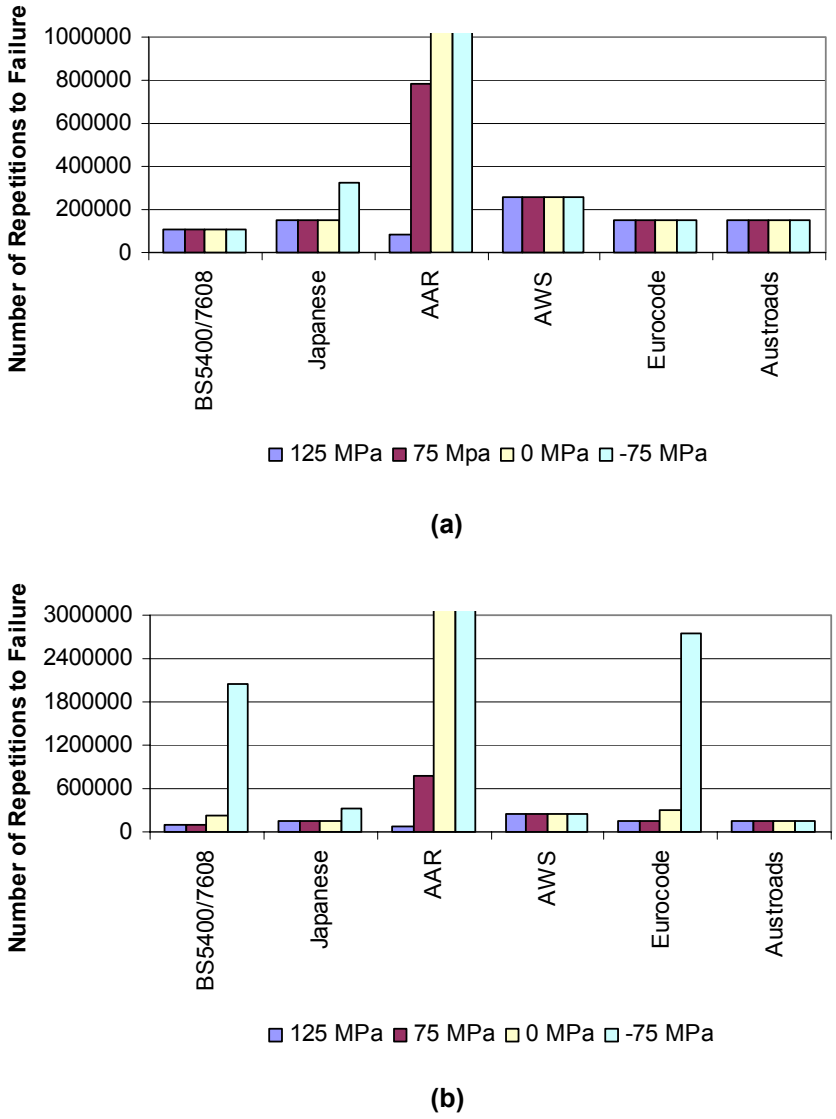

Figure 2.7.5. Fatigue life for a longitudinally welded joint to stresses of varying mean stress. (a) welded, (b) welded and stress relieved

The remaining life estimated by the AAR code is infinite for both the 0 MPa and –75 MPa mean stress cases.

Effect of Correction and Safety Factors

The effects of the correction factors, listed in Table 2.7.2, and of the safety factors, discussed in Section 2.7.2.3, on the estimates for remaining life for a longitudinally welded joint detail, are shown in Figure 2.7.6. A stress history made up of a repeating unit of one stress cycle with a range of 150 MPa and ten stress cycles with a range of 100 MPa, all about a mean stress of 75MPa is used. For codes that allow for correction for material thickness, a thickness of 34 mm has been used. For the BS7608 and AWS codes, remaining life is predicted using code recommendations for correction of S-N data to account for weld enhancement. The estimate for remaining life for the AWS code for minimum factor of safety is taken from the S-N curve for redundant structures. The uncorrected estimate is taken from the S-N curve for redundant structures. All other maximum and minimum factors of safety are defined in the codes.

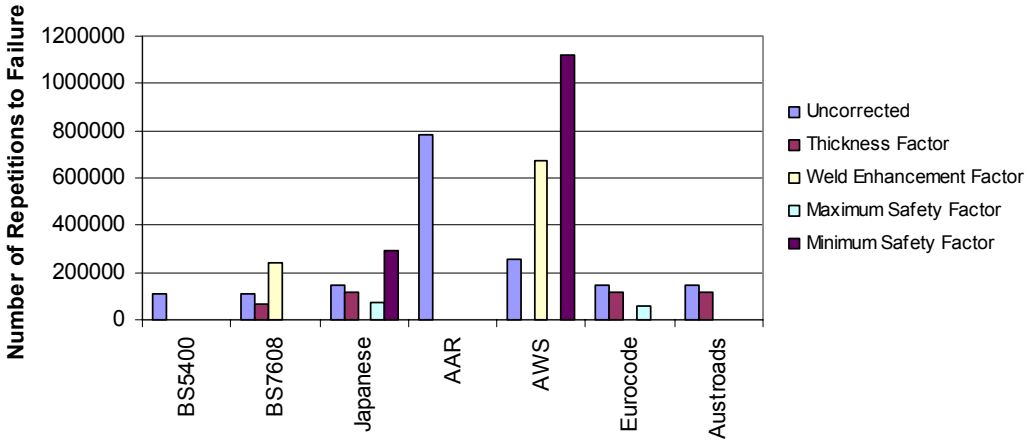

Figure 2.7.6. Fatigue life for a longitudinally welded joint including correction and safety factors.

Effect of Stress Spectra

The effect of stress spectra is also comPared on a longitudinally welded joint detail (Figure 2.7.7). A stress history made up of a repeating unit of one stress cycle with a range of 150 MPa and ten stress cycles with a range of 100 MPa, all about a mean stress of 75MPa is used. Three cases are considered, the first using raw cycles and the second uses stress cycles adjusted within a stress spectrum ranging from –175 MPa to 175 MPa with 40 intervals or 'bins'. The third case has the same range this time with 20 intervals.

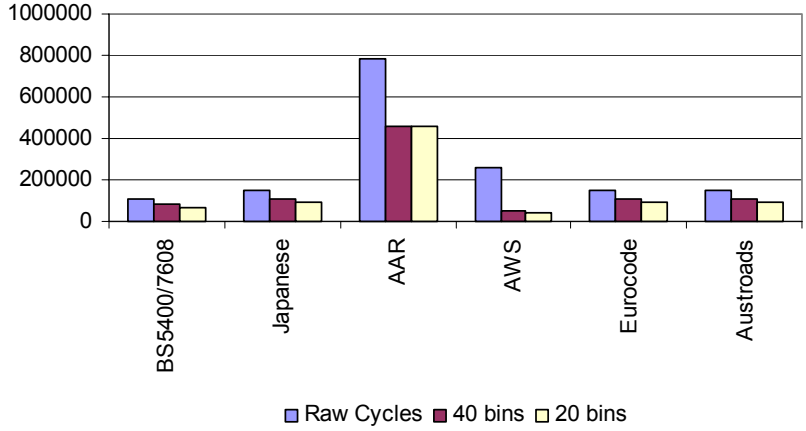

Figure 2.7.7. Comparison of the effect of using a stress spectrum.

2.7.3.3 Discussion

From the trials presented here, the British Standard codes tend to be more conservative in their estimates of remaining life, for welded joint details and for non-welded or stress-relieved details with moderate to high mean stresses, than the other codes critiqued within this study. See Figures 2.7.3, 2.7.5, 2.7.6 and 2.7.7 and Tables 2.7.6 to 2.7.9. The most significant factors contributing to this include the following:

1. The uncorrected S-N curves of the British Standard codes tend to be lower on the stress axis, than other codes for most joint details (Figure 2.7.1).

2. The British codes do not assume a cut-off limit and therefore accumulate damage for minor cycles, which the other codes tend to ignore (Figure 2.7.1, Figure 2.7.3 and Table 2.7.2).
3. The plate thickness correction factor of BS7608, $\sqrt[4]{16/t}$, yields more conservative results than the plate thickness correction factor, $\sqrt[4]{25/t}$, used in the Japanese code, Eurocode and the Austroads Bridge Design Code (Figure 2.7.6 and Table 2.7.3)

The Austroads code, the Eurocode and the Japanese code tend to give comparative estimates of remaining life. Estimates of remaining life from these codes tend to be less conservative than the British Standard codes, but generally more conservative than the AAR and AWS codes (Figures 2.7.3, 2.7.5, 2.7.6 and 2.7.7 and Tables 2.7.6 to 2.7.9).

The welded cover plate detail is an exception to the trend outlined above (Figure 2.7.4 and Table 2.7.10). For welded cover plate details the American codes tend to be most conservative and the British Standard codes only slightly more conservative than the remaining codes.

The effect of mean stress tends to be greatest in the British Standard code and Eurocode estimates of remaining life, for non-welded or welded and stress-relieved joints, than in the other codes studied. For negative or low positive values of mean stress these codes tend to be less conservative than most other codes studied (Figure 2.7.5 (b). The reason is that the British Standard codes and the Eurocode use just sixty percent of the compressive portion of stresses for non-welded or welded and stress-relieved joint details, increasing estimates for fatigue life (Table 2.7.2). All codes account for the

effect of mean stress by correcting either the applied load or S-N curves, except the Austroads and AWS where the effect of mean stress is not considered.

Correction factors, for the effects of weld enhancement and safety, have a significant effect on remaining life estimates (Figure 2.7.6), as expected, and greatly vary from code to code.

The use of stress spectra increases the conservatism of remaining life estimates (Figure 2.7.7), by increasing the stress range of the counted cycles. One assumes that the use of stress spectra is based on historical assessment, where handling many cycles was difficult and it became efficient in analysis to group cycles together in a spectrum. This is no longer the case, since little computational effort is required to sum the fatigue damage of all cycles without sorting cycles into a stress spectrum.

2.7.3.4 Conclusions

The work presented here summarises a comparative study of seven international fatigue codes. The motivation for the study arose from the fact many codes exist and are used, which yield equally as many, often wildly different, estimates for remaining life. The study consists of the comparison of the assessment method of each code, broken into manageable units to simplify comparison. In addition, numerical results from the codes have been compared for a number of stress histories and joint classes. The effect of various factors, such as the use of stress spectra and code defined correction factors, on the estimates of remaining life made using the codes has been demonstrated and compared. Of the codes studied, the British Standard codes tend to be most conservative in their estimate of remaining life, for most welded joint details and for

non-welded or stress-relieved details with stress ranges with moderate to high mean stresses. The Austroads, Eurocode and the Japanese codes are generally comparable and follow, while the American codes provide the least conservative estimates for remaining life. This trend is shown to be largely the result of uncorrected S-N curve form. Exceptions to this general trend have been identified for cover plate details and stress cycles with negative or low positive values of mean stress.

3. DEMONSTRATION

3.1 The Mullet Creek Railway Bridge

3.1.1 The Mullet Creek Railway Bridge

The bridge used for the demonstration of the methods and assessment techniques developed in this research is the Mullet Creek Railway Bridge (Figure 3.1.1). The bridge was commissioned in the mid 1960's, replacing a timber viaduct, built in 1887, over Mullet Creek at Kembla Grange, approximately ten kilometres south of the city Wollongong in NSW, Australia [119]. The bridge is fifty-eight metres in length and consists of twenty-four steel girder approach spans, ranging from six to eight and half metres in length (Figure 3.1.2), and a main plate-welded girder through span of approximately twenty-seven metres in length (Figure 3.1.3).

Figure 3.1.1. Mullet Creek Railway Bridge.

Figure 3.1.2. Typical Mullet Creek Railway Bridge approach span.

Figure 3.1.3. Mullet Creek Railway Bridge main span.

The bridge supports a single track, which is subject to relatively light passenger traffic and conditional freight traffic including coal trains, starch trains and ballast trains. The bridge is ideal for case study investigation; it is typical in design to many steel bridges in Australia, has easy access, is relatively new and has relatively simple traffic flow.

3.1.2 The Mullet Creek Railway Bridge Approach Spans

The approach spans in particular are used to develop and then to demonstrate the method proposed here. The approach spans are especially ideal for demonstration due to their sensitivity to fatigue. Being relatively short (just six to eight and a half metres in length), the approach spans are subject to relatively more major loading cycles than larger spans [34, 120]. The short approach spans are subjected to a peak loading cycle for each pair of wagon or passenger train bogies (i.e. the trailing bogie of one carriage and the leading bogie of the next) and for each bogie of a locomotive. A longer span would be subjected to perhaps only one peak cycle for an entire train. Figure 3.1.4 demonstrates the relative number of peak stress cycles for the main span and one of the approach spans under the passage of two six-axle locomotives and two four-axle

carriages. The stress histories shown in Figure 3.1.4 were generated in the dynamic analytical model developed in this research, for a typical approach span and the main through span of the Mullet Creek Railway Bridge.

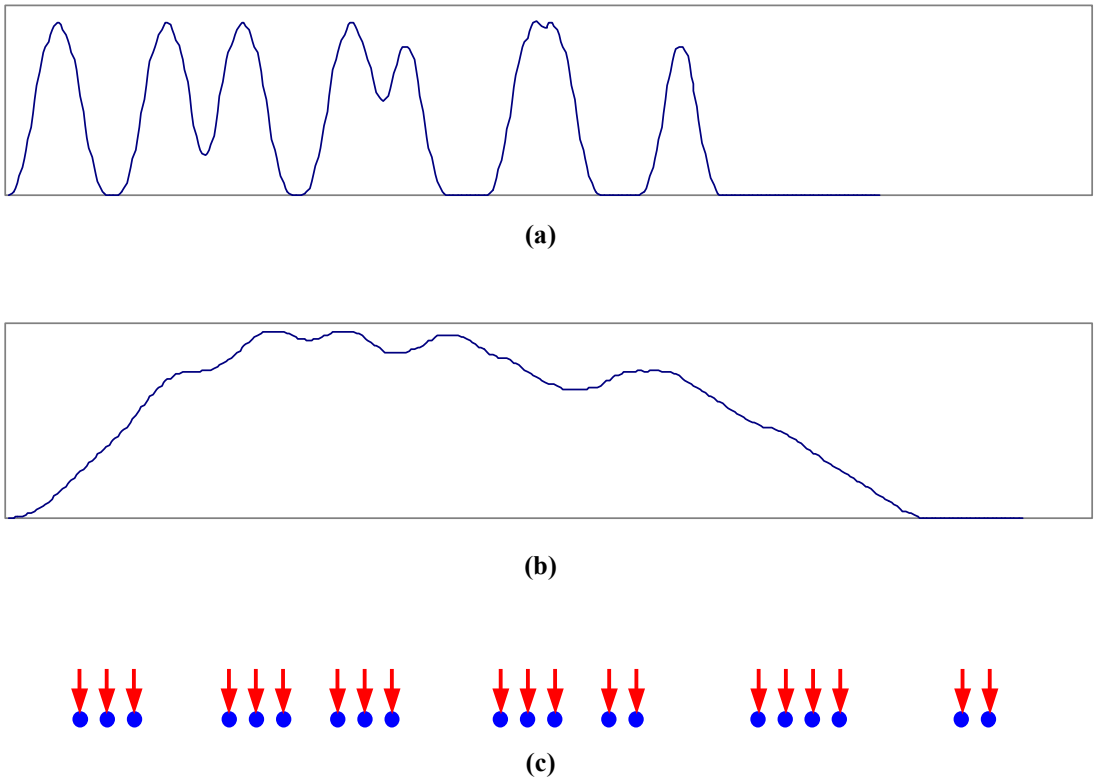

(a)

(b)

(c)

Figure 3.1.4. Typical stress history at the mid-span of the short approach spans (a) and the long main span (b) under the passage of two locomotives and two carriages with axle spacing shown in (c).

The main girders of the approach spans are predominately 30” x 12” x 176# BFBs (Broad Flange Beams), with web-stiffeners welded to the top flange and web, at one-third span length intervals (Figure 3.1.5). The approach spans have four 15” x 4” x 36.37# PFC (Parallel Flange Channel) cross girders, which are bolted to the web stiffeners, as well as 3.5” x 3.5” x 3/8” EA (Equal Angle) sway bracing, bolted to gussets welded to the inside of the web (Figure 3.1.6). 10” x 6.5” x 9’-0” transoms are bolted to the outside edge of the top flange of the BFBs.

Figure 3.1.5. Broad Flange Beam with web-stiffeners welded on the top flange and web.

Figure 3.1.6. Cross girder and sway bracing connections.

The approach spans have fixed bearings at one end and expansion bearings at the other. The expansion bearings are a simple steel-on-steel design. The bearing details are shown in Figure 3.1.7. Concrete piers support pairs of one fixed bearing set and one expansion bearing set. Complete engineering drawings for the approach spans of the Mullet Creek Railway Bridge are presented in Appendix F.

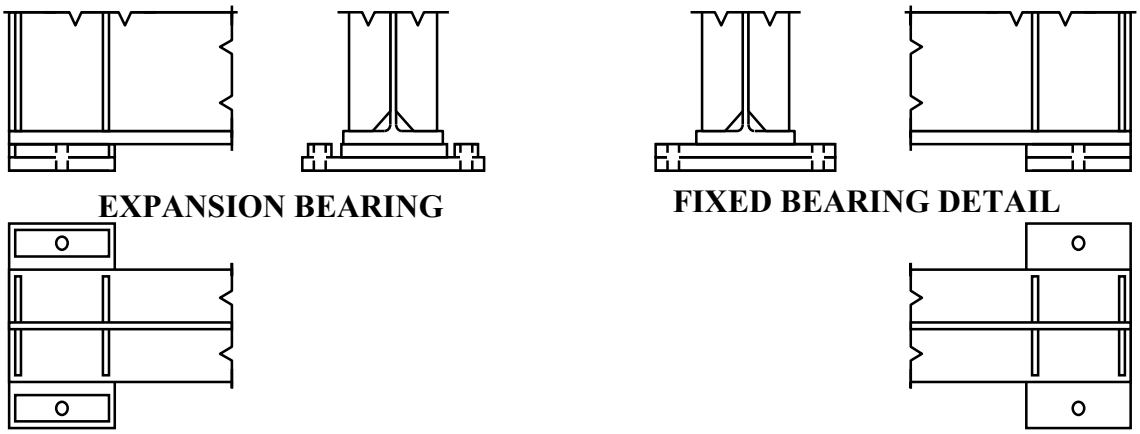

Figure 3.1.7. Expansion and fixed bearing details.

3.1.3 The Significance of Some Design Aspects on Remaining Life and Structural Integrity

Local Bending and Torsional Effects of Transom Loading

A particular issue in bridges of the Mullet Creek design is high localised stresses from induced torsion in the top flange of the Broad Flange Beams. This issue is well known to Australian railway engineers [13, 14]. Due to the eccentricity of the rail to the centre line of the Broad Flange Beams, the transoms undergo bending, causing the transoms to load the inside edge of the top flange (Figure 3.1.8). In some bridges this problem has been so severe that it has been known to plastically deform the top flange and to cause cracking at the edge of the flange for rolled sections, particularly when occurring with corrosion under the transom, and to cause cracking at the fillet between the web and flange in longitudinally welded sections [13, 14].

Figure 3.1.8. Eccentric loading causing the transoms to load the inside edge of the top flange.

Damage at Fixed Bearings

The Mullet Creek Railway Bridge is designed ideally as simply supported, with an expansion bearing at one end and a fixed bearing at the other. The field-test measurements (Section 3.3) and subsequent analytical and finite element model tuning (Section 3.4), indicate that the spans do not in fact behave as if simply supported but exhibit a rotational stiffness about the bearing. As Section 3.4 and the discussion in Chapter 4 details further, this appears to lead to locally high shear loading and, possibly, damage at the fixed bearings.

3.2 Finite Element Models of the Mullet Creek Railway Bridge

3.2.1 Finite Element Sensitivity Model

As has been noted in Section 2.2, beam element models have been predominantly used for analysis in this research. Of course whenever finite element analysis is used, the trade off between the level of detail in the model and the time and the expense of the analysis must be considered. For complete dynamic analysis, using the method presented in Section 2.2, beam models offer a satisfactory balance and deliver relatively efficient and usable results. The majority of finite element modelling has been carried out using the G&D Computing Strand7 package, although MSC Nastran has also been used within the project with similar results. The rendered approach span beam element sensitivity model is shown in Figure 3.2.1.

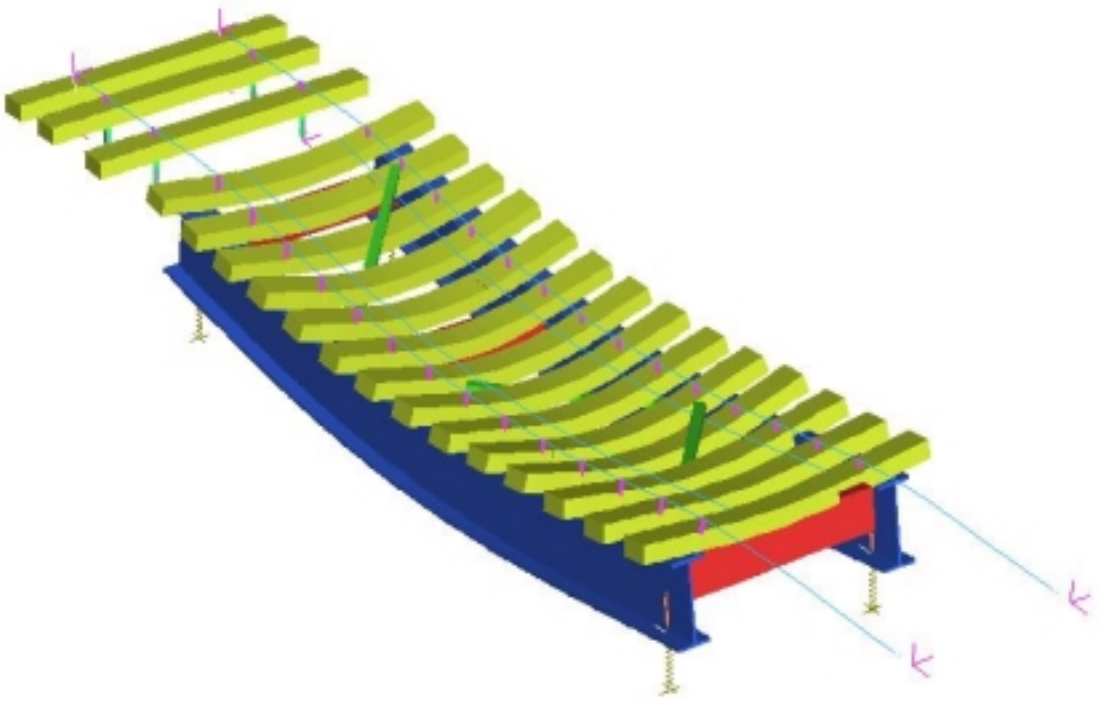

Figure 3.2.1. Rendered approach span beam element sensitivity model.

Model statistics include: 304 nodes, 306 beam elements and 112 link elements. All beam properties are taken from structural drawings supplied by RSA (presented in Appendix F) which were subsequently confirmed by site measurements. The support conditions at the piers are as per structural drawings, with both ends free to rotate and the expansion bearing end free to translate longitudinally. Vertical spring-damper elements are modelled at rail-transom, sleepers-ballast and bearing-substructure connections. Spring-damper elements allow the distribution of wheel loads through the rails and transoms, and irregularities or damage of transoms and abutments to be modelled and adjusted. Longitudinal springs are modelled at the rail-transom and transom - broad flange beam connections. The intention in this case is to allow adjustment of the modelled rail-transom rail clip connection and the transom-BFB hold-down bolts. These connections have been shown to have a significant effect on the behaviour of the bridge. This is discussed further in Section 3.4 and Chapter 4. Preliminary values of damping and stiffness at the rails, transoms and ballast were taken from the very useful text by Esveld [121]. Transom beam elements are connected to broad flange beam elements via a master-slave link allowing some translation of the transom, along its longitudinal axis, and rotation, about the broad flange beam longitudinal axis. Loads are transmitted vertically through the transom, eccentrically about the broad flange beam axis, Figure 3.2.2. The approach span model includes three sleepers leading up to the span. Sleepers on the approach to the span have been modelled, so the approach conditions of the bridge may be accurately simulated in dynamic analysis. The spacing between these sleepers is irregular representing actual site measurements, which differ from structural drawings and ideal conditions of regular sleeper spacing. The rails have been extended 2.5 metres beyond each end of the span at either end and fixed in all three rotations and translations.

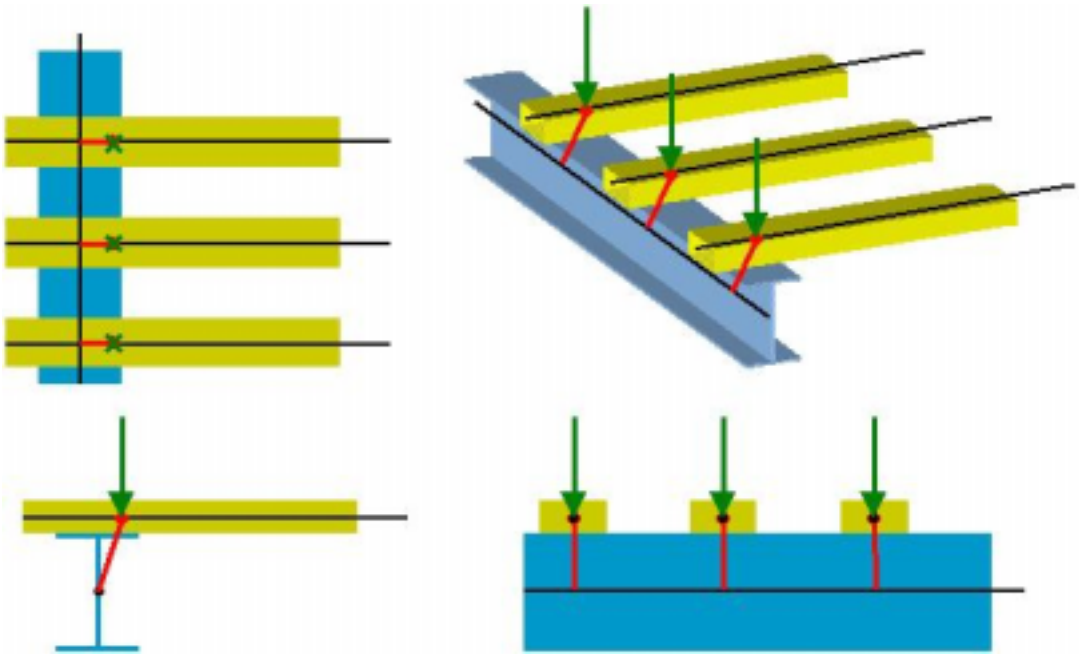

Figure 3.2.2. Transom-broad flange beam connection.

A preliminary beam element model was verified early in the project via strain gauging of one of the approach spans under the static load of a locomotive. Further details of the preliminary testing and verification work may be found in Sorrenson [122].

3.2.2 Stress Data Recovery from Beam Element Sensitivity Models

The available stress output from Strand7, for dynamic analysis using beam models, has not been helpful for complete structural integrity and remaining life assessment. Instead beam force and moment output have been converted to stresses and used in analysis. Details of the method of stress conversion used are presented in Appendix G.

3.2.3 High-Detail Finite Element Model

In order to consider the effect of stress concentrations due to joint details, a high detail model of the span using continuum elements has been developed, Figure 3.2.3.

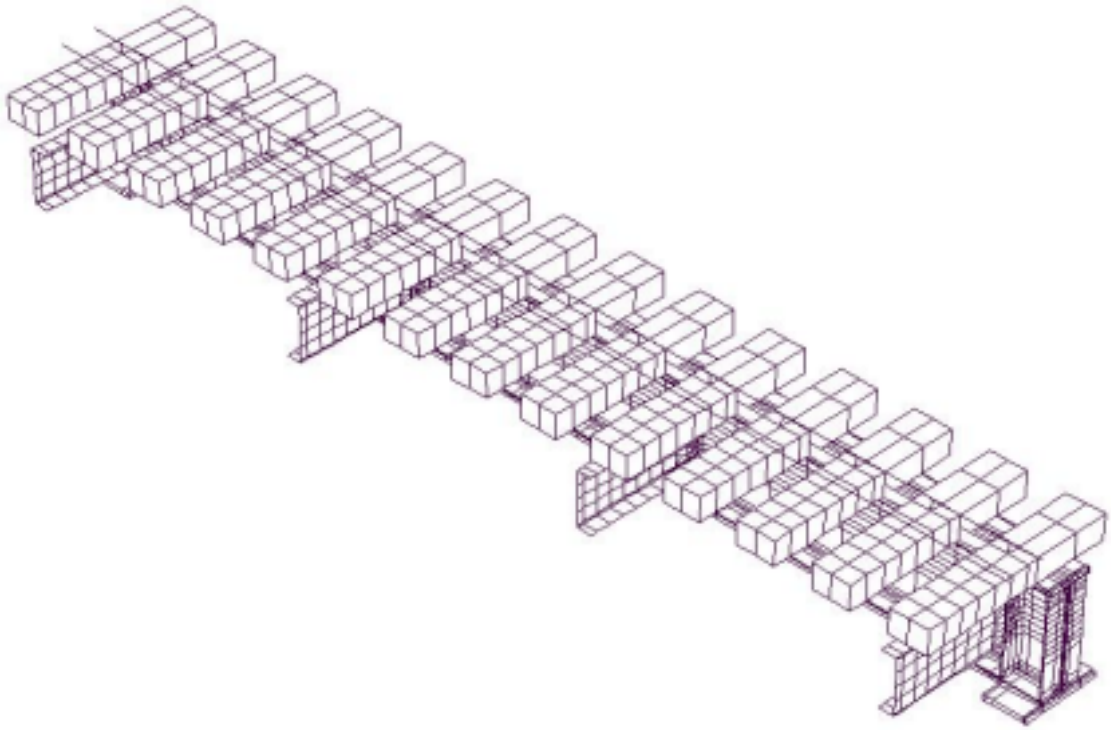

Figure 3.2.3. High detail finite element model.

This model, although unsuitable for dynamic analysis, was solved using static loads to investigate potential stress concentrations, not identified by the beam sensitivity model. The beam model yields comparable and sufficiently accurate results to the high detail model shown, with the exception at the top flange, where bending in the transom gives rise to high localised stresses. The best location for field testing of secondary bending at the top flange was identified to be above web stiffeners by the high detail model, Figure 3.2.4.

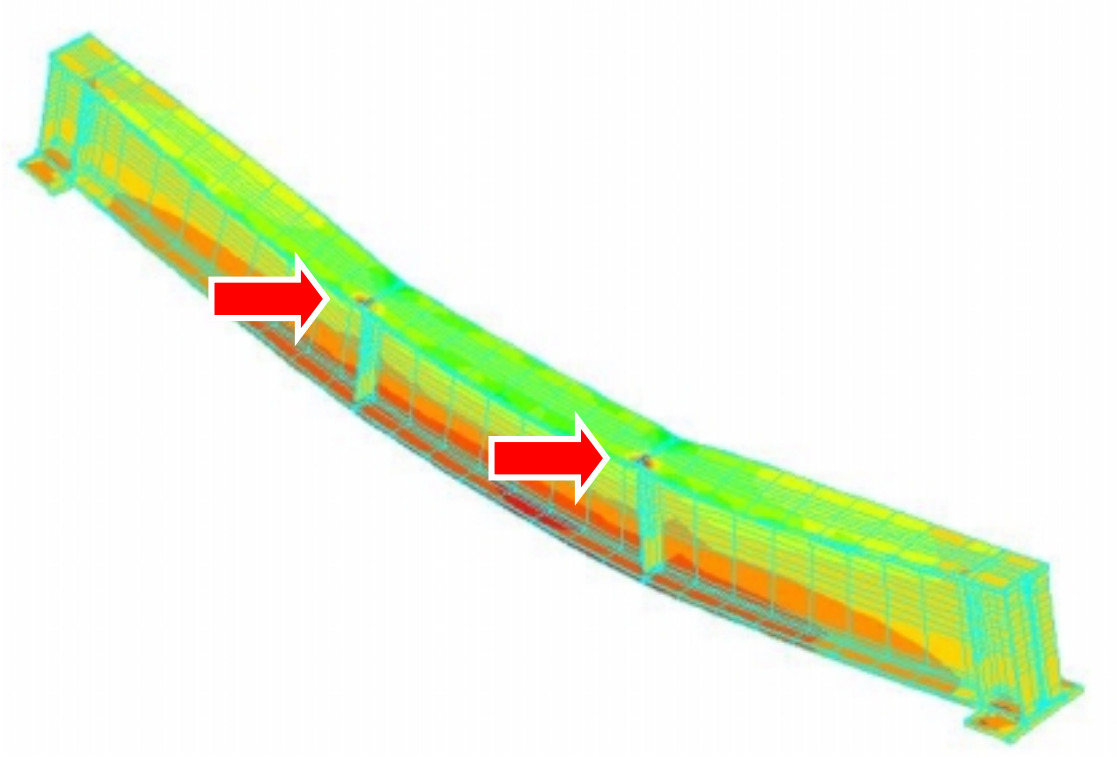

Figure 3.2.4. High detail finite element model identifying critical locations of high localised stresses in the top flange due to transom bending.

3.2.4 Plate Element Sub-Model

Some work has been carried out in this research to build simple plate element sub-model for the web stiffener detail. The loads and constraints applied to the sub-model are based on the global response of the beam model. Kiss and Dunai [123,124] present a technique for automatic computation of numerical stress histories in steel truss railway bridges using finite element sub-models. They term their technique multi-level. In it they model a truss bridge, using a beam element model, and determine the unit deformations of the structure under load, they then apply these unit deformations to plate element sub-models of joints, in order to consider geometric influences on stresses. The numerical stress histories are obtained using influence-line based summations, so are somewhat quasi-static rather than completely dynamic. It is

proposed in future work that sub-models be used to further investigate the top flange of the Mullet Creek Railway Bridge approach span BFBs. As in the work of Kiss and Dunai, the intention is not to replace global beam element models, but to complement them with plate element sub-models for components that cannot be modelled accurately using only beam elements. Complex components may be modelled in detail using plate elements and assessed using dynamic deformations from the beam element model. As has been noted, some preliminary work has been carried out in this research using a sub-model for the web-stiffener connection. Considerably more work is required before results from the sub-model developed this project are useful.

The preliminary web-stiffener connection plate element sub-model is illustrated in Figure 3.2.5. The preliminary sub-model is two thirds of one of the BFB main girders modelled from the inside edge of one of the bearings. This enables investigation of the flange above the web-stiffener connection, as well at other locations along the beam.

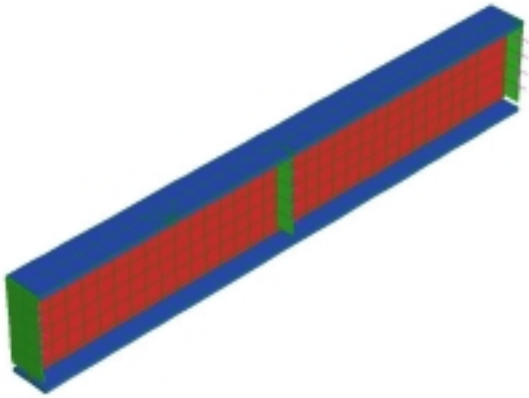

Figure 3.2.5. Preliminary web-stiffener plate element sub-model.

3.3 Field Testing

3.3.1 Field Test Program

Three rounds of field-testing were carried out during the course of the present research. The first round of testing was carried out in the preliminary research leading up to this thesis [122]. The second and third rounds of testing were carried out in 2000 and 2001 [72] and are detailed below.

3.3.2 Test Equipment

Equipment used during field-testing, Figure 3.3.1, included the following:

- Power Drill with Sanding Pad for Cleaning Back Steel Surfaces
- Small Generator for Power Drill
- Single Axis 120 Ohm Strain Gauges
- Rectangular 120 Ohm Rosette Strain Gauges
- Custom Built Strain Gauge Amplifier
- Eight Channel TEAC RD-135T DAT Data Recorder
- Custom Built Battery Power Supply for Strain Gauge Amplifier and Data Recorder
- Three Bruel & Kjaer 4384 V Accelerometers with Electrically Isolated Magnets
- Bruel & Kjaer Conditioning Amplifier Amplifier with Battery Supply
- National Instruments BNC-2110 Adapter and Hardware for Digitising Data
- Custom Built Digitising Software

Figure 3.3.1. Equipment used during testing.

3.3.3 2000 Field Testing

In November of 2000, dynamic testing of the approach spans of the Mullet Creek Railway Bridge was carried out. The work was delayed considerably due to logistical difficulties in co-ordinating participants from various organisations, as well as difficulties settling on appropriate safety procedures and work-site supervision. After much discussion the appropriate level of work site supervision was settled upon. Work site supervision was carried out by qualified Rail Services Australia employees, to the satisfaction of maintenance contractors Fluor Australia. Groups co-ordinated for the work were Rail Services Australia, BHP, Network Control (Rail Access Corporation), Fluor Australia and the University of Wollongong.

The 2000 round of testing did not adhere completely to the technique presented earlier in this paper, since the method was under development. The passage of a known locomotive at 'crawl' speed was not recorded during testing and as a result the

measured response was not useful for model validation. The 2000 round of testing did however provide a significant amount of test data for vehicles at normal speed, which was useful for load identification and correlation of results for traffic at normal speed.

For the test set-up strain gauges and accelerometers were installed on a twenty four foot approach span, the third span from the northern end of the bridge, shown in Figure 3.3.2.

Figure 3.3.2. Approach span chosen for the first round of testing.

Six strain gauges were attached to the underside bottom flanges of the broad flange beam girders (three on each girder), at one-quarter span length intervals. One strain gauge was located to the top side of the top flange of the BFBs, above one of the web-stiffeners, to measure the high localised stresses caused by transoms loaded eccentrically to the BFB girders, Figure 3.3.3.

Figure 3.3.3. Strain gauge located on the top flange of the Broad Flange Beams above one of the web-stiffeners.

As was noted in the previous section, the location of the strain gauge for the top flange was identified as an area of high localised stress, by preliminary high level finite element analysis carried out prior to testing (Figure 3.3.4).

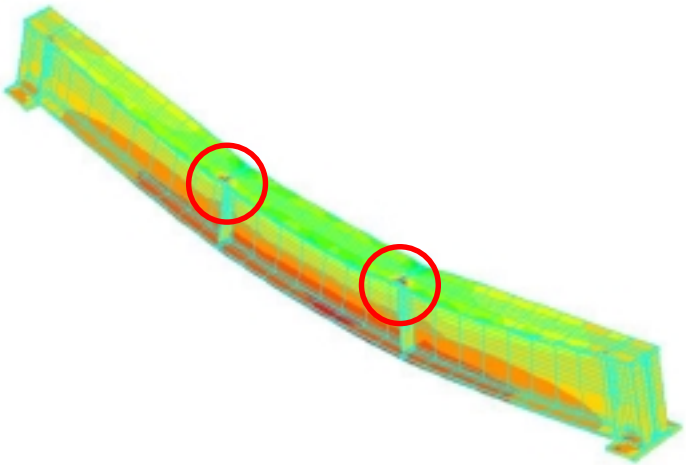

Figure 3.3.4. High level FEA identifying critical locations of high localised stresses.

Four ninety-degree rosette strain gauges were attached to the rails to gain a relative measure of axle load and to measure the speed of rolling stock, where axle spacing is known. The strain gauges were set up on the outside face of the rail web, at the neutral axis of the rail, approximately forty-five degrees from the edge of the sole plate. Strain

gauges were then connected in a Wheatstone bridge in order to measure a single axle load. The strain gauge set up and Wheatstone bridge are shown in Figures 3.3.5 and 3.3.6. The measurement set-up is adapted from Fryba [41].

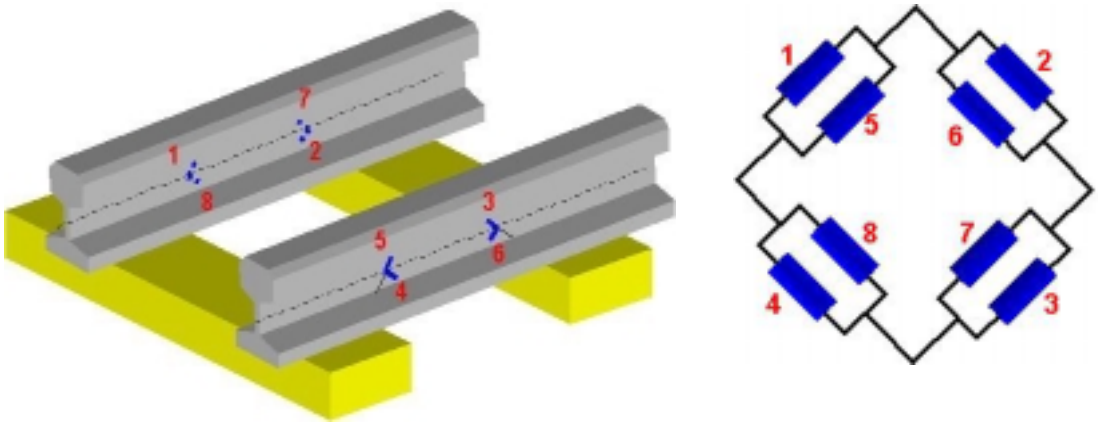

Figure 3.3.5. Strain gauge set-up and Wheatstone bridge for relative axle load measurement.

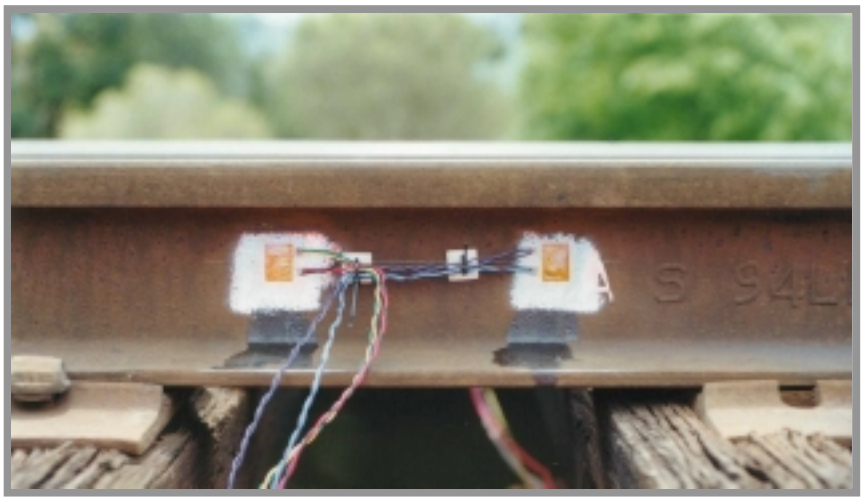

Figure 3.3.6. Strain gauge set-up for relative axle load measurement.

Three accelerometers were attached to the span via electrically isolated magnets, to measure acceleration response. The intention was to use the twice-integrated acceleration response signal for model tuning and load identification. The location of accelerometers was varied during testing. Figure 3.3.7 illustrates the accelerometers at one of the fixed bearings.

Figure 3.3.7. Accelerometers at one of the fixed bearings.

Figure 3.3.8 shows a schematic the complete set up of test equipment.

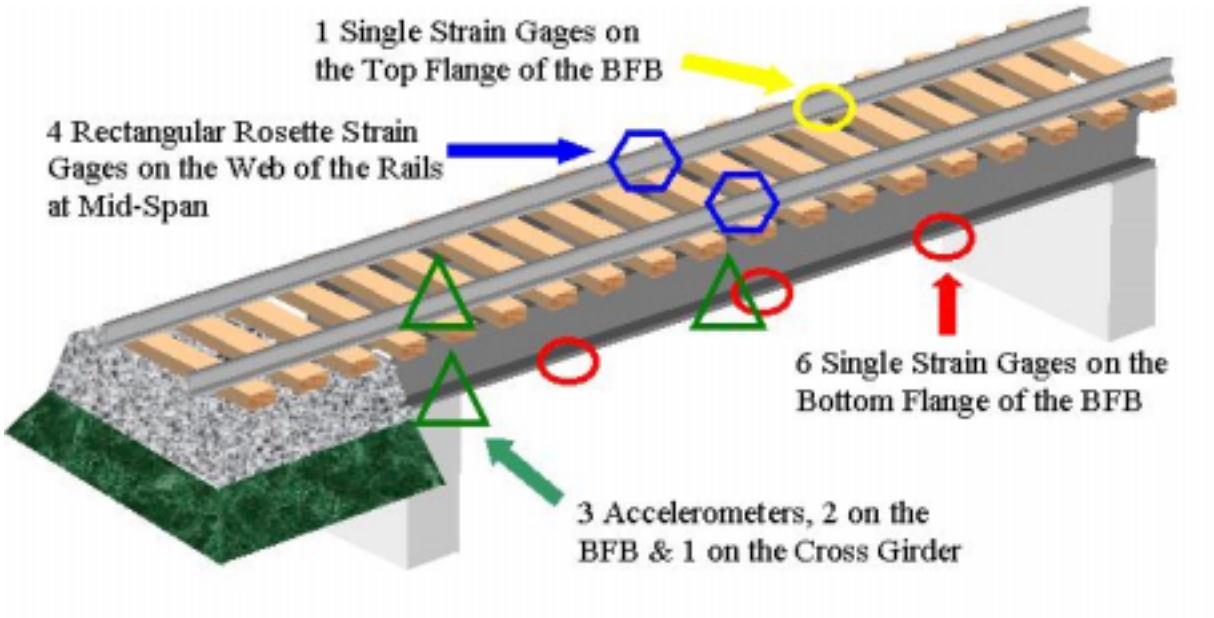

Figure 3.3.8. Schematic of test set up.

In order to calibrate the test equipment, a BHP locomotive was stopped on the span. Calibration was carried out twice, once for each of the locomotive bogies. Figure 3.3.9 shows the locomotive being used to calibrate the test equipment.

Figure 3.3.9. Locomotive stopped at mid span for equipment calibration.

After the equipment was calibrated, data was recorded for thirty-three trains over a period of approximately ten days. Train types, times and directions of travel were noted to complement recorded data and were compared and confirmed against current working timetables. Recorded data has been catalogued both in order of event and in groups of train type and direction of travel. Catalogued data for both the 2000 and 2001 rounds of testing is included in Appendix H. Data was recorded for ballast trains, Manildra starch trains, BHP coal trains, and diesel and electric passenger trains. Data was recorded on an eight channel DAT data recorder and converted to digital format via a program written as part of the project in C language, using a National Instruments Analogue to Digital card. The analogue to digital conversion software is included in Appendix I. A sample of digitised data is presented in Figure 3.3.10, illustrating stresses at the top flange above the web stiffener, the bottom flange at mid span and the rail gauges, for the passage of 100t Manildra wagons.

The data recorded by field measurement gave bending stress results that differed from the assumed simply supported finite element model. The measured bending stresses were generally slightly lower than the predicted stresses from simply supported models, suggesting an increased stiffness in the actual bridge structure. Bending stresses also

varied from the simply supported prediction along the length of the span in a manner that suggested a stiffness at the span ends, that varied from the assumed simply supported condition. Bending stresses were not symmetrical about the centre of the span, instead stresses from the gauge at the expansion bearing end of the span were greater than stresses from the gauge at the fixed bearing end of the span.

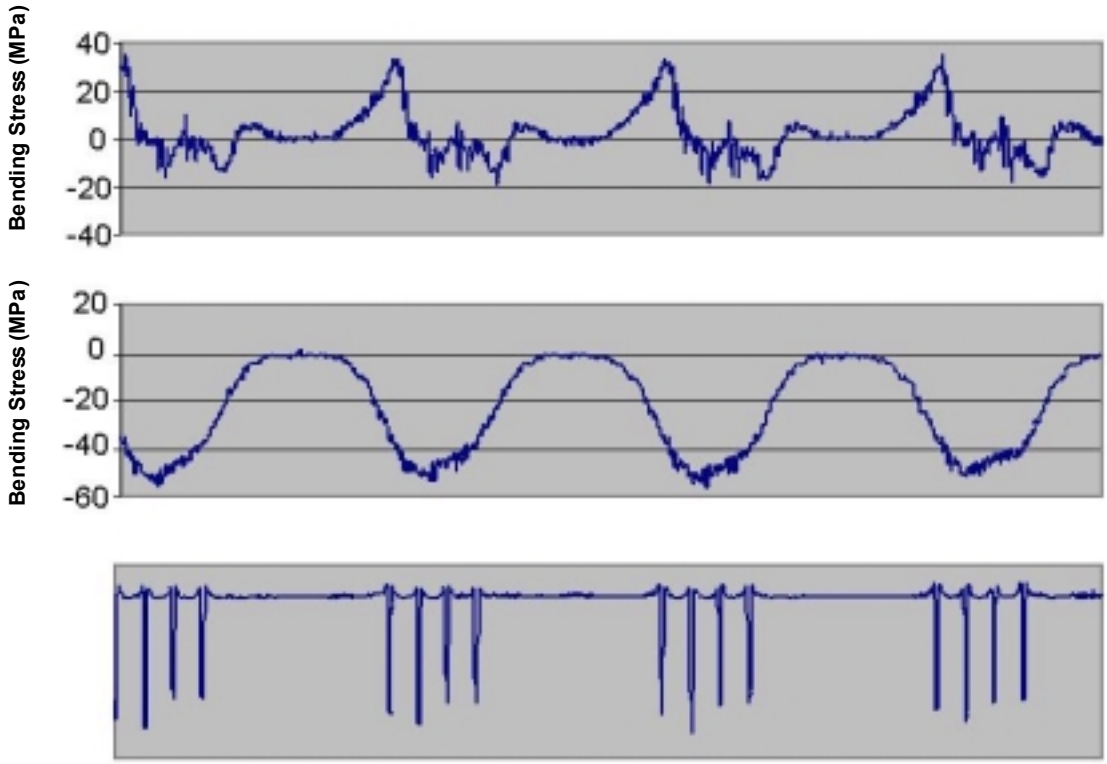

Figure 3.3.10. Sample of digitised test data.

3.3.4 2001 Field Testing

Early in 2001, the final round of testing was carried out. Logistically this round of testing was much easier to organise than the previous testing. On this occasion instrumentation consisted of strain gauges on the underside bottom flanges of the broad flange beam girders (three on each girder), at one-quarter span length intervals and accelerometers at the same locations. Since at no stage was anyone required to work at

track level, the set-up of equipment was considerably easier than in previous testing and safe work procedures were carried out without disrupting normal traffic.

On this occasion, rather than stopping a locomotive on the span, the slow pass (10 km/hr) of a BHP locomotive was recorded to calibrate equipment. The dynamic data recorded during the slow pass was also used to validate and fine tune the analytical and finite element sensitivity models, and to account for the unexpected bending stress results. This is demonstrated in the following section.

Using the tuned analytical model described in section 2.4 and dynamic bending stress histories from field testing, loads may be identified from structural response. The strain gauges set up on the rail in the first round of testing to measure relative axle load are therefore unnecessary. This greatly simplifies the test set-up and reduces traffic disruption as was noted above. Load identification from the structural response of the Mullet Creek Bridge is demonstrated further in Section 3.5.

Dynamic bending stress and accelerometer data was recorded for a further twenty-four Manildra starch trains, BHP coal trains and diesel and electric passenger trains, bringing the total number of trains catalogued over both rounds of testing to fifty-seven. The catalogue of recorded data is presented in Appendix H.

3.4 Validation of Finite Element Models

3.4.1 Variation of Field Test Results from Predicted Response

As was noted in the previous section, the bending stress results measured during field-testing varied from predictions based on simply supported beam behaviour. The measured bending stresses were generally slightly lower than the simply supported predictions and the bending stresses were not symmetrical about the mid-span. This suggests that the stiffness at the supports varied from simply supported assumptions. Figure 3.4.1 demonstrates the bending stress results from field testing for the slow pass of a BHP locomotive and the predicted bending stress results, assuming simply supported conditions. Recall that bending stress results were measured at one-quarter span length intervals. In the figure below, starting from left to right, the bending stress results are shown for the strain gauge measurement taken at a one-quarter span length from the expansion bearing, the measurement taken at mid-span and the measurement taken at a three-quarter span length from the expansion bearing, i.e. a one quarter-span length from the fixed bearing.

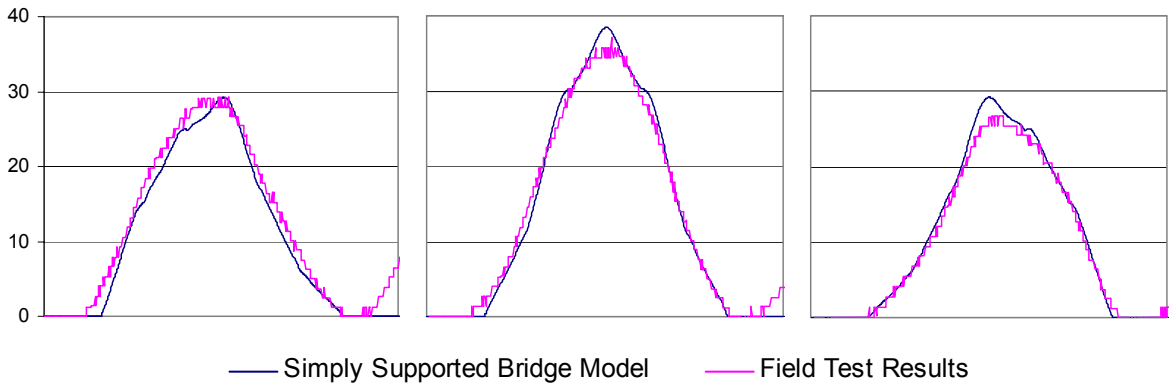

Figure 3.4.1. Bending stress (MPa) versus time results from field-testing and the predicted bending stress results assuming simply supported conditions.

3.4.2 Finite Tuning of Analytical Model Response to Field Test Results

As has been detailed in full in Section 2.3, the method for validating and fine tuning the finite element model built for this project, and presented in Section 3.2, uses dynamic field test results and the analytical model developed in Section 2.4. Recall that the analytical model is used as an intermediate step, in order to provide guidance to final finite element model tuning. (The tuned analytical model is also essential for accurate load identification.) Recall also that the analytical model may be tuned for overall structural properties, rotational stiffness at supports and the length of load distributions. The analytical model is presented again in Figure 3.4.2.

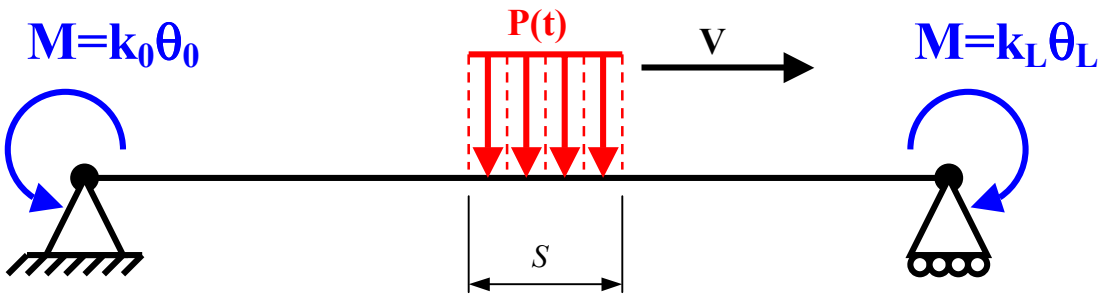

Figure 3.4.2. Analytical model with tuneable load distribution length, rotational stiffness at supports and overall stiffness.

The properties of the preliminary analytical model, like the preliminary finite element model, were based on structural drawings (Appendix F) and site inspection. The properties of the preliminary analytical model were then tuned, so that its response matched the measured results for the locomotive of known wheel loads and axle spacing moving at 10 km/hr. The analytical model was then further verified against data for normal traffic. The response of the tuned analytical model and the field test results for the slow moving locomotive are presented in Figure 3.4.3. The final properties of the tuned analytical model are listed in Table 3.4.1.

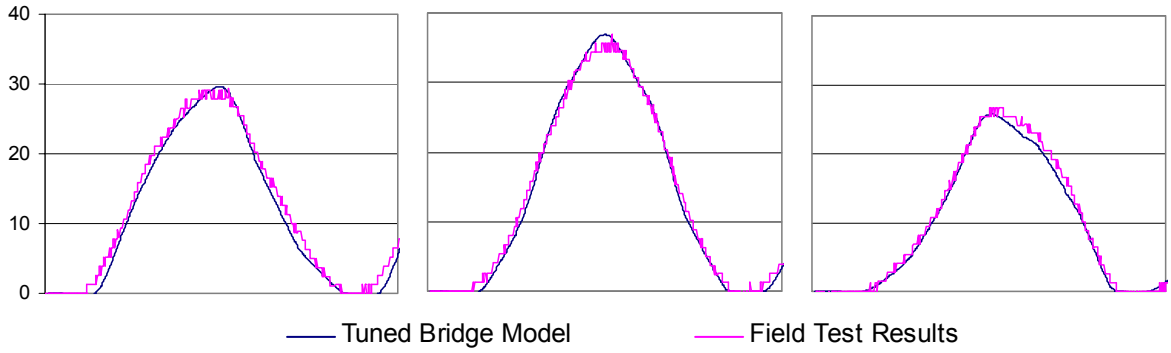

Figure 3.4.3. Bending stress (MPa) versus time results from field-testing and the bending stress results from the tuned model.

Beam Properties		
Cross Sectional Area	3.33×10^{-2}	m^2
Mass Density	7.85×10^{3}	$kg.m^{-3}$
Damping Ratio	0.1	%
Length	6.812	m
Modulus of Elasticity (E)	207	GPa
Original Second Moment of Area (I)	3.26×10^{-3}	m^4
Factored Second Moment of Area (I)	3.05×10^{-3}	m^4
Velocity	3.10	$m.s^{-1}$
Distance from Neutral Axis (y)	0.375	m
Distance from Origin (x)	1.747	m
Tunable Beam Properties		
End Rotational Stiffness (k_O)	0	$N.m.rad^{-1}$
End Rotational Stiffness (k_L)	4.50×10^{7}	$N.m.rad^{-1}$
Overall Stiffness Factor	1.07	
Contact Patch Length	1.7	m

Table 3.4.1. Final properties of the tuned analytical model.

The properties of the analytical model, which are tuned in order to match the modelled response to the measured response, are listed separately in the table. As was noted in Section 2.4, a quasi-static analytical model was developed in order to speed up the process of tuning the analytical response to measured results for a slow moving vehicle.

Once the properties were found for the quasi-static model, these were then used in the fully dynamic model for load identification, as per Section 2.5.

From the tuneable beam properties of Table 3.4.1 it is clear that the end conditions are not simply supported, as originally assumed, but in fact exhibit a rotational stiffness at the fixed bearing.

3.4.3 Fine Tuning of the Finite Element Sensitivity Model Response

Guided by the tuning of the analytical model, the finite element sensitivity model was then tuned. Clearly it is not sufficient to simply include rotationally stiffened constraints to the fixed bearing in the finite element model. The true structural response and the stress variations that accompany it for the entire structure are sought, so that the entire finite element model behaves in a manner closely approximating reality. Instead then, with the guidance of the analytical model, the structure was investigated in order to find a reasonable cause for the variation from simply supported behaviour. Finite element models were built to investigate a number of potential causes. After a great deal of consideration, a number of discussions with project partners and sponsors, and further finite element modelling and site inspection, the most likely cause of the variation from simply supported conditions was settled upon.

The likely cause of the increased stiffness at the fixed bearing is that the BFB-transom and transom-rail connections possess some stiffness. This may appear both obvious and insignificant, however when coupled with the resistance of the fixed bearing to move longitudinally (located well below the neutral axis of the broad flange beams), and the resistance of the rails to move longitudinally, a significant moment effect is set

up at the bearing. This effect has been confirmed, to some extent, in subsequent tuning of the finite element model. Recall from Section 3.2, that the rails have been extended 2.5 metres beyond each end of the span at either end and fixed in all three rotations and translations. Recall also that longitudinal spring elements (along the rail axis) have been modelled at the rail-transom and transom-BFB connections. The intention was to allow adjustment of the modelled pandrol rail clip connection. By adjusting the stiffness of these spring elements it has been possible to tune the finite element sensitivity model such that modelled bending stress results match the test and analytical results.

Figure 3.4.4 shows the bending moment distribution of the approach span finite element sensitivity model, with tuned longitudinal spring elements at the rail-transom and transom-broad flange beam connections, under a stationary locomotive load. Also shown is the moment effect set up by the stiffness in the rail-transom-broad flange beam connection and the resistance of the fixed bearing to move longitudinally.

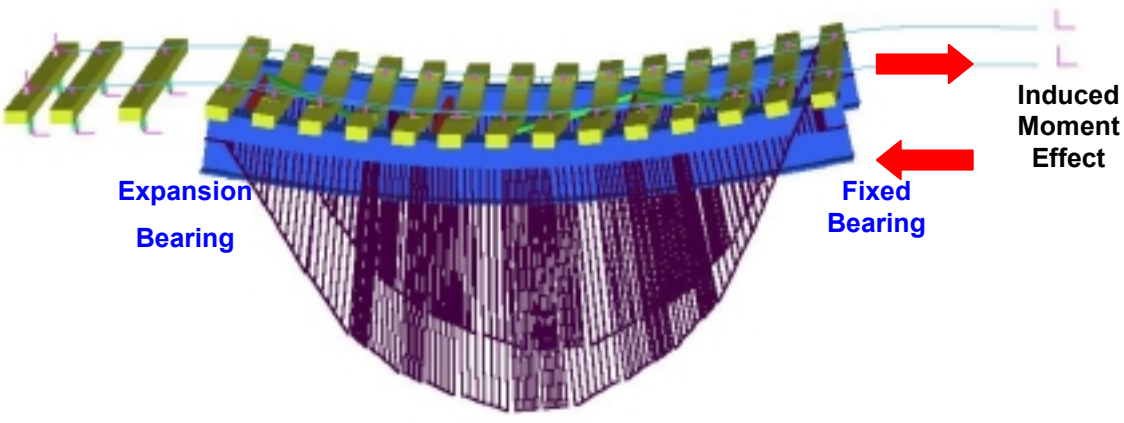

Figure 3.4.4. Bending stress distribution of the approach span under a static locomotive load.

The finite element sensitivity model was also tuned to account for the length of the load distribution identified from the analytical model. This was achieved using the vertical

spring-damper elements modelled at the rail-transom connections. Softening or stiffening the vertical spring stiffness has allowed the load distribution to be tuned and modelled.

3.4.4 The Significance of the Variation from the Simply Supported Assumption

Considering only the modelled bending stress results, presented in Figures 3.4.1 and 3.4.3, it may appear that the stiffness set up at the fixed bearing has an insignificant effect on the structural integrity of the Mullet Creek Railway Bridge, or indeed any bridge of this type. This is not the case. The variation of the Mullet Creek Railway Bridge from the simply supported assumption, and the expected variation of other bridges of this type, is likely to have a significant effect on the structural integrity of the bridge. This will be discussed in greater detail in Chapter 4. However in this section, it is observed that in other bridges of this type, where the main girders are welded sections, the fixed bearings have undergone cracking apparently not seen in the expansion bearing. See Figure 3.4.5, from a bridge in Richmond, NSW, which is of similar design to the Mullet Creek bridge showing cracking at the fixed bearings of two consecutive spans. Note that the expansion bearings are not damaged.

Figure 3.4.5. Cracking at the fixed bearings of consecutive spans of a similar bridge in Richmond, NSW [Rail Infrastructure Corporation].

In the Mullet Creek bridge, the sections are rolled rather than welded. As one would expect then, no cracking has been observed at the fixed or expansion bearings. Instead, however, the piers under the fixed bearings show signs of damage not seen at the expansion bearings. Figure 3.4.6 shows damage at the piers under the fixed bearing. Note that there is no damage under the expansion bearing.

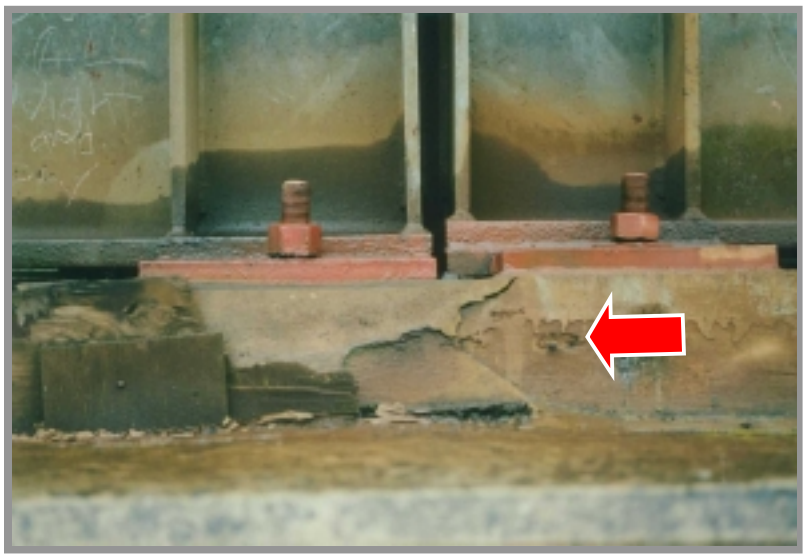

Figure 3.4.6. Damage at the pier beneath the fixed bearing at one of the Mullet Creek Railway Bridge approach spans.

A summary of this section is presented in Sorrenson and West [72].

3.5 Load Identification from Structural Response

3.5.1 Identification of 'Noisy' and 'Quiet' Response Signals from Test Data

It is not feasible to identify the time varying magnitude of every load which crosses the Mullet Creek Railway Bridge, instead a sample of loads are identified for each type of rolling stock

The applied load from a wheel with defects, such as out-of-round wheels or wheel flats, will differ significantly from the applied load caused by a wheel without defects. In this project, an attempt has been made to consider both cases, by identifying wheels with defects and wheels that are relatively defect free, from measured dynamic response. The response for every train recorded during testing was investigated and the strain cycles for each train sorted into two categories, either relatively noisy or relatively quiet. 'Noisy' signals are assumed to be the result of the interaction between wheel defects or other defects and the structure, and 'quiet' signals are assumed to be the result of the interaction between relatively defect free wheels and the structure. Once all the strain cycles are separated into noisy or quiet categories, a typical noisy signal and a typical quiet signal are chosen for each type of rolling stock and load identification carried out on each. Recorded strain results for a number of trains are shown in figures 3.5.1 – 3.5.5. The number of noisy and quiet responses identified from the measured data for a number of train types is shown in table 3.5.1

Figure 3.5.1 illustrates the strain response for a series of Manildra wagons. The wagons have all been classified 'quiet', though since the signal from all the wagons are similar it would make little difference whether the wagons were classified quiet or

noisy, since the classification is merely so that a typical response may be chosen for load identification.

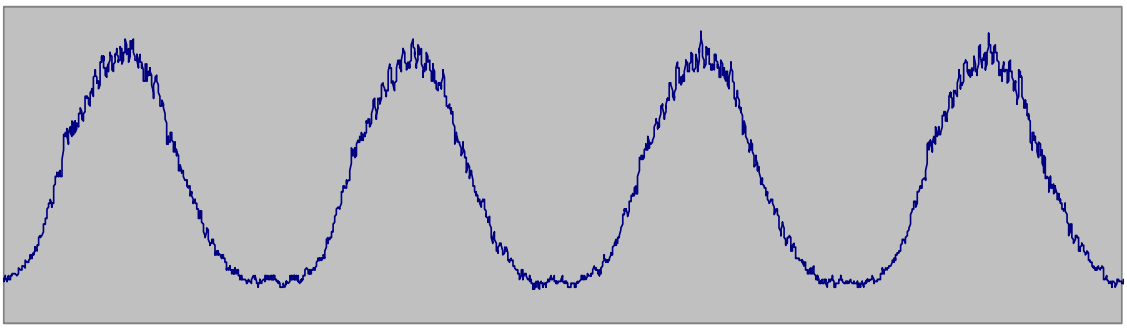

Figure 3.5.1. The measured strain versus time response for a series of Manildra wagons (tape 2, event 10).

Figure 3.5.2 illustrates the response for a series of BHP wagons. The first, second and fourth response cycles are relatively quiet, while the third response cycle is relatively noisy.

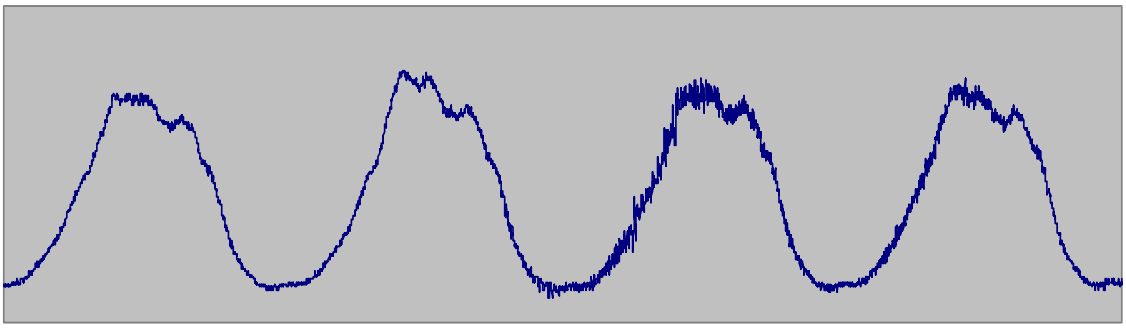

Figure 3.5.2. The measured strain versus time response for a series of BHP wagons (tape 2, event 31).

Figure 3.5.3 also illustrates the response for a series of BHP wagons. In this case the first, and fourth response cycles were considered relatively quiet, while the second and third response cycles were considered relatively noisy.

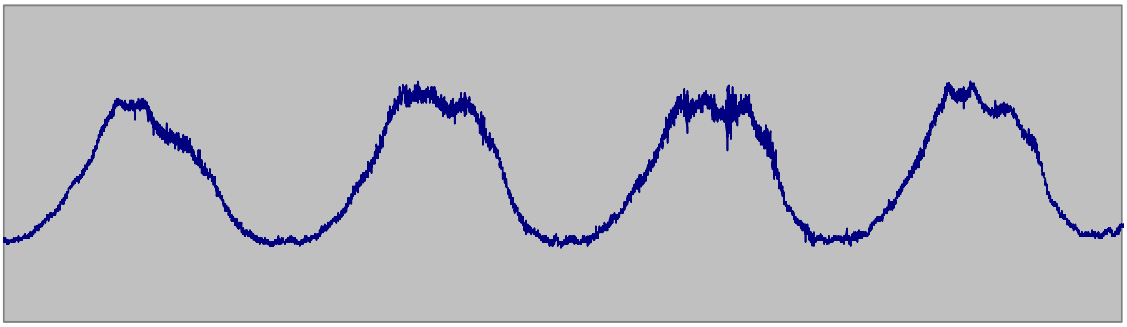

Figure 3.5.3. The measured strain versus time response for a series of BHP wagons (tape 2, event 24).

Figure 3.5.4 illustrates the response for a Tangara train. The signal is almost entirely 'noisy'. Tangara trains travel at relatively high speeds and are somewhat notorious for having a high number of wheel defects.

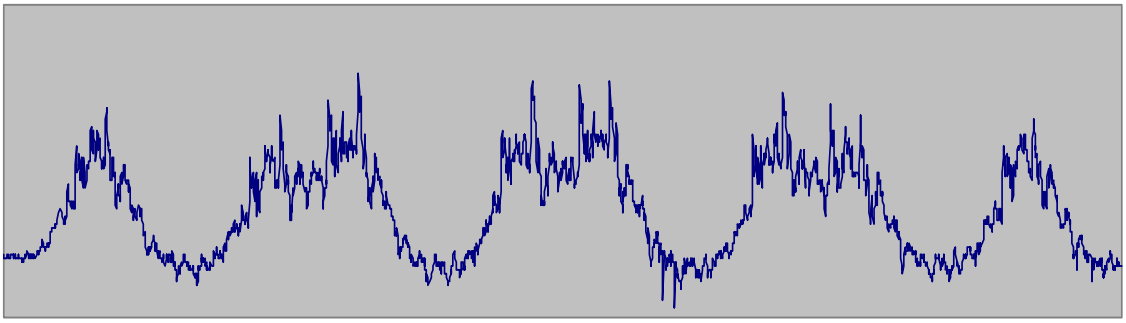

Figure 3.5.4. The measured strain versus time response for a Tangara train (tape 2, event 21).

Figure 3.5.5 illustrates the response for a City Rail Electric train.

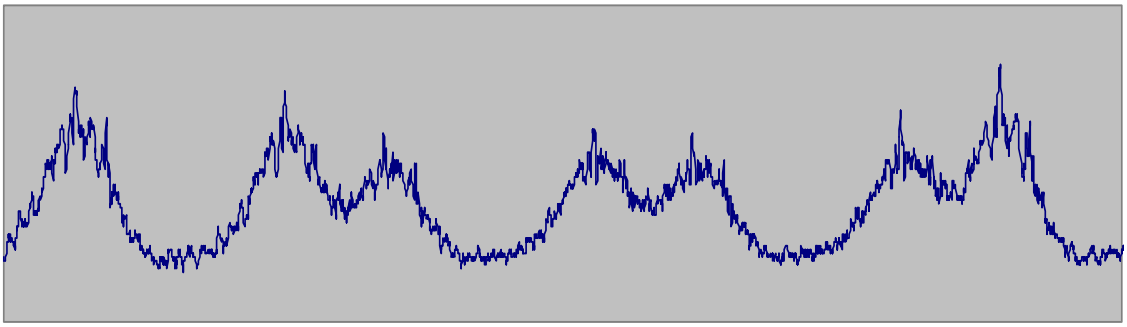

Figure 3.5.5. The measured strain versus time response for a City Rail Electric train (tape 2, event 20).

The complete set of recorded test data was categorised as either ‘noisy’ or ‘quiet’ response. Table 3.5.1 presents the results. All of the Manildra wagons yielded similar responses, which have all been categorised as ‘quiet’. Tangara trains yielded the highest percentage of noisy responses. The response of BHP trains in the up direction was relatively quiet in comparison to BHP trains in the down direction. (Note that the “up” direction is toward Sydney Central Station and the “down” direction is away from Sydney Central Station). The speed of BHP trains in the up direction is generally lower than the speed of BHP trains in the down direction on the Mullet Creek Bridge. This is due to the fact that BHP trains travelling in the up direction generally start from rest at a branch line just 1 or 2 kilometres south of Mullet Creek Bridge.

Rolling Stock Type	'Noisy' Response	**'Quiet' Response**	**% 'Noisy' Response**
Assorted Freight			
Locomotives	2	8	20%
Wagons	10	26	28%
BHP (Down)			
Locomotives	10	14	42%
Wagons	14	27	34%
BHP (Up)			
Locomotives	3	23	12%
Wagons	9	43	17%
Manildra			
Locomotives	7	5	58%
Wagons	0	36	0%
Passenger Trains			
City Rail Electric (Down)	42	39	52%
City Rail Electric (Up)	74	66	53%
City Rail Diesel (Down)	6	6	50%
City Rail Diesel (Up)	6	10	38%
Tangara	12	4	75%

Table 3.5.1. The complete set of test data categorised into 'noisy' or 'quiet' response.

3.5.2 Identification of Loads from 'Noisy' and 'Quiet' Response Signals

Loads have been identified from a typical noisy and quiet response for each train type. The recorded events chosen for load identification are listed in table 3.5.2.

Train Type	Tape & Event	Speed ($km.h^{-1}$)	Axle Spacing (m)			Static Load (kN)	Noisy / Quiet Response
Electric Passenger	Tape 2, Event 27	90.6	2.45	5.326	2.45	74	N & Q
Diesel Passenger	Tape 2, Event 6	88.2	2.4	5.5	2.4	72	N & Q
Tangara	Tape 2, Event 21	104.1	2.4	3.876	2.4	65	N & Q
442 Class Loco	Tape 2, Event 26	49.4	1.702	1.702		93.7	Q
81 Class Loco	Tape 1, Event 6	81.6	1.905	1.905		106.2	N
BHP 67t Wagon	Tape 2, Event 24	16	1.676	2.236	1.676	83.385	N & Q
Manildra 100t Wagon	Tape 2, Event 10	82.6	1.9	1.9	1.9	122.63	Q

Table 3.5.2. Recorded events chosen for load identification.

Loads have been identified using the method outlined in Section 2.5. Figures 3.5.6(a), 3.5.7(a), 3.5.8(a) and 3.5.9(a) present the raw identified loads, for four of the chosen train types. Note the large spikes as the load enters and leaves the span. This is the same problem identified in Section 2.5. The stress response from the forward solution of the analytical model yields results which are identical to the measured response. The raw identified loads are unusable in the finite element simulations however, due to the very large and unrealistic spikes. Figures 3.5.6(b), 3.5.7(b), 3.5.8(b) and 3.5.9(b) present the identified loads after cropping the load values with a lower and upper bound. Recall from Section 2.5 that the relative error of using a lower and upper bound is assessed by using the corrected load values in a 'forward' solution, generating a structural response which is compared against the measured response. Upper and lower bounds are then adjusted if the analytical response using the corrected load values differs greatly from the measured response. Figures 3.5.6(c), 3.5.7(c), 3.5.8(c) and

3.5.9(c) present the comparison of the analytical model forward solution using the corrected load values and the measured response, for several train types.

Figure 3.5.6 presents the raw identified loads, the corrected identified loads with a lower bound of 100 kN and an upper bound of 150 kN, and a comparison of forward solution with the test results for the 'noisy' 81 Class Manildra Loco of tape 1, event 6.

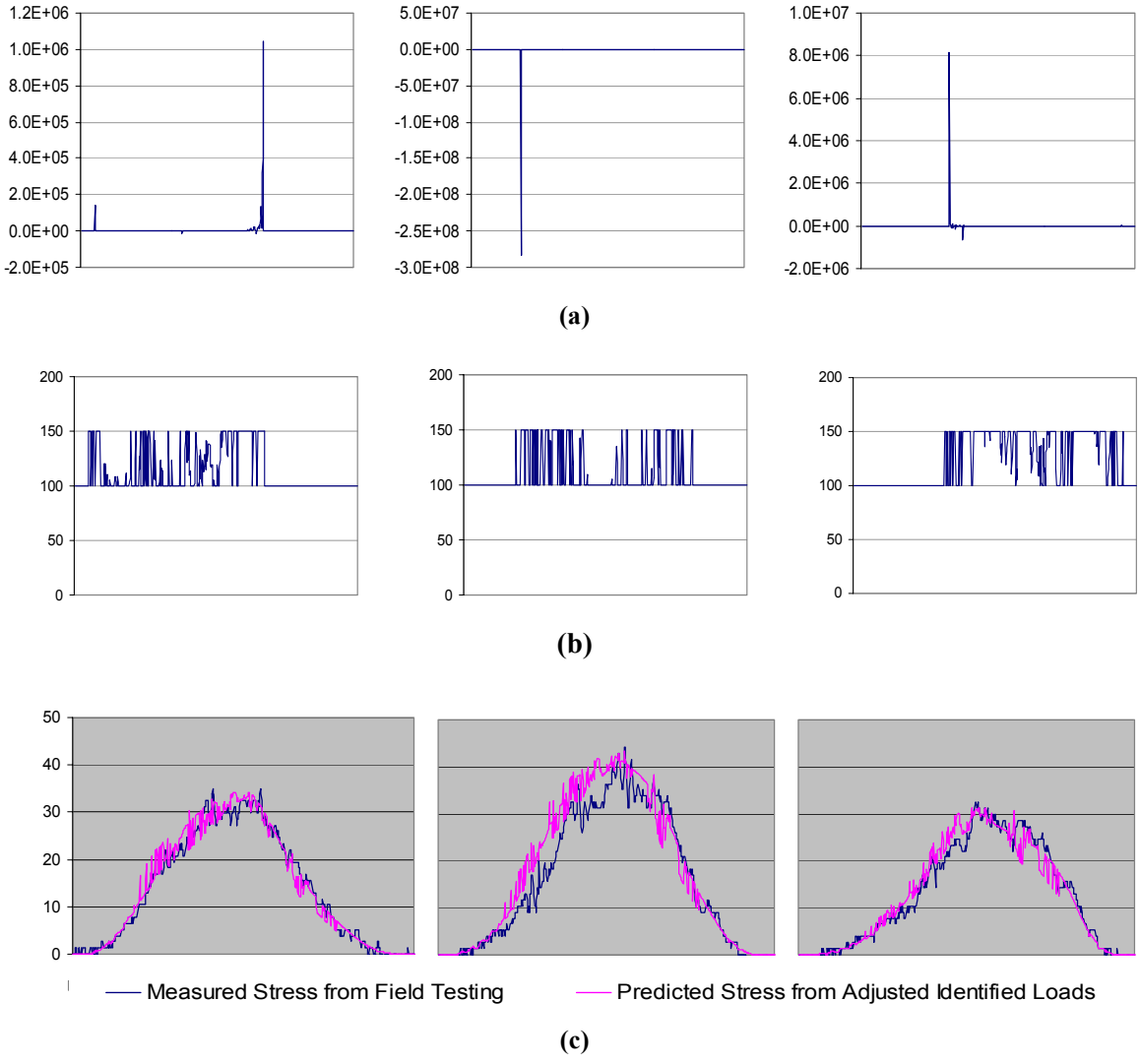

Figure 3.5.6. Load identification for the 'noisy' 81 Class Locomotive; tape 1, event 6.

(a) Raw identified loads (in kN);

(b) Corrected identified loads (in kN); lower bound of 100 kN and upper bound of 150 kN;

(c) Comparison of forward solution using corrected loads and test response (in MPa).

Figure 3.5.7 presents the raw identified loads, the corrected identified loads with a lower bound of 60 kN and an upper bound of 100 kN, and a comparison of forward solution with the test results for the 'noisy' diesel passenger train of tape 2, event 6.

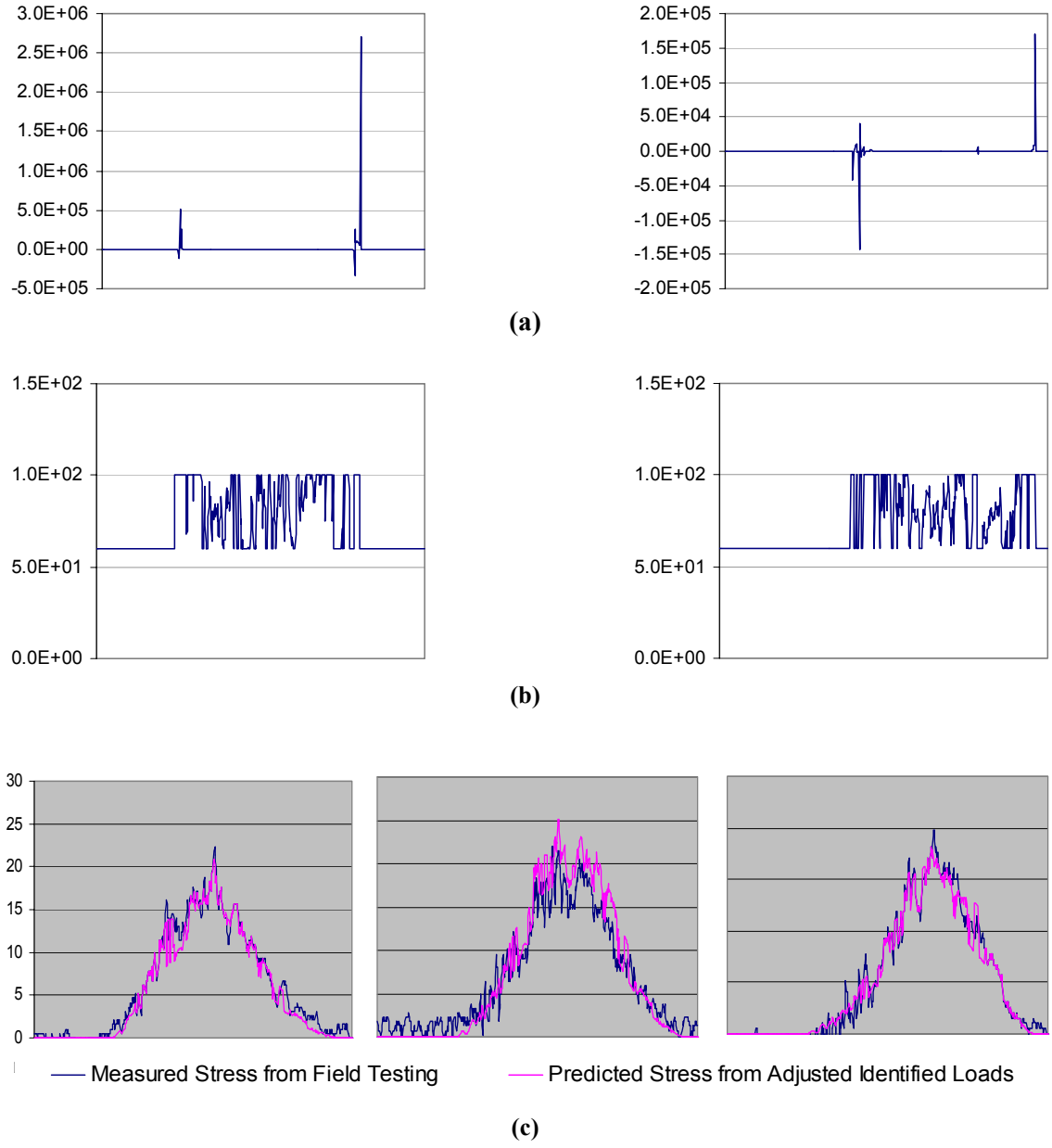

Figure 3.5.7. Load identification for the 'noisy' diesel passenger train; tape 2, event 6.

(a) Raw identified loads (in kN);

(b) Corrected identified loads (in kN); lower bound of 60 kN and upper bound of 100 kN;

(c) Comparison of forward solution using corrected loads and test response (in MPa).

Figure 3.5.8 presents the raw identified loads, the corrected identified loads with a lower bound of 40 kN and an upper bound of 100 kN, and a comparison of forward solution with the test results for the 'noisy' Tangara passenger train of tape 2, event 21.

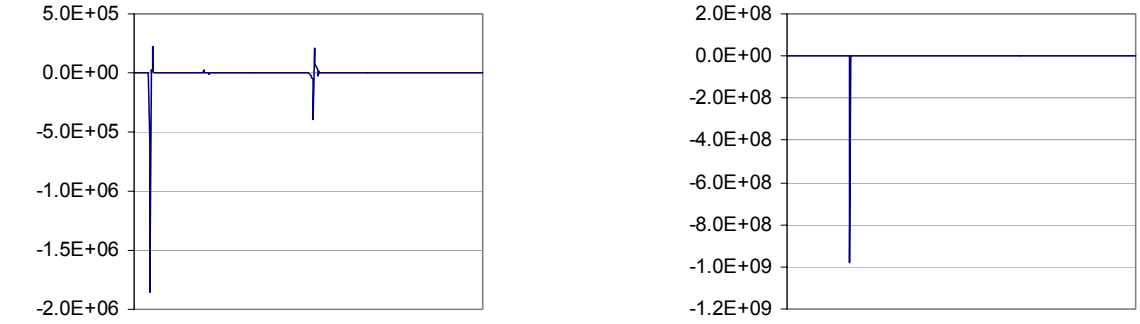

(a)

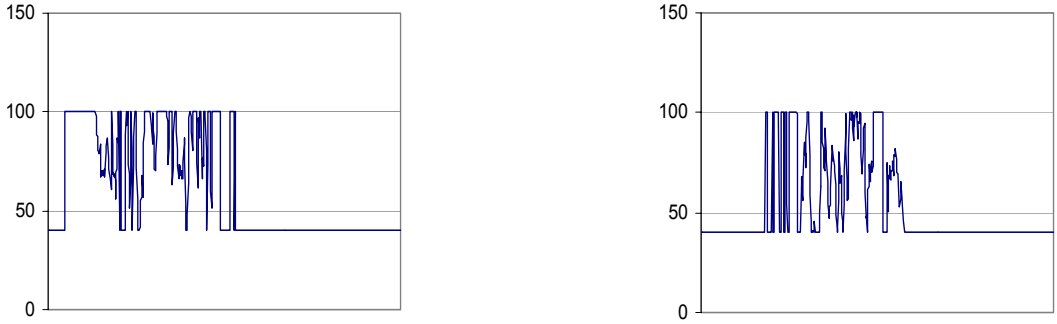

(b)

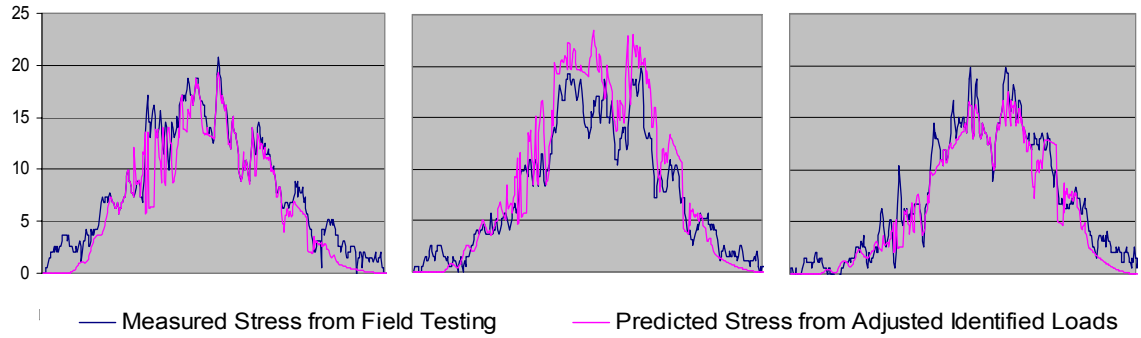

(c)

Figure 3.5.8. Load identification for the 'noisy' Tangara passenger train; tape 2, event 21.

(a) Raw identified loads (in kN);

(b) Corrected identified loads (in kN); lower bound of 40 kN and upper bound of 100 kN;

(c) Comparison of forward solution using corrected loads and test response (in MPa).

Figure 3.5.9 presents the raw identified loads, the corrected identified loads with a lower bound of 70 kN and an upper bound of 130 kN, and a comparison of forward solution with the test results for the 'noisy' electric passenger train of tape 2, event 27.

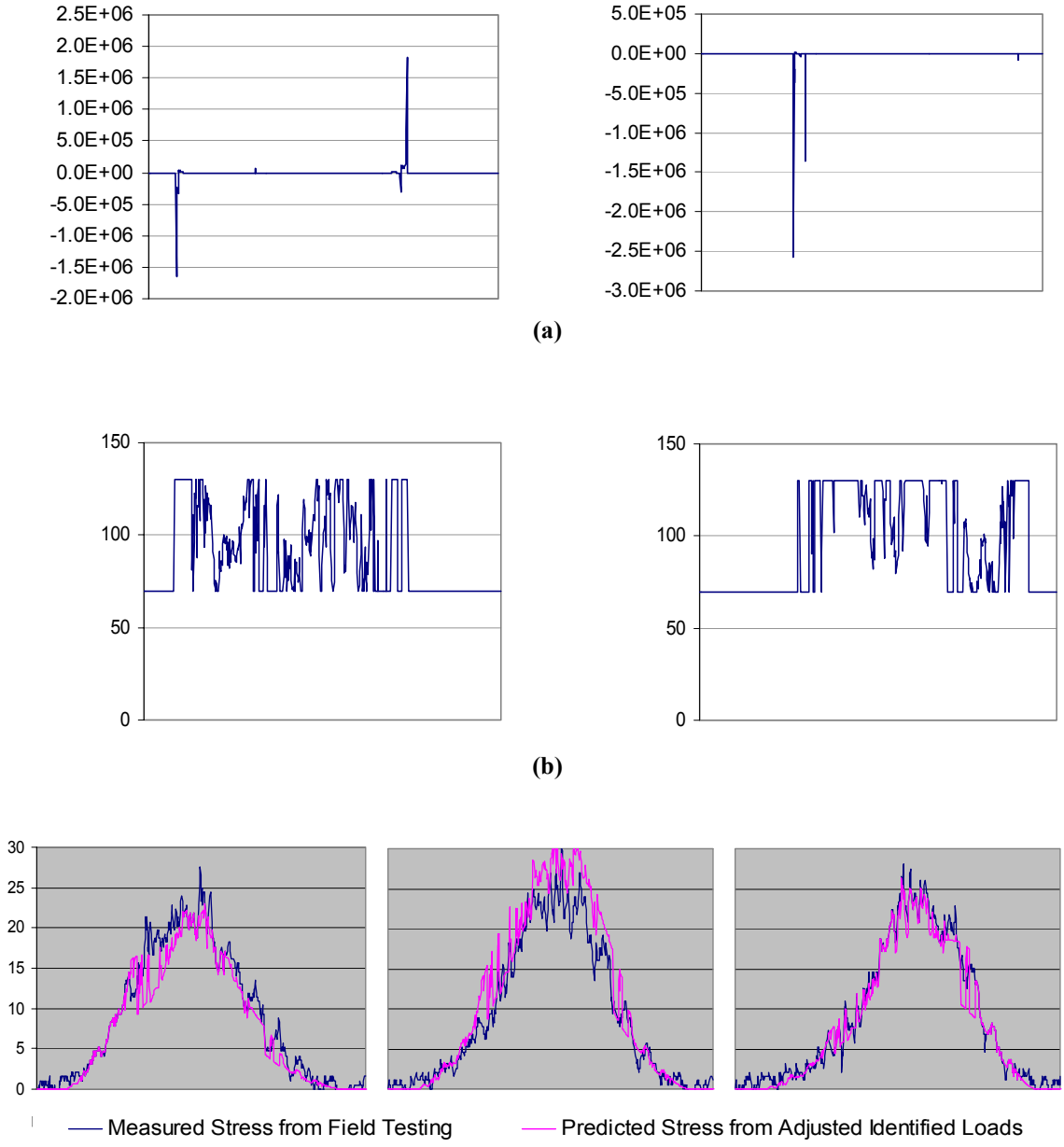

Figure 3.5.9. Load identification for the 'noisy' electric passenger train; tape 2, event 27.

(a) Raw identified loads (in kN);

(b) Corrected identified loads (in kN); lower bound of 70 kN and upper bound of 130 kN;

(c) Comparison of forward solution using corrected loads and test response (in MPa).

3.6 Duty Cycle Development

3.6.1 Duty Cycle Development

As was outlined in Section 2.6, in this research a somewhat traditional approach has been followed in developing the loading history for the Mullet Creek Railway Bridge.

5. Identify Potential Sources of Loading
6. Identify Loading History from those Sources
7. Simplify Loading into Representative Units
8. Clearly Document Loading History, Reference Information Sources and Outline Assumptions and Uncertainties

3.6.2 Potential Sources of Loading

Potential sources of loading include local industries and rail operators. The potential sources of loading identified for the Mullet Creek Railway Bridge are listed below.

- Passenger and Goods Traffic (Rail Services Australia)
- Bombo Quarry Freight Traffic (Rail Services Australia)
- Wongawilli Coal Mine Freight Traffic (BHP)
- Dunmore Quarry Freight Traffic (Boral)
- Australian Paper Freight Traffic
- Manildra Starch Plant Freight Traffic
- National Rail (Rolling Stock Operator for Some of the Above Plants)
- Freight Corp. (Rolling Stock Operator for Some of the Above Plants)

3.6.3 Load History

The following pages present the raw load data identified, as well as brief referencing indicating where this data was obtained. Assumptions and references presented in these pages are minimal and are repeated in full in section 3.6.5. Tables 3.6.1 – 3.6.4 present a summary of raw data gathered from four working timetables. Table 3.6.5 presents raw data gathered for some of the major local industries. Figure 3.6.1 contains photos of many of the locomotives that have crossed the Mullet Creek Railway Bridge. Photos are reproduced with permission from the Railpage web site (www.railpage.org.au), individual authors are acknowledged in the figure caption. Figures 3.6.2 – 3.6.9 show schematics for common passenger trains that have crossed the Mullet Creek Railway Bridge. Passenger train images are reproduced from the City Rail web site (www.cityrail.nsw.gov.au/trains).

Train Type	Frequency (/wk)	Number of Carriages	Tonnes (/train)	Other Information
Diesel / Electric Freight				
(Goods)	57		900	maximum tonnage for single 42,44,25 or 421 Class Loco (p91 - 94)
				maximum length = 60 x 4 wheeled vehicles (p91 - 94)
			750	maximum tonnage for single 48 or 49 Class Loco (p91 - 94)
				maximum length = 45 x 4 wheeled vehicles (p91 - 94)
			1500	maximum tonnage for double 48 or 49 Class Loco (p91 - 94)
				maximum length = 60 x 4 wheeled vehicles (p91 - 94)
(Mixed)	6		310	maximum length = 35 x 4 wheeled vehicles (p91 - 94)
(Pick-Up)	17			
(Milk)	8		500	
Diesel / Electric Passenger				
	6	8	390	maximum tonnage for single 43,44 or 421 Class Loco (p91 - 94)
	5	6	260	maximum tonnage for single 48 or 49 Class Loco (p91 - 94)
	6	2		
	19		200	
	16		230	
(Fast)	5		273	
	3		300	
	8		?	
				For BHP trains to Wongawilli see page 102

Table 3.6.1. Raw data from the 1968 NSW Department of Railways Working Timetable.

Train Type	Frequency (/wk)	Number of Carriages	Tonnes (/train)	Other Information
Freight	86		590	single branch line (p89)
			1175	double branch line (p89)
CPH	15	3		
	19	2		
	11	1		
BUDD	21	5		
Diesel / Electric	15	5	155	47,48 or 49 Class Locos, maximum load per loco 280 tonne (p3 / p83)
	5	7	180	
	6	2	55	
	1	8	200	
	1	8	231	
	5	4	184	
	5	7	205	
	1	10	205	
	1	10	280	
	1	8	231	
Diesel	1	5		
	9	4		
	26	2		

Table 3.6.2. Raw data from the 1979 Public Transport Commission of NSW Working Timetable.

Train Type	Frequency (/wk)	Number of Carriages	Tonnes (/train)	Other Information
Loco Hauled	95			
2 Car Diesel	87	2		
4 Car Diesel	9	4		
DEB Set	8			
Diesel	50	2		
	13	Daylight Express		

Table 3.6.3. Raw data from the 1985 State Rail Authority of NSW Working Timetable.

Train Type	Frequency (/wk)	Number of Carriages	Tonnes (/train)	Other Information
G-Set	64	4		
IC	140	4		
	77	6		
	1	8		
Endeavour	115	2		
	11	4		

Table 3.6.4. Raw data from the 2000 State Rail Authority of NSW Working Timetable.

Source	Freq. (/wk)	Type of Loco	No. of Locos	Type of Wagon	No. of Wagons	Tonnes (/train)	Tonnes (/yr)	Reference
BHP- Wongawilli: (1965 - 2000)								
Up - Loaded	5					1000		Freight Corp.
Down - Loaded	5							
				67	12 - 16	(1964 - 1984+)		A Railway History of the Illawarra & Proposed Waste Emplacement at Wongawilli
							2000000	The Collieries Handbook
		D34	1	(1969+)				railpage.org.au
		45 & 442		(1995+)				railpage.org.au & observation
		442	2					railpage.org.au & observation
Boral- Dunmore Quarry: (1965 - 1993, 2000 -)								
Up - Loaded	3 / mth						3000 / mth	National Rail
Down - Unloaded	3 / mth							
RSA - Bombo Quarry: (1965 - 2000)								
Up - Loaded	2	48	1			2000		RSA - Sydney
		or 81	2					
Down - Unloaded	2							
				20	75			Freight Corp.
				41	(‘til '96)			RSA - Bombo
				54	(after '96)			RSA - Bombo
						pre 1994	300000	RSA - Bombo
						1994	280000	
						1995	327000	
						1996	167000	
						1997	238000	
						1998	67000	
						1999	132000	
Australian Paper - Bomaderry: (1965 - 1987)								
Up - Loaded							60000	Australian Paper
Down - Unloaded								
Manildra - Bomaderry: (1973 - 2000)								
Up - Loaded	6			100	11 - 22			Bomaderry Station
Down - Loaded	6			25				
		81	2	100	14			Observation

Table 3.6.5 Raw data from the some of the Illawarra’s local industries.

(a)

(b)

(c)

(d)

(e)

(f)

Figure 3.6.1. Locomotives which have crossed the Mullet Creek Railway Bridge.

(a) D34 Locomotive *(Brad Peadon)*.

(b) 44 Class Locomotive *(Frank Archer)*.

(c) 442 Class Locomotive *(Brad Peadon)*.

(d) 45 Class Locomotive *(Brad Peadon)*.

(e) 48 Class Locomotive *(David Johnston)*.

(f) 81 Class Locomotive *(Mal McDonald)*.

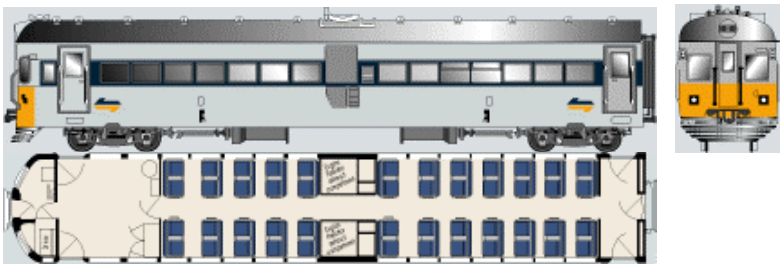

Figure 3.6.2. 620 Class driver motor railcar with luggage area.

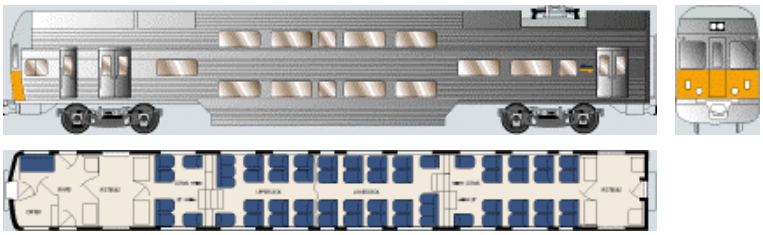

Figure 3.6.3. V Set driver motor carriage (intercity services).

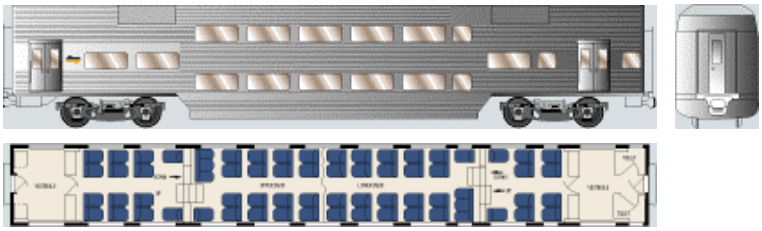

Figure 3.6.4. V Set trailer carriage (intercity services).

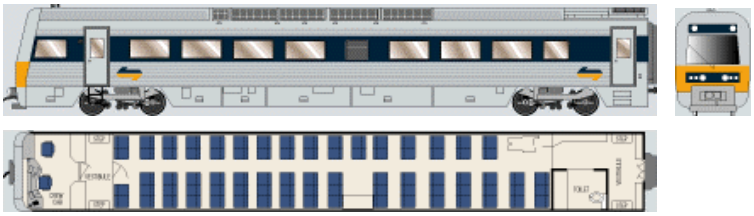

Figure 3.6.5. TE Endeavour driver motor railcar with toilet.

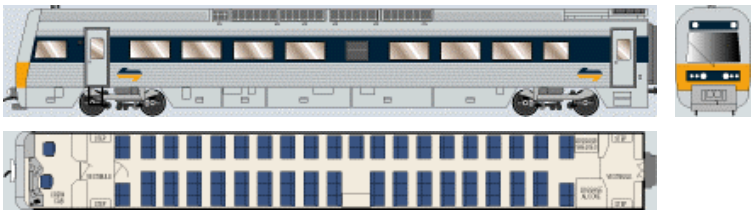

Figure 3.6.6. LE Endeavour driver motor railcar with luggage area.

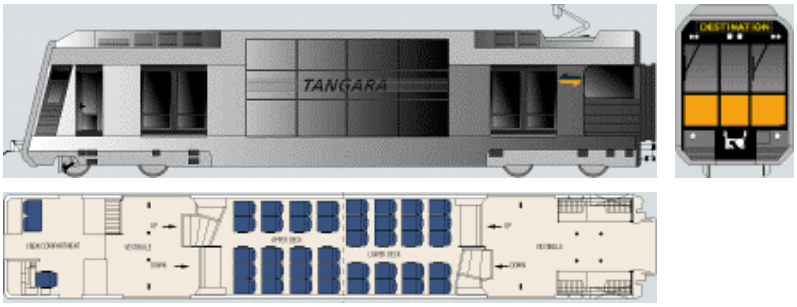

Figure 3.6.7. G Set (Tangara) driver trailer (intercity and suburban services).

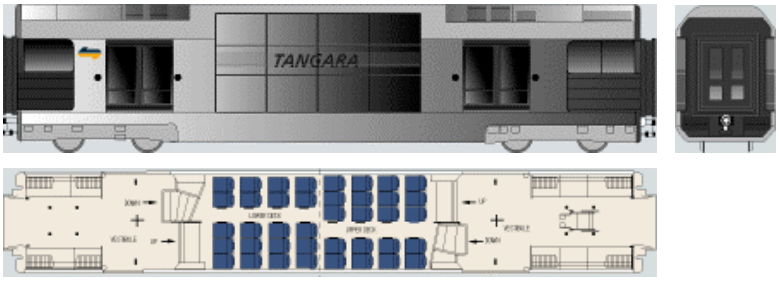

Figure 3.6.8. G Set (Tangara) motor carriage (intercity and suburban services).

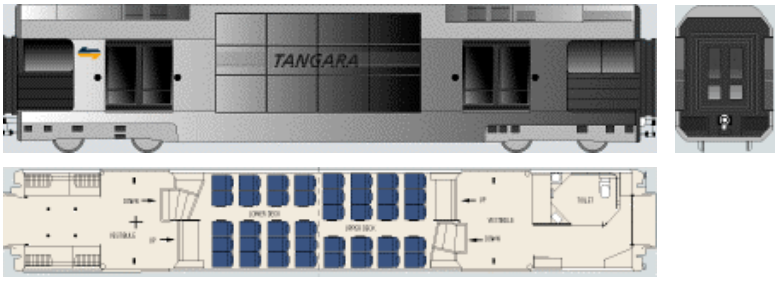

Figure 3.6.9. G Set (Tangara) motor carriage with toilet (intercity suburban services).

3.6.4 Load History Simplified into Representative Units

Raw data has been simplified into representative units of traffic in two stages, data is simplified once according to loading source and then data is simplified again into the final representative units of traffic. The results of the first step of simplifying raw data are presented in Appendix J. The final results, the representative units of traffic used in analysis of the Mullet Creek Bridge, are presented below in tables 3.6.6 – 3.6.13.

Tables 3.6.6 – 3.6.11 present simplified duty cycle data for all traffic since the commissioning of the bridge in 1965 until 2000. Tables 3.6.12 and 3.6.13 present simplified duty cycle data for current traffic.

Train Type	Passes (total)	Speed (km/hr)	Type of Loco	No. of Locos	Type of Carriage	No. of Carriages
Loco Hauled	60840	84	44 Class	1	620 Class	6
	29120	84	48 Class	1	620 Class	4
	13520	84	48 Class	1	620 Class	2
BUDD	20800	84			BUDD	5
Diesel / Electric	96720	92			V-Set IC	2
	62400	92			V-Set IC	4
	20280	92			V-Set IC	6
Endeavour	35620	84			TE / LE	2
G-Set	16640	102			G-Set	4

Table 3.6.6 Representative passenger traffic (1965 – 2000).

Train Type	Wheel Load (kN)											
	Axle 1	2	3	4	5	6	7	8	9	10	11	12
44 Class	92.7	92.7	92.7	92.7	92.7	92.7	92.7	92.7	92.7	92.7	92.7	92.7
48 Class	63.7	63.7	63.7	63.7	63.7	63.7	63.7	63.7	63.7	63.7	63.7	63.7
620 Class Carriage	93	93	93	93								
BUDD	64	64	64	64								
V-Set IC Driver/Trailer	74	74	74	74								
V-Set IC Carriage	49	49	49	49								
TE / LE	72	72	72	72								
G-Set Driver/Trailer	55	55	55	55								
G-Set Motor	65	65	65	65								

Table 3.6.7 Representative passenger traffic wheel load specifications.

Train Type	Axle Spacing (mm)												
	Coupler-1	1-2	2-3	3-4	4-5	5-6	6-7	7-8	8-9	9-10	10-11	11-12	12-13
44 Class	2143	2096	2096	5080	2096	2096	4540	2096	2096	5080	2096	2096	4540
48 Class	2147	1676	1981	3150	1981	1676	4293	1676	1981	3150	1981	1676	4293
620 Class Carriage	2095	1981	11888	1981	1257								
BUDD	2552.7	2591	13564	2591	2553								
V-Set IC Driver/Trailer	2663	2450	13777	2450	2663								
V-Set IC Carriage	2663	2450	13777	2450	2663								
TE / LE	3300	2400	14400	2400	2750								
G-Set Driver/Trailer	2038	2400	11544	2400	1938								
G-Set Motor	1938	2400	11544	2400	1938								

Table 3.6.8 Representative passenger traffic axle spacing specifications.

Train Type	Passes (total)	Speed (km/hr)	Type of Loco	No. Of Locos	Type of Wagon	No. of Wagons
BHP- Wongawilli:						
Up - Loaded	7800	23	D34		67 tonne	15
Down - Loaded	7800	42	D34		67 tonne	15
Up - Loaded	1300	23	442	2	67 tonne	15
Down - Loaded	1300	42	442	2	67 tonne	15
Dunmore & Bombo Quarry, Australian Paper and Freight Trains:						
Up - Loaded	57890	66	48	1	41 t (loaded)	25
Down - Unloaded	57890	66	48	1	41 t (empty – 10 t)	25
Manildra - Bomaderry:						
Up - Loaded	8424	82	81	2	100 tonne	20
Down - Loaded	8424	82	81	2	100 tonne	20

Table 3.6.9 Representative freight traffic (1965 – 2000).

Train Type	Wheel Load (kN)											
	Axle 1	2	3	4	5	6	7	8	9	10	11	12
D34	108	108	108	108	108	108	108	108	108	108	108	108
442 Class	93.7	93.7	93.7	93.7	93.7	93.7	93.7	93.7	93.7	93.7	93.7	93.7
67 t Wagon	83.385	83.4	83.4	83.4	83.4	83.4	83.4	83.4	83.4	83.4	83.4	83.4
48 Class	63.7	63.7	63.7	63.7	63.7	63.7	63.7	63.7	63.7	63.7	63.7	63.7
41 t Wagon	50	50	50	50	50	50	50	50	50	50	50	50
10 t (empty 41 t Wagon)	12	12	12	12	12	12	12	12	12	12	12	12
81 Class	106.2	106	106	106	106	106	106	106	106	106	106	106
100 t Wagon	122.63	122.63	122.63	122.63	122.63	122.63	122.63	122.63	122.63	122.63	122.63	122.63

Table 3.6.10 Representative freight traffic wheel load specifications.

Train Type	Axle Spacing (mm)												
	Coupler-1	1-2	2-3	3-4	4-5	5-6	6-7	7-8	8-9	9-10	10-11	11-12	12-13
D34	2311.4	1702	1702	7239	1702	1702	4623	1702	1702	7239	1702	1702	4623
442 Class	2311.4	1702	1702	7239	1702	1702	4623	1702	1702	7239	1702	1702	4623
67 t Wagon	1118	1676	8687	1676	2236	1676	8687	1676					
48 Class	2147	1676	1981	3150	1981	1676	4293	1676	1981	3150	1981	1676	4293
41 t Wagon	1118	1676	8687	1676	2236	1676	8687	1676					
10 t (empty 41 t Wagon)													
81 Class	2438	1905	1905	8660	1905	1905	4876	1905	1905	8660	1905	1905	4876
100 t Wagon	950	1900	12000	1900	1900	1900	12000	1900					

Table 3.6.11 Representative freight traffic axle spacing specifications.

Train Type	Passes (/yr)	Speed (km/hr)	Type of Loco	No. of Locos	Type of Carriage	No. of Carriages
Diesel / Electric	7384	92			V-Set IC	4
	4004	92			V-Set IC	6
Endeavour	7124	84			TE / LE	2
G-Set	3328	102			G-Set	4

Table 3.6.12 Representative passenger traffic (current annual).

Train Type	Passes (/yr)	Speed (km/hr)	Type of Loco	No. Of Locos	Type of Wagon	No. of Wagons
BHP- Wongawilli:						
Up - Loaded	260	23	442	2	67 tonne	15
Down - Loaded	260	42	442	2	67 tonne	15
Dunmore & Bombo Quarry and Freight Trains:						
Up - Loaded	156	66	48	1	41 t (loaded)	25
Down - Unloaded	156	66	48	1	41 t (empty – 10 t)	25
Manildra - Bomaderry:						
Up - Loaded	312	82	81	2	100 tonne	20
Down - Loaded	312	82	81	2	100 tonne	20

Table 3.6.13 Representative freight traffic (current annual).

3.6.5 Information Sources, Assumptions and Uncertainties

Information Sources

Many sources were explored in order to develop the duty cycle for the Mullet Creek Bridge, with varying usefulness. The most useful sources are referenced below.

- Rail Transport Museum (Illawarra Chapter) - *meets the first Tuesday of the month at BHP Northgate Visitors Centre, Port Kembla, NSW, Australia.*
- RSA Working Timetables (1968, 1979, 1985 and 2000) – *available from NSW State Records and The NSW State Library.*
- NSW Dept. of Environment and Planning, *Proposed Waste Emplacement at Wongawilli – Environmental Impact Statement*, Sydney : Dept. of Environment and Planning, 1984.
- BHP Steel Collieries Division, *The Collieries Handbook*, Wollongong, NSW : BHP, 1993.
- Southern, J.L.N, *A railway history of the Illawarra*, Melbourne : B.H.P., 1978.
- Dept. of Environment and Planning, *Planning for blue metal quarrying in the municipalities of Shellharbour and Kiama and Tablelands Sub-region*, Dept. of Environment and Planning, 1982.
- General information at http://www.railpage.org.au.
- Locomotive information at http://locopage.railpage.org.au
- Information on passenger trains at http://www.cityrail.nsw.gov.au/trains
- For rail operating statistics http://www.freightcorp.com.au
- International rail server at http://www.railserve.com

The co-operation of individuals in a number of organisations has greatly assisted the process of gathering information. Freight Corp. and Bombo Quarry and RSA deserve

special mention and were particularly helpful. Many notes, advice and vehicle specifications were provided by RSA. A vehicle database provided by RSA was particularly useful. The locopage web site has a number of similar specifications for locomotives.

Some other Internet sites which, although not used in this project, may be helpful when searching for duty cycle data are listed below.

- Commonwealth Railways at http://www.railpage.org.au/comrails
- Australian Motive Power Rosters at http://members.tripod.com/amrp/index.htm
- Australian Association of Time Table Collectors at http://www.aattc.org.au
- ARHS – Archives at http://www.accsoft.com.au/~arhsnsw/archives.htm
- Australian Railway Maps at http://people.enternet.com.au/~cbrnbill/maps/austrail.htm
- International rail server at http://trainweb.com

Assumptions and Uncertainties

For the development of representative passenger traffic:

- Only four working timetables have been used for passenger train information. These have been assumed to be indicative of the decade in which they fall.
- Passenger trains have been reduced to nine representative units only. Although this is extremely simplified and many types of locomotives and carriages have been omitted, it is assumed to provide a practical estimate.
- It is assumed that half of the passenger rail traffic passes in the up direction and half in the down.

- 44 Class & 48 Class locomotive specifications are taken from the Vehicle Database provided by RSA.
- BUDD & G-Set (Tangara) specifications are taken from drawings provided by RSA.
- Endeavour and 620 Class specifications are provided by RSA, coupler dimensions for 620 Class trains are estimates.
- V-Set axle specifications are from provided by RSA, other dimensions derived from diagrams on cityrail.com.au.

For the development of representative freight traffic;

- Information regarding the rail movements of BHP came from many sources. The exact configuration of a BHP coal train to Wongawilli was difficult to obtain. Various sources suggested that BHP trains haul approximately 1000 tonnes per trip and 67 tonne wagons have historically been used. The collieries handbook suggests that the Wongawilli mine produces approximately 2 000 000 tonnes per year which confirms the tonnage per train and number of trips suggested by representatives of Freight Corp. The D34 main line locomotive is assumed to have been in service from 1965 to 1995. After which 45 class and 442 class locomotives are assumed to have been used for transporting coal. This assumption is supported by both observations of current trains and the railpage web site.
- The administration officer from Bombo Quarry was very helpful, providing information regarding the wagons that have been used as well as annual tonnages for the Boombo Quarry. Freight Corp. supplied information regarding a typical train makeup of two 48-class locos and a 2000 tonne haul.

- Little information was available regarding the make up of Dunmore Quarry or Paper Mill trains, although tonnages were provided. It was indicated that Dunmore quarry trains hauled around 1000 tonne.
- For simplicity Dunmore Quarry, Bombo Quarry, Australian Paper Mill and Freight trains are all assumed to haul 1000 tonne loads made up of 41 tonne wagons and one 48 class loco. Wagons are assumed to be loaded in the up direction only.
- Manildra train information was difficult to gather. Observation of locos hauling Manildra wagons as well as information from a local train station gave some indication of a typical train consist and the frequency of running. These trains are assumed to be loaded in both directions. This is as per directions given by station staff, although observations indicate that this is not always the case.
- The number of Bombo trains have been doubled and assumed 1000t instead of 2000t, to simplify the number of representative trains.
- Working timetables give little indication of freight train loads. Freight trains from working timetables are assumed to be the same configuration as quarry trains.
- Dunmore and Bombo Quarry, Australian Paper and freight trains are assumed to have the same configuration as one another and have been simplified to one representative train type with the appropriate number of passes.
- 48 Class, 442 Class and 81 Class locomotive specifications are taken from the Vehicle Database provided by RSA.
- D34 specifications are derived from the locopage web site, the wheel base is assumed to be the same as 442 Class locomotives.
- Wagon specifications are taken from a Vehicle Database provided by RSA.
- The 67t wagon listed is assumed to be NGAF (68t), NGBA or NGBF wagons.

- 41t wagons are assumed to have the same wheel spacing as NGAF (68t), NGBA or NGBF wagons with a 41t load.
- 100 t Manildra wagons are assumed to be MGFH wagons.
- Empty wagon wheel loads are assumptions only.

All train speeds are taken from field-test results, with some additional guidance from Working Time Tables and railpage.com.au.

3.7 Stress Recovery from Identified Loads and Duty Cycle Data

3.7.1 Stress Recovery

Identified loads and duty cycle data have been used to generate a complete stress history of the Mullet Creek Railway Bridge and to project future stresses.

Where the structural response was measured during field testing, for a particular current train type, the identified loads for that train have been used to generate load tables for use in finite element analysis. For historical trains, which no longer run on the Mullet Creek Railway Bridge, identified loads measured from the structural response under current traffic have been adjusted and used to generate load tables for analysis. Where the historical train is considered to have a similar interaction with the structure as a current train, the structural responses from current trains have been used to estimate applied loads. For example BUDD passenger trains, which no longer run on the Mullet Creek Railway Bridge, have been considered similar to current diesel passenger trains in their interaction with the structure. The identified loads from current diesel passenger trains have been used for the simulation of BUDD passenger trains by shifting the identified loads of diesel passenger trains, according to the shift in the magnitude of wheel load specifications for diesel passenger trains to BUDD passenger trains. Wheel load specifications for diesel passenger trains are 72 kN and for BUDD passenger trains are 64 kN (Table 3.6.7). Therefore, for the generation of load tables BUDD train, wheel loads are assumed to be equivalent to diesel train wheel loads, shifted by 8 kN and spaced according to BUDD passenger train axle spacing specifications (Table 3.6.8). Wheel loads for all trains for which loads were not identified from test results have been similarly assumed.

3.7.2 Comparison of the Finite Element Response with Analytical and Field Test Results

Figures 3.7.1 and 3.7.2 compare the predicted bending stress response from the tuned finite element beam model with the analytical model response, for the representative duty cycle 'noisy' electric passenger train and 'noisy' 81 Class locomotive. Figures 3.7.3 and 3.7.4 compare the predicted bending stress response from the tuned finite element model with the measured field-test response for the same 'noisy' electric passenger train and 'noisy' 81 Class locomotive.

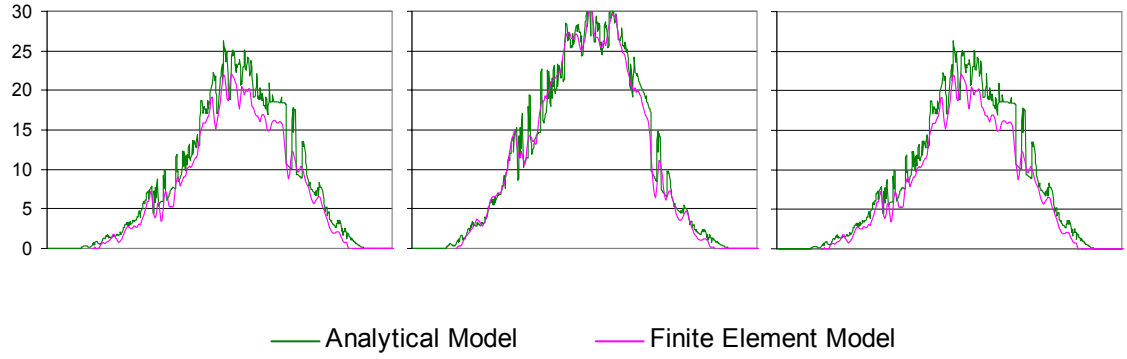

Figure 3.7.1. Comparison of the predicted bending stress versus time response (in MPa) from the tuned finite element model with the analytical model response for the representative duty cycle 'noisy' electric passenger train.

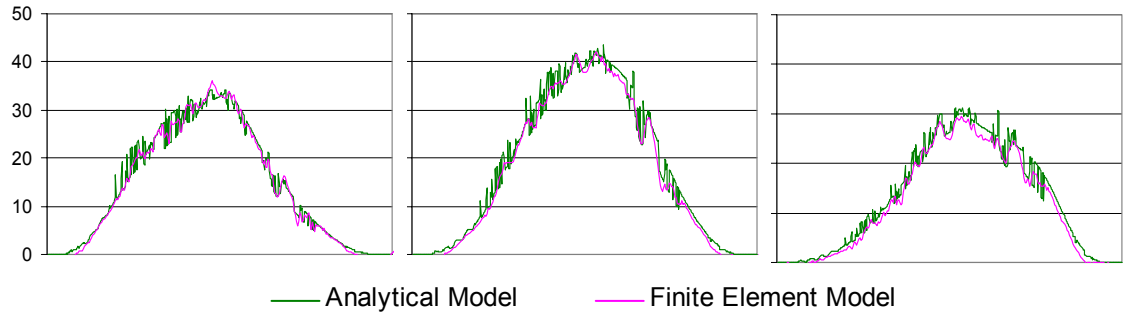

Figure 3.7.2. Comparison of the predicted bending stress versus time response (in MPa) from the tuned finite element model with the analytical model response for the representative duty cycle 'noisy' 81 Class locomotive.

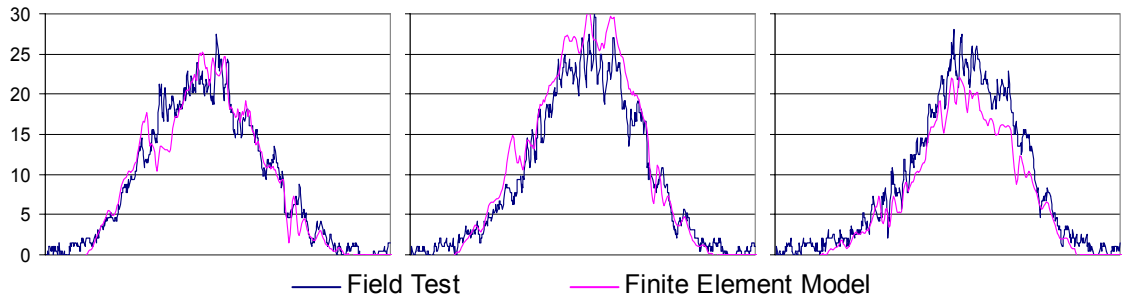

Figure 3.7.3. Comparison of the predicted bending stress versus time response (in MPa) from the tuned finite element model with the measured field-test response for the representative duty cycle 'noisy' electric passenger train.

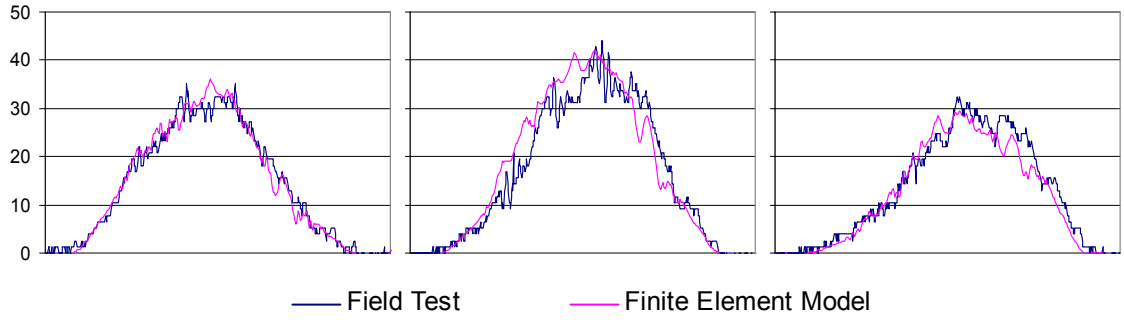

Figure 3.7.4. Comparison of the predicted bending stress versus time response (in MPa) from the tuned finite element model with the measured field-test response for the representative duty cycle 'noisy' 81 Class locomotive.

Load tables for all of the representative duty cycle trains have been applied to the tuned finite element model and the structural response generated. For long trains, particularly freight trains, short units have been modelled and the structural response from those short units summed for the complete response. For example, for a Manildra freight train, with two locomotives and twenty wagons, only the structural response to the locomotives and two of the wagons has been simulated. The response of the complete duty cycle train is then easily found, by summing the response of additional wagons, using the simulated response of the two wagons modelled (Figure 3.7.6).

Figure 3.7.5 compares the predicted bending stress response from the preliminary web-stiffener connection plate element model, with the measured field test response for the representative duty cycle 'noisy' 81 Class locomotive. The stress response from the preliminary plate element sub-model built in this project does not match the test results with sufficient accuracy to be used with confidence.

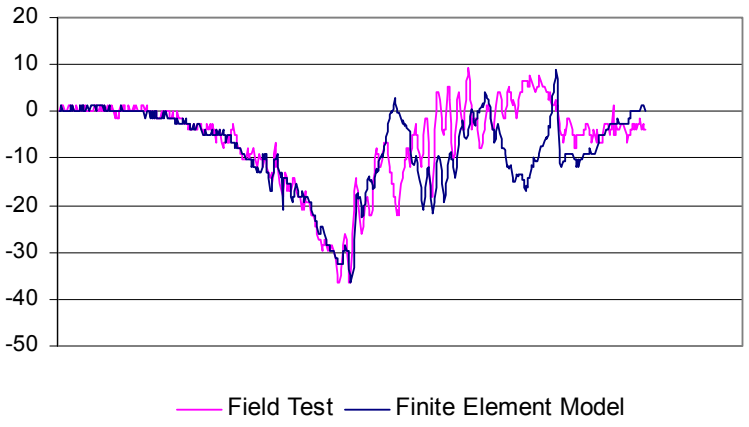

Figure 3.7.5. Comparison of the predicted bending stress versus time response (in MPa) from the web-stiffener connection plate element model with the measured field-test response for the representative duty cycle 'noisy' 81 Class locomotive.

It was decided that further pursuit of the use of sub-models to model complex components was beyond the scope of this thesis. Further investigation is highly recommended in future work.

3.7.3 Manipulation of Applied Loads

The response of the complete set of duty cycle trains has been found for both 'noisy' and 'quiet' trains. The complete finite element bending stress response at mid-span and the shear stress response at the fixed bearing, for the 'noisy' duty cycle Manildra train and the 'noisy' duty cycle six carriage electric passenger train, are shown in Figures 3.7.6 – 3.7.9. The complete finite element bending stress response at mid-span and the

shear stress response at the fixed bearing, for the 'noisy' duty cycle two carriage diesel passenger train is shown in Figure 3.7.10.

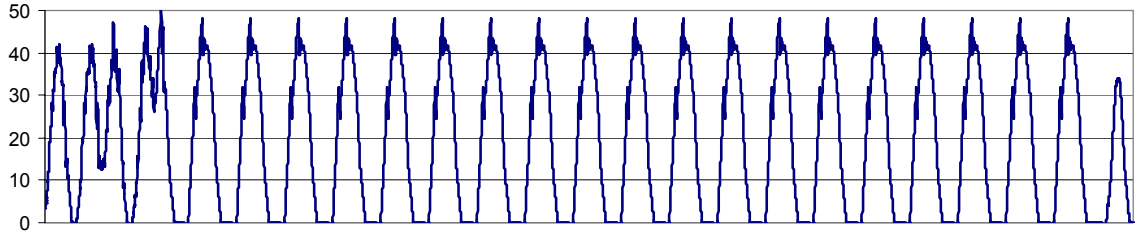

Figure 3.7.6. The complete finite element bending stress versus time response (in MPa) at mid-span for the 'noisy' duty cycle Manildra train.

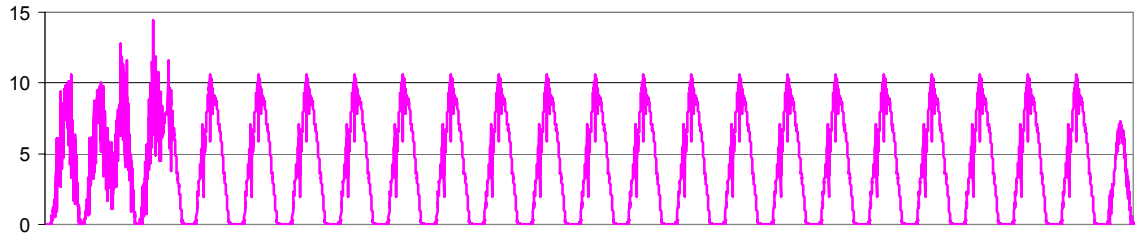

Figure 3.7.7. The complete finite element shear stress versus time response (in MPa) at the fixed bearing for the 'noisy' duty cycle Manildra train.

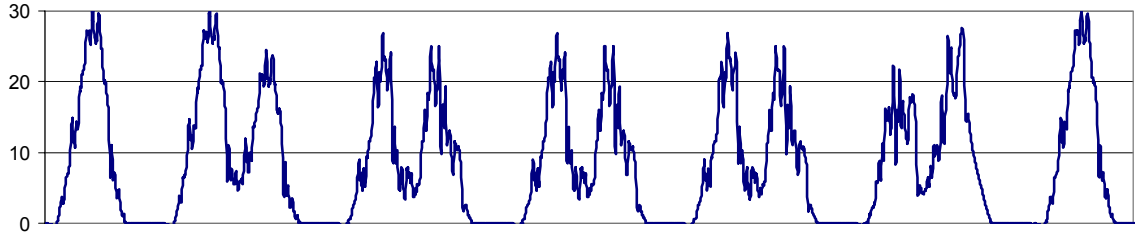

Figure 3.7.8. The complete finite element bending stress versus time response (in MPa) at mid-span for the 'noisy' duty cycle six carriage electric passenger train.

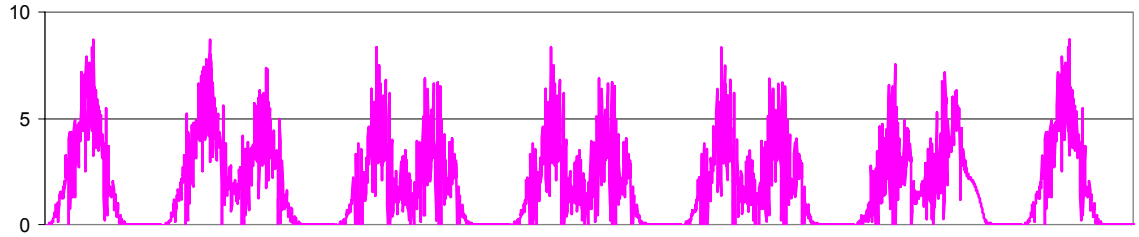

Figure 3.7.9. The complete finite element shear stress versus time response (in MPa) at the fixed bearing for the 'noisy' duty cycle six carriage electric passenger train.

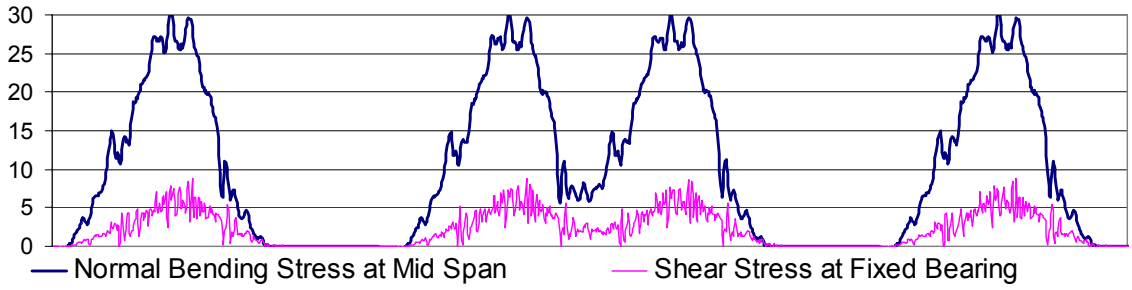

Figure 3.7.10. The complete finite element bending stress versus time response (in MPa) at mid-span and the shear stress response at the fixed bearing for the 'noisy' duty cycle two carriage diesel passenger train.

3.7.4 Manipulation of Structural Conditions

In order to measure the effect that manipulation of the structural conditions has on structural integrity and remaining life, two separate changes have been assessed.

In the first change the longitudinal stiffness of the modelled pandrol rail clip was reduced to zero. This is structurally possible by using zero toe load pandrol clips at the transom-rail connection. The moment effect at the fixed bearing is reduced effectively to zero and so too is shear stress at the fixed bearing. The effect of the change on the bending stress response, at quarter span intervals, for a 'noisy' duty cycle bogie of an electric passenger train, is shown in Figure 3.7.11.

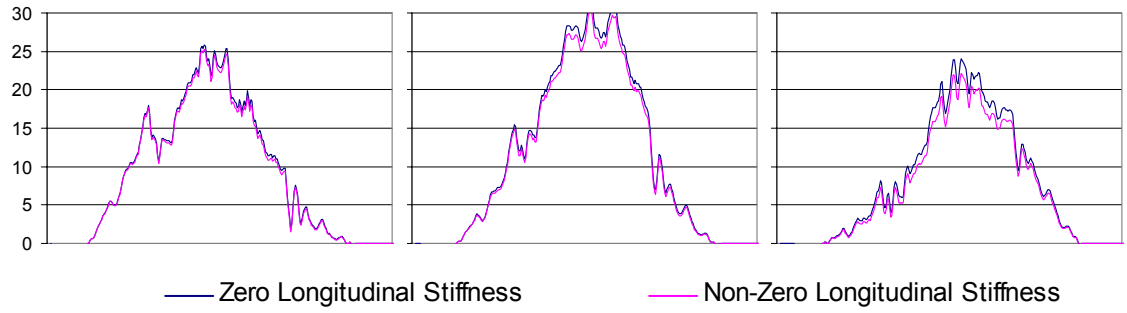

Figure 3.7.11. The effect of reducing the longitudinal stiffness of the modelled pandrol clip connection on the bending stress versus time response (in MPa) at quarter span intervals for a 'noisy' duty cycle bogie of an electric passenger train.

The second change made, simulated moving the location of loads transmitted from the transoms to the BFBs from the inner edge of the BFB compression flange to directly above the axis of beam. This is structurally possible using resilient bearing pads between the transoms and the broad flange beams, so that the load from the transom no longer acts on the inner edge of the BFB flange but instead over the axis. In theory, the effect of the change is to remove the high localised stresses in the top flange. Ideally this would be modelled using a plate sub-model. In the absence of a reliable plate element model for the web-stiffener connection, the beam element model has been used to simulate the structural change. The simulated stress history, for the case where the loads are applied above the beam axis, is assumed to be equivalent to the bending stress history of the Mullet Creek Railway Bridge finite element beam model. This is reasonable since the finite element beam model models bending stress without the high localised stresses above the web-stiffener connection caused by eccentric loading of the transom. A comparison of the measured field-test results with the bending stress in the top flange of the finite element beam model is shown in Figure 3.7.12.

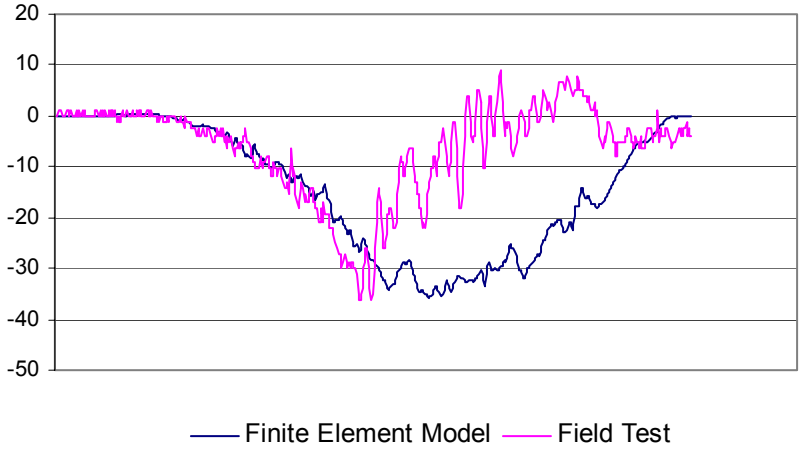

Figure 3.7.12. The effect on the bending stress versus time response in the compression flange above the web-stiffener (in MPa) of moving the point of application of the loads from a position above the inner edge of the BFB compression flange to directly above the beam axis.

3.8 Structural Integrity and Remaining Life Assessment

3.8.1 Structural Integrity and Remaining Life

Three components of the Mullet Creek Railway Bridge have been chosen for analysis.

- The BFB at Mid-Span,
- The Fixed Bearing Component, and
- The BFB Web-Stiffener Component.

3.8.1.1 Broad Flange Beam at Mid-Span and Fixed Bearing Component

Assuming the approach spans behave as concentrically loaded simple beams and ignoring local stress concentrations, the bottom flange at mid-span is the component with the highest peak stresses. This component is unlikely to be critical on the Mullet Creek Railway Bridge, since it is a non-welded rolled section and is therefore unlikely to be sensitive to fatigue. This component is useful for comparison with other bridges, however.

The fixed bearing component has been shown to be significant since, contrary to design, the fixed bearing joint carries considerable shear stress, as demonstrated in Section 3.7. While for the majority of the Mullet Creek Railway Bridge approach spans the component is a non-welded BFB, a welded section has been considered given the failure of the component at other bridges of the same design such, as the Richmond River Underbridge, discussed in Section 3.4.

Figure 3.8.1 illustrates these two components.

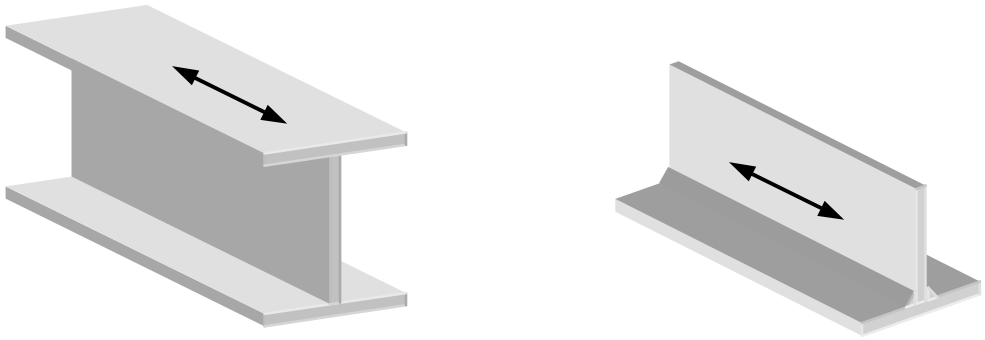

(a) **(b)**

Figure 3.8.1. (a) Rolled non-welded section of the BFB at mid-span,

(b) Weld loaded in shear of the fixed bearing connection.

Both the mid-span of the BFB and the fixed bearing connection may be assessed for structural integrity and remaining life using the stress output of the tuned finite element model. The remaining life of the BFB mid-span has been calculated using the fatigue assessment software described in Section 2.7, nominating the British Standard BS7608 code [110] and Australian Standard Austroads Bridge Design Code [116]. The British Standard and Austroads codes have been chosen since they tend to be most popular for assessment of bridges in Australia. The Eurocode is also popular, although it has not been used since it often yields results identical to the Austroads code. The fixed bearing connection has been assessed using the assessment software, nominating the Austroads Bridge Design Code only. BS7608 was not used on this occasion since it does not offer an appropriate joint detail for the shear loaded fixed bearing component.

The fatigue code detail categories, for the mid-span of the broad flange beam and the fixed bearing connection, are presented in Table 3.8.1.

Joint Class	Detail Category	
	BS7608	Austroads
Non-Welded BFB at Mid-Span	B	160
Shear Loaded Fixed Bearing		80

Table 3.8.1. Detail categories of the mid-span and fixed bearing components.

Remaining life assessment has been carried out separately for the finite element stress response of each duty cycle train. Using the number of passes from the simplified duty cycle data for all traffic since the commissioning of the bridge in 1965 until 2000 (Tables 3.6.6 – 3.6.11), the damage for the period 1965 – 2000 may be calculated. Combining the damage for the period 1965 - 2000 and the simplified duty cycle data for current traffic (Tables 3.6.12 and 3.6.13) within the Palmgren-Miner rule, the remaining life of the span, assuming the current traffic volume remains constant, may be calculated. 'Noisy' and 'quiet' duty cycle trains are analysed separately and their remaining life summed within Miner's rule at the percentages found from testing (Table 3.5.1). Equation 3.8.1 is used to find the remaining life of the span in years.

$$\left[\sum \frac{N_i}{N_{fi}}\right]_{1965-2000} + B_f\left[\sum \frac{N_j}{N_{fj}}\right]_{per\ year} = 1$$

$$B_f = \frac{1-\left[\sum \frac{N_i}{N_{fi}}\right]_{1965-2000}}{\left[\sum \frac{N_j}{N_{fj}}\right]_{per\ year}} \qquad (3.8.1)$$

B_f = number of repetitions to failure,
N_i = number of cycles of applied stress, i,
N_{fi} = number of cycles to failure from the SN curve for applied stress, i,
N_j = number of cycles of applied stress, i,
N_{fj} = number of cycles to failure from the SN curve for applied stress, i.

Remaining life estimates for the non-welded BFB at mid-span and shear loaded fixed bearing connection are listed in Table 3.8.2. Details of the remaining life calculations are presented in Appendix K.

Joint Class	**Remaining Life Estimate**	
	BS7608	**Austroads**
Non-Welded BFB at Mid-Span	30 000 years	infinite
Shear Loaded Fixed Bearing		infinite

Table 3.8.2. Remaining life estimates for the mid-span and fixed bearing components.

3.8.1.2 Broad Flange Beam Web-Stiffener Component

The third component considered was the connection between the web-stiffener and the top flange of the BFBs. For assessment using finite element generated stresses, a plate sub-model is needed. The stress response from the preliminary plate sub-model built in this project, while helpful, does not match the test results with sufficient accuracy to be

used with confidence. Instead then, test results are used to provide a preliminary investigation. Complete analysis of this joint is deferred for future work. In order to use test results, stress cycles for duty cycle fatigue trains are built by taking measured stresses at the web-stiffener connection for current trains, and manipulating measured stresses in order to simulate historical trains, which no longer run on the Mullet Creek Railway Bridge. In order to simulate historical loading the magnitude of stress cycles from current trains are factored according to the change in the magnitude of wheel load specifications, in a manner similar to that used to construct wheel loads for historical trains from identified loads. For example, a BUDD passenger train, which no longer runs on the Mullet Creek Bridge, has a wheel load specification of 72 kN. In order to generate stress cycles for the web-stiffener connection for this train, where no measured results are available, the stress cycles for a diesel passenger train with wheel specifications of 64 kN are factored by 72/64. Clearly this is not the most ideal method for carrying out fatigue assessment. The important effect of axle spacing, particularly important for short spans like the Mullet Creek approach spans, is ignored. Only the joint measured during field-testing may be assessed and only the loads applied may be assessed reliably. It is not possible to manipulate applied loads and generally it is not possible to simulate manipulation of structural conditions. Regardless, however, assessment has been carried out using measured results to provide a preliminary assessment until a complete assessment may be carried out in future work. The remaining life of the web-stiffener connection has been calculated using the fatigue assessment software described in Section 2.7 nominating the British Standard BS7608 code [110], the Australian Standard Austroads Bridge Design Code [116], the Japanese Society of Steel Construction code [112] and the American Association of Railways

code [113]. A number of codes were used on this occasion due to the variability in the way the codes deal with negative mean stress.

The transverse fillet welded web-stiffener connection is shown in Figure 3.8.2 and the detail categories from the codes are presented in Table 3.8.3.

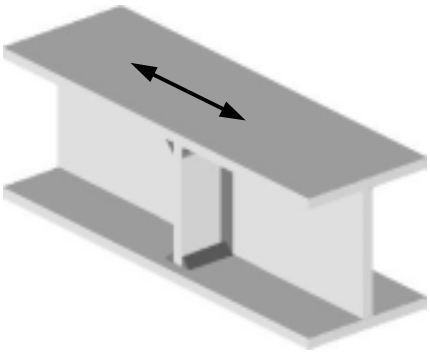

Figure 3.8.2. Transverse fillet welded section of the web-stiffener connection.

Joint Class	**Detail Category**			
	BS7608	**Austroads**	**Japanese**	**AAR**
Transverse Fillet Welded Web-Stiffener Connection	F2	71	E	3.1.6

Table 3.8.3. Detail categories for the transverse fillet web-stiffener connection.

Remaining life estimates for the transverse fillet welded web-stiffener connection are listed in Table 3.8.4. Details of the remaining life calculations are presented in Appendix I.

Joint Class	Remaining Life Estimate			
	BS7608	Austroads	Japanese	AAR
Transverse Fillet Welded Web-Stiffener Connection	Nil	Nil	14 years	infinite

Table 3.8.4. Remaining life estimates for the transverse fillet web-stiffener connection.

3.8.2 Effect of Manipulating Applied Loads

Where the dynamic stress history used in analysis is based on stresses generated via a tuned finite element model, rather than on measured stresses only, loads may be manipulated and the resulting stress history from any load pattern assessed. For the Mullet Creek Railway Bridge loads have been separated into 'noisy' and 'quiet' duty cycle trains. Manipulating loads in this way, estimates for remaining life for all noisy and all quiet trains may be made and compared. Estimates for remaining life for all noisy trains, all quiet trains and the percentage of noisy and quiet trains identified during field-testing is presented in Table 3.8.5 for the BFB at mid-span from the BS7608 code.

Joint Class	Remaining Life Estimate		
	100% 'noisy'	100% 'quiet'	Measured % of 'noisy' and 'quiet'
Non-Welded BFB at Mid-Span	26 000 years	33 000 years	30 000 years

Table 3.8.5. Remaining life estimates for the non-welded BFB at mid-span after manipulation of applied loads.

It is not possible to manipulate applied loads for the web-stiffener connection, since measured results were used rather than finite element generated stress histories.

3.8.3 Effect of Manipulating Structural Conditions

As outlined in Section 3.7.4 two changes to the structural conditions of the Mullet Creek Railway Bridge have been modelled.

The first was a change to the longitudinal stiffness of the modelled pandrol clip. Reducing the stiffness to zero the shear stress at the fixed bearing is removed. The bending stress in the broad flange beam is increased slightly, though remaining life is still infinite according to the Austroads code, and effectively infinite according the BS7608 code.

The second change was to assume loads to be directly above the axis of the BFBs. Ideally, the effect of the change is assumed to remove the secondary bending stresses in the top flange. The effect of this change, on the remaining life of the connection, has been assessed by comparing estimates of remaining life from field-test results to estimates from beam model finite element results, where the effect of secondary bending is nil. Using the Austroads and BS7608 codes, where the Miner's sum is already greater than unity, the remaining life is increased by a factor of approximately 2.25 (Appendix K). Using the Japanese code the remaining life is increased from 14 years to 40 years, a factored remaining life increase of 2.86 (Appendix K).

4. DISCUSSION

4.1 Review

The methodology proposed in this research has been shown to be largely successful, by the application of the method to the Mullet Creek Railway Bridge approach spans.

In Section 2.1, a review of the literature highlighted that where structural models are used for assessment, dynamic interaction is often ignored, or else accounted for by a single amplification factor applied to dead load stresses. Where true dynamic behaviour is included in assessment, generally only measured stresses are used. In the present work, structural models are used to simulate true dynamic behaviour under load. Structural models are built in finite element software, with loads applied via nodal load tables. In Section 2.2, it was noted that the method developed here for modelling the dynamic response of structures in finite element software is equivalent to the method developed and published by Wu, Whittaker and Cartmell [35], for mobile gantry cranes in finite element software. However, in their research Wu, Whittaker and Cartmell do not use identified loads, have not validated their research against field-test results and do not use the method for structural integrity and remaining life assessment. In this project, identified loads are used for the simulation of true dynamic response, the simulated response is verified against field-testing and is used for structural integrity and remaining life assessment.

A number of methods for field-testing of bridge structures have been reviewed in Section 2.3. Dynamic field-testing techniques using strain gauges have been used in the present research for model validation and tuning, as well as for load identification from structural response. The 2001 round of testing was more efficient than previous

rounds of testing. Due to the development of load identification, derived from bending stress response, measurement of the relative axle load was unnecessary. Consequently no person was required to work at track level, thus disruption to normal traffic was avoided. For the Mullet Creek Railway Bridge, field-testing confirmed the predicted high stresses at the web stiffener-top flange connection and identified non-symmetrical bending stress behaviour along the length of the span (Figure 3.4.1).

Much of the literature presenting analysis of bridges subjected to moving loads assumes bridges are simply supported and applied loads are concentrated. In this work, an analytical model has been developed for Euler-Bernoulli beams with rotational stiffness at supports subjected to multiple distributed loads. This is important for model validation and load identification of railway bridges. The Heaviside function is a traditional approach to modelling distributed loads on beams. The response of the analytical model developed in this research has been shown to differ from the response of the Heaviside approximation (Figures 2.4.10 – 2.4.13). This is most notable in the acceleration response where the response of the model developed here appears to more closely resemble field-test results, though further testing and verification is recommended.

The finite element sensitivity model built for the Mullet Creek approach spans (Section 3.2) has proven to be appropriate for model tuning. Of particular importance are the vertical and longitudinal stiffness elements at the rail-transom connection. Tuning of the analytical model to measured test results identified a rotational stiffness at the fixed bearing end of the Mullet Creek approach spans (Table 3.4.1). Subsequent tuning of the finite element model identified the likely cause of the stiffness, as the interaction

between the rails, transoms and the fixed bearing (Section 3.4). While not apparently significant in terms of bending stress at and near mid span, it would appear to be very significant at the fixed bearing where damage is common on bridges of the Mullet Creek type (Figures 3.4.5 and 3.4.6).

Load identification has been employed in this research to determine applied loads. The majority of published research into load identification from structural response is centred on simply supported beams traversed by concentrated loads, and most research has been carried out on road bridges. Due to the analytical model of Section 2.4, load identification theory has been extended to non-simply supported beams with distributed applied loads. An approximate method has been presented to allow feasible load identification of the multiple loads applied to a railway bridge structure. The magnitudes of identified loads have been corrected with a lower an upper bound on load magnitudes (Section 3.5). While this is a somewhat simplified approach, the 'forward' solution of the analytical model, using the identified loads, yields an appropriate comparison with measured field-test bending stress response (Figure 3.5.6 – 3.5.9).

Stresses generated from identified loads and duty cycle data, in finite element beam sensitivity models, compare well with field test results (Figures 3.7.3 and 3.7.4). Since simulated results compare well at locations of field-test results, one may confidently assume that the finite element response elsewhere on the model may be reliably used in assessment. Results from the preliminary plate element sub-model presented in this thesis, while a useful indicator, do not compare with measured results with sufficient accuracy to be used in assessment (Figure 3.7.5).

Three components of the Mullet Creek Railway Bridge approach spans have been chosen for structural integrity and remaining life assessment. The remaining life of the broad flange beam at mid-span and the fixed bearing connection, have been estimated to be infinite according to the BS7608 and Austroads codes (Table 3.8.2). This is as expected for the lightly trafficked Mullet Creek bridge. The estimates for the remaining life of the web-stiffener detail vary greatly according to the codes (Table 3.8.4). The BS7608 and Austroads code suggest the component is beyond failure since the Miner's summation exceeds unity. The Japanese code gives the component 14 years of remaining life, under the current traffic volume, before Miner's sum exceeds unity and the AAR code estimates infinite life. These predictions would appear to reveal more about the codes themselves and the way they deal with negative mean stress, than they do about the web-stiffener detail. The life estimates made by each of the codes relate directly to how the codes account for mean stress. The BS7608 and Austroads codes ignore mean stress for welded components and the Japanese and AAR codes account for mean stress to varying degrees (Figure 2.7.5).

Once the finite element sensitivity models are validated against field test results using identified loads, the applied loads and structural conditions may be manipulated, and the impact on the structural integrity and remaining life assessed (Figures 3.7.11 and 3.7.12). Loading and structural conditions may be adjusted at this point and the integrity and remaining life of the structure evaluated for virtually any combination of structural and loading condition. While the process is largely academic, for the BFB mid-span, whose life is infinite according to the codes, it has been shown that applied loads may be manipulated and the effect on remaining life assessed. If 100% 'noisy' signals are assumed (i.e. noisy vehicle-structure interaction due to defects) the

estimated remaining life is reduced by 25%, compared with the estimated life assuming 100% 'quiet' signals (Table 3.8.5). For the simply designed Mullet Creek Railway Bridge approach spans, where loads are transmitted through transoms supported by main BFB girders, this is a moderate change in life. For more complex structures, like the main span of the Mullet Creek Railway Bridge, where transoms are supported by short stringers rather than long main girders, a much greater effect on remaining life is expected.

Reducing the longitudinal stiffness of the rail-transom connection to zero, in the finite element model, has allowed assessment of the effect of manipulating structural conditions. As a result of the change the shear stress at the fixed bearing was effectively removed. A manipulation of structural conditions has also been simulated at the web-stiffener detail, by using the global compressive stresses of the finite element beam model in the place of measured results. This simulates a shift in the location of loads from the edge of the flange, to a position over the axis of the beam. Although the coded estimates for remaining life have been shown to be unhelpful for the web-stiffener detail, the increase in remaining life predicted by the codes offers some guidance. The simulated change results in a factored increase in estimated remaining life, ranging from 2.25 from the Austroads code to 2.86 from the Japanese code (Section 3.7.4 and Appendix K).

Stress based fatigue assessment is relied upon in the presented methodology, for estimates of remaining life. Software capable of carrying out assessment, via a number of international codes has been written and used in assessment (Appendix E). This

software has been used to provide a critical comparison of international fatigue codes (Section 2.7.3).

4.2 Implications and Recommendations

The method presented here provides the ability to model truly dynamic response for identified loading, at both test measured and non-measured locations on a structure. The generation of a detailed stress history from finite element modelling, based on identified dynamic loads rather than peak static stress, is achievable to sufficient accuracy. Applied loads and structural conditions may be manipulated, to allow reliable consideration of proposed or historical changes. The time and cost of field-testing is greatly reduced through dynamic methods. Dynamic field-testing, carried out according to the final round of field-testing presented in this thesis, greatly reduces disruption to normal traffic and is recommended for future assessments. Model tuning is sped up through the analytical model intermediate step, and final assessment is made more efficient through the use of a software system for structural fatigue codes.

It has been demonstrated that railway bridges have the potential to behave as non-simply supported structures with distributed rather than concentrated applied loads and that sensitivity in finite element modelling therefore is important.

A useful foundation has been built in the present research. There remains a great deal of scope however, for the method developed here to be improved and the research extended. It is recommended that in future work the method be used for other more complicated structures. It is planned that the method will be used for the main span of the Mullet Creek Railway Bridge.

Some work was carried out during field-testing using accelerometers. The aim was to integrate the acceleration signal twice, to enable model tuning and load identification from acceleration response. The equipment used was not appropriate, however, and further accelerometer testing is planned. If successful, this is expected to greatly increase the efficiency of field-testing, and greatly reduce the time of the test set-up and therefore cost of field-testing.

It is recommended that the analytical model developed in this research be further verified, particularly against laboratory and field-test acceleration response. It is recommended that consideration be given to extend the analytical model to include more parameters for load identification of more complex structures. Despite the research presented here, more work is recommended on load identification from structural response, particularly load identification from railway bridge structural response. To overcome the problem of large unrealistic load spikes as the load enters or leaves the span, individual loads could be set to a constant magnitude for a set period. This will greatly impact the identification of other loads during that period, but may be expected to be more accurate than applying an upper and lower bound to identified loads. Surprisingly there appears to have been little work published for moving load identification where the applied load is measured both at the source, the railway vehicle wheel in our case, as well as from structural response. This would be useful in validating load identification approximations.

The use of finite element sub-models for a complex component has been only lightly treated in this research. It is highly recommended that use of sub-models be explored

in greater depth in future work if the methodology developed in this research is to reach its potential and be useful for complex joint details.

A final recommendation is that a commercial software system, with a user-friendly interface, be written for each step of the methodology developed here, to provide a tool for the assessment railway bridges. Of particularly value would be the writing of software for the analytical model step, the load identification from structural response step, the algorithm which writes load tables for finite element models, and the fatigue code software system.

4.3 Implications and Recommendations for the Mullet Creek Railway Bridge

For the Mullet Creek Railway Bridge, and like designed bridges, the significant effect of transom bending has been confirmed and to some extent quantified. The effect of the interaction between the rails and transoms, and the fixed bearing, has also been identified. In order to extend the life of the Mullet Creek Railway Bridge, it is recommended that rail clips at the rail-transom connections be replaced with zero toe load pandrol clips, and that resilient pads be included between the transoms and broad flange beams.

It is also recommended that the web-stiffener connections and the fixed bearing components be given priority during the inspection of these types of bridges.

5. CONCLUSIONS

5.1 Aims of the Research Fulfilled

The aims of this research were:

- to work toward addressing the problem of ageing steel railway bridges, by formulating a clear, repeatable methodology for high-level structural assessment,
- to develop a method, which integrates the state-of-the-art in modelling, testing and fatigue code tools and uses transient digital data for testing, modelling and assessment, and
- to demonstrate the methodology, by assessing the steel girder approach spans of the Mullet Creek Railway Bridge, Dapto, NSW, Australia.

While the most significant contribution of this research is expected to be the fulfilment of the aims above, a further aim of the work has been:

- to extend current research in some individual steps of the methodology.

The aims of the research have been fulfilled. Though, as was noted in the previous chapter, there remains scope for the method to be further improved and the research extended.

A clear, repeatable methodology for high-level structural assessment has been formulated. The method does integrate the state-of-the-art in modelling, testing and fatigue code tools and does use transient digital data for testing, modelling and assessment. The method begins with a finite element sensitivity model which is tuned and validated against transient digital data from the dynamic field-test response of a

slow moving vehicle of known load, through a dynamic analytical model intermediate step. The dynamic field-test response of normal traffic is then recorded and time-varying axle loads identified, from the digitised measured response, using the analytical model as a transfer function. Identified loads are applied to the tuned finite element sensitivity model and the dynamic stress history generated for virtually any bridge component. Dynamic stress histories are then entered directly into a software system, which estimates remaining life via a choice of several international fatigue codes. Loading and structural conditions may be adjusted at this point and the integrity and remaining life of the structure evaluated for virtually any combination of structural and loading condition.

The method has been demonstrated by the assessment of the steel girder approach spans of the Mullet Creek Railway Bridge. Three components of the Mullet Creek Railway Bridge approach spans were chosen for structural integrity and remaining life assessment. Structural conditions and applied loading conditions were altered and the impact of the changes investigated. From the structural integrity and remaining life assessment, two locations have been identified as fatigue critical and recommendations made to project sponsors Rail Infrastructure Corporation for structural changes and ongoing inspection.

Current research has been extended in some individual steps of the methodology, including dynamic response simulation of railway bridges in finite element software, finite element sensitivity modelling, load identification, analytical modelling of railway bridges and development of a software system for coded fatigue assessment.

- The use of nodal load tables, for modelling the dynamic response of structures in finite element software, has been published by others in the literature. In the material published for modelling the dynamic response of structures, loads identified from test results have not been used, research has not been validated against field test results and the method is not used for structural integrity and remaining life assessment. In this research, modelling of the dynamic response of structures in finite element software has been extended by the use of identified loads for dynamic response simulation, verification of simulated response against field-test results, and the use of simulated response for structural integrity and remaining life assessment.
- The importance of sensitivity analysis in finite element models has been demonstrated, with the Mullet Creek approach spans varying from typical simply supported assumptions.
- A suitable railway bridge analytical model was developed for beams with rotational stiffness at supports subjected to multiple distributed loads.
- Due to the analytical model developed in this research, load identification theory has been extended to non-simply supported beams with distributed applied loads
- A software system capable of carrying out assessment via a number of international codes has been written and used in assessment. This software has been used to provide a critical comparison of international fatigue codes.

5.2 Overall Importance of the Research

The problem of ageing infrastructure has been shown to be widespread with potentially catastrophic consequences. Railway bridge assessment is particularly difficult due to changes in structural conditions, between different bridges of like design, and over the life of any particular bridge. The dynamic interaction between rolling stock and bridge structures also has a dramatic effect on modelling and assessment. Different methods of assessment are often used and differing assumptions made, making repeatable and verifiable assessment difficult. The most important contribution of the research presented in this thesis is the provision of a clear and repeatable method of high-level structural assessment. Dynamic interaction is dealt with simply, using identified loads, and sensitivity models are used, allowing structural and loading changes to be modelled.

The method presented here has been shown to be capable of modelling truly dynamic response, for identified loading, at both field-test measured and non-measured locations on a structure. The generation of a detailed stress history, from finite element modelling, based on identified dynamic loads rather than peak static stress, has been shown to be achievable to sufficient accuracy. Where the detailed stress history generated from a finite element model is verified against test measured conditions, applied loads and structural conditions may be manipulated to allow reliable consideration of proposed or historical changes.

It has been demonstrated that railway bridges have the potential to behave as non-simply supported structures with distributed, rather than concentrated, applied loads and that sensitivity analysis in finite element modelling is therefore significant. An

awareness of the potential for railway bridges to behave as non-simply supported structures with distributed applied loads is highly important in structural integrity and remaining life assessment.

The time and cost of field-testing, model tuning and remaining life assessment is greatly reduced through the dynamic methods used in this research. From the recommendations of Chapter 4 it would appear possible to reduce the time and therefore cost of field-testing even further, using accelerometer measurement for model validation and load identification. Model tuning is sped up through the analytical model intermediate step and final assessment is made more efficient through the use of a software system for structural fatigue codes. Where the cost of field-testing, model tuning and clear repeatable assessment is reduced, high-level assessment becomes an increasingly attractive proposition and is more accessible to infrastructure managers and maintenance providers.

REFERENCES

1. Liebowitz H. Fracture: an advanced treatise. New York: Academic Press, 1968

2. Hayes B. Classic brittle failures in large welded structures. Engineering Failure Analysis 1996: 3(2): 115-127.

3. Fischer JW. Fatigue and fracture in steel bridges. New York: Wiley, 1984

4. Jackson B. Rail has been revived, but it needs more care if it is to prosper. Engineers Australia 1999: 71(10): 50-52.

5. Productivity Commission Report. Progress in rail reform. Australian Commonwealth Government, 2000.

6. IEAust. 2000 Australian Infrastructure Report Card. IEAust, 2000.

7. Institute of Civil Engineers (UK). State of the Nation. ICE (UK), 2000.

8. ASCE. 1998 Report Card for America's Infrastructure. ASCE. 1998.

9. ASCE. 2001 Report Card for America's Infrastructure. ASCE. 2001.

10. Yates A. Jackson B. Crumbling infrastructure needs urgent funding. Engineers Australia 2001: 73(8): 26-29.

11. IEAust. 2001 Australian Infrastructure Report Card. IEAust, 2001

12. West MP. Life cycle support for railway bridge infrastructure. Australasian Welding Journal 1999: 44(4):26-28.

13. Marcer JR. Design aspects significantly affecting rating and fatigue life of railway underbridges. Melbourne, Australia: Asia - Pacific Symposium on Bridge Loading and Fatigue, 1996.

14. Chung B. Marcer JR. Structural assessment of a historically significant underbridge in NSW. Adelaide, Australia: Austroads 4th Bridge Conference, 2000.

15. Timoshenko SP. On the forced vibration of bridges. Philosophical Magazine 1922: 42: 1018-1019.

16. Inglis CE. A Mathematical Treatise on Vibrations in Railway Bridges. London: Cambridge University Press, 1934.

17. Meacham H.C. Ahlbeck DR. A computer study of dynamic loads caused by vehicle track interaction. Trans ASME. Journal of Engineering for Industry, Series B 1969: 91(3): 808-816.

18. Tajaddini A. Testing the effects of wheel impact loads on bridges. Railway Track and Structures 1996: March: 17-20.

19. Muller JF. Dux PF. Prestressed-concrete railway-bridge live-load strains. Journal of Structural Engineering 1992: 118(2): 359-375.

20. Tunna JM. Wheel/rail forces due to wheel irregularities. Ninth International Wheelset Congress 1988: 6(2): Paper 6-2.

21. Hino J. Yoshimura T. Konishi K. Ananthanarayana N. A finite element method prediction of the vibration of a bridge subject to a moving vehicle load. Journal of Sound and Vibration 1984: 96(1): 45-53.

22. Wang TL. Huang D. Shahawy M. Huang K. Dynamic response of highway girder bridges. Computers and Structures 1996: 60(6): 1021-1027.

23. Green M. F. Cebon D. Dynamic interaction between heavy vehicles and highway bridges. Computers and Structures 1997: 62(2): 253-264.

24. Fafard M. Laflamme M. Savard M. Bennur M Dynamic analysis of existing continuous bridge. Journal of Bridge Engineering 1998: 3(1): 28-37.

25. Zhai W. Cai Z. Dynamic interaction between a lumped mass vehicle and a discretely supported continuous rail track. Computers and Structures 1997: 63(5): 987-997.

26. Delgado RM. Santos SM. Modelling of railway bridge-vehicle interaction on high speed tracks. Computers and Structures 1997: 63(3): 511-523.

27. Byers WG. Marley MJ. Mohammadi J. Nielson RJ. Sarkani S. Fatigue reliability reassessment procedures; state of the art paper. Journal of Structural Engineering 1997: 123(3): 271-276.

28. Byers WG. Marley MJ. Mohammadi J. Nielson RJ. Sarkani S. Fatigue reliability reassessment procedures; state of the art paper. Journal of Structural Engineering 1997: 123(3): 277-285.

29. Yamada K. Kato K. Ishiguro Y. Uemura A. Field stress measurements of a plate girder bridge carrying a 116 tonf truck. Bridge Management 3: London 1996:311-320.

30. Korondi L. Szittner A. Kally M. Kristy L. Determination of fatigue safety and remaining life on a riveted railway bridge by measurement. Journal of Constructional Steel Research 1998: 46(1-3): Paper No. 327.

31. Marcer JR. Bhavnagri VS. Strain gauging and fatigue assessment of old rail bridges in NSW. Melbourne, Australia: Conference On Railway Engineering, 1995.

32. Bhavnagri VS. Analysis and testing of an old lattice girder rail bridge. Australian Civil Engineering Transactions 1995: 37(3): 229-239

33. Grundy P. Deutch GP. Hardcastle RTA. Park A. Integrity and capacity of Melton viaduct. First National Structural Engineering Conference: Melbourne, Australia 1987: 42-49

34. Chung B. Fatigue assessment of rail underbridges. Melbourne, Australia: Austroads 2nd Bridge Conference, 1993.

35. Wu JJ. Whittaker AR. Cartmell MP. The use of finite element techniques for calculating the dynamic response of structures to moving loads. Computers and Structures 2000: 78(6): 789-799.

36. Willis R. Appendix to the report of the Royal Commissioners appointed to inquire into the application of iron to railway structures. London: H.M. Stationery Office, 1849.

37. Stokes GG. Discussions of a differential equation related to the breaking of railway bridges. Transactions of the Cambridge Philosophical Society 1867: 8(5): 707-735.

38. Ayre RS. Ford G. Jacobsen LS. Transverse vibration of a two-span beam under action of a moving constant force. Journal of Applied Mechanics 1950: 17: 1-12.

39. Ayre RS. Jacobsen LS. HSU CS. Transverse vibration of one and two span beams under the action of a moving mass load. Proceedings of the first US national congress of applied mechanics 1952: 81-90.

40. Fryba L. Vibration of Solids and Structures under Moving Loads. Groningen, The Netherlands: Noordhoff International, 1972.

41. Fryba L. Dynamics of railway bridges. London: T. Telford, New York: American Society of Civil Engineers, 1996.

42. Lin YH. Trethewey MW. Finite element analysis of elastic beams subjected to moving loads. Journal of Sound and Vibration 1990: 136(2): 323-342.

43. Karaolides CK. Kounadis AN. Forced motion of a simple frame subjected to a moving force. Journal of Sound and Vibration 1983: 88(1): 27-45.

44. Biggs JM. Introduction to structural dynamics. New York: McGraw Hill, 1964.

45. Clough RW. Penzien J. Dynamics of structures. New York: McGraw Hill, 1975.

46. Yang YB. Yau JD. Hsu LC. Vibration of simple beams due to trains moving at high speeds. Engineering Structures 1997: 19(11): 936-944.

47. Law SS. Chan THT. Zeng QH. Moving force identification: a time domain method. Journal of Sound and Vibration 1997: 201(1): 1-22.

48. Chen YH. Li CY. Dynamic response of elevated high-speed railway. Journal of Bridge Engineering 2000: 5(2): 124-130.

49. Wu JS. Dai CW. Dynamic responses of multispan nonuniform beam due to moving loads. Journal of Structural Engineering 1987: 113(3): 458-74.

50. Olsson M. Finite element, modal co-ordinate analysis of structures subjected to moving loads. Journal of Sound and Vibration 1985: 99(1): 1-12.

51. Hino J. Yoshimura T. Ananthanarayana N. Vibration analysis of non-linear beams subjected to a moving load using the finite element method. Journal of Sound and Vibration 1985: 100(4): 477-491.

52. Fryba L. Nakagiri S. Yoshikawa N. Stochastic finite elements for a beam on a random foundation with uncertain damping under a moving force. Journal of Sound and Vibration 1993: 163(1): 31-45.

53. Thambiratnam D. Zhuge Y. Dynamic analysis of beams on elastic foundation subject to moving loads. Journal of Sound and Vibration 1996: 198(2): 149-169.

54. Henchi K. Fafard M. Dhatt G. Talbot M. Dynamic behaviour of multi-span beams under moving loads. Journal of Sound and Vibration 1997: 199(1): 33-50.

55. Wang RT. Vibration of multi-span Timonshenko beams to a moving force. Journal of Sound and Vibration 1997: 207(5): 731-742.

56. Saadeghvazari MA. Finite element analysis of highway bridges subjected to moving loads. Computers and Structures 1993: 49(5): 837-842.

57. Grundy P. Impact factors in railway bridge loading codes. Asia - Pacific Symposium on Bridge Loading and Fatigue. Melbourne 1996

58. Jackson B. Photography to monitor railway viaducts. Engineers Australia 1991: 63(21): 34.

59. Olaszek P. Investigation of the dynamic characterisation of bridge structures using a computer vision method. Measurement 1999: 25(3): 227-236.

60. Paternak H. Horvath L. Investigation of steel members under cyclic loading by thermovision. Journal of Construction Steel Research 1998: 46 (1-3): Paper No. 254.

61. Gong Z. Nyborg EO. Oommen G. Acoustic emission monitoring of steel railroad bridges. Materials Evaluation 1992: 50(7): 883-887.

62. Otsuka H. Hikosaka H. Miyatake H. Nakamura S. Estimation of maximum stress in old railway riveted I-girder bridges using acoustic emission signals. Journal of Acoustic Emission 1991-1992: 10(1-2): s13-s17.

63. Elliot JF. Quarrie IR. Continuous acoustic monitoring of bridges. Adelaide, Australia: Austroads 4th Bridge Conference, 2000.

64. Faber MH. Val DV. Stewart MG. Proof load testing for bridge assessment and upgrading. Engineering Structures 2000:22(12): 1677-1689.

65. Barker MG. Steel girder bridge field test procedures. Construction and Building Materials 1999: 13(4): 229-239

66. Haritos N. Abu-Aisheh E. The role of dynamic testing methods in bridge structural assessment. Adelaide, Australia: Austroads 4th Bridge Conference, 2000.

67. Ventura CE. Determination of the dynamic characteristics of the Colquitz River Bridge by full-scale testing. Canadian Journal of Civil Engineering 1996: 23(2): 536-548.

68. Casas JR. Full-scale dynamic testing of the Alamillo cable-stayed bridge in Sevilla (Spain). Earthquake Engineering and Structural Dynamics 1995: 24: 35-51.

69. Idriss RL. White KR. Woodward CB. Jauregui DV. Evaluation and testing of a fracture critical bridge. NDT&E International 1995: 28(6): 339-347.

70. Mohammad K. Mahmud SK. Bridge load testing - the Malaysian experience. Adelaide, Australia: Austroads 4th Bridge Conference, 2000.

71. Salawu OS. Williams C. Review of full-scale dynamic testing of bridge structures. Engineering Structures 1995: 17(2): 113-121.

72. Sorrenson PJ. West MP. Field Test Validation of a Railway Bridge Model by Structural Dynamic Sensitivity Analysis. Wollongong, Australia: RTSA Conference on Railway Engineering, 2002.

73.Gbadeyan J.A. Oni S. T. Dynamic behaviour of beams and retangular plates under moving loads. Journal of Sound and Vibration 1995: 182: 677-695.

74. Lee U. Revisiting the moving mass problem: onset of separation between the mass and beam. Journal of Vibration and Acoustics 1996: 118: 516-521

75. Norman OK. Hopkins RC. Weighing vehicles in motion. Highway Research Board Bulletin 50, National Research Council, Washington, DC 1952.

76. Stiffert M. Determination of the volume and composition of traffic: weigh bridges. Third International Conference on the Structural Design of Asphalt Pavements 1972: II: 35-39.

77. Bergan AT. Dyck GJ. The development of an automatic highway scale. Presented at Roads and Transportation Association of Canada Project Committee Meeting, Saskatchewan, Canada, 1976.

78. Tritt B. Richards. Determination of vehicle axle mass - a description and demonstration of the ARRB system. Proceedings Axle Mass Determination Workshop, ARRB 1978.

79. Moses F. Weigh-in-motion system using instrumented bridge. Journal of Transport Engineering ASCE 1984: 105(TE): 233-49

80. Peters RJ. An unmanned and detectable highway speed vehicle weighing system. Proceedings of 13th ARRB and 5th REAAA Combined Conference 1985: 6: 70-83

81. Davis P. Sommerville F. Low-cost axle load determination. Proceedings of the 13th ARRB and 5th REAAA Combined Conference 1986: 6: 297-301

82. Doyle JF. An experimental method for determining the dynamic contact law. Experimental Mechanics 1984: 1: 10-16.

83 Doyle JF. Further developments in determining the dynamic contact law. Experimental Mechanics 1984: 4: 265-270.

84. Hillary B. Ewins DJ The use of strain gauges in force determination and frequency response measurements. Proceedings of the 2nd International Modal Analysis Conference: Orlando, Florida 1984: 627-634.

85. Stevens KK. Force identification: an overview. Proceedings of the SEM Conference on Experimental Mechanics 1987: 838-834.

86. Hoshiya M. Maruyama O. Identification of a running load on a beam system. Journal of Engineering Mechanics 1987: 113(6): 813-824.

87. O'Connor C. Chan THT. Wheel loads from bridge strains: laboratory studies. Journal of Structural Engineering 1988: 114(8): 1724-1740.

88. O'Connor C. Chan THT. Dynamic wheel loads from bridge strains. Journal of Structural Engineering 1988: 114(8): 1703-1723.

89. Chan THT. Yung TH. A theoretical study of force identification using prestressed concrete bridges. Engineering Structures 2000:23(11): 1529-1537.

90. Saiidi M. Douglas B. Feng S. Prestress force effect on vibration frequency of concrete bridges. Journal of Structural Engineering 1994: 120: 2233-2241

91. Chan THT. Yung TH. Moving force identification using an existing prestressed concrete bridges. Engineering Structures 2000:22(10): 1261-1270.

92. Grundy P. Fatigue life of Australian railway bridges. Australian Civil Engineering Transactions 1982: 24(3): 267-282.

93. Bruestle KE. Prucz Z. Fatigue of steel bridges. Proceedings Area 1991: Bulletin 736 92: 177-197.

94. Tang J. ZhaoJ. A practical approach for predicting reliability under random cyclic loading. Reliability Engineering and System Safety 1995: 50(1): 7-15.

95. Szerszen MM. Nowak AS. Laman JA. Fatigue reliability of steel bridges. Journal of Constructional Steel Research 1999: 52(1): 83-92.

96. Tobias DH. Foutch DA. Reliability-based method for fatigue evaluation of railway bridges. Journal of Bridge Engineering 1997: 2(2): 53-60.

97. Le X. Peterson ML. A method for fatigue based reliability when the loading of a component is unknown. International Journal of Fatigue 1999: 21(6): 603-610.

98. Maragakis E Sanders DH. Fatigue reliability analysis program for railroad steel riveted bridges. Proceedings AREA 1995: Bulletin 751 96: 191-209.

99. Singh R. Koenke C. Simulation framework for risk assessment of damage tolerant structures. Computers and Structures 2000: 77(1): 101-115.

100. Grundy P. Khalaf H. Boully G. Direct risk assessment of ageing bridges - traffic loads. Adelaide, Australia: Austroads 4th Bridge Conference, 2000.

101. Colombi P. Dolonski K. Fatigue lifetime of welded joints under random loading: rainflow cycle vs. cycle sequence method. Probabilistic Engineering Mechanics 2001: 16(1): 61-71.

102. Jones A. Hudd RC. Cyclic stress-strain curves generated from random cyclic strain amplitude tests. International Journal of Fatigue 1999: 21(6): 521-530.

103. Miller KJ. O'Donnell WJ. The fatigue limit and its elimination. Fatigue Fract Mater Struct 1999: 22(7): 545-557.

104. Zheng X. Li Z. Fatigue performance of old bridge steel and the procedures for life prediction with given survivability. Engineering Fracture Mechanics 1996: 53(2): 251-262.

105. Agerskov H. Fatigue in steel structures under random loading. Journal of Constructional Steel Research 2000: 53(3): 283-305.

106. Agerskov H. Nielson JA. Fatigue in steel highway bridges under random loading. Journal of Structural Engineering 1999: 125(2): 152-162.

107. Liou HY. Wu WF. Shin CS. A modified model for the estimation of fatigue life derived from random vibration theory. Probabilistic Engineering Mechanics 1999: 14(3): 281-288

108. Fatemi A. Yang L. Cumlative fatigue damage and life prediction theories: a survey of the state of the art for homogeneous materials. International Journal of Fatigue 1998: 20(1): 9-34.

109. Fryba L. Gajdos L. Fatigue properties of orthotropic decks on railway bridges. Engineering Structures 1999: 21(7) 639-652.

110. Caramelli S. Croce P. Messina bridge: testing assisted deck fatigue design. Florence, Italy: Proceedings of: IIW International Conference Welded constructions: Achievements and perspectives for the new millennium, July 2000.

111. BS 7608 Fatigue design and assessment of steel structures, British Standards, 1993.

112. BS 5400 Steel, concrete and composite bridges part 10 code of practice for fatigue, British Standards, 1980.

113. Fatigue design recommendations for steel structures (English version), Japanese Society of Steel Construction, 1995

114. Fatigue design of new freight cars, Association of American Railroads, 1988

115. Structural welding code- steel, American Welding Society, 1996

116. ENV 1993-1-1 Eurocode - Design of Steel Structures, 1992

117. Australian bridge design code, Austroads, 1996

118. Grundy P. Preface to conference proceedings. Melbourne, Australia: Asia-Pacific Symposium on Bridge Loading and Fatigue, 1996.

119. Singleton CC. Railway History in Illawarra NSW. Australia: Illawarra Historical Museum: 1964.

120. Drew FP. Structural fatigue - how much of a factor in railroad bridges? Railway Track and Structures 1966: December: 19-22.

121. Esveld C. Modern railway track. Duisburg, West Germany: MRT Productions, 1989.

122. Sorrenson PJ. Fatigue life of steel girder bridges. Wollongong, Australia: Proceedings of International Conference on Mechanics of Structures, Materials and Systems, 1999.

123. Kiss K. Dunai L. Stress history generation for truss bridges using multi-level models. Computers and Structures 2000: 78(1-3): 329-339.

124. Kiss K. Dunai L. Advanced model for the stress analysis of steel truss bridges. Journal of Constructional Steel Research 1998: 46(1-3): 76-78.

BIBLIOGRAPHY

Anton H. Calculus: 4th Ed. New York: Wiley, 1992.

Anton H. Elementary Linear Algebra: 6th Ed. New York: Wiley,1991.

West MP. Essential Nastran. Wollongong: University of Wollongong, 1997.

West MP. Finite Element Methods in Theory and Practice. Wollongong: University of Wollongong, 1997.

Blakely K. MSC/NASTRAN Basic Dynamic Analysis Users Guide: Version 68. Los Angeles: MacNeal-Schwendler Corp., 1993.

Kilroy K. MSC/NASTRAN Version 70 Quick Reference Guide. Los Angeles: MacNeal-Schwendler Corp., 1993.

Boswell LF. D'Mello C. Dynamics of Structural Systems. Oxford [England]; Boston: Blackwell Publications1993.

Rao SS. Mechanical Vibrations: 3rd Ed. Reading, Mass: Addison-Wesly, 1995.

Doyle NF. Railway Track Design: A Review of Current Practice. Canberra: Australian Government Publishing Service, 1980.

Garg VK. Dukkipati RV. Dynamics of Railway Vehicle Systems. Ontario: Academic Press, 1984.

Popov EP. Engineering Mechanics of Solids. Englewood Cliffs, N.J.: Prentice-Hall, 1968

Gere JM. Timoshenko SP. Mechanics of Materials: 4th Ed. Boston: PWS Pub Co., 1997

Dowling NE. Mechanical Behaviour of Materials: 2nd Ed. Upper Saddle River, NJ: Prentice-Hall, 1999.

Bennett D. The Creation of Bridges. London: Aurum, 1999.

Leonhardt F. Bridges: Aesthetics and Design. Stuttgart: Deutsche Verlags-Anstalt, 1982.

Railway Bridge Design Manual. Australian and New Zealand Railway Conferences, 1974.

BLH Electronics. SR-4 Strain Gage Hand book. Waltham M.A.: BLH Electronics, 1980.

APPENDICES

Appendix A - Mode Shape Function for Euler-Bernoulli Beams with Rotational Stiffness at Supports

In order to determine the modes of a beam with continuous mass, the only force assumed to be resisting motion is the beam's inertial force.

The inertial force is

$$q(x) = -\bar{m}a = -\bar{m}\frac{\partial^2 v}{\partial t^2} \tag{A.1}$$

where $\bar{m} = \frac{m}{l}$

The bending-moment (A.2), shear-force (A.3) and load equation (A.4) are

$$M(x) = EI\frac{\partial^2 v}{\partial x^2} \tag{A.2}$$

$$V(x) = \frac{\partial M}{\partial x} = EI\frac{\partial^3 v}{\partial x^3} \tag{A.3}$$

$$q(x) = \frac{\partial V}{\partial x} = EI\frac{\partial^4 v}{\partial x^4} \tag{A.4}$$

Equating (A.1 and A.4),

$$EI\frac{\partial^4 v}{\partial x^4} = -\bar{m}\frac{\partial^2 v}{\partial t^2} \tag{A.5}$$

$$EI\frac{\partial^4 v}{\partial x^4} + \bar{m}\frac{\partial^2 v}{\partial t^2} = 0$$

which is the equation of motion for the natural vibrations in a beam of continuous mass.

Assume the function v(x,t) has a separable solution.

$$\text{i.e.} \quad v(x,t) = \mathrm{X}(x)\,\mathrm{T}(t) \tag{A.6}$$

$$\frac{\partial^4 v}{\partial x^4} = \mathrm{X}^{IV}(x)\,\mathrm{T}(t) \tag{A.7}$$

$$\frac{\partial^2 v}{\partial t^2} = \mathrm{X}(x)\,\ddot{\mathrm{T}}(t) \tag{A.8}$$

$$EI\mathrm{X}^{IV}\mathrm{T} + \bar{m}\mathrm{X}\ddot{\mathrm{T}} = 0 \tag{A.9}$$

$$EI\mathrm{X}^{IV}\mathrm{T} = -\bar{m}\mathrm{X}\ddot{\mathrm{T}}$$

Dividing throughout by $EI\mathrm{XT}$

yields $$\frac{\mathrm{X}^{IV}}{\mathrm{X}} = -\frac{\bar{m}}{EI}\frac{\ddot{\mathrm{T}}}{\mathrm{T}}$$

which may be separated and rewritten

$$\frac{\mathrm{X}^{IV}}{\mathrm{X}} = \lambda$$

and $$-\frac{\bar{m}}{EI}\frac{\ddot{\mathrm{T}}}{\mathrm{T}} = \lambda.$$

or $$\ddot{\mathrm{T}} + \frac{\bar{m}}{EI}\mathrm{T}\lambda = 0 \tag{A.10}$$

and $$\mathrm{X}^{IV} - \lambda\mathrm{X} = 0 \tag{A.11}$$

Solving (A.10),

$$\ddot{\mathrm{T}} + \frac{EI}{\bar{m}}\lambda\mathrm{T} = 0$$

$$\mathrm{T} = Ae^{i\omega t}$$

$$\dot{\mathrm{T}} = i\omega Ae^{i\omega t}$$

$$\ddot{\mathrm{T}} = -\omega^2 Ae^{i\omega t}$$

$$-\omega^2 Ae^{i\omega t} + \frac{EI}{\bar{m}}\lambda Ae^{i\omega t} = 0$$

$$\omega^2 = \lambda\frac{EI}{\bar{m}} \tag{A.12}$$

Solving (A.11),

$$X^{IV} - \lambda X = 0$$

(A.11) may be rewritten as a fourth order differential equation, leading to

$$D^4 - \lambda = 0$$

where, $D = \pm\lambda^{\frac{1}{4}}, \pm i.\lambda^{\frac{1}{4}}$

Therefore,

$$X = C_1 e^{i\lambda^{\frac{1}{4}}x} + C_2 e^{-i\lambda^{\frac{1}{4}}x} + C_3 e^{-\lambda^{\frac{1}{4}}x} + C_4 e^{\lambda^{\frac{1}{4}}x} \tag{A.13}$$

Recall,

$$\cos(\lambda^{\frac{1}{4}}x) = \frac{e^{i\lambda^{\frac{1}{4}}x} + e^{-i\lambda^{\frac{1}{4}}x}}{2}$$

$$\sin(\lambda^{\frac{1}{4}}x) = \frac{e^{i\lambda^{\frac{1}{4}}x} - e^{-i\lambda^{\frac{1}{4}}x}}{2i}$$

$$\cosh(\lambda^{\frac{1}{4}}x) = \frac{e^{\lambda^{\frac{1}{4}}x} + e^{-\lambda^{\frac{1}{4}}x}}{2}$$

$$\sinh(\lambda^{\frac{1}{4}}x) = \frac{e^{\lambda^{\frac{1}{4}}x} - e^{-\lambda^{\frac{1}{4}}x}}{2}$$

A.13 may be rewritten,

$$\begin{aligned} X = {} & C_1\left(\cos(\lambda^{\frac{1}{4}}x) + i\sin(\lambda^{\frac{1}{4}}x)\right) + C_2\left(\cos(\lambda^{\frac{1}{4}}x) - i\sin(\lambda^{\frac{1}{4}}x)\right) \\ & + C_3\left(\cosh(\lambda^{\frac{1}{4}}x) - \sinh(\lambda^{\frac{1}{4}}x)\right) + C_4\left(\cosh(\lambda^{\frac{1}{4}}x) + \sinh(\lambda^{\frac{1}{4}}x)\right) \end{aligned} \tag{A.14}$$

Grouping constant coefficients;

$$\begin{aligned}\mathrm{X} &= (C_1 + C_2)\cos\left(x\lambda^{\frac{1}{4}}\right) + i(C_1 - C_2)\sin\left(x\lambda^{\frac{1}{4}}\right) \\ &+ (C_3 + C_4)\cosh\left(x\lambda^{\frac{1}{4}}\right) + (C_3 + C_4)\sinh\left(x\lambda^{\frac{1}{4}}\right)\end{aligned} \tag{A.15}$$

Which after coefficients renaming yields;

$$\mathrm{X} = A\cos\left(x\lambda^{\frac{1}{4}}\right) + B\sin\left(x\lambda^{\frac{1}{4}}\right) + C\cosh\left(x\lambda^{\frac{1}{4}}\right) + D\sinh\left(x\lambda^{\frac{1}{4}}\right) \tag{A.16}$$

$$\mathrm{X}^{I} = -A\lambda^{\frac{1}{4}}\sin\left(x\lambda^{\frac{1}{4}}\right) + B\lambda^{\frac{1}{4}}\cos\left(x\lambda^{\frac{1}{4}}\right) + C\lambda^{\frac{1}{4}}\sinh\left(x\lambda^{\frac{1}{4}}\right) + D\lambda^{\frac{1}{4}}\cosh\left(x\lambda^{\frac{1}{4}}\right) \tag{A.17}$$

$$\mathrm{X}^{II} = -A\lambda^{\frac{1}{2}}\cos\left(x\lambda^{\frac{1}{4}}\right) - B\lambda^{\frac{1}{2}}\sin\left(x\lambda^{\frac{1}{4}}\right) + C\lambda^{\frac{1}{2}}\cosh\left(x\lambda^{\frac{1}{4}}\right) + D\lambda^{\frac{1}{2}}\sinh\left(x\lambda^{\frac{1}{4}}\right) \tag{A.18}$$

$$\mathrm{X}^{III} = A\lambda^{\frac{3}{4}}\cos\left(x\lambda^{\frac{1}{4}}\right) - B\lambda^{\frac{3}{4}}\sin\left(x\lambda^{\frac{1}{4}}\right) + C\lambda^{\frac{3}{4}}\cosh\left(x\lambda^{\frac{1}{4}}\right) + D\lambda^{\frac{3}{4}}\sinh\left(x\lambda^{\frac{1}{4}}\right) \tag{A.19}$$

$$\mathrm{X}^{IV} = A\lambda\sin\left(x\lambda^{\frac{1}{4}}\right) + B\lambda\cos\left(x\lambda^{\frac{1}{4}}\right) + C\lambda\sinh\left(x\lambda^{\frac{1}{4}}\right) + D\lambda\cosh\left(x\lambda^{\frac{1}{4}}\right) \tag{A.20}$$

For a beam with rotational stiffness at the supports, the boundary conditions are

$$\begin{aligned} v(0) &= 0 \\ \frac{\partial v}{\partial x}(0) &= -\theta(0) \\ \frac{\partial^2 v}{\partial x^2}(0) &= -\frac{k_0\theta(0)}{EI} \end{aligned} \qquad \text{and} \qquad \begin{aligned} v(L) &= 0 \\ \frac{\partial v}{\partial x}(L) &= \theta(L) \\ \frac{\partial^2 v}{\partial x^2}(L) &= -\frac{k_L\theta(L)}{EI} \end{aligned}$$

from which it follows

$$\begin{aligned} X(0) &= 0 \\ X^{I}(0) &= -\theta(0) \\ X^{II}(0) &= \frac{-k_0\theta(0)}{EI} \\ X^{II}(0) - \frac{k_0\theta(0)}{EI} &= 0 \end{aligned} \qquad \text{and} \qquad \begin{aligned} X(L) &= 0 \\ X^{I}(L) &= \theta(L) \\ X^{II}(L) &= -\frac{k_L\theta(L)}{EI} \\ X^{II}(L) + \frac{k_L\theta(L)}{EI} &= 0 \end{aligned}$$

In order to determine the modal frequencies and the mode shape function, the equations for $X(0)=0$, $X(L)=0$, $X^{II}(0)-\frac{k_0\theta(0)}{EI}=0$ and $X^{II}(L)+\frac{k_L\theta(L)}{EI}=0$ are solved simultaneously.

$$\begin{bmatrix} 1 & 0 & 1 & 0 \\ \cos\left(L\lambda^{\frac{1}{4}}\right) & \cos\left(L\lambda^{\frac{1}{4}}\right) & \cos\left(L\lambda^{\frac{1}{4}}\right) & \cos\left(L\lambda^{\frac{1}{4}}\right) \\ -\lambda^{\frac{1}{2}} & -\frac{\lambda^{\frac{1}{4}}k_0}{E.I} & \lambda^{\frac{1}{2}} & -\frac{\lambda^{\frac{1}{4}}k_0}{EI} \\ \left(-\lambda^{\frac{1}{2}}\cos\left(L\lambda^{\frac{1}{4}}\right)\right) & \left(-\lambda^{\frac{1}{2}}\sin\left(L\lambda^{\frac{1}{4}}\right)\right) & \left(\lambda^{\frac{1}{2}}\sinh\left(L\lambda^{\frac{1}{4}}\right)\right) & \left(\lambda^{\frac{1}{2}}\sinh\left(L\lambda^{\frac{1}{4}}\right)\right) \\ \left(-\frac{\lambda^{\frac{1}{4}}k_L}{EI}\sin\left(L\lambda^{\frac{1}{4}}\right)\right) & \left(+\frac{\lambda^{\frac{1}{4}}k_L}{EI}\cos\left(L\lambda^{\frac{1}{4}}\right)\right) & \left(+\frac{\lambda^{\frac{1}{4}}k_L}{EI}\cosh\left(L\lambda^{\frac{1}{4}}\right)\right) & \left(+\frac{\lambda^{\frac{1}{4}}k_L}{EI}\sin\left(L\lambda^{\frac{1}{4}}\right)\right) \end{bmatrix} \begin{bmatrix} A \\ B \\ C \\ D \end{bmatrix} = \begin{bmatrix} 0 \\ 0 \\ 0 \\ 0 \end{bmatrix} \quad \text{(A.21)}$$

Equating the determinant of the first matrix to zero yields,

$$\det[A]=0$$

$$0 = 4\lambda^{\frac{1}{2}}\sin\left(L\lambda^{\frac{1}{4}}\right)\sinh\left(L\lambda^{\frac{1}{4}}\right)+\left(2-2\cos\left(L\lambda^{\frac{1}{4}}\right)\cosh\left(L\lambda^{\frac{1}{4}}\right)\right)\frac{k_0k_L}{(EI)^2} + 2\lambda^{\frac{1}{4}}\left(\cosh\left(L\lambda^{\frac{1}{4}}\right)\sin\left(L\lambda^{\frac{1}{4}}\right)-\sinh\left(L\lambda^{\frac{1}{4}}\right)\cos\left(L\lambda^{\frac{1}{4}}\right)\right)\frac{(k_0+k_L)}{EI} \quad \text{(A.22)}$$

λ is found by iterating equation (A.22) and the modal frequencies found by substituting into equation (A.12).

Solving (A.21) for the coefficients A, B, C and D yields,

$$C=-A$$
$$D=-\Delta B$$

where,

$$\Delta = \left\{ \frac{\frac{k_0}{2\lambda^{\frac{1}{4}} EI}\left[\cosh\left(L\lambda^{\frac{1}{4}}\right) - \cos\left(L\lambda^{\frac{1}{4}}\right)\right] + \sin\left(L\lambda^{\frac{1}{4}}\right)}{\frac{k_0}{2\lambda^{\frac{1}{4}} EI}\left[\cosh\left(L\lambda^{\frac{1}{4}}\right) - \cos\left(L\lambda^{\frac{1}{4}}\right)\right] + \sinh\left(L\lambda^{\frac{1}{4}}\right)} \right\}$$

Substituting these into equation (A.16) at L, i.e. $X(L) = 0$,

$$0 = A\left(\cos\left(L\lambda^{\frac{1}{4}}\right) - \cosh\left(L\lambda^{\frac{1}{4}}\right)\right) + B\left(\sin\left(L\lambda^{\frac{1}{4}}\right) - \Delta\sinh\left(L\lambda^{\frac{1}{4}}\right)\right)$$

$$B = \frac{-A\left(\cos\left(L\lambda^{\frac{1}{4}}\right) - \cosh\left(L\lambda^{\frac{1}{4}}\right)\right)}{\left(\sin\left(L\lambda^{\frac{1}{4}}\right) - \Delta\sinh\left(L\lambda^{\frac{1}{4}}\right)\right)}$$

Substituting into $X(x)$, the expression for the mode shape function becomes,

$$\mathrm{X}(x) = \gamma\left\{\left(\cos\left(x\lambda^{\frac{1}{4}}\right) - \cosh\left(x\lambda^{\frac{1}{4}}\right)\right) - \alpha\left(\sin\left(x\lambda^{\frac{1}{4}}\right) + \beta\sinh\left(x\lambda^{\frac{1}{4}}\right)\right)\right\} \tag{A.23}$$

where,

$$\alpha = \frac{\cos\left(L\lambda^{\frac{1}{4}}\right) - \cosh\left(L\lambda^{\frac{1}{4}}\right)}{\sin\left(L\lambda^{\frac{1}{4}}\right) - \Delta\sinh\left(L\lambda^{\frac{1}{4}}\right)}$$

$$\beta = \frac{\cos\left(L\lambda^{\frac{1}{4}}\right) - \cosh\left(L\lambda^{\frac{1}{4}}\right)}{\sin\left(L\lambda^{\frac{1}{4}}\right) - \Delta\sinh\left(L\lambda^{\frac{1}{4}}\right)}\Delta$$

γ = modal normalising constant.

Appendix B - Quasi-Static Analytical Model for Euler-Bernoulli Beams with Rotational Stiffness at Supports Subjected to Multiple Moving Uniformly Distributed Loads

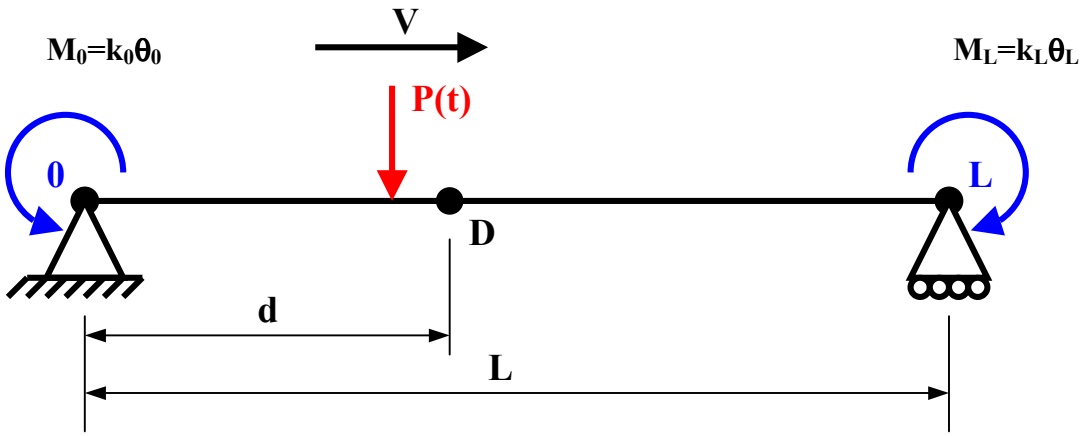

Figure B.1. Statically indeterminate beam with rotational stiffness at supports subjected to a single moving concentrated load.

The statically indeterminate beam of Figure B.1 may be solved by the method of superposition (also known as the flexibility method or the force method of analysis), using the equations of equilibrium, the equations of compatibility and the force-displacement relations. By the method of superposition the applied load, P, is solved first (Load Case 1), second the moment at x = 0, M_0, is solved (Load Case 2) and finally the moment at x = L, M_L, is solved (Load Case 3). The results of each solution are superimposed.

Equations of Equilibrium

$$R_0 = \frac{P(L-Vt)}{L} + \frac{M_0}{L} - \frac{M_L}{L} \tag{B.1}$$

$$R_L = \frac{PVt}{L} - \frac{M_0}{L} + \frac{M_L}{L} \tag{B.2}$$

$$M_0 = k_0\theta_0 \tag{B.3}$$

$$M_L = k_L\theta_L \tag{B.4}$$

$$R_0 = \frac{P(L-Vt)}{L} + \frac{k_0\theta_0}{L} - \frac{k_L\theta_L}{L} \tag{B.5}$$

$$R_L = \frac{PVt}{L} - \frac{k_0\theta_0}{L} + \frac{k_L\theta_L}{L} \tag{B.6}$$

Equations of Compatibility

$$\theta_0 = (\theta_0)_{LC1} - (\theta_0)_{LC2} - (\theta_0)_{LC3} \tag{B.8}$$

$$\theta_L = (\theta_L)_{LC1} - (\theta_L)_{LC2} - (\theta_L)_{LC3} \tag{B.7}$$

(negative sign in summation due to opposite sense of angular rotation)

Force-Displacement Relations

(force-displacement relations taken from any solid mechanics text)

$$(\theta_0)_{LC1} = \frac{PVt(L-Vt)(2L-Vt)}{6LEI} \tag{B.9}$$

$$(\theta_L)_{LC1} = \frac{PVt(L-Vt)(L+Vt)}{6LEI} \tag{B.10}$$

$$(\theta_0)_{LC2} = \frac{M_0 L}{3EI} \tag{B.11}$$

$$(\theta_L)_{LC2} = \frac{M_0 L}{6EI} \tag{B.12}$$

$$(\theta_0)_{LC3} = \frac{M_L L}{6EI} \tag{B.13}$$

$$(\theta_L)_{LC3} = \frac{M_L L}{3EI} \tag{B.14}$$

substituting into the equations of compatibility

$$\theta_0 = \frac{PVt(L-Vt)(2L-Vt)}{6LEI} - \frac{k_0\theta_0 L}{3EI} - \frac{k_L\theta_L L}{6EI} \tag{B.13}$$

$$\theta_L = \frac{PVt(L-Vt)(L+v.t)}{6LEI} - \frac{k_0\theta_0 L}{6EI} - \frac{k_L\theta_L L}{3EI} \tag{B.14}$$

solving for θ_0 and θ_L

$$\theta_0 = PVt(L-Vt)\left[\frac{(2L-Vt)6LEI + 3(L-Vt)L^2 k_L}{(6LEI)^2 + 3L^4 k_0 k_L + 12L^3 EI(k_L + k_0)}\right] \tag{B.17}$$

$$\theta_L = PVt(L-Vt)\left[\frac{(L+Vt)6LEI + 3L^2 Vtk_0}{(6LEI)^2 + 3L^4 k_0 k_L + 12L^3 EI(k_L + k_0)}\right] \tag{B.18}$$

θ_0 and θ_L are substituting into equation (B.19) below to find the bending moment at D which in turn is substituted in to equation (B.20) to find the bending stress.

$$\begin{aligned} M_D &= R_0 d - k_0\theta_0 - P(d-vt) \\ &= \left(\frac{P(L-Vt)}{L} + \frac{k_0\theta_0}{L} - \frac{k_L\theta_L}{L}\right)d - k_0\theta_0 - P(d-Vt) \qquad \text{for } 0 \le Vt \le d \end{aligned}$$

$$\begin{aligned} M_D &= R_0 d - k_0\theta_0 \\ &= \left(\frac{P(L-Vt)}{L} + \frac{k_0\theta_0}{L} - \frac{k_L\theta_L}{L}\right)d - k_0\theta_0 \qquad \text{for } d \le Vt \le L \end{aligned} \tag{B.19}$$

$$\sigma_B = \frac{My}{I} \tag{B.20}$$

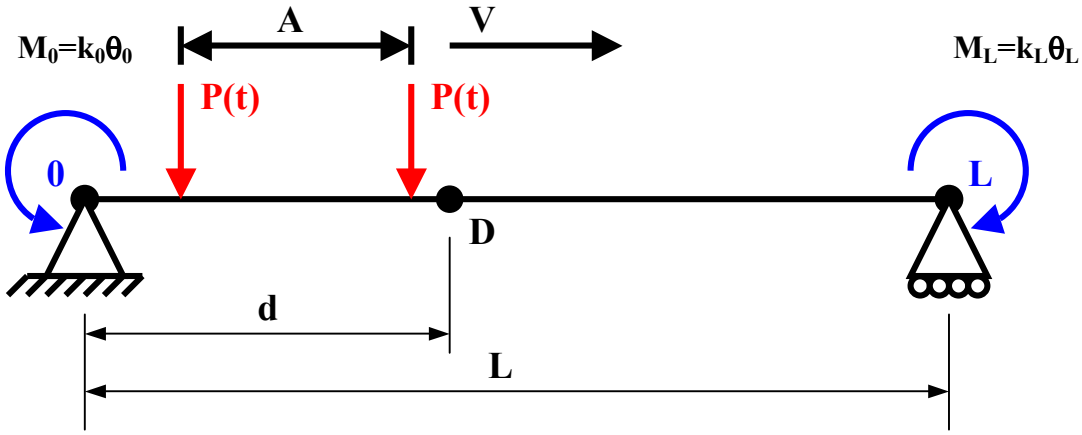

Figure B.2. Statically indeterminate beam with rotational stiffness at supports subjected to two moving concentrated loads.

For a second load, separated from the first by a distance 'A' (Figure B.2), the complete response is found via superposition of the solutions for both loads. The response for the second load is solved from the same formula, noting that the position of the load along the beam may be expressed as Vt-A in place of Vt. For multiple loads, Vt-A_n is used where A_n is the distance of the first load from the nth load, a distance of zero for the first load itself. The magnitude of each load we express as P_n where n is the load number. The total number of loads is m.

$$M_D = \sum_{n=1}^{m}\left\{\left(\frac{P_n(L-Vt+A_n)}{L}+\frac{k_0\theta_0}{L}-\frac{k_L\theta_L}{L}\right)d-k_0\theta_0-P_n(d-Vt+A_n)\right\} \qquad \text{for } 0 \le Vt \le d$$

$$M_D = \sum_{n=1}^{m}\left\{\left(\frac{P_n(L-Vt+A_n)}{L}+\frac{k_0\theta_0}{L}-\frac{k_L\theta_L}{L}\right)d-k_o\theta_0\right\} \qquad \text{for } d \le Vt \le L \qquad \text{(B.21)}$$

where

$$\theta_0 = P_n(Vt-A_n)(L-Vt+A_n)\left[\frac{(2L-Vt+A_n)6LEI+3(L-Vt+A_n)L^2k_L}{(6LEI)^2+3L^4k_0k_L+12L^3EI(k_L+k_0)}\right]$$

$$\theta_L = P_n(Vt-A_n)(L-Vt+A_n)\left[\frac{(L+Vt-A_n)6LEI+3L^2(Vt-A_n)k_0}{(6LEI)^2+3L^4k_0k_L+12L^3EI(k_L+k_0)}\right]$$

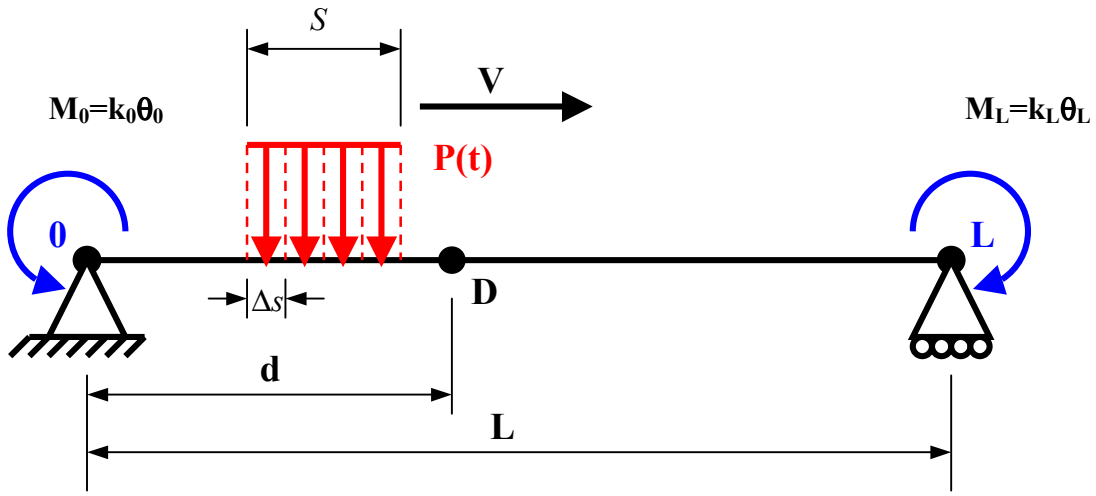

Figure B.3. Statically indeterminate beam with rotational stiffness at supports subjected to a moving uniformly distributed load.

For a uniformly distributed load (Figure B.3), the distributed load is approximated as a set of point loads. The magnitude of the load at each point is approximated as the total load divided by the number of divisions.

The number of divisions may be expressed as;

$$n = \frac{S}{\Delta s} \tag{B.22}$$

While the magnitude of each load may be expressed as;

$$P_m = \frac{P}{n} = \frac{P\Delta s}{S} \tag{B.23}$$

Considering the distributed load as a series of point loads, the distance from the first load A, of equation (B.21), to each successive load varies from 0 to 'S', where 'S'

represents the total length of the uniformly distributed load. The magnitude of each load is $\frac{P\Delta s}{S}$

$$M_D = \sum_{n=0}^{m} \left\{ \left(\frac{\frac{P\Delta s}{S}(L - Vt + s)}{L} + \frac{k_0\theta_0}{L} - \frac{k_L\theta_L}{L} \right) d - k_0\theta_0 - \frac{P\Delta s}{S}(d - Vt + s) \right\} \quad \text{for } 0 \le Vt \le d$$

$$M_D = \sum_{n=0}^{m} \left\{ \left(\frac{\frac{P\Delta s}{S}(L - Vt + s)}{L} + \frac{k_0\theta_0}{L} - \frac{k_L\theta_L}{L} \right) d - k_0\theta_0 \right\} \quad \text{for } d \le Vt \le L \qquad \text{(B.24)}$$

where

$$\theta_0 = \frac{P\Delta A}{S}(Vt - s)(L - Vt + s)\left[\frac{(2L - Vt + s)6LEI + 3(L - Vt + s)L^2 k_L}{(6LEI)^2 + 3L^4 k_0 k_L + 12L^3 EI(k_L + k_0)} \right]$$

$$\theta_L = \frac{P\Delta A}{S}(Vt - s)(L - Vt + s)\left[\frac{(L + Vt - s)6LEI + 3L^2(Vt - s)k_o}{(6LEI)^2 + 3L^4 k_o k_L + 12L^3 EI(k_L + k_o)} \right]$$

For a distributed load assume Δs approaches 0 and replace Σ with $\int$, Δs with ds and integrate from 0 to S.

$$M_D = \int_0^s \left\{ \left(\frac{\frac{Pds}{S}(L - Vt + s)}{L} + \frac{k_0\theta_0}{L} - \frac{k_L\theta_C}{L} \right) d - k_0\theta_0 - \frac{P.ds}{S}(d - Vt + s) \right\} \quad \text{for } 0 \le Vt \le d$$

$$M_D = \int_0^s \left\{ \left(\frac{\frac{Pds}{S}(L - Vt + s)}{L} + \frac{k_0\theta_0}{L} - \frac{k_L\theta_L}{L} \right) d - k_0\theta_0 \right\} \quad \text{for } d \le Vt \le L \qquad \text{(B.25)}$$

where

$$\theta_0 = \frac{Pds}{S}(Vt - s)(L - Vt + s)\left[\frac{(2L - Vt + s)6LEI + 3(L - Vt + s)L^2 k_C}{(6LEI)^2 + 3L^4 k_0 k_L + 12L^3 EI(k_L + k_0)} \right]$$

$$\theta_L = \frac{Pds}{S}(Vt - s)(L - Vt + s)\left[\frac{(L + Vt - s)6LEI + 3L^2(Vt - s)k_0}{(6LEI)^2 + 3L^4 k_0 k_L + 12L^3 EI(k_L + k_0)} \right]$$

which upon integrating between 0 and s becomes

$$M_D = \left(\frac{\frac{Ps}{S}\left(L - Vt + \frac{s}{2}\right)}{L} + \frac{k_0\theta_0}{L} - \frac{k_L\theta_L}{L} \right) d - k_0\theta_0 - \frac{Ps}{S}\left(d - Vt + \frac{s}{2}\right) \qquad \text{for } 0 \le Vt \le d$$

$$M_D = \left(\frac{\frac{Ps}{S}\left(L - Vt + \frac{s}{2}\right)}{L} + \frac{k_0\theta_0}{L} - \frac{k_L\theta_L}{L} \right) d - k_0\theta_0 - \frac{Ps}{S}\left(\frac{d - Vt + s}{2}\right) \qquad \text{for } d \le Vt \le d + S$$

$$M_D = \left(\frac{\frac{Ps}{S}\left(L - Vt + \frac{s}{2}\right)}{L} + \frac{k_0\theta_0}{L} - \frac{k_L\theta_L}{L} \right) d - k_0\theta_0 \qquad \text{for } d + S \le Vt \le L$$

$$M_D = \left(\frac{\frac{Ps}{S}\left(\frac{L - Vt + S}{2}\right)}{L} + \frac{k_0\theta_0}{L} - \frac{k_L\theta_L}{L} \right) d - k_0\theta_0 \qquad \text{for } L \le Vt \le L + S \qquad \text{(B.26)}$$

where

$$\theta_0 = \frac{Ps}{S}\left[\left(-\frac{s^3}{4} - s^2L + s^2Vt + 3sVtL - sL^2 - \frac{3s(Vt)^2}{2} + (Vt)^3 - 3(Vt)^2L + 2VtL^2 \right) 6LEI \right.$$
$$\left. + \left(-\frac{3s^3}{4} - 2s^2L + 3s^2Vt + 6sVtL - \frac{3sL^2}{2} - \frac{9s(Vt)^2}{2} + 3(Vt)^3 - 6(Vt)^2L + 3VtL^2 \right) L^2k_L \right]$$
$$\div \left[(6LEI)^2 + 3L^4k_0k_L + 12L^3EI(k_L + k_0) \right]$$

$$\theta_L = \frac{Ps}{S}\left[\left(\frac{s^3}{4} - s^2Vt - \frac{sL^2}{2} + \frac{3s(Vt)^2}{2} - (Vt)^3 + VtL^2 \right) 6LEI \right.$$
$$\left. + \left(\frac{s^3}{4} + \frac{s^2L}{3} - s^2Vt + \frac{3s(Vt)^2}{2} - (Vt)^3 + (Vt)^2L - s(Vt)L \right) 3L^2k_0 \right]$$
$$\div \left[(6LEI)^2 + 3L^4k_0k_L + 12L^3EI(k_L + k_0) \right]$$

Note the use of lower case ‘s’ and upper case ‘S’ in the above formulae. The upper case ‘S’ refers to the entire load distribution, while the lower case ‘s’ refers to the

portion of the distributed load on the beam. This will be less than 'S' as the load enters and leaves the span. Note also the additional expression for $D \leq Vt \leq d + S$. The only difference between this expression and the one preceding it for $0 \leq Vt \leq d$ is the term which represents the moving distributed force as it meets the point D and travels over that point (Figure B.4).

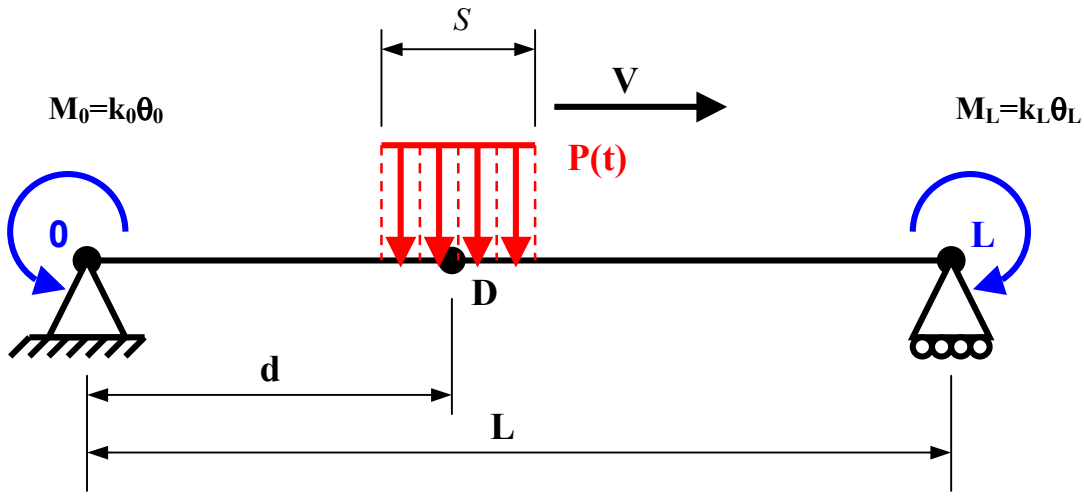

Figure B.4 Statically indeterminate beam with rotational stiffness at supports subjected to a moving uniformly distributed load travelling over point D.

Note finally the additional expression for $L \leq Vt \leq L + S$. The only difference between this and the expression preceding it for $d + S \leq Vt \leq L$ is the term for the moving distributed load as it meets and travels over the end of the beam (Figure B.5). Note also that this change may equivalently be expressed $\frac{s}{2}$ rather than $\frac{L - Vt - S}{2}$ as it is in the expression above.

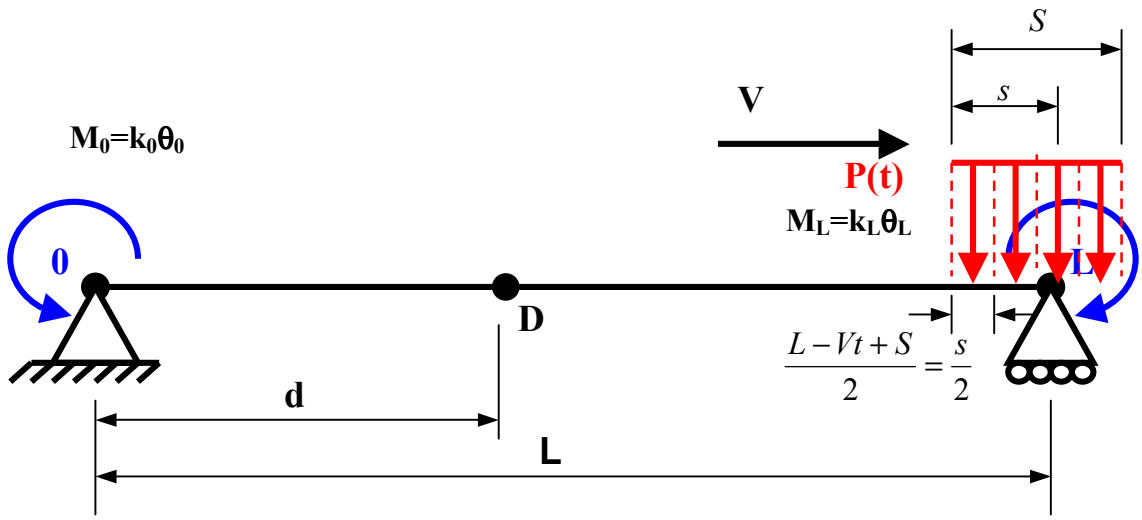

Figure B.5 Statically indeterminate beam with rotational stiffness at supports subjected to a moving uniformly distributed load travelling over the end of the span.

For multiple moving uniformly distributed loads (Figure B.6) Vt is replaced with Vt-A_n where A_n is the distance of the first load from each successive load, a distance of zero for the first load itself. Each load is denoted $P_n(t)$ since the loads may be time varying in nature.

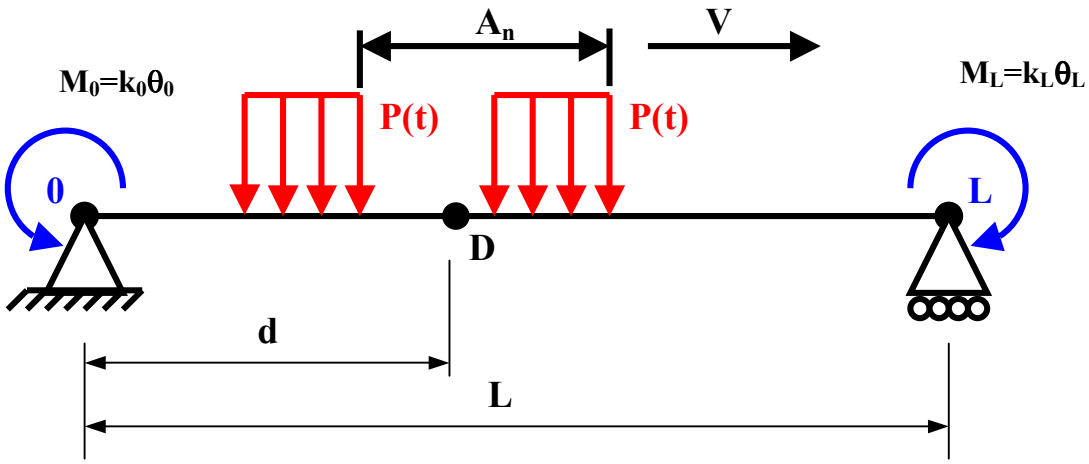

Figure B.6 Statically indeterminate beam with rotational stiffness at supports subjected to multiple moving uniformly distributed loads.

$$M_D = \sum_{n=1}^{m} \left\{ \left(\frac{\frac{P_n(t)s}{S}\left(L - Vt + A_n + \frac{s}{2}\right)}{L} + \frac{k_0\theta_0}{L} - \frac{k_L\theta_L}{L} \right) d - k_0\theta_0 - \frac{P_n(t)s}{S}\left(d - Vt + A_n + \frac{s}{2}\right) \right\} \qquad \text{for } 0 \le \text{Vt-A}_\text{n} \le \text{d}$$

$$M_D = \sum_{n=1}^{m} \left\{ \left(\frac{\frac{P_n(t)s}{S}\left(L - Vt + A_n + \frac{s}{2}\right)}{L} + \frac{k_0\theta_0}{L} - \frac{k_L\theta_L}{L} \right) d - k_0\theta_0 - \frac{P_n(t)s}{S}\left(\frac{d - Vt + A_n + s}{2}\right) \right\} \qquad \text{for } \text{d} \le \text{Vt-A}_\text{n} \le \text{d} + \text{S}$$

$$M_D = \sum_{n=1}^{m} \left\{ \left(\frac{\frac{P_n(t)s}{S}\left(L - Vt + A_n + \frac{s}{2}\right)}{L} + \frac{k_0\theta_0}{L} - \frac{k_C\theta_C}{L} \right) d - k_A\theta \right\} \qquad \text{for } \text{d} + \text{S} \le \text{Vt-A}_\text{n} \le \text{L}$$

$$M_D = \sum_{n=1}^{m} \left\{ \left(\frac{\frac{P_n(t)s}{S}\left(\frac{L - Vt + A_n + S}{2}\right)}{L} + \frac{k_0\theta_0}{L} - \frac{k_L\theta_L}{L} \right) d - k_A\theta \right\} \qquad \text{for } \text{L} \le \text{Vt-A}_\text{n} \le \text{L} + \text{S} \qquad \text{(B.27)}$$

where

$$\theta_0 = \frac{P_n(t)s}{S}\left[\left(-\frac{s^3}{4} - s^2L + s^2(Vt - A_n) + 3s(Vt - A_n)L - sL^2 - \frac{3s(Vt - A_n)^2}{2} + (Vt - A_n)^3 - 3(Vt - A_n)^2L + 2(Vt - A_n)L^2 \right) 6LEI \right.$$
$$\left. + \left(-\frac{3s^3}{4} - 2s^2L + 3s^2(Vt - A_n) + 6s(Vt - A_n)L - \frac{3sL^2}{2} - \frac{9s(Vt - A_n)^2}{2} + 3(Vt - A_n)^3 - 6(Vt - A_n)^2L + 3(Vt - A_n)L^2 \right) L^2k_L \right]$$
$$\div \left[(6LEI)^2 + 3L^4k_0k_L + 12L^3EI(k_L + k_0) \right]$$

$$\theta_L = \frac{P_n(t)s}{S}\left[\left(\frac{s^3}{4} - s^2(Vt - A_n) - \frac{sL^2}{2} + \frac{3s(Vt - A_n)^2}{2} - (Vt - A_n)^3 + (Vt - A_n)L^2 \right) 6LEI \right.$$
$$\left. + \left(\frac{s^3}{4} + \frac{s^2L}{3} - s^2(Vt - A_n) + \frac{3s(Vt - A_n)^2}{2} - (Vt - A_n)^3 + (Vt - A_n)^2L - s(Vt - A_n)L \right) 3L^2k_0 \right]$$
$$\div \left[(6LEI)^2 + 3L^4k_0k_L + 12L^3EI(k_L + k_0) \right]$$

Appendix C - Acceleration Response for Euler-Bernoulli Beams with Rotational Stiffness at Supports Subjected to Multiple Moving Uniformly Distributed Loads

For $0 \le t \le \frac{S}{V}$,

$$
\begin{aligned}
\ddot{\xi}_i = & -P\gamma \Big/ \left[Sm_i \left(\left(\omega_i^{\,2} - \Omega^2 \right)^2 + (2\zeta_i \omega_i \Omega)^2 \right) \right] \\
& \bullet \Bigg\{ \left[C_1(t)\left(\omega_i^{\,2} - \Omega^2 \right) + C_3(t)(2\zeta_i \omega_i \Omega) \right] \times \left[-\Omega^2 \cos(\Omega t) + \left(\omega_{iD}^{\,2} - \zeta^2{}_i \omega_i^{\,2} \right) e^{-\zeta_i \omega_i t} \left(\left(\frac{\zeta_i \omega_i}{\omega_{iD}} \right) \sin(\omega_{iD} t) + \cos(\omega_{iD} t) \right) \right. \\
& \left. + 2\zeta_i \omega_i \omega_{iD} e^{-\zeta_i \omega_i t} \left(\left(\frac{\zeta_i \omega_i}{\omega_{iD}} \right) \cos(\omega_{iD} t) - \sin(\omega_{iD} t) \right) \right] \\
& - \left[C_3(t)\left(\omega_i^{\,2} - \Omega^2 \right) - C_1(t)(2\zeta_i \omega_i \Omega) \right] \times \left[-\Omega^2 \sin(\Omega t) + \left(\Omega \omega_{iD} - \frac{\Omega \zeta^2{}_i \omega_i^{\,2}}{\omega_{iD}} \right) e^{-\zeta_i \omega_i t} \sin(\omega_{iD} t) + 2\zeta_i \omega_i \Omega e^{-\zeta_i \omega_i t} \cos(\omega_{iD} t) \right] \\
& + 2 \times \left[\dot{C}_1(t)\left(\omega_i^{\,2} - \Omega^2 \right) + \dot{C}_3(t)(2\zeta_i \omega_i \Omega) \right] \\
& \bullet \left[-\Omega \sin(\Omega t) + \zeta_i \omega_i e^{-\zeta_i \omega_i t} \left(\left(\frac{\zeta_i \omega_i}{\omega_{iD}} \right) \sin(\omega_{iD} t) + \cos(\omega_{iD} t) \right) - \omega_{iD} e^{-\zeta_i \omega_i t} \left(\left(\frac{\zeta_i \omega_i}{\omega_{iD}} \right) \cos(\omega_{iD} t) - \sin(\omega_{iD} t) \right) \right] \\
& - 2 \times \left[\dot{C}_3(t)\left(\omega_i^{\,2} - \Omega^2 \right) - \dot{C}_1(t)(2\zeta_i \omega_i \Omega) \right] \times \left[-\Omega \cos(\Omega t) + \frac{\Omega \zeta_i \omega_i}{\omega_{iD}} e^{-\zeta_i \omega_i t} \sin(\omega_{iD} t) - \Omega e^{-\zeta_i \omega_i t} \cos(\omega_{iD} t) \right] \\
& + \left[\ddot{C}_1(t)\left(\omega_i^{\,2} - \Omega^2 \right) + \ddot{C}_3(t)(2\zeta_i \omega_i \Omega) \right] \times \left[\cos(\Omega t) - e^{-\zeta_i \omega_i t} \left(\left(\frac{\zeta_i \omega_i}{\omega_{iD}} \right) \sin(\omega_{iD} t) + \cos(\omega_{iD} t) \right) \right] \\
& - \left[\ddot{C}_3(t)\left(\omega_i^{\,2} - \Omega^2 \right) - \ddot{C}_1(t)(2\zeta_i \omega_i \Omega) \right] \times \left[\sin(\Omega t) - \frac{\Omega}{\omega_{iD}} e^{-\zeta_i \omega_i t} \sin(\omega_{iD} t) \right] \Bigg\} \\
& + P\gamma \Big/ \left[Sm_i \left(\left(\omega_i^{\,2} + \Omega^2 \right)^2 - (2\zeta_i \omega_i \Omega)^2 \right) \right] \\
& \bullet \Bigg\{ \left[C_2(t)\left(\omega_i^{\,2} + \Omega^2 \right) + C_4(t)(2\zeta_i \omega_i \Omega) \right] \times \left[\Omega^2 \cosh(\Omega t) + \left(\omega_{iD}^{\,2} - \zeta_i^{\,2} \omega_i^{\,2} \right) e^{-\zeta_i \omega_i t} \left(\left(\frac{\zeta_i \omega_i}{\omega_{iD}} \right) \sin(\omega_{iD} t) + \cos(\omega_{iD} t) \right) \right. \\
& \left. + 2\zeta_i \omega_i \omega_{iD} e^{-\zeta_i \omega_i t} \left(\left(\frac{\zeta_i \omega_i}{\omega_{iD}} \right) \cos(\omega_{iD} t) - \sin(\omega_{iD} t) \right) \right] \\
& - \left[C_4(t)\left(\omega_i^{\,2} + \Omega^2 \right) + C_2(t)(2\zeta_i \omega_i \Omega) \right] \times \left[\Omega^2 \sinh(\Omega t) + \left(\Omega \omega_{iD} - \frac{\Omega \zeta_i^{\,2} \omega_i^{\,2}}{\omega_{iD}} \right) e^{-\zeta_i \omega_i t} \sin(\omega_{iD} t) + 2\zeta_i \omega_i \Omega e^{-\zeta_i \omega_i t} \cos(\omega_{iD} t) \right] \\
& + 2 \times \left[\dot{C}_2(t)\left(\omega_i^{\,2} + \Omega^2 \right) + \dot{C}_4(t)(2\zeta_i \omega_i \Omega) \right] \\
& \bullet \left[\Omega \sinh(\Omega t) + \zeta_i \omega_i e^{-\zeta_i \omega_i t} \left(\left(\frac{\zeta_i \omega_i}{\omega_{iD}} \right) \sin(\omega_{iD} t) + \cos(\omega_{iD} t) \right) - \omega_{iD} e^{-\zeta_i \omega_i t} \left(\left(\frac{\zeta_i \omega_i}{\omega_{iD}} \right) \cos(\omega_{iD} t) - \sin(\omega_{iD} t) \right) \right] \\
& - 2 \times \left[\dot{C}_4(t)\left(\omega_i^{\,2} + \Omega^2 \right) + \dot{C}_2(t)(2\zeta_i \omega_i \Omega) \right] \times \left[\Omega \cosh(\Omega t) + \frac{\Omega \zeta_i \omega_i}{\omega_{iD}} e^{-\zeta_i \omega_i t} \sin(\omega_{iD} t) - \Omega e^{-\zeta_i \omega_i t} \cos(\omega_{iD} t) \right] \\
& + \left[\ddot{C}_2(t)\left(\omega_i^{\,2} + \Omega^2 \right) + \ddot{C}_4(t)(2\zeta_i \omega_i \Omega) \right] \times \left[\cosh(\Omega t) - e^{-\zeta_i \omega_i t} \left(\left(\frac{\zeta_i \omega_i}{\omega_{iD}} \right) \sin(\omega_{iD} t) + \cos(\omega_{iD} t) \right) \right] \\
& - \left[\ddot{C}_4(t)\left(\omega_i^{\,2} + \Omega^2 \right) + \ddot{C}_2(t)(2\zeta_i \omega_i \Omega) \right] \times \left[\sinh(\Omega t) - \frac{\Omega}{\omega_{iD}} e^{-\zeta_i \omega_i t} \sin(\omega_{iD} t) \right] \Bigg\}
\end{aligned}
\tag{C.1}
$$

Where,

$$C_1(t) = \frac{1}{\lambda^{\frac{1}{4}}}\left(\sin(\Omega t) - \alpha\cos(\Omega t) + \alpha\right)$$

$$C_2(t) = \frac{1}{\lambda^{\frac{1}{4}}}\left(\sinh(\Omega t) + \beta\cosh(\Omega t) - \beta\right)$$

$$C_3(t) = \frac{1}{\lambda^{\frac{1}{4}}}\left(\alpha\sin(\Omega t) + \cos(\Omega t) - 1\right)$$

$$C_4(t) = \frac{1}{\lambda^{\frac{1}{4}}}\left(\beta\sinh(\Omega t) + \cosh(\Omega t) - 1\right)$$

$$\dot{C}_1(t) = \frac{\Omega}{\lambda^{\frac{1}{4}}}\left(\cos(\Omega t) + \alpha\sin(\Omega t)\right)$$

$$\dot{C}_2(t) = \frac{\Omega}{\lambda^{\frac{1}{4}}}\left(\cosh(\Omega t) + \beta\sinh(\Omega t)\right)$$

$$\dot{C}_3(t) = \frac{\Omega}{\lambda^{\frac{1}{4}}}\left(\alpha\cos(\Omega t) - \sin(\Omega t)\right)$$

$$\dot{C}_4(t) = \frac{\Omega}{\lambda^{\frac{1}{4}}}\left(\beta\cosh(\Omega t) + \sinh(\Omega t)\right)$$

$$\ddot{C}_1(t) = \frac{\Omega^2}{\lambda^{\frac{1}{4}}}\left(-\sin(\Omega t) + \alpha\cos(\Omega t)\right)$$

$$\ddot{C}_2(t) = \frac{\Omega^2}{\lambda^{\frac{1}{4}}}\left(\sinh(\Omega t) + \beta\cosh(\Omega t)\right)$$

$$\ddot{C}_3(t) = \frac{\Omega^2}{\lambda^{\frac{1}{4}}}\left(-\alpha\sin(\Omega t) - \cos(\Omega t)\right)$$

$$\ddot{C}_4(t) = \frac{\Omega^2}{\lambda^{\frac{1}{4}}}\left(\beta\sinh(\Omega t) + \cosh(\Omega t)\right)$$

For $\frac{S}{V} \le t \le \frac{L}{V}$,

$$
\begin{aligned}
\ddot{\xi}_i = & -P\gamma \Big/ \left[Sm_i \left(\left(\omega_i^{\,2} - \Omega^2 \right)^2 + (2\zeta_i \omega_i \Omega)^2 \right) \right] \\
& \bullet \Bigg\{ \left[C_1(S)\left(\omega_i^{\,2} - \Omega^2 \right) + C_3(S)(2\zeta_i \omega_i \Omega) \right] \times \Bigg[-\Omega^2 \cos(\Omega t) + \left(\omega_{iD}^{\,2} - \zeta^2{}_i \omega_i^{\,2} \right) e^{-\zeta_i \omega_i t} \left(\left(\frac{\zeta_i \omega_i}{\omega_{iD}} \right) \sin(\omega_{iD} t) + \cos(\omega_{iD} t) \right) \\
& + 2\zeta_i \omega_i \omega_{iD} e^{-\zeta_i \omega_i t} \left(\left(\frac{\zeta_i \omega_i}{\omega_{iD}} \right) \cos(\omega_{iD} t) - \sin(\omega_{iD} t) \right) \Bigg] \\
& - \left[C_3(S)\left(\omega_i^{\,2} - \Omega^2 \right) - C_1(S)(2\zeta_i \omega_i \Omega) \right] \times \left[-\Omega^2 \sin(\Omega t) + \left(\Omega \omega_{iD} - \frac{\Omega \zeta^2{}_i \omega_i^{\,2}}{\omega_{iD}} \right) e^{-\zeta_i \omega_i t} \sin(\omega_{iD} t) + 2\zeta_i \omega_i \Omega e^{-\zeta_i \omega_i t} \cos(\omega_{iD} t) \right] \\
& + \left[\mathcal{C}_1(S)\left(\omega_i^{\,2} - \Omega^2 \right) + \mathcal{C}_3(S)(2\zeta_i \omega_i \Omega) \right] \times \left[\cos\left(S\lambda^{\frac{1}{4}} \right) - e^{-\zeta_i \omega_i \frac{S}{V}} \left(\left(\frac{\zeta_i \omega_i}{\omega_{iD}} \right) \sin\left(\omega_{iD} \frac{S}{V} \right) + \cos\left(\omega_{iD} \frac{S}{V} \right) \right) \right] \\
& \bullet \left[\left(\frac{\zeta^2{}_i \omega_i^{\,2}}{\omega_{iD}} - \omega_{iD} \right) e^{-\zeta_i \omega_i \left(t - \frac{S}{V} \right)} \sin\left(\omega_{iD} \left(t - \frac{S}{V} \right) \right) - 2\zeta_i \omega_i e^{-\zeta_i \omega_i \left(t - \frac{S}{V} \right)} \left(\frac{\zeta_i \omega_i}{\omega_{iD}} \right) \cos\left(\omega_{iD} \left(t - \frac{S}{V} \right) \right) \right] \\
& - \left[\mathcal{C}_3(S)\left(\omega_i^{\,2} - \Omega^2 \right) - \mathcal{C}_1(S)(2\zeta_i \omega_i \Omega) \right] \times \left[\sin\left(S\lambda^{\frac{1}{4}} \right) - \frac{\Omega}{\omega_{iD}} e^{-\zeta_i \omega_i \frac{S}{V}} \sin\left(\omega_{iD} \frac{S}{V} \right) \right] \\
& \times \left[\left(\frac{\zeta^2{}_i \omega_i^{\,2}}{\omega_{iD}} - \omega_{iD} \right) e^{-\zeta_i \omega_i \left(t - \frac{S}{V} \right)} \sin\left(\omega_{iD} \left(t - \frac{S}{V} \right) \right) - 2\zeta_i \omega_i e^{-\zeta_i \omega_i \left(t - \frac{S}{V} \right)} \left(\frac{\zeta_i \omega_i}{\omega_{iD}} \right) \cos\left(\omega_{iD} \left(t - \frac{S}{V} \right) \right) \right] \Bigg\} \\
& + P\gamma \Big/ \left[Sm_i \left(\left(\omega_i^{\,2} + \Omega^2 \right)^2 - (2\zeta_i \omega_i \Omega)^2 \right) \right] \\
& \bullet \Bigg\{ \left[C_2(S)\left(\omega_i^{\,2} + \Omega^2 \right) + C_4(S)(2\zeta_i \omega_i \Omega) \right] \times \Bigg[\Omega^2 \cosh(\Omega t) + \left(\omega_{iD}^{\,2} - \zeta^2{}_i \omega_i^{\,2} \right) e^{-\zeta_i \omega_i t} \left(\left(\frac{\zeta_i \omega_i}{\omega_{iD}} \right) \sin(\omega_{iD} t) + \cos(\omega_{iD} t) \right) \\
& + 2\zeta_i \omega_i \omega_{iD} e^{-\zeta_i \omega_i t} \left(\left(\frac{\zeta_i \omega_i}{\omega_{iD}} \right) \cos(\omega_{iD} t) - \sin(\omega_{iD} t) \right) \Bigg] \\
& - \left[C_4(S)\left(\omega_i^{\,2} + \Omega^2 \right) + C_2(S)(2\zeta_i \omega_i \Omega) \right] \times \left[\Omega^2 \sinh(\Omega t) + \left(\Omega \omega_{iD} - \frac{\Omega \zeta^2{}_i \omega_i^{\,2}}{\omega_{iD}} \right) e^{-\zeta_i \omega_i t} \sin(\omega_{iD} t) + 2\zeta_i \omega_i \Omega e^{-\zeta_i \omega_i t} \cos(\omega_{iD} t) \right] \\
& + \left[\mathcal{C}_2(S)\left(\omega_i^{\,2} + \Omega^2 \right) + \mathcal{C}_4(S)(2\zeta_i \omega_i \Omega) \right] \times \left[\cosh\left(S\lambda^{\frac{1}{4}} \right) - e^{-\zeta_i \omega_i \frac{S}{V}} \left(\left(\frac{\zeta_i \omega_i}{\omega_{iD}} \right) \sin\left(\omega_{iD} \frac{S}{V} \right) + \cos\left(\omega_{iD} \frac{S}{V} \right) \right) \right] \\
& \bullet \left[\left(\frac{\zeta^2{}_i \omega_i^{\,2}}{\omega_{iD}} - \omega_{iD} \right) e^{-\zeta_i \omega_i \left(t - \frac{S}{V} \right)} \sin\left(\omega_{iD} \left(t - \frac{S}{V} \right) \right) - 2\zeta_i \omega_i e^{-\zeta_i \omega_i \left(t - \frac{S}{V} \right)} \left(\frac{\zeta_i . \omega_i}{\omega_{iD}} \right) \cos\left(\omega_{iD} \left(t - \frac{S}{V} \right) \right) \right] \\
& - \left[\mathcal{C}_4(S)\left(\omega_i^{\,2} + \Omega^2 \right) + \mathcal{C}_2(S)(2\zeta_i \omega_i \Omega) \right] \times \left[\sinh\left(S\lambda^{\frac{1}{4}} \right) - \frac{\Omega}{\omega_{iD}} e^{-\zeta_i \omega_i \frac{S}{V}} \sin\left(\omega_{iD} \frac{S}{V} \right) \right] \\
& \times \left[\left(\frac{\zeta^2{}_i \omega_i^{\,2}}{\omega_{iD}} - \omega_{iD} \right) e^{-\zeta_i \omega_i \left(t - \frac{S}{V} \right)} \sin\left(\omega_{iD} \left(t - \frac{S}{V} \right) \right) - 2\zeta_i \omega_i e^{-\zeta_i \omega_i \left(t - \frac{S}{V} \right)} \left(\frac{\zeta_i \omega_i}{\omega_{iD}} \right) \cos\left(\omega_{iD} \left(t - \frac{S}{V} \right) \right) \right] \Bigg\}
\end{aligned}
\tag{C.2}
$$

Where,

$$C_1(S) = \frac{1}{\lambda^{\frac{1}{4}}}\left(\sin\left(S\lambda^{\frac{1}{4}}\right) - \alpha\cos\left(S\lambda^{\frac{1}{4}}\right) + \alpha\right)$$

$$C_2(S) = \frac{1}{\lambda^{\frac{1}{4}}}\left(\sinh\left(S\lambda^{\frac{1}{4}}\right) + \beta\cosh\left(S\lambda^{\frac{1}{4}}\right) - \beta\right)$$

$$C_3(S) = \frac{1}{\lambda^{\frac{1}{4}}}\left(\alpha\sin\left(S\lambda^{\frac{1}{4}}\right) + \cos\left(S\lambda^{\frac{1}{4}}\right) - 1\right)$$

$$C_4(S) = \frac{1}{\lambda^{\frac{1}{4}}}\left(\beta\sinh\left(S\lambda^{\frac{1}{4}}\right) + \cosh\left(S\lambda^{\frac{1}{4}}\right) - 1\right)$$

$$\mathcal{C}_1(S) = \frac{\Omega}{\lambda^{\frac{1}{4}}}\left(\cos\left(S\lambda^{\frac{1}{4}}\right) + \alpha\sin\left(S\lambda^{\frac{1}{4}}\right)\right)$$

$$\mathcal{C}_2(S) = \frac{\Omega}{\lambda^{\frac{1}{4}}}\left(\cosh\left(S\lambda^{\frac{1}{4}}\right) + \beta\sinh\left(S\lambda^{\frac{1}{4}}\right)\right)$$

$$\mathcal{C}_3(S) = \frac{\Omega}{\lambda^{\frac{1}{4}}}\left(\alpha\cos\left(S\lambda^{\frac{1}{4}}\right) - \sin\left(S\lambda^{\frac{1}{4}}\right)\right)$$

$$\mathcal{C}_4(S) = \frac{\Omega}{\lambda^{\frac{1}{4}}}\left(\beta\cosh\left(S\lambda^{\frac{1}{4}}\right) + \sinh\left(S\lambda^{\frac{1}{4}}\right)\right)$$

For $\frac{L}{V} \le t \le \frac{L+S}{V}$,

$$\ddot{\xi}_i = -P\gamma \Big/ \left[Sm_i \left(\left(\omega_i^2 - \Omega^2 \right)^2 + (2\zeta_i \omega_i \Omega)^2 \right) \right]$$

$$\bullet \left\{ \left[C_1(S)\left(\omega_i^2 - \Omega^2\right) + C_3(S)(2\zeta_i\omega_i\Omega) \right] \times \left[-\Omega^2 \cos(\Omega t) + \left(\omega_{iD}^2 - \zeta^2{}_i \omega_i^2 \right) e^{-\zeta_i \omega_i t} \left(\left(\frac{\zeta_i \omega_i}{\omega_{iD}} \right) \sin(\omega_{iD} t) + \cos(\omega_{iD} t) \right) \right. \right.$$

$$\left. + 2\zeta_i \omega_i \omega_{iD} e^{-\zeta_i \omega_i t} \left(\left(\frac{\zeta_i \omega_i}{\omega_{iD}} \right) \cos(\omega_{iD} t) - \sin(\omega_{iD} t) \right) \right]$$

$$- \left[C_3(S)\left(\omega_i^2 - \Omega^2\right) - C_1(S)(2\zeta_i\omega_i\Omega) \right] \times \left[-\Omega^2 \sin(\Omega t) + \left(\Omega \omega_{iD} - \frac{\Omega \zeta^2{}_i \omega_i^2}{\omega_{iD}} \right) e^{-\zeta_i \omega_i t} \sin(\omega_{iD} t) + 2\zeta_i \omega_i \Omega e^{-\zeta_i \omega_i t} \cos(\omega_{iD} t) \right]$$

$$+ \left[\dot{C}_1(S)\left(\omega_i^2 - \Omega^2\right) + \dot{C}_3(S)(2\zeta_i\omega_i\Omega) \right] \times \left[\cos\left(S\lambda^{\frac{1}{4}} \right) - e^{-\zeta_i \omega_i \frac{S}{V}} \left(\left(\frac{\zeta_i \omega_i}{\omega_{iD}} \right) \sin\left(\omega_{iD} \frac{S}{V} \right) + \cos\left(\omega_{iD} \frac{S}{V} \right) \right) \right]$$

$$\bullet \left[\left(\frac{\zeta^2{}_i \omega_i^2}{\omega_{iD}} - \omega_{iD} \right) e^{-\zeta_i \omega_i \left(t - \frac{S}{V} \right)} \sin\left(\omega_{iD} \left(t - \frac{S}{V} \right) \right) - 2\zeta_i \omega_i e^{-\zeta_i \omega_i \left(t - \frac{S}{V} \right)} \left(\frac{\zeta_i \omega_i}{\omega_{iD}} \right) \cos\left(\omega_{iD} \left(t - \frac{S}{V} \right) \right) \right]$$

$$- \left[\dot{C}_3(S)\left(\omega_i^2 - \Omega^2\right) - \dot{C}_1(S)(2\zeta_i\omega_i\Omega) \right] \times \left[\sin\left(S\lambda^{\frac{1}{4}} \right) - \frac{\Omega}{\omega_{iD}} e^{-\zeta_i \omega_i \frac{S}{V}} \sin\left(\omega_{iD} \frac{S}{V} \right) \right]$$

$$\bullet \left[\left(\frac{\zeta^2{}_i \omega_i^2}{\omega_{iD}} - \omega_{iD} \right) e^{-\zeta_i \omega_i \left(t - \frac{S}{V} \right)} \sin\left(\omega_{iD} \left(t - \frac{S}{V} \right) \right) - 2\zeta_i \omega_i e^{-\zeta_i \omega_i \left(t - \frac{S}{V} \right)} \left(\frac{\zeta_i \omega_i}{\omega_{iD}} \right) \cos\left(\omega_{iD} \left(t - \frac{S}{V} \right) \right) \right]$$

$$+ \frac{1}{\lambda^{\frac{1}{4}}} \left[\alpha\left(\omega_i^2 - \Omega^2\right) + (-1)(2\zeta_i\omega_i\Omega) \right] \times \left[\cos\left(L\lambda^{\frac{1}{4}} \right) + \left(\omega_{iD}^2 - \zeta^2{}_i \omega_i^2 \right) e^{-\zeta_i \omega_i t} \left(\left(\frac{\zeta_i . \omega_i}{\omega_{iD}} \right) \sin(\omega_{iD} t) + \cos(\omega_{iD} t) \right) \right.$$

$$\left. + 2\zeta_i \omega_i \omega_{iD} e^{-\zeta_i \omega_i t} \left(\left(\frac{\zeta_i . \omega_i}{\omega_{iD}} \right) \cos(\omega_{iD} t) - \sin(\omega_{iD} t) \right) + \sin\left(L\lambda^{\frac{1}{4}} \right) \right.$$

$$\bullet \left\langle \left(\Omega \omega_{iD} - \frac{\Omega \zeta^2{}_i \omega_i^2}{\omega_{iD}} \right) e^{-\zeta_i \omega_i \left(t - \frac{L}{V} \right)} \sin\left(\omega_{iD} \left(t - \frac{L}{V} \right) \right) + 2\zeta_i \omega_i e^{-\zeta_i \omega_i \left(t - \frac{L}{V} \right)} \left(\frac{\zeta_i . \omega_i}{\omega_{iD}} \right) \cos\left(\omega_{iD} \left(t - \frac{L}{V} \right) \right) \right\rangle \Bigg]$$

$$- \frac{1}{\lambda^{\frac{1}{4}}} \left[(-1)\left(\omega_i^2 - \Omega^2\right) - \alpha(2\zeta_i\omega_i\Omega) \right] \times \left[\sin\left(L\lambda^{\frac{1}{4}} \right) + \left(\omega_{iD}^2 - \zeta^2{}_i \omega_i^2 \right) e^{-\zeta_i \omega_i t} \left(\left(\frac{\zeta_i \omega_i}{\omega_{iD}} \right) \sin(\omega_{iD} t) + \cos(\omega_{iD} t) \right) \right.$$

$$\left. + 2\zeta_i \omega_i \omega_{iD} e^{-\zeta_i \omega_i t} \left(\left(\frac{\zeta_i \omega_i}{\omega_{iD}} \right) \cos(\omega_{iD} t) - \sin(\omega_{iD} t) \right) - \cos\left(L\lambda^{\frac{1}{4}} \right) \right.$$

$$\left. \bullet \left\langle \left(\Omega \omega_{iD} - \frac{\Omega \zeta^2{}_i \omega_i^2}{\omega_{iD}} \right) e^{-\zeta_i \omega_i \left(t - \frac{L}{V} \right)} \sin\left(\omega_{iD} \left(t - \frac{L}{V} \right) \right) + 2\zeta_i \omega_i e^{-\zeta_i \omega_i \left(t - \frac{L}{V} \right)} \left(\frac{\zeta_i \omega_i}{\omega_{iD}} \right) \cos\left(\omega_{iD} \left(t - \frac{L}{V} \right) \right) \right\rangle \Bigg] \right\}$$

(continued over the page…)

$$+ P\gamma / \left[Sm_i \left(\left(\omega_i^{\,2} + \Omega^2 \right)^2 - (2\zeta_i \omega_i \Omega)^2 \right) \right]$$

$$\bullet \left\{ \left[C_2(S)\left(\omega_i^{\,2} + \Omega^2 \right) + C_4(S)(2\zeta_i \omega_i \Omega) \right] \times \left[\Omega^2 \cosh(\Omega t) + \left(\omega_{iD}^{\,2} - \zeta^2{}_i \omega_i^{\,2} \right) e^{-\zeta_i \omega_i t} \left(\left(\frac{\zeta_i \omega_i}{\omega_{iD}} \right) \sin(\omega_{iD} t) + \cos(\omega_{iD} t) \right) \right. \right.$$

$$\left. \left. + 2\zeta_i \omega_i \omega_{iD} e^{-\zeta_i \omega_i t} \left(\left(\frac{\zeta_i \omega_i}{\omega_{iD}} \right) \cos(\omega_{iD} t) - \sin(\omega_{iD} t) \right) \right] \right.$$

$$- \left[C_4(S)\left(\omega_i^{\,2} + \Omega^2 \right) + C_2(S)(2\zeta_i \omega_i \Omega) \right] \times \left[\Omega^2 \sinh(\Omega t) + \left(\Omega \omega_{iD} - \frac{\Omega \zeta^2{}_i \omega_i^{\,2}}{\omega_{iD}} \right) e^{-\zeta_i \omega_i t} \sin(\omega_{iD} t) + 2\zeta_i \omega_i \Omega e^{-\zeta_i \omega_i t} \cos(\omega_{iD} t) \right]$$

$$+ \left[\mathcal{C}_2(S)\left(\omega_i^{\,2} + \Omega^2 \right) + \mathcal{C}_4(S)(2\zeta_i \omega_i \Omega) \right] \times \left[\cosh\left(S\lambda^{\frac{1}{4}} \right) - e^{-\zeta_i \omega_i \frac{S}{V}} \left(\left(\frac{\zeta_i . \omega_i}{\omega_{iD}} \right) \sin\left(\omega_{iD} \frac{S}{V} \right) + \cos\left(\omega_{iD} \frac{S}{V} \right) \right) \right]$$

$$\bullet \left[\left(\frac{\zeta^2{}_i \omega_i^{\,2}}{\omega_{iD}} - \omega_{iD} \right) e^{-\zeta_i \omega_i \left(t - \frac{S}{V} \right)} \sin\left(\omega_{iD} \left(t - \frac{S}{V} \right) \right) - 2\zeta_i \omega_i e^{-\zeta_i \omega_i \left(t - \frac{S}{V} \right)} \left(\frac{\zeta_i \omega_i}{\omega_{iD}} \right) \cos\left(\omega_{iD} \left(t - \frac{S}{V} \right) \right) \right]$$

$$- \left[\mathcal{C}_4(S)\left(\omega_i^{\,2} + \Omega^2 \right) + \mathcal{C}_2(S)(2\zeta_i \omega_i \Omega) \right] \times \left[\sinh\left(S\lambda^{\frac{1}{4}} \right) - \frac{\Omega}{\omega_{iD}} e^{-\zeta_i \omega_i \frac{S}{v}} \sin\left(\omega_{iD} \frac{S}{V} \right) \right]$$

$$\bullet \left[\left(\frac{\zeta^2{}_i \omega_i^{\,2}}{\omega_{iD}} - \omega_{iD} \right) e^{-\zeta_i \omega_i \left(t - \frac{S}{V} \right)} \sin\left(\omega_{iD} \left(t - \frac{S}{V} \right) \right) - 2\zeta_i \omega_i e^{-\zeta_i \omega_i \left(t - \frac{S}{V} \right)} \left(\frac{\zeta_i \omega_i}{\omega_{iD}} \right) \cos\left(\omega_{iD} \left(t - \frac{S}{V} \right) \right) \right]$$

$$+ \frac{1}{\lambda^{\frac{1}{4}}} \left[(-\beta)\left(\omega_i^{\,2} + \Omega^2 \right) + (-1)(2\zeta_i \omega_i \Omega) \right] \times \left[\cosh\left(L\lambda^{\frac{1}{4}} \right) + \left(\omega_{iD}^{\,2} - \zeta^2{}_i \omega_i^{\,2} \right) e^{-\zeta_i \omega_i t} \left(\left(\frac{\zeta_i \omega_i}{\omega_{iD}} \right) \sin(\omega_{iD} t) + \cos(\omega_{iD} t) \right) \right.$$

$$\left. + 2\zeta_i \omega_i \omega_{iD} e^{-\zeta_i \omega_i t} \left(\left(\frac{\zeta_i \omega_i}{\omega_{iD}} \right) \cos(\omega_{iD} t) - \sin(\omega_{iD} t) \right) + \sinh\left(L\lambda^{\frac{1}{4}} \right) \right.$$

$$\bullet \left\langle \left(\Omega \omega_{iD} - \frac{\Omega \zeta^2{}_i \omega_i^{\,2}}{\omega_{iD}} \right) e^{-\zeta_i \omega_i \left(t - \frac{L}{V} \right)} \sin\left(\omega_{iD} \left(t - \frac{L}{V} \right) \right) + 2\zeta_i \omega_i e^{-\zeta_i \omega_i \left(t - \frac{L}{V} \right)} \left(\frac{\zeta_i \omega_i}{\omega_{iD}} \right) \cos\left(\omega_{iD} \left(t - \frac{L}{V} \right) \right) \right\rangle \Bigg]$$

$$- \frac{1}{\lambda^{\frac{1}{4}}} \left[(-1)\left(\omega_i^{\,2} + \Omega^2 \right) + (-\beta)(2\zeta_i \omega_i \Omega) \right] \times \left[\sinh\left(L\lambda^{\frac{1}{4}} \right) + \left(\omega_{iD}^{\,2} - \zeta^2{}_i \omega_i^{\,2} \right) e^{-\zeta_i \omega_i t} \left(\left(\frac{\zeta_i \omega_i}{\omega_{iD}} \right) \sin(\omega_{iD} t) + \cos(\omega_{iD} t) \right) \right.$$

$$\left. + 2\zeta_i \omega_i \omega_{iD} e^{-\zeta_i \omega_i t} \left(\left(\frac{\zeta_i . \omega_i}{\omega_{iD}} \right) \cos(\omega_{iD} t) - \sin(\omega_{iD} t) \right) + \cosh\left(L\lambda^{\frac{1}{4}} \right) \right.$$

$$\left. \bullet \left\langle \left(\Omega \omega_{iD} - \frac{\Omega \zeta^2{}_i \omega_i^{\,2}}{\omega_{iD}} \right) e^{-\zeta_i \omega_i \left(t - \frac{L}{V} \right)} \sin\left(\omega_{iD} \left(t - \frac{L}{V} \right) \right) + 2\zeta_i \omega_i e^{-\zeta_i \omega_i \left(t - \frac{L}{V} \right)} \left(\frac{\zeta_i \omega_i}{\omega_{iD}} \right) \cos\left(\omega_{iD} \left(t - \frac{L}{V} \right) \right) \right\rangle \Bigg] \right\} \qquad \text{(C.3)}$$

Where,

$$C_1(S) = \frac{1}{\lambda^{\frac{1}{4}}}\left(\sin\left(S\lambda^{\frac{1}{4}}\right) - \alpha\cos\left(S\lambda^{\frac{1}{4}}\right)\right)$$

$$C_2(S) = \frac{1}{\lambda^{\frac{1}{4}}}\left(\sinh\left(S\lambda^{\frac{1}{4}}\right) + \beta\cosh\left(S\lambda^{\frac{1}{4}}\right)\right)$$

$$C_3(S) = \frac{1}{\lambda^{\frac{1}{4}}}\left(\alpha\sin\left(S\lambda^{\frac{1}{4}}\right) + \cos\left(S\lambda^{\frac{1}{4}}\right)\right)$$

$$C_4(S) = \frac{1}{\lambda^{\frac{1}{4}}}\left(\beta\sinh\left(S\lambda^{\frac{1}{4}}\right) + \cosh\left(S\lambda^{\frac{1}{4}}\right)\right)$$

$$\mathcal{C}_1(S) = \frac{\Omega}{\lambda^{\frac{1}{4}}}\left(\cos\left(S\lambda^{\frac{1}{4}}\right) + \alpha\sin\left(S\lambda^{\frac{1}{4}}\right)\right)$$

$$\mathcal{C}_2(S) = \frac{\Omega}{\lambda^{\frac{1}{4}}}\left(\cosh\left(S\lambda^{\frac{1}{4}}\right) + \beta\sinh\left(S\lambda^{\frac{1}{4}}\right)\right)$$

$$\mathcal{C}_3(S) = \frac{\Omega}{\lambda^{\frac{1}{4}}}\left(\alpha\cos\left(S\lambda^{\frac{1}{4}}\right) - \sin\left(S\lambda^{\frac{1}{4}}\right)\right)$$

$$\mathcal{C}_4(S) = \frac{\Omega}{\lambda^{\frac{1}{4}}}\left(\beta\cosh\left(S\lambda^{\frac{1}{4}}\right) + \sinh\left(S\lambda^{\frac{1}{4}}\right)\right)$$

Appendix D - Example Output from Fatigue Assessment Software

DATA INPUT

Name and location of stress history input file: a:data1.txt

DATA INPUT FOR THE GENERIC METHODOLOGY ANALYSIS

Value of Stress at Fracture: 430 MPa

Points which define the S-N Curve.

N	S (MPa)
100000	200
10000000	43
1000000000	43

DATA INPUT FOR BS7608 CODE ANALYSIS

M Value (inverse slope): 3

Fatigue limit: 86 Mpa

Detail assumed non-welded or stress relieved.

Thickness correction factor chosen with a thickness of 20 mm

Further modification factor of 1.3 used

DATA INPUT FOR BS5400 CODE ANALYSIS

M Value (inverse slope): 3

Fatigue limit: 86 Mpa

Detail assumed welded and not stress relieved.

DATA INPUT FOR JAPANESE CODE ANALYSIS

Basic Allowable Stress: 147 MPa

Stress range at cut off (fatigue) limit: 86 Mpa

Redundancy partial safety factor: 1.1

Importance partial safety factor: 1.05

Inspection partial safety factor: 1.05

DATA INPUT FOR AAR CODE ANALYSIS

(Data entered in Imperial units as per the code and converted to Metric units here)

Steel chosen for analysis, with a fatigue limit at 2,000,000 cycles.

Y intercept of MGD:	124.795 MPa
Slope of the MGD:	0.71
Slope of the S-N Curve:	0.33

DATA INPUT FOR AWS CODE ANALYSIS

Points which define the Corrected S-N Curve.

N	S (MPa)
100000	520
10000000	111.8

Modification factor	1.3

DATA INPUT FOR EUROCODE ANALYSIS

Value Detail Category:	147 MPa
Thickness correction factor chosen with a thickness of	30 mm
Detail assumed non-welded or stress relieved.	
Partial safety factor for fatigue loading:	1.1
Partial safety factor for fatigue strength:	1.1

DATA INPUT FOR AUSTROADS CODE ANALYSIS

Value Detail Category:	147 MPa
Thickness correction factor chosen with a thickness of	30 mm

FILTERED STRESS HISTORY

-120
-20
-50
60
10
150
-50
120
-100
20
-120

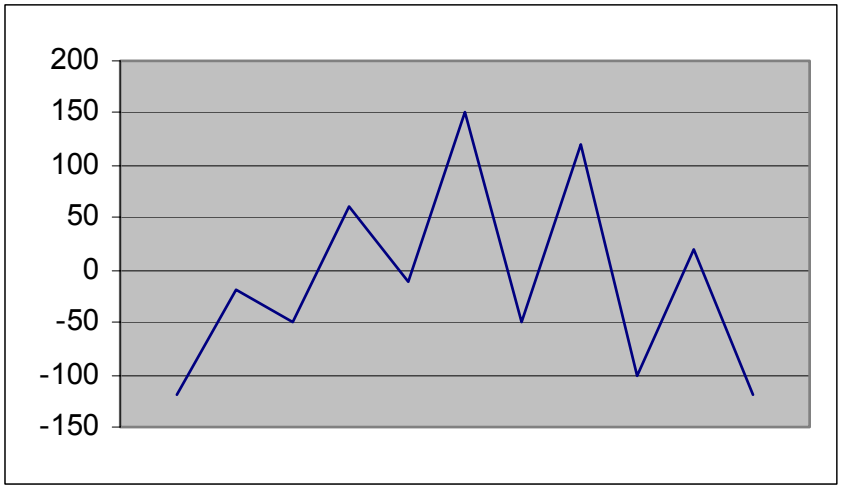

STRESS SPECTRUM

Bin No		1	2	3	4	5	6	7	8	Total
	Bin From	-160	-120	-80	-40	0	40	80	120	
1	-160	0	0	0	0	0	0	0	0	0
2	-120	0	0	0	0	1	0	0	1	2
3	-80	0	0	0	1	0	0	0	1	2
4	-40	0	0	0	0	0	1	0	0	1
5	0	0	0	0	0	0	0	0	0	0
6	40	0	0	0	0	0	0	0	0	0
7	80	0	0	0	0	0	0	0	0	0
8	120	0	0	0	0	0	0	0	0	0
Total		0	0	0	1	1	1	0	2	5

NORMALISED STRESS SPECTRUM

Bin No		1	2	3	4	5	6	7	8	Total
	Bin From	-160	-120	-80	-40	0	40	80	120	
1	-160	0	0	0	0	0	0	0	0	0
2	-120	0	0	0	0	0.2	0	0	0.2	0.4
3	-80	0	0	0	0.2	0	0	0	0.2	0.4
4	-40	0	0	0	0	0	0.2	0	0	0.2
5	0	0	0	0	0	0	0	0	0	0
6	40	0	0	0	0	0	0	0	0	0
7	80	0	0	0	0	0	0	0	0	0
8	120	0	0	0	0	0	0	0	0	0
Total		0	0	0	0.2	0.2	0.2	0	0.4	1

REPETITIONS TO FAILURE FROM GENERIC METHODOLOGY

The number of repetitions to failure from the stress spectra data is: **127927**

The number of repetitions to failure from the raw data is: **213184**

REPETITIONS TO FAILURE FROM THE BS7608 CODE

The number of repetitions to failure from the stress spectra data is: **492486**

The number of repetitions to failure from the raw data is: **802972**

REPETITIONS TO FAILURE FROM THE BS5400 CODE

The number of repetitions to failure from the stress spectra data is: **151287**

The number of repetitions to failure from the raw data is: **239528**

REPETITIONS TO FAILURE FROM THE JAPANESE CODE

The number of repetitions to failure from the stress spectra data is: **77011**

The number of repetitions to failure from the raw data is: **121148**

REPETITIONS TO FAILURE FROM THE AAR CODE

The number of repetitions to failure from the stress spectra data is: **138942**

The number of repetitions to failure from the raw data is: **228001**

REPETITIONS TO FAILURE FROM THE AWS CODE

The number of repetitions to failure from the stress spectra data is: **336968**

The number of repetitions to failure from the raw data is: **532439**

REPETITIONS TO FAILURE FROM THE EUROCODE

The number of repetitions to failure from the stress spectra data is: **130050**

The number of repetitions to failure from the raw data is: **209424**

REPETITIONS TO FAILURE FROM THE AUSTROADS CODE

The number of repetitions to failure from the stress spectra data is: **132227**

The number of repetitions to failure from the raw data is: **209249**

Appendix E - Fatigue Assessment Software Source Code

```
//--------------------------------------------------------------------------
//
//        Fatigue Assessment Software
//
//--------------------------------------------------------------------------


#include <string.h>
#include <stdlib.h>
#include <stdio.h>
#include <conio.h>
#include <time.h>
#include <math.h>
#include <errno.h>
#include <dos.h>
#include <io.h>

//        Function Declarations
void B10_introduction(void);
void B20_readfile(void);
void B30_cyclecount(void);
void C10_snlifecycle(void);
void C20_bs7608lifecycle(void);
void C30_bs5400lifecycle(void);
void C40_japlifecycle(void);
void C50_aarlifecycle(void);
void C60_awslifecycle(void);
void C70_eurolifecycle(void);
void C80_auslifecycle(void);
void C90_screenoutput(void);
void C100_fileoutput(void);

//        Global Variables
char name_out[20],name_in[20],infile[10],outfile[10],*cell[2][21],string[90];
char floatstring1[20],floatstring2[20],view,history,bin;

int bin_no,i,j,k,l,m,n,p,q,r,s,t,u,v,point[2000001],T_row[100],T_col[100];

float stress[2000001],temp_stress[2000001],max[1000000],min[1000000];
float upper,lower,binsize,smin,smax,min_stress;
float norm_T_row,norm_T_col,norm_T_all,norm_spectrum,T_all;

//        SN Curve Variables
float Spoint1,Spoint2,Spoint3,Npoint1,Npoint2,Npoint3;
float fracture_stress,m1,m2,b1,b2,N;
float amplitude,mean,n_N,n_amplitude,n_mean;
float spectrum[100][100],n_reversed_stress[1000000],reversed_stress[100][100];
```

```
//      BS7608/BS5400 Variables
char weld,bs7608,bs54,bs_thick,bs_mod;

float bs_t,bs_sn,bs_factor;
float bs_m,bs_s0,n_bs_range[1000000],bs_range[100][100];
float bs7608N,n_bs7608N,total_bs7608N,n_total_bs7608N,bs7608Bf,n_bs7608Bf;
float bs5400N,n_bs5400N,total_bs5400N,n_total_bs5400N,bs5400Bf,n_bs5400Bf;

//      Japanese Code Variables
char jap_thick,jap,jap_part;

float jap_factor,jap_a,jap_b,jap_c,jap_p;
float jap_all,jap_N,jap_S,jap_t,n_jap_range[1000000],jap_range[100][100];
float japN,n_japN,cor_all,cor_S,total_japN,n_total_japN,japBf,n_japBf;

//      AAR Variables
char sn,material,aar;

float n_total_N,n_Bf,total_N,Bf,n_total_aarN,n_aarBf,total_aarN,aarBf;
float Se,maxs,mins,aar_r,Ne,aar_b,aar_m,aar_k,aarN,n_aarN;

//      AWS Variables
char aws,aws_mod;

float Naws1,Saws1,Naws2,Saws2,aws_m,maws,baws;
float Naws,total_Naws,n_Naws,n_total_Naws,awsBf,n_awsBf;

//      Eurocode Variables
char eur,euro_thick,euro_part;

float euro_cat,euro_t,euro_det,euro_l,euro_s;
float euroN,n_euroN,total_euroN,n_total_euroN,euroBf,n_euroBf;

//      Austroads Code Variables
char aus,aus_thick;

float aus_cat,aus_det,aus_t,n_aus_range[1000000],aus_range[100][100];
float ausN,n_ausN,total_ausN,n_total_ausN,ausBf,n_ausBf;
```

```
//=====================================================================
//                  A Level
//=====================================================================

//---------------------------------------------------------------------
//                  A10 The Main Module
//---------------------------------------------------------------------

void main()
{
        B10_introduction();
        B20_readfile();
        B30_cyclecount();
}

//=====================================================================
//                  B Level
//=====================================================================

//---------------------------------------------------------------------
//                  B10 Introduction
//---------------------------------------------------------------------

void B10_introduction(void)
{
//      Print assumptions to screen
        printf("This version of the fatigue assessment program makes the following a
        ssumptions\n");
        printf("\n");
        printf("Assumed stress state is plane stress with one normal stress equal to
        zero.\n");
        printf("The stress state therefore becomes uniaxial normal stress and shear
        stress.\n");
        printf("Shear stresses are assumed to vary simultaneously with normal
        stress.\n");
        printf("Where shear stress is less than 0.15 of normal stress, normal stress to be
        used in analysis.\n");
        printf("Where shear stress is greater than 0.15 of normal stress, principal stress
        used.\n");
        printf("It is left to the user to ensure appropriate stresses are used in
        analysis.\n");
        printf("\n");

//      Request the text file to be viewed
        printf("Enter the text file you would like to read the stress-time history
        from:\n");
        scanf("%s",&infile);
        sprintf(name_in,"b:%s.txt",infile);
        printf("\n");
```

```
//      Request whether the user would like to arrange cycles into a stress spectrum
        printf("Would you like to arrange cycles in a stress spectrum (y/n)?\n");
        scanf("%s",&bin);

        if(bin=='y'||bin=='Y')
        {
                printf("Enter the upper bound of the stress spectrum table: ");
                scanf("%f",&upper);
                printf("\n");
                printf("Enter the lower bound of the stress spectrum table: ");
                scanf("%f",&lower);
                printf("\n");
                printf("Enter the number of bins (maximum permissible = 100): ");
                scanf("%d",&bin_no);
                printf("\n");
        }

//      Request output location
        printf("Where would you like to view the output?");
        printf("\nIf you would like to view the output on the screen, press 1:");
        printf("\nIf you would like to send the output to disk, press 2:");
        scanf("%s",&view);

//      Request the file to which the filtered data is to be sent
        if (view=='2')
        {
                printf("\n\nEnter the name of the text file you would like to write the
                output to: ");
                scanf("%s",&outfile);
                sprintf(name_out,"b:%s.txt",outfile);
        }
        printf("\n\n");

//              Request whether the user would like to analyse via assumed current
                methodology
        printf("Would you like to a conduct fatigue analysis via assumed current
        methodology (y/n)?");
        scanf("%s",&sn);

        if (sn=='y'||sn=='Y')
        {
//      Request the value for true stress at fracture
                printf("\n\nEnter the value for the true stress at fracture for conversion to
                fully reversed");
                printf("stress amplitudes (MPa):");
                scanf("%f",&fracture_stress);
```

```
//      Request S-N curve data
            printf("\nEnter points 1,2 & 3 for the S-N curve:");
            printf("\nPoint 1 (N): ");
            scanf("%f",&Npoint1);
            printf("Point 1 (S) (MPa): ");
            scanf("%f",&Spoint1);
            printf("\nPoint 2 (N): ");
            scanf("%f",&Npoint2);
            printf("Point 2 (S) (MPa): ");
            scanf("%f",&Spoint2);
            printf("\nPoint 3 (N): ");
            scanf("%f",&Npoint3);
            printf("Point 3 (S) (MPa): ");
            scanf("%f",&Spoint3);
      }
      printf("\n\n");

//      Request whether the user would like to analyse via the BS7608 code
      printf("Would you like to a conduct fatigue analysis as per BS7608 (y/n)?");
      scanf("%s",&bs7608);

      if (bs7608=='y'||bs7608=='Y')
      {
//      Request S-N curve data and weld detail
            printf("\n\nEnter class details:");
            printf("\n\nEnter the m value: ");
            scanf("%f",&bs_m);
            printf("\nEnter the S0 value (MPa): ");
            scanf("%f",&bs_s0);
            printf("\nIs the detail welded and not stress relieved (y/n)?");
            scanf("%s",&weld);
            printf("\nIs a thickness correction factor required - (y/n)?");
            scanf("%s",&bs_thick);

            bs_t=16.;

            if (bs_thick=='y'||bs_thick=='Y')
            {
                  printf("\n\nEnter the plate thickness (must be greater than or
                  equal to 16mm):");
                  scanf("%f",&bs_t);
            }

            printf("\nAre any other S-N curve modification factors required (y/n)?");
            scanf("%s",&bs_mod);

            bs_sn=1.0;
```

```
            if (bs_mod=='y'||bs_mod=='Y')
            {
                printf("\n\nEnter the appropriate value of the modification
                factor.");
                printf("\nFor example 1.3 for controlled machining or grinding
                of the weld toe.");
                scanf("%f",&bs_sn);
            }

            bs_factor = pow(16./bs_t,0.25) * bs_sn;

        }
        printf("\n\n");

//          Request whether the user would like to analyse via the BS5400 code
        printf("Would you like to a conduct fatigue analysis as per BS5400 (y/n)?");
        scanf("%s",&bs54);

        if (bs54=='y'||bs54=='Y')
        {
            if (bs7608=='y'||bs7608=='Y')
            {
                printf("\n\nClass details entered for BS7608 will be used.");
            }
            else
            {
//          Request S-N curve data and weld detail
                printf("\n\nEnter class details:");
                printf("\n\nEnter the m value: ");
                scanf("%f",&bs_m);
                printf("\nEnter the S0 value (MPa): ");
                scanf("%f",&bs_s0);
                printf("\nIs the detail welded and not stress relieved (y/n)?");
                scanf("%s",&weld);
            }
        }
            printf("\n\n");

//      Request whether the user would like to analyse via the Japanese code
        printf("Would you like to a conduct fatigue analysis as per the Japanese Code
        (y/n)?");
        scanf("%s",&jap);
```

```
        if (jap=='y'||jap=='Y')
        {
//              Request S-N curve data and stress ranges
                printf("\n\nEnter the basic allowable stress range at 2,000,000 cycles
                (MPa):");
                scanf("%f",&jap_all);
                printf("\nEnter the stress range at the cut off (fatigue) limit (MPa): ");
                scanf("%f",&jap_S);
                printf("\nIs a thickness correction factor required - (y/n)?");
                scanf("%s",&jap_thick);

                jap_t=25.0;

                if (jap_thick=='y'||jap_thick=='Y')
                {
                        printf("\n\nEnter the plate thickness (must be greater than or
                        equal to 25mm):");
                        scanf("%f",&jap_t);
                }

                printf("\nAre partial safety factors required - (y/n)?");
                scanf("%s",&jap_part);

                jap_p=1.0;

                if (jap_part=='y'||jap_part=='Y')
                {
                        printf("\n\nEnter the redundancy partial safety factor:");
                        scanf("%f",&jap_a);
                        printf("\n\nEnter the importance partial safety factor:");
                        scanf("%f",&jap_b);
                        printf("\n\nEnter the inspection partial safety factor:");
                        scanf("%f",&jap_c);

                        jap_p = jap_a * jap_b * jap_c;
                }

                jap_factor = pow(25./jap_t,0.25);

        }
        printf("\n\n");

//      Request whether the user would like to analyse via the AAR code
        printf("Would you like to a conduct fatigue analysis as per the AAR code
        (y/n)?");
        scanf("%s",&aar);
```

```
if (aar=='y'||aar=='Y')
        {
//      Select the material type
                printf("\n\nWould you like to analyse steel or aluminium?");
                printf("\nIf you would like to analyse steel (ie Ne = 2000000), press
                1:");
                printf("\nIf you would like to analyse aluminium (ie Ne = 10000000),
                press 2:");
                scanf("%s",&material);

                if (material=='1') Ne=2000000.;
                else if (material=='2') Ne=10000000.;

//      Request material data from AAR code
                printf("\nEnter the Y-intercept of MGD (ksi):");
                scanf("%f",&aar_b);
                aar_b=6.89476*aar_b;
                printf("\nEnter the MGD slope:");
                scanf("%f",&aar_m);
                printf("\nEnter the S-N Slope: ");
                scanf("%f",&aar_k);
        }
        printf("\n\n");

//      Request whether the user would like to analyse via the AWS code
        printf("Would you like to a conduct fatigue analysis as per the AWS code
        (y/n)?");
        scanf("%s",&aws);

        if (aws=='y'||aws=='Y')
        {

//      Request S-N curve data
                printf("\nEnter points 1 & 2 for the AWS S-N curve:");
                Naws1 = 100000;
                printf("\nStress Range at 10 0000 cycles: (MPa): ");
                scanf("%f",&Saws1);
                printf("\nCycles at the endurance limt: ");
                scanf("%f",&Naws2);
                printf("Stress Range at the endurance limt (MPa): ");
                scanf("%f",&Saws2);

                printf("\nAre any S-N curve modification factors required (y/n)?");
                scanf("%s",&aws_mod);

                aws_m = 1.0;
```

```
            if (aws_mod=='y'||aws_mod=='Y')
            {
                printf("\n\nEnter the appropriate value of the modification
                factor.");
                printf("\nFor example 1.3 for toe grinding, hammer peening or
                TIG dressing,");
                printf("\nor 1.5 for the cummulative affect of toe grinding and
                hammer peening.");
                scanf("%f",&aws_m);
            }

            Saws1 = Saws1 * aws_m;
            Saws2 = Saws2 * aws_m;
        }

        printf("\n\n");

//      Request whether the user would like to analyse via the Eurocode
        printf("Would you like to a conduct fatigue analysis as per the Eurocode
        (y/n)?");
        scanf("%s",&eur);

        if (eur=='y'||eur=='Y')
        {
//      Request detail category
            printf("\n\nEnter the value of the Detail Category (MPa):");
            scanf("%f",&euro_cat);
            printf("\nIs a thickness correction factor required - (y/n)?");
            scanf("%s",&euro_thick);

            euro_t=25.;

            if (euro_thick=='y'||euro_thick=='Y')
            {
                printf("\n\nEnter the plate thickness (must be greater than or
                equal to 25mm):");
                scanf("%f",&euro_t);
            }
```

```
            if(bs7608=='y'||bs7608=='Y')
            {
                if (weld!='y'&&weld!='Y')
                {
                    printf("\nDetail assumed unwelded or welded and stress
                    relieved as per BS7608.\n");
                }
                if (weld=='y'||weld=='Y')
                {
                    printf("\nDetail assumed welded and not stress relieved
                    as per BS7608.\n");
                }
            }

            else
            {
                printf("\nIs the detail welded and not stress relieved (y/n)?");
                scanf("%s",&weld);
            }

            printf("\nAre partial safety factors required - (y/n)?");
            scanf("%s",&euro_part);

            euro_l = 1.0;

            euro_s = 1.0;

            if (euro_part=='y'||euro_part=='Y')
            {
                printf("\n\nEnter the partial safety factor for fatigue loading:");
                scanf("%f",&euro_l);
                printf("\n\nEnter the partial safety factor for fatigue strength:");
                scanf("%f",&euro_s);
            }

            euro_det=pow(25./euro_t,0.25)*pow(2.5,(-1./3.))
            *euro_cat/(euro_l*euro_s);
        }

        printf("\n\n");

//      Request whether the user would like to analyse via the Austroads code
        printf("Would you like to a conduct fatigue analysis as per the Austroads Code
        (y/n)?");
        scanf("%s",&aus);

        if (aus=='y'||aus=='Y')
        {
//      Request detail category
            printf("\n\nEnter the value of the Detail Category (MPa):");
```

```
                scanf("%f",&aus_cat);
                printf("\nIs a thickness correction factor required - (y/n)?");
                scanf("%s",&aus_thick);

                aus_t=25.;

                if (aus_thick=='y'||aus_thick=='Y')
                {
                        printf("\n\nEnter the plate thickness (must be greater than or
                        equal to 25mm):");
                        scanf("%f",&aus_t);
                }

                aus_det=pow(25./aus_t,0.25)*pow(2.5,(-1./3.))*aus_cat;
        }

//      Request for filtered Stress History
        if (view=='2')
        {
                printf("\n\n\n\n\nWould you like the filtered Stress History Sent to file
                (y/n)?");
                scanf("%s",&history);
        }
}
```

```
//---------------------------------------------------------------------------
//                  B20 Read File
//---------------------------------------------------------------------------

void B20_readfile(void)
{
        FILE *fp;       // File declaration

//      Open the requested text file for reading only
        if ((fp=fopen(name_in,"r"))==NULL)
        {
                printf("\nCannot open file %s",name_in);
                getch();
                exit(1);
        }

        j=0;

        while (!feof(fp))
        {
//      Read in data file line by line
                fgets(string,20,fp);

//      Establish string and get the first token:
                m=0;
                cell[m][10] = strtok(string,"    ");

                while( cell[m][10] != NULL )
                {
                        m=m+1;

//      Get next token:
                        cell[m][10] = strtok(NULL,"  ");
                }

//      Convert to a floating point number from a string
                sprintf(floatstring2,"%s",cell[1][10]);
                stress[j] = atof(floatstring2);

                j=j+1;
        }
        fclose(fp);

                j=j-1;
}
```

```
//-------------------------------------------------------------------------
//                  B30 Cycle Count
//-------------------------------------------------------------------------

void B30_cyclecount(void)
{
//      Find lowest stress entry
        for (i=0;i<j+1;i++)
        {
                if (i==0)
                {
                        min_stress = stress[0];
                        l = 0;
                }

                if (stress[i]<min_stress)
                {
                        min_stress = stress[i];
                        l = i;
                }
        }

//      Shift data so that first point is the minimum stress value
        for (i=0;i<j+1;i++)
        {
                if (i<=(j-l))
                {
                        temp_stress[i] = stress[i+l];
                }
                else
                {
                        temp_stress[i] = stress[i-j+l];
                }
        }

//      Store only points which define peaks or valleys
        k=0;
        for (i=1;i<j;i++)
        {
                n=0;
                while ((temp_stress[i+1+n]-temp_stress[i+n])==0) n=n+1;

                if (((temp_stress[i+1+n]-temp_stress[i])
                                *(temp_stress[i]-temp_stress[i-1]))<0)
                {
                        k=k+1;
                        stress[k]=temp_stress[i];
                }
                i=i+n;
        }
```

```
        k=k+1;
        stress[k]=temp_stress[0];
        stress[0]=temp_stress[0];

//      Rain flow cycle count shifted data
        n=0;
        v=0;
        for (i=0;i<k+1;i++)
        {
                point[v]=i;
                v=v+1;
        }
        v=v-1;
        while ((k-2*n)>2)
        {
                u=v-1;
                v=0;
                i=0;
                t=0;
                while (i<u)
                {
                        if ((t<1)&&(fabs(stress[point[i+2]]-stress[point[i+1]])
                                        >=fabs(stress[point[i+1]]-stress[point[i]])))
                        {
                                if (stress[point[i+1]]>stress[point[i]])
                                {
                                        min[n] = stress[point[i]];
                                        max[n] = stress[point[i+1]];
                                }

                                else if (stress[point[i+1]]<stress[point[i]])
                                {
                                        max[n] = stress[point[i]];
                                        min[n] = stress[point[i+1]];
                                }

//      Record details for S-N Curve calculations
                                if (sn=='y'||sn=='Y')
                                {
```

```
//      Record stress details for exact calculation
                        n_amplitude=(max[n]-min[n])/2.;
                        n_mean=(max[n]+min[n])/2.;
                        if (n_mean<0)
                        {
                                n_reversed_stress[n]=n_amplitude;
                        }
                        else
                        {
                                n_reversed_stress[n]=
                                n_amplitude/(1.-
                                (n_mean/fracture_stress));
                        }
                }

//      Record details for BS7608/BS5400 and Eurocode calculations
                if (bs7608=='y'||bs7608=='Y'||bs54=='y'
                ||bs54=='Y'||eur=='y'||eur=='Y')
                {
                        if (weld=='y'||weld=='Y')
                                n_bs_range[n]=max[n]-min[n];
                        else
                        {
                                if (max[n]<0&&min[n]<0)
                                        n_bs_range[n]=0.;
                                else if (min[n]<0&&max[n]>=0)
                                        n_bs_range[n]=0.6*(0.-
                                        min[n])+max[n];

                                else if (min[n]>=0&&max[n]>=0)
                                        n_bs_range[n]=max[n]-min[n];
                        }
                }

//      Record details for Japanese Code calculations
                if (jap=='y'||jap=='Y')
                        n_jap_range[n]=max[n]-min[n];
```

```
//      Record details for Austroads and AWS Code calculations
                        if (aus=='y'||aus=='Y'||aws=='y'||aws=='Y')
                                n_aus_range[n]=max[n]-min[n];

                        n=n+1;
                        i=i+2;
                        t=1;
                }
                else
                {
                        point[v]=point[i];
                        v=v+1;
                        i=i+1;
                }
        }
        if (i>u)
        {
                point[v]=point[i];
        }
        else
        {
                point[v]=point[i];
                v=v+1;
                point[v]=point[i+1];
        }
}

max[n] = stress[point[1]];
min[n] = stress[point[0]];

//      Record details for S-N Curve calculations
if (sn=='y'||sn=='Y')
{
//      Record stress details for exact calculation
        n_amplitude=(max[n]-min[n])/2.;
        n_mean=(max[n]+min[n])/2.;
        if (n_mean<0)
        {
                n_reversed_stress[n]=n_amplitude;
        }
        else
        {
                n_reversed_stress[n]=
                n_amplitude/(1.-(n_mean/fracture_stress));
        }
}
```

```
//      Record details for BS7608/BS5400 and Eurocode calculations
        if (bs7608=='y'||bs7608=='Y'||bs54=='y'||bs54=='Y'||eur=='y'||eur=='Y')
        {
                if (weld=='y'||weld=='Y')
                        n_bs_range[n]=max[n]-min[n];
                else
                {
                        if (max[n]<0&&min[n]<0)    n_bs_range[n]=0.;
                        else if (min[n]<0&&max[n]>=0)
                                n_bs_range[n]=0.6*(0.-min[n])+max[n];
                        else if (min[n]>=0&&max[n]>=0)
                                n_bs_range[n]=max[n]-min[n];
                }
        }

//      Record details for Japanese Code calculations
        if (jap=='y'||jap=='Y')
                n_jap_range[n]=max[n]-min[n];

//              Record details for Austroads and AWS Code calculations
        if (aus=='y'||aus=='Y'||aws=='y'||aws=='Y')
                n_aus_range[n]=max[n]-min[n];

        n=n+1;

//      Establish bin size
        binsize = (upper-lower)/bin_no;

//      Put counted cycles into the appropriate bins and determine the mean,
//      amplitude and fully reversed stress
        for (q=0;q<bin_no;q++)
        {
                for (r=0;r<bin_no;r++)
                {
                        smin = lower + q*binsize;
                        smax = lower + r*binsize;

                        for (i=0;i<n;i++)
                        {
                                if (smin<=min[i]&&min[i]<(smin+binsize)
                                &&smax<=max[i]&&max[i]<(smax+binsize))
                                {
                                        spectrum[q][r]=spectrum[q][r]+1;
```

```
//      Record details for S-N Curve calculations
                                        if (sn=='y'||sn=='Y')
                                        {
                                                amplitude=((smax+binsize)-smin)/2.;
                                                mean=((smax+binsize)+smin)/2.;
                                                if (mean<0)
                                                {
                                                        reversed_stress[q][r]=amplitude;
                                                }
                                                else
                                                {
                                                        reversed_stress[q][r]=
                                                                amplitude/(1.-
                                                                (mean/fracture_stress));
                                                }
                                        }

//      Record details for BS7608/BS5400 and Eurocode calculations
                                        if (bs7608=='y'||bs7608=='Y'||bs54=='y'
                                        ||bs54=='Y'||eur=='y'||eur=='Y')
                                        {
                                                if (weld=='y'||weld=='Y')
                                                        bs_range[q][r]=(smax+binsize)-
                                                        smin;
                                                else
                                                {
                                                        if ((smax+binsize)<0&&smin<0)
                                                                bs_range[q][r]=0.;
                                                        else if (smin<0
                                                        &&(smax+binsize)>=0)
                                                                bs_range[q][r]=0.6*(0.-
                                                                smin)+smax+binsize;
                                                        else if (smin>=0
                                                        &&(smax+binsize)>=0)
                                                                bs_range[q][r]
                                                                =smax+binsize-smin;
                                                }
                                        }
//      Record details for Japanese Code calculations
                                        if (jap=='y'||jap=='Y')
                                                jap_range[q][r]=(smax+binsize)-smin;

//      Record details for Austroads and AWS Code calculations
                                        if (aus=='y'||aus=='Y'||aws=='y'||aws=='Y')
                                                aus_range[q][r]=(smax+binsize)-smin;
                                }
                        }
                }
        }
```

```
//      Find row totals
        for (q=0;q<bin_no;q++)
        {
                for (r=0;r<bin_no;r++)
                {
                        T_row[q]=T_row[q]+spectrum[q][r];
                }
                T_all=T_all+T_row[q];
        }

//      Find column totals
        for (r=0;r<bin_no;r++)
        {
                for (q=0;q<bin_no;q++)
                {
                        T_col[r]=T_col[r]+spectrum[q][r];
                }
        }

        if (sn=='y'||sn=='Y') C10_snlifecycle();

        if (bs7608=='y'||bs7608=='Y') C20_bs7608lifecycle();

        if (bs54=='y'||bs54=='Y') C30_bs5400lifecycle();

        if (jap=='y'||jap=='Y') C40_japlifecycle();

        if (aar=='y'||aar=='Y')  C50_aarlifecycle();

        if (aws=='y'||aws=='Y') C60_awslifecycle();

        if (eur=='y'||eur=='Y') C70_eurolifecycle();

        if (aus=='y'||aus=='Y') C80_auslifecycle();

        if (view=='1')  C90_screenoutput();
        else if (view=='2') C100_fileoutput();
}
```

```
//---------------------------------------------------------------------------
//                  C10 S-N Life Cycle
//---------------------------------------------------------------------------

void C10_snlifecycle(void)
{
//      Find equations for the S-N lines
        m1=log10(Spoint2/Spoint1)/log10(Npoint2/Npoint1);
        b1=log10(Spoint1)-m1*log10(Npoint1);

        m2=log10(Spoint3/Spoint2)/log10(Npoint3/Npoint2);
        b2=log10(Spoint2)-m2*log10(Npoint2);

        if(bin=='y'||bin=='Y')
        {
//      Calculated life cycles from bin data
        N=0;
        total_N=0;
        for (q=0;q<bin_no;q++)
        {
                for (r=0;r<bin_no;r++)
                {
                        if (spectrum[q][r]>0)
                        {
                                if (reversed_stress[q][r]>Spoint1)
                                {
                                        printf("\nReversed Stress has exceeded S-N
                                        limits! - ASSUMED CURRENT
                                        METHODOLOGY");
                                        getch();
                                        exit(1);
                                }
                                else if (Spoint1>=reversed_stress[q][r]&&
                                        reversed_stress[q][r]>=Spoint2)
                                {
                                        N=spectrum[q][r]/
                                        (pow(reversed_stress[q][r],
                                        (1./m1))*pow(10.,(-b1/m1)));
                                        total_N=total_N+N;
                                }
                                else if (reversed_stress[q][r]<Spoint2&&m2!=0)
                                {
                                        N=spectrum[q][r]/
                                        (pow(reversed_stress[q][r],
                                        (1./m2))*pow(10.,(-b2/m2)));
                                        total_N=total_N+N;
                                }
                        }
                }
        }
```

```
        }

//      Calculated life cycles from exact values
        n_N=0;
        n_total_N=0;
        for (i=0;i<n;i++)
        {
                if (n_reversed_stress[i]>Spoint1)
                {
                        printf("\nReversed Stress has exceeded S-N limits! - ASSUMED
                        CURRENT METHODOLOGY");
                        getch();
                        exit(1);
                }
                else if (Spoint1>=n_reversed_stress[i]&&
                        n_reversed_stress[i]>=Spoint2)
                {
                        n_N=1./(pow(n_reversed_stress[i],(1./m1))*pow(10.,(-b1/m1)));
                        n_total_N=n_total_N+n_N;
                }

                else if (n_reversed_stress[i]<Spoint2&&m2!=0)
                {
                        n_N=1./(pow(n_reversed_stress[i],(1./m2))
                                *pow(10.,(-b2/m2)));
                        n_total_N=n_total_N+n_N;
                }
        }

//      Calculate number of repetitions to failure from bin data
        Bf=1./total_N;
//      Calculate number of repetitions to failure from exact values
        n_Bf=1./n_total_N;
}
```

```
//---------------------------------------------------------------------------
//                  C20 BS7608 Life Cycle
//---------------------------------------------------------------------------

void C20_bs7608lifecycle(void)
{
        if(bin=='y'||bin=='Y')
        {
//      Calculated life cycles from bin data
        bs7608N=0;
        total_bs7608N=0;
        for (q=0;q<bin_no;q++)
        {
                for (r=0;r<bin_no;r++)
                {
                        if (spectrum[q][r]>0&&bs_range[q][r]!=0.)
                        {
                                if (bs_range[q][r]>(bs_s0*pow(.01,-1./bs_m)*bs_factor))
                                {
                                        printf("\nCorrected Stress has exceeded S-N
                                        limits! - BS7608 CODE");
                                        getch();
                                        exit(1);
                                }
                                else if ((bs_s0*pow(.01,-1./bs_m)*bs_factor)
                                >=bs_range[q][r]&&
                                bs_range[q][r]>=(bs_s0*bs_factor))
                                {
                                        bs7608N=spectrum[q][r]/
                                        (10000000.*pow((bs_s0*
                                        bs_factor/bs_range[q][r]),bs_m));
                                        total_bs7608N=total_bs7608N+bs7608N;
                                }

                                else if (bs_range[q][r]<(bs_s0*bs_factor))
                                {
                                        bs7608N=spectrum[q][r]/
                                        (10000000.*pow((bs_s0
                                        *bs_factor/bs_range[q][r]),(bs_m+2.)));
                                        total_bs7608N=total_bs7608N+bs7608N;
                                }
                        }
                }
        }
        }
```

```
//      Calculated life cycles from exact values
        n_bs7608N=0;
        n_total_bs7608N=0;
        for (i=0;i<n;i++)
        {
                if (n_bs_range[i]!=0.)
                {
                        if (n_bs_range[i]>(bs_s0*pow(.01,-1./bs_m)*bs_factor))
                        {
                                printf("\nCorrected Stress has exceeded S-N limits! -
                                BS7608 CODE");
                                getch();
                                exit(1);
                        }
                        else if ((bs_s0*pow(.01,-1./bs_m)*bs_factor)
                        >=n_bs_range[i]&&n_bs_range[i]>=(bs_s0*bs_factor))
                        {
                                n_bs7608N=1./(10000000.*pow((bs_s0
                                *bs_factor/n_bs_range[i]),bs_m));
                                n_total_bs7608N=n_total_bs7608N+n_bs7608N;
                        }

                        else if (n_bs_range[i]<(bs_s0*bs_factor))
                        {
                                n_bs7608N=1./(10000000.*pow((bs_s0
                                *bs_factor/n_bs_range[i]),(bs_m+2.)));
                                n_total_bs7608N=n_total_bs7608N+n_bs7608N;
                        }
                }
        }
//      Calculate number of repetitions to failure from bin data
        bs7608Bf=1./total_bs7608N;
//      Calculate number of repetitions to failure from exact values
        n_bs7608Bf=1./n_total_bs7608N;
}
```

```
//---------------------------------------------------------------------------
//                  C30 BS5400 Life Cycle
//---------------------------------------------------------------------------

void C30_bs5400lifecycle(void)
{
        if(bin=='y'||bin=='Y')
        {
//      Calculated life cycles from bin data
        bs5400N=0;
        total_bs5400N=0;
        for (q=0;q<bin_no;q++)
        {
                for (r=0;r<bin_no;r++)
                {
                        if (spectrum[q][r]>0&&bs_range[q][r]!=0.)
                        {
                                if (bs_range[q][r]>(bs_s0*pow(.01,-1./bs_m)))
                                {
                                        printf("\nCorrected Stress has exceeded S-N
                                        limits! - BS5400 CODE");
                                        getch();
                                        exit(1);
                                }
                                else if ((bs_s0*pow(.01,-1./bs_m))>=bs_range[q][r]&&
                                        bs_range[q][r]>=bs_s0)
                                {
                                        bs5400N=spectrum[q][r]/
                                        (10000000.*pow((bs_s0/
                                        bs_range[q][r]),bs_m));
                                        total_bs5400N=total_bs5400N+bs5400N;
                                }

                                else if (bs_range[q][r]<bs_s0)
                                {
                                        bs5400N=spectrum[q][r]/
                                        (10000000.*pow((bs_s0/
                                        bs_range[q][r]),(bs_m+2.)));
                                        total_bs5400N=total_bs5400N+bs5400N;
                                }
                        }
                }
        }
        }
```

```
//      Calculated life cycles from exact values
        n_bs5400N=0;
        n_total_bs5400N=0;
        for (i=0;i<n;i++)
        {
                if (n_bs_range[i]!=0.)
                {
                        if (n_bs_range[i]>(bs_s0*pow(.01,-1./bs_m)))
                        {
                                printf("\nCorrected Stress has exceeded S-N limits! -
                                BS5400 CODE");
                                getch();
                                exit(1);
                        }
                        else if ((bs_s0*pow(.01,-1./bs_m))>=n_bs_range[i]
                        &&n_bs_range[i]>=bs_s0)
                        {
                                n_bs5400N=1./(10000000.
                                *pow((bs_s0/n_bs_range[i]),bs_m));
                                n_total_bs5400N=n_total_bs5400N+n_bs5400N;
                        }

                        else if (n_bs_range[i]<bs_s0)
                        {
                                n_bs5400N=1./(10000000.
                                *pow((bs_s0/n_bs_range[i]),(bs_m+2.)));
                                n_total_bs5400N=n_total_bs5400N+n_bs5400N;
                        }
                }
        }
//      Calculate number of repetitions to failure from bin data
        bs5400Bf=1./total_bs5400N;
//      Calculate number of repetitions to failure from exact values
        n_bs5400Bf=1./n_total_bs5400N;
}
```

```
//---------------------------------------------------------------------------
//                  C40 Japanese Code Life Cycle
//---------------------------------------------------------------------------

void C40_japlifecycle(void)
{
        if(bin=='y'||bin=='Y')
        {
//      Calculated life cycles from bin data

        japN=0;
        total_japN=0;
        for (q=0;q<bin_no;q++)
        {
                for (r=0;r<bin_no;r++)
                {
                        if (spectrum[q][r]>0)
                        {
                                mins = lower + q*binsize;
                                maxs = lower + (r+1)*binsize;

                                if (mins<=0&&maxs<=0)
                                {
                                        cor_all=1.3*jap_factor*jap_all;
                                        cor_S=1.3*jap_factor*jap_S;
                                }

                                else if (mins/maxs<=-1)
                                {
                                        cor_all=(1.3*(1.-mins/maxs)/(1.6-
                                        mins/maxs))*jap_factor*jap_all;
                                        cor_S=(1.3*(1.-mins/maxs)/(1.6-
                                        mins/maxs))*jap_factor*jap_S;
                                }

                                else
                                {
                                        cor_all=jap_factor*jap_all;
                                        cor_S=jap_factor*jap_S;
                                }

                                if (jap_range[q][r]>(cor_all*pow(2000.,1./3.)))
                                {
                                        printf("\nCorrected Stress has exceeded S-N
                                        limits! - JAPANESE CODE - bin");
                                        getch();
                                        exit(1);
```

```
                        }
                        else if ((cor_all*pow(2000.,1./3.))>=jap_range[q][r]&&
                                jap_range[q][r]>=(cor_S))
                        {
                                japN=spectrum[q][r]/(2000000.*
                                pow(cor_all/jap_range[q][r],3.));
                                total_japN=total_japN+japN;
                        }
                }
        }
        }

//      Calculated life cycles from exact values
        n_japN=0;
        n_total_japN=0;
        for (i=0;i<n;i++)
        {
                mins = min[i];
                maxs = max[i];

                if (mins<=0&&maxs<=0)
                {
                        cor_all=1.3*jap_factor*jap_all;

                }

                else if (mins/maxs<=-1)
                {
                        cor_all=(1.3*(1.-mins/maxs)/(1.6-mins/maxs))
                        *jap_factor*jap_all;
                        cor_S=(1.3*(1.-mins/maxs)/(1.6-mins/maxs))*jap_factor*jap_S;
                }

                else
                {
                        cor_all=jap_factor*jap_all;
                        cor_S=jap_factor*jap_S;
                }

                if (n_jap_range[i]>(cor_all*pow(2000.,1./3.)))
                {
                        printf("\nCorrected Stress has exceeded S-N limits! -
                        JAPANESE CODE");
                        getch();
                        exit(1);
                }
```

```
                else if ((cor_all*pow(2000.,1./3.))>=n_jap_range[i]&&
                n_jap_range[i]>=(cor_S))
                {
                        n_japN=1./(2000000.*pow(cor_all/n_jap_range[i],3.));

                n_total_japN=n_total_japN+n_japN;
                }
        }
//      Calculate number of repetitions to failure from bin data
        japBf=1./(pow(jap_p,3.)*total_japN);
//      Calculate number of repetitions to failure from exact values
        n_japBf=1./(pow(jap_p,3.)*n_total_japN);
}
```

```
//---------------------------------------------------------------------------
//                  C50 AAR Life Cycle
//---------------------------------------------------------------------------

void C50_aarlifecycle(void)
{
        if(bin=='y'||bin=='Y')
        {
//      Calculated life cycles from bin data
        aarN=0;
        total_aarN=0;
        for (q=0;q<bin_no;q++)
        {
                for (r=0;r<bin_no;r++)
                {
                        if (spectrum[q][r]>0)
                        {
                                mins = lower + q*binsize;
                                maxs = lower + (r+1)*binsize;

                                aar_r=mins/maxs;
                                if (aar_r>1||aar_r<-1)
                                {
                                        aar_r=-1.0;
                                        maxs = (maxs-mins)/2.;
                                }

                                Se = aar_b/(1.-aar_m*aar_r);

                                if (Se<maxs)
                                {
                                        if (maxs>(Se*pow(Ne/100000.,aar_k)))
                                        {
                                                printf("\nCorrected Stress has exceeded S-
                                                N limits! - AAR CODE");
                                                getch();
                                                exit(1);
                                        }

                                        else
                                        {
                                        aarN=spectrum[q][r]/
                                        (Ne/(pow(maxs/Se,1./aar_k)));
                                        total_aarN=total_aarN+aarN;
                                        }
                                }
                        }
                }
        }
        }
```

```
//      Calculated life cycles from exact data

        n_aarN=0;
        n_total_aarN=0;
        for (i=0;i<n;i++)
        {
                mins=min[i];
                maxs=max[i];
                aar_r=mins/maxs;
                if (aar_r>1||aar_r<-1)
                {
                        aar_r=-1.0;
                        maxs = (maxs-mins)/2.;
                }

                Se = aar_b/(1.-aar_m*aar_r);

                if (Se<maxs)
                {

                        if (maxs>(Se*pow(Ne/100000.,aar_k)))
                        {
                                printf("\nCorrected Stress has exceeded S-N limits! -
                                AAR CODE");
                                getch();
                                exit(1);
                        }
                        else
                        {
                                n_aarN=1./(Ne/(pow(maxs/Se,1./aar_k)));
                                n_total_aarN=n_total_aarN+n_aarN;
                        }
                }
        }
//      Calculate number of repetitions to failure from bin data
        aarBf=1./total_aarN;
//      Calculate number of repetitions to failure from exact values
        n_aarBf=1./n_total_aarN;
}
```

```
//-------------------------------------------------------------------------
//                  C60 AWS Life Cycle
//-------------------------------------------------------------------------

void C60_awslifecycle(void)
{
//      Find equations for the S-N lines
        maws=log10(Saws2/Saws1)/log10(Naws2/Naws1);
        baws=log10(Saws1)-maws*log10(Naws1);

        if(bin=='y'||bin=='Y')
        {
//      Calculated life cycles from bin data
        N=0;
        total_N=0;
        for (q=0;q<bin_no;q++)
        {
                for (r=0;r<bin_no;r++)
                {
                        if (spectrum[q][r]>0)
                        {
                                if (aus_range[q][r]>Saws1)
                                {
                                        printf("\nCorrected Stress has exceeded S-N
                                        limits! - AWS CODE");
                                        getch();
                                        exit(1);
                                }
```

```
                        else if (Saws1>=aus_range[q][r]&&
                                aus_range[q][r]>=Saws2)
                        {
                                Naws=spectrum[q][r]/
                                (pow(aus_range[q][r],(1./maws))
                                *pow(10.,(-baws/maws)));
                                total_Naws=total_Naws+Naws;
                        }
                }
        }
        }

//      Calculated life cycles from exact values
        n_Naws=0;
        n_total_Naws=0;
        for (i=0;i<n;i++)
        {
                if (n_aus_range[i]>Saws1)
                {
                        printf("\nCorrected Stress has exceeded S-N limits! - AWS
                        CODE");
                        getch();
                        exit(1);
                }
                else if (Saws1>=n_aus_range[i]&&
                        n_aus_range[i]>=Saws2)
                {
                        n_Naws=1./(pow(n_aus_range[i],(1./maws))
                        *pow(10.,(-baws/maws)));
                        n_total_Naws=n_total_Naws+n_Naws;
                }
        }

//      Calculate number of repetitions to failure from bin data
        awsBf=1./total_Naws;
//      Calculate number of repetitions to failure from exact values
        n_awsBf=1./n_total_Naws;
}
```

```
//---------------------------------------------------------------------------
//                  C70 Eurocode Life Cycle
//---------------------------------------------------------------------------

void C70_eurolifecycle(void)
{
        if(bin=='y'||bin=='Y')
        {
//      Calculated life cycles from bin data
        euroN=0;
        total_euroN=0;
        for (q=0;q<bin_no;q++)
        {
                for (r=0;r<bin_no;r++)
                {
                        if (spectrum[q][r]>0)
                        {
                                if (bs_range[q][r]>(euro_det*pow(.002,-1./3.)))
                                {
                                        printf("\nCorrected Stress has exceeded S-N
                                        limits! - EUROCODE");
                                        getch();
                                        exit(1);
                                }
                                else if ((euro_det*pow(.002,-1./3.))>=bs_range[q][r]
                                &&bs_range[q][r]>=euro_det)
                                {
                                        euroN=spectrum[q][r]/(5000000.
                                        *pow((euro_det/bs_range[q][r]),3.));
                                        total_euroN=total_euroN+euroN;
                                }

                                else if (euro_det>bs_range[q][r]&&bs_range[q][r]
                                >=(euro_det*pow(.05,1./5.)))
                                {
                                        euroN=spectrum[q][r]/(5000000.*
                                        pow((euro_det/bs_range[q][r]),5.));
                                        total_euroN=total_euroN+euroN;
                                }
                        }
                }
        }
        }
```

```
//      Calculated life cycles from exact values
        n_euroN=0;
        n_total_euroN=0;
        for (i=0;i<n;i++)
        {
                if (n_bs_range[i]>(euro_det*pow(.002,-1./3.)))
                {
                        printf("\nCorrected Stress has exceeded S-N limits! -
                        EUROCODE");
                        getch();
                        exit(1);
                }
                else if ((euro_det*pow(.002,-1./3.))>=n_bs_range[i]
                &&n_bs_range[i]>=euro_det)
                {
                        n_euroN=1./(5000000.*pow((euro_det/n_bs_range[i]),3.));
                        n_total_euroN=n_total_euroN+n_euroN;
                }

                else if (euro_det>=n_bs_range[i]&&
                n_bs_range[i]>=(euro_det*pow(.05,1./5.)))
                {
                        n_euroN=1./(5000000.*pow((euro_det/n_bs_range[i]),5.));
                        n_total_euroN=n_total_euroN+n_euroN;
                }
        }
//      Calculate number of repetitions to failure from bin data
        euroBf=1./total_euroN;
//      Calculate number of repetitions to failure from exact values
        n_euroBf=1./n_total_euroN;
}
```

```
//---------------------------------------------------------------------------
//                  C80 Austroads Code Life Cycle
//---------------------------------------------------------------------------

void C80_auslifecycle(void)
{
        if(bin=='y'||bin=='Y')
        {
//      Calculated life cycles from bin data
        ausN=0;
        total_ausN=0;
        for (q=0;q<bin_no;q++)
        {
                for (r=0;r<bin_no;r++)
                {
                        if (spectrum[q][r]>0)
                        {
                                if (aus_range[q][r]>(aus_det*pow(.02,-1./3.)))
                                {
                                        printf("\nCorrected Stress has exceeded S-N
                                        limits! - AUSTROADS CODE");
                                        getch();
                                        exit(1);
                                }
                                else if ((aus_det*pow(.02,-1./3.))>=aus_range[q][r]
                                &&aus_range[q][r]>=aus_det)
                                {
                                        ausN=spectrum[q][r]/(5000000.*
                                        pow((aus_det/aus_range[q][r]),3.));
                                        total_ausN=total_ausN+ausN;
                                }

                                else if (aus_det>aus_range[q][r]&&aus_range[q][r]
                                >=(aus_det*pow(.05,1./5.)))
                                {
                                        ausN=spectrum[q][r]/(5000000.
                                        *pow((aus_det/aus_range[q][r]),5.));
                                        total_ausN=total_ausN+ausN;
                                }
                        }
                }
        }
        }
```

```
//      Calculated life cycles from exact values
        n_ausN=0;
        n_total_ausN=0;
        for (i=0;i<n;i++)
        {
                if (n_aus_range[i]>(aus_det*pow(.02,-1./3.)))
                {
                        printf("\nCorrected Stress has exceeded S-N limits! -
                        AUSTROADS CODE");
                        getch();
                        exit(1);
                }
                else if ((aus_det*pow(.02,-1./3.))>=n_aus_range[i]
                &&n_aus_range[i]>=aus_det)
                {
                        n_ausN=1./(5000000.*pow((aus_det/n_aus_range[i]),3.));
                        n_total_ausN=n_total_ausN+n_ausN;
                }

                else if (aus_det>n_aus_range[i]&&
                n_aus_range[i]>=(aus_det*pow(.05,1./5.)))
                {
                        n_ausN=1./(5000000.*pow((aus_det/n_aus_range[i]),5.));
                        n_total_ausN=n_total_ausN+n_ausN;
                }
        }
//      Calculate number of repetitions to failure from bin data
        ausBf=1./total_ausN;
//      Calculate number of repetitions to failure from exact values
        n_ausBf=1./n_total_ausN;
}
```

```
//---------------------------------------------------------------------------
//                  C90 Screen Output
//---------------------------------------------------------------------------

void C90_screenoutput(void)
{
//      Write the data to the screen
        printf("\n\n");

        if (sn=='y'||sn=='Y')
        {
                printf("DATA INPUT FOR PARTICULAR S-N CURVE
                ANALYSIS\n\n");
                printf("\n\nValue of Stress at Fracture: %3.3f MPa",fracture_stress);
                printf("\n\nPoints which define the S-N Curve.");
                printf("\nN                       S");
                printf("\n%3.0f                          %3.2f",Npoint1,Spoint1);
                printf("\n%3.0f                          %3.2f",Npoint2,Spoint2);
                printf("\n%3.0f                  %3.2f",Npoint3,Spoint3);
        }

        if (bs7608=='y'||bs7608=='Y')
        {
                printf("\n\n");
                printf("DATA INPUT FOR BS7608 CODE ANALYSIS\n\n");
                printf("\n\nM Value (inverse slope) = %3.3f",bs_m);
                printf("\n\nFatigue limit = %3.3f Mpa",bs_s0);
                if (weld!='y'&&weld!='Y')
                {
                        printf("\n\nDetail assumed unwelded or welded and stress
                        relieved.");
                }
                if (weld=='y'||weld=='Y')
                {
                        printf("\n\nDetail assumed welded and not stress relieved.");
                }
                if (bs_thick=='y'||bs_thick=='Y')
                {
                        printf("\n\nThickness correction factor chosen with a thickness
                        of %3.3f mm",bs_t);
                }
                if (bs_mod=='y'||bs_mod=='Y')
                {
                        printf("\n\nFurther modification factor of %3.3f used",bs_sn);
                }
        }
```

```
if (bs54=='y'||bs54=='Y')
{
        printf("\n\n");
        printf("DATA INPUT FOR BS5400 CODE ANALYSIS\n\n");
        printf("\n\nM Value (inverse slope) = %3.3f",bs_m);
        printf("\n\nFatigue limit = %3.3f Mpa",bs_s0);
        if (weld!='y'&&weld!='Y')
        {
                printf("\n\nDetail assumed unwelded or welded and stress
                relieved.");
        }
        if (weld=='y'||weld=='Y')
        {
                printf("\n\nDetail assumed welded and not stress relieved.");
        }
}

if (jap=='y'||jap=='Y')
{
        printf("\n\n");
        printf("DATA INPUT FOR JAPANESE CODE ANALYSIS\n\n");
        printf("\n\nBasic Allowable Stress = %3.3f MPa",jap_all);
        printf("\n\nStress range at cut off (fatigue) limit = %3.3f Mpa",jap_S);
        if (jap_thick=='y'||jap_thick=='Y')
        {
                printf("\n\nThickness correction factor chosen with a thickness
                of %3.3f mm",jap_t);
        }

        if (jap_part=='y'||jap_part=='Y')
        {
                printf("\n\nRedundancy partial safety factor of %3.3f
                used",jap_a);
                printf("\n\nImportance partial safety factor of %3.3f
                used",jap_b);
                printf("\n\nInspection partial safety factor of %3.3f used",jap_c);
        }
}
```

```
if (aar=='y'||aar=='Y')
{
	printf("\n\n");
	printf("DATA INPUT FOR AAR CODE ANALYSIS\n\n");
	if (material=='1')
	{
		printf("\n\nSteel chosen for analysis, with a fatigue limit at
		2,000,000 cycles.");
	}
	if (material=='2')
	{
		printf("\n\nAluminium Alloy chosen for analysis, with a fatigue
		limit at 10,000,000 cycles.");
	}
	printf("\n\nY intercept of MGD = %3.3f MPa",aar_b);
	printf("\n\nSlope of the MGD = %3.3f",aar_m);
	printf("\n\nSlope of the S-N Curve = %3.3f MPa",aar_k);
}

if (aws=='y'||aws=='Y')
{
	printf("DATA INPUT FOR PARTICULAR AWS CODE
	ANALYSIS\n\n");
	printf("\n\nPoints which define the S-N Curve.");
	printf("\nN                    S (MPa)");
	printf("\n%3.0f                    %3.2f",Naws1,Saws1);
	printf("\n%3.0f                    %3.2f",Naws2,Saws2);

	if (aws_mod=='y'||aws_mod=='Y')
	{
		printf("\n\nModification factor of %3.3f used",aws_m);
	}
}

if (eur=='y'||eur=='Y')
{
	printf("\n\n");
	printf("DATA INPUT FOR EUROCODE ANALYSIS\n\n");
	printf("\n\nValue Detail Category = %3.3f MPa",euro_cat);
	if (euro_thick=='y'||euro_thick=='Y')
	{
		printf("\n\nThickness correction factor chosen with a thickness
		of %3.3f mm",euro_t);
	}
	if (weld!='y'&&weld!='Y')
	{
		printf("\n\nDetail assumed unwelded or welded and stress
		relieved.");
	}
	if (weld=='y'||weld=='Y')
```

```
        {
                printf("\n\nDetail assumed welded and not stress relieved.");
        }
        if (euro_part=='y'||euro_part=='Y')
        {
                printf("\n\nPartial safety factor for fatigue loading
                %3.3f",euro_l);
                printf("\n\nPartial safety factor for fatigue strength
                %3.3f",euro_s);
        }
}

if (aus=='y'||aus=='Y')
{
        printf("\n\n");
        printf("DATA INPUT FOR AUSTROADS CODE ANALYSIS\n\n");
        printf("\n\nValue Detail Category = %3.3f MPa",aus_cat);
        if (aus_thick=='y'||aus_thick=='Y')
        {
                printf("\n\nThickness correction factor chosen with a thickness
                of %3.3f mm",aus_t);
        }
}

if(bin=='y'||bin=='Y')
{
printf("\n\n");
printf("STRESS SPECTRUM\n\n");
printf("Bin No     ");
for (r=0;r<bin_no;r++)
        {
                printf("%5d",r+1);
        }
        printf("  Total\n");
        printf("      From");
for (r=0;r<bin_no;r++)
        {
                printf("%5.0f",lower+r*binsize);
        }
        printf("\n");
        getch();
```

```
for (q=0;q<bin_no;q++)
{
        printf("%5d %5.0f",q+1,lower+q*binsize);
        for (r=0;r<bin_no;r++)
        {
                printf("%5.0f",spectrum[q][r]);
        }
        printf("%5d\n",T_row[q]);
        getch();
}

printf("Total      ");
for (r=0;r<bin_no;r++)
        {
                printf("%5d",T_col[r]);
        }
printf("%5.0f",T_all);

printf("\n\n");
printf("NORMALISED STRESS SPECTRUM\n\n");
printf("Bin No     ");
for (r=0;r<bin_no;r++)
        {
                printf("%5d",r+1);
        }
        printf("  Total\n");
        printf("       From");
for (r=0;r<bin_no;r++)
        {
                printf("%5.0f",lower+r*binsize);
        }
        printf("\n");
        getch();

for (q=0;q<bin_no;q++)
{
        printf("%5d %5.0f",q+1,lower+q*binsize);
        for (r=0;r<bin_no;r++)
        {
                norm_spectrum=spectrum[q][r]/T_all;
                printf("%5.1f",norm_spectrum);
        }
        norm_T_row=T_row[q]/T_all;
        printf("%5.1f\n",norm_T_row);
        getch();
}
```

```
printf("Total      ");
for (r=0;r<bin_no;r++)
        {
                norm_T_col=T_col[r]/T_all;
                printf("%5.1f",norm_T_col);
        }
norm_T_all=T_all/T_all;
printf("%5.1f",norm_T_all);
}

printf("\n\n");
if (sn=='y'||sn=='Y')
{
        printf("REPETITIONS TO FAILURE FROM THE ASSUMED
        CURRENT METHODOLOGY");
        if(bin=='y'||bin=='Y')
        {
                if (Bf>=1.e+30)
                        printf("\nThe number of repetitions to failure from the
                        bin data is infinite.");
                else
                        printf("\nThe number of repetitions to failure from the
                        bin data is: %3.0lf",Bf);
        }
                if (n_Bf>=1.e+30)
                        printf("\nThe number of repetitions to failure from the
                        exact values is infinite.\n\n\n");
                else
                        printf("\nThe number of repetitions to failure from the
                        exact values is: %3.0lf\n\n\n",n_Bf);
}
if (bs7608=='y'||bs7608=='Y')
{
        printf("REPETITIONS TO FAILURE FROM THE BS7608 CODE");
        if(bin=='y'||bin=='Y')
        {
                if (bs7608Bf>=1.e+30)
                        printf("\nThe number of repetitions tofailure from the bin
                        data is infinite.");
                else
                        printf("\nThe number of repetitions to failure from the
                        bin data is: %3.0lf",bs7608Bf);
        }
        if (n_bs7608Bf>=1.e+30)
                printf("\nThe number of repetitions to failure from the exact
                values is infinite.\n\n\n");
        else
                printf("\nThe number of repetitions to failure from the exact
                values is: %3.0lf\n\n\n",n_bs7608Bf);
}
```

```
if (bs54=='y'||bs54=='Y')
{
        printf("REPETITIONS TO FAILURE FROM THE BS5400 CODE");
        if(bin=='y'||bin=='Y')
        {
                if (bs5400Bf>=1.e+30)
                        printf("\nThe number of repetitions to failure from the
                        bin data is infinite.");
                else
                        printf("\nThe number of repetitions to failure from the
                        bin data is: %3.0lf",bs5400Bf);
        }
        if (n_bs5400Bf>=1.e+30)
                printf("\nThe number of repetitions to failure from the exact
                values is infinite.\n\n\n");
        else
                printf("\nThe number of repetitions to failure from the exact
                values is: %3.0lf\n\n\n",n_bs5400Bf);
}
if (jap=='y'||jap=='Y')
{
        printf("REPETITIONS TO FAILURE FROM THE JAPANESE
        CODE");
        if(bin=='y'||bin=='Y')
        {
                if (japBf>=1.e+30)
                        printf("\nThe number of repetitions to failure from the
                        bin data is infinite.");
                else
                        printf("\nThe number of repetitions to failure from the
                        bin data is: %3.0lf",japBf);
        }

        if (n_japBf>=1.e+30)
                printf("\nThe number of repetitions to failure from the exact
                values is infinite.\n\n\n");
        else
                printf("\nThe number of repetitions to failure from the exact
                values is: %3.0lf\n\n\n",n_japBf);
}
if (aar=='y'||aar=='Y')
{
        printf("REPETITIONS TO FAILURE FROM THE AAR CODE");
        if(bin=='y'||bin=='Y')
        {
                if (aarBf>=1.e+30)
                        printf("\nThe number of repetitions to failure from the
                        bin data is infinite.");
```

```
                else
                        printf("\nThe number of repetitions to failure from the
                        bin data is: %3.0lf",aarBf);
        }
        if (n_aarBf>=1.e+30)
                printf("\nThe number of repetitions to failure from the exact
                values is infinite.\n\n\n");
        else
                printf("\nThe number of repetitions to failure from the exact
                values is: %3.0lf\n\n\n",n_aarBf);
}
if (aws=='y'||aws=='Y')
{
        printf("REPETITIONS TO FAILURE FROM THE AWS CODE");
        if(bin=='y'||bin=='Y')
        {
                if (awsBf>=1.e+30)
                        printf("\nThe number of repetitions to failure from the
                        bin data is infinite.");
                else
                        printf("\nThe number of repetitions to failure from the
                        bin data is: %3.0lf",awsBf);
        }
        if (n_awsBf>=1.e+30)
                printf("\nThe number of repetitions to failure from the exact
                values is infinite.\n\n\n");
        else
                printf("\nThe number of repetitions to failure from the exact
                values is: %3.0lf\n\n\n",n_awsBf);
}
if (eur=='y'||eur=='Y')
{
        printf("REPETITIONS TO FAILURE FROM THE EUROCODE");
        if(bin=='y'||bin=='Y')
        {
                if (euroBf>=1.e+30)
                        printf("\nThe number of repetitions to failure from the
                        bin data is infinite.");
                else
                        printf("\nThe number of repetitions to failure from the
                        bin data is: %3.0lf",euroBf);
        }
        if (n_euroBf>=1.e+30)
                printf("\nThe number of repetitions to failure from the exact
                values is infinite.\n\n\n");
        else
                printf("\nThe number of repetitions to failure from the exact
                values is: %3.0lf\n\n\n",n_euroBf);
}
```

```
        if (aus=='y'||aus=='Y')
        {
                printf("REPETITIONS TO FAILURE FROM THE AUSTROADS
                CODE");
                if(bin=='y'||bin=='Y')
                {
                        if (ausBf>=1.e+30)
                                printf("\nThe number of repetitions to failure from the
                                bin data is infinite.");
                        else
                                printf("\nThe number of repetitions to failure from the
                                bin data is: %3.0lf",ausBf);
                }
                if (n_ausBf>=1.e+30)
                        printf("\nThe number of repetitions to failure from the exact
                        values is infinite.\n\n\n");
                else
                        printf("\nThe number of repetitions to failure from the exact
                        values is: %3.0lf\n\n\n",n_ausBf);
        }
        getch();
}
```

```
//---------------------------------------------------------------------------
//                  C100 File Output
//---------------------------------------------------------------------------

void C100_fileoutput(void)
{
        FILE *fp;       // File declaration

//      Open the created text file for writing only
        if ((fp=fopen(name_out,"w"))==NULL)
        {
                printf("\nCannot open file %s",name_out);
                getch();
                exit(1);
        }

//      Write the data to the file
        fprintf(fp,"DATA INPUT\n\n");
        fprintf(fp,"Name and location of stress history input file:%s",name_in);
        if (sn=='y'||sn=='Y')
        {
                fprintf(fp,"\n\nDATA INPUT FOR ASSUMED CURRENT
                METHODOLOGY ANALYSIS");
                fprintf(fp,"\n\nValue of Stress at Fracture: %3.3f MPa",fracture_stress);
                fprintf(fp,"\n\nPoints which define the S-N Curve.");
                fprintf(fp,"\n   N       S (MPa)");
                fprintf(fp,"\n   %f      %f",Npoint1,Spoint1);
                fprintf(fp,"\n   %f      %f",Npoint2,Spoint2);
                fprintf(fp,"\n   %f      %f",Npoint3,Spoint3);
        }

        if (bs7608=='y'||bs7608=='Y')
        {
                fprintf(fp,"\n\nDATA INPUT FOR BS7608 CODE ANALYSIS");
                fprintf(fp,"\n\nM Value (inverse slope):       %3.3f",bs_m);
                fprintf(fp,"\n\nFatigue limit:  %3.3f  Mpa",bs_s0);
                if (weld!='y'&&weld!='Y')
                {
                        fprintf(fp,"\n\nDetail assumed unwelded or stress relieved.");
                }
                if (weld=='y'||weld=='Y')
                {
                        fprintf(fp,"\n\nDetail assumed welded and not stress relieved.");
                }
                if (bs_thick=='y'||bs_thick=='Y')
                {
                        fprintf(fp,"\n\nThickness correction factor chosen with a
                        thickness of %3.3f      mm",bs_t);
                }
```

```
        if (bs_mod=='y'||bs_mod=='Y')
        {
                fprintf(fp,"\n\n Further modification factor of %3.3f
                used",bs_sn);
        }
}

if (bs54=='y'||bs54=='Y')
{
        fprintf(fp,"\n\nDATA INPUT FOR BS5400 CODE ANALYSIS");
        fprintf(fp,"\n\nM Value (inverse slope): %3.3f",bs_m);
        fprintf(fp,"\n\nFatigue limit:%3.3f Mpa",bs_s0);
        if (weld!='y'&&weld!='Y')
        {
                fprintf(fp,"\n\nDetail assumed unwelded or stress relieved.");
        }
        if (weld=='y'||weld=='Y')
        {
                fprintf(fp,"\n\nDetail assumed welded and not stress relieved.");
        }
}

if (jap=='y'||jap=='Y')
{
        fprintf(fp,"\n\nDATA INPUT FOR JAPANESE CODE ANALYSIS");
        fprintf(fp,"\n\nBasic Allowable Stress: %3.3f MPa",jap_all);
        fprintf(fp,"\n\nStress range at cut off (fatigue) limit: %3.3f
        Mpa",jap_S);
        if (jap_thick=='y'&&weld=='Y')
        {
                fprintf(fp,"\n\nThickness correction factor chosen with a
                thickness of %3.3f      mm",jap_t);
        }
        if (jap_part=='y'||jap_part=='Y')
        {
                fprintf(fp,"\n\nRedundancy partial safety factor: %3.3f",jap_a);
                fprintf(fp,"\n\nImportance partial safety factor: %3.3f",jap_b);
                fprintf(fp,"\n\nInspection partial safety factor: %3.3f",jap_c);
        }
}
```

```
if (aar=='y'||aar=='Y')
{
        fprintf(fp,"\n\nDATA INPUT FOR AAR CODE ANALYSIS");
        if (material=='1')
        {
                fprintf(fp,"\n\nSteel chosen for analysis, with a fatigue limit at
                2,000,000 cycles.");
        }
        if (material=='2')
        {
                fprintf(fp,"\n\nAluminium Alloy chosen for analysis, with a
                fatigue limit at 10,000,000 cycles.");
        }
        fprintf(fp,"\n\nY intercept of MGD:          %3.3f  MPa",aar_b);
        fprintf(fp,"\n\nSlope of the MGD:            %3.3f",aar_m);
        fprintf(fp,"\n\nSlope of the S-N Curve:      %3.3f",aar_k);
}

if (aws=='y'||aws=='Y')
{
        fprintf(fp,"\n\nDATA INPUT FOR AWS CODE ANALYSIS");
        fprintf(fp,"\n\nPoints which define the Corrected S-N Curve.");
        fprintf(fp,"\n   N       S (MPa)");
        fprintf(fp,"\n   %f      %f",Naws1,Saws1);
        fprintf(fp,"\n   %f      %f",Naws2,Saws2);

        if (aws_mod=='y'||aws_mod=='Y')
        {
                fprintf(fp,"\n\nModification factor %3.3f",aws_m);
        }
}

if (eur=='y'||eur=='Y')
{
        fprintf(fp,"\n\nDATA INPUT FOR EUROCODE ANALYSIS");
        fprintf(fp,"\n\nValue Detail Category: %3.3f MPa",euro_cat);
        if (euro_thick=='y'||euro_thick=='Y')
        {
                fprintf(fp,"\n\nThickness correction factor chosen with a
                thickness of %3.3f      mm",euro_t);
        }
        if (weld!='y'&&weld!='Y')
        {
                fprintf(fp,"\n\nDetail assumed unwelded or stress relieved.");
        }
        if (weld=='y'||weld=='Y')
        {
                fprintf(fp,"\n\nDetail assumed welded and not stress relieved.");
        }
```

```
        if (euro_part=='y'||euro_part=='Y')
        {
                fprintf(fp,"\n\nPartial safety factor for fatigue loading:
                %3.3f",euro_l);
                fprintf(fp,"\n\nPartial safety factor for fatigue strength:
                %3.3f",euro_s);
        }
}

if (aus=='y'||aus=='Y')
{
        fprintf(fp,"\n\nDATA INPUT FOR AUSTROADS CODE
        ANALYSIS");
        fprintf(fp,"\n\nValue Detail Category: %3.3fMPa",aus_cat);
        if (aus_thick=='y'||aus_thick=='Y')
        {
                fprintf(fp,"\n\nThickness correction factor chosen with a
                thickness of %3.3f      mm",aus_t);
        }
}
```

```
if(bin=='y'||bin=='Y')
{
fprintf(fp,"\n\n\nSTRESS SPECTRUM\n\n");
fprintf(fp,"      Bin No");
for (r=0;r<bin_no;r++)
        {
                fprintf(fp,"      %d",r+1);
        }
        fprintf(fp,"      Total\n");
fprintf(fp,"                Bin From");
for (r=0;r<bin_no;r++)
        {
                fprintf(fp,"      %3.2f",lower+r*binsize);
        }
        fprintf(fp,"\n");
for (q=0;q<bin_no;q++)
{
        fprintf(fp,"      %d      %3.2f",q+1,lower+q*binsize);
        for (r=0;r<bin_no;r++)
        {
                fprintf(fp,"      %3.0f",spectrum[q][r]);
        }
        fprintf(fp,"      %d\n",T_row[q]);
}
fprintf(fp,"      Total    ");
for (r=0;r<bin_no;r++)
        {
                fprintf(fp,"      %d",T_col[r]);
        }
fprintf(fp,"      %3.0f",T_all);

fprintf(fp,"\n\n\nNORMALISED STRESS SPECTRUM\n\n");
fprintf(fp,"      Bin No");
for (r=0;r<bin_no;r++)
        {
                fprintf(fp,"      %d",r+1);
        }
        fprintf(fp,"      Total\n");
fprintf(fp,"                Bin From");
for (r=0;r<bin_no;r++)
        {
                fprintf(fp,"      %3.2f",lower+r*binsize);
        }
        fprintf(fp,"\n");
```

```
for (q=0;q<bin_no;q++)
{
        fprintf(fp,"      %d      %3.2f",q+1,lower+q*binsize);
        for (r=0;r<bin_no;r++)
        {
                norm_spectrum=spectrum[q][r]/T_all;
                fprintf(fp,"      %3.2f",norm_spectrum);
        }
        norm_T_row=T_row[q]/T_all;
        fprintf(fp,"      %3.2f\n",norm_T_row);
}
fprintf(fp,"      Total    ");
for (r=0;r<bin_no;r++)
        {
                norm_T_col=T_col[r]/T_all;
                fprintf(fp,"      %3.2f",norm_T_col);
        }
norm_T_all=T_all/T_all;
fprintf(fp,"      %3.2f\n",norm_T_all);
}

if (sn=='y'||sn=='Y')
{
        fprintf(fp,"\n\nREPETITIONS TO FAILURE FROM ASSUMED
        CURRENT METHODOLOGY");
        if(bin=='y'||bin=='Y')
        {
                if (Bf>=1.e+30)
                        fprintf(fp,"\nThe number of repetitions to failure from the
                        bin values is infinite.");
                else
                        fprintf(fp,"\nThe number of repetitions to failure from the
                        bin data is: %3.0lf",Bf);
        }
        if (n_Bf>=1.e+30)
                fprintf(fp,"\nThe number of repetitions to failure from the exact
                values is infinite.");
        else
                fprintf(fp,"\nThe number of repetitions to failure from the exact
                values is: %3.0lf",n_Bf);
}
```

```
if (bs7608=='y'||bs7608=='Y')
{
        fprintf(fp,"\n\nREPETITIONS TO FAILURE FROM THE BS7608
        CODE");
        if(bin=='y'||bin=='Y')
        {
                if (bs7608Bf>=1.e+30)
                        fprintf(fp,"\nThe number of repetitions to failure from the
                        bin values is infinite.");
                else
                        fprintf(fp,"\nThe number of repetitions to failure from the
                        bin data is: %3.0lf",bs7608Bf);
        }
        if (n_bs7608Bf>=1.e+30)
                fprintf(fp,"\nThe number of repetitions to failure from the exact
                values is infinite.");
        else
                fprintf(fp,"\nThe number of repetitions to failure from the exact
                values is: %3.0lf",n_bs7608Bf);
}

if (bs54=='y'||bs54=='Y')
{
        fprintf(fp,"\n\nREPETITIONS TO FAILURE FROM THE BS5400
        CODE");
        if(bin=='y'||bin=='Y')
        {
                if (bs5400Bf>=1.e+30)
                        fprintf(fp,"\nThe number of repetitions to failure from the
                        bin values is infinite.");
                else
                        fprintf(fp,"\nThe number of repetitions to failure from the
                        bin data is: %3.0lf",bs5400Bf);
        }
        if (n_bs5400Bf>=1.e+30)
                fprintf(fp,"\nThe number of repetitions to failure from the exact
                values is infinite.");
        else
                fprintf(fp,"\nThe number of repetitions to failure from the exact
                values is: %3.0lf",n_bs5400Bf);
}
```

```
if (jap=='y'||jap=='Y')
{
        fprintf(fp,"\n\nREPETITIONS TO FAILURE FROM THE JAPANESE
        CODE");
        if(bin=='y'||bin=='Y')
        {
                if (japBf>=1.e+30)
                        fprintf(fp,"\nThe number of repetitions to failure from the
                        bin values is infinite.");
                else
                        fprintf(fp,"\nThe number of repetitions to failure from the
                        bin data is: %3.0lf",japBf);
        }
        if (n_japBf>=1.e+30)
                fprintf(fp,"\nThe number of repetitions to failure from the exact
                values is infinite.");
        else
                fprintf(fp,"\nThe number of repetitions to failure from the exact
                values is: %3.0lf",n_japBf);
}

if (aar=='y'||aar=='Y')
{
        fprintf(fp,"\n\nREPETITIONS TO FAILURE FROM THE AAR
        CODE");
        if(bin=='y'||bin=='Y')
        {
                if (aarBf>=1.e+30)
                        fprintf(fp,"\nThe number of repetitions to failure from the
                        bin values is infinite.");
                else
                        fprintf(fp,"\nThe number of repetitions to failure from the
                        bin data is: %3.0lf",aarBf);
        }
        if (n_aarBf>=1.e+30)
                fprintf(fp,"\nThe number of repetitions to failure from the exact
                values is infinite.");
        else
                fprintf(fp,"\nThe number of repetitions to failure from the exact
                values is: %3.0lf",n_aarBf);
}
```

```
        if (aws=='y'||aws=='Y')
        {
                fprintf(fp,"\n\nREPETITIONS TO FAILURE FROM THE AWS
                CODE");
                if(bin=='y'||bin=='Y')
                {
                        if (awsBf>=1.e+30)
                                fprintf(fp,"\nThe number of repetitions to failure from the
                                bin values is infinite.");
                        else
                                fprintf(fp,"\nThe number of repetitions to failure from the
                                bin data is: %3.0lf",awsBf);
                }
                if (n_awsBf>=1.e+30)
                        fprintf(fp,"\nThe number of repetitions to failure from the exact
                        values is infinite.");
                else
                        fprintf(fp,"\nThe number of repetitions to failure from the exact
                        values is: %3.0lf",n_awsBf);
        }

        if (eur=='y'||eur=='Y')
        {
                fprintf(fp,"\n\nREPETITIONS TO FAILURE FROM THE
EUROCODE");
                if(bin=='y'||bin=='Y')
                {
                        if (euroBf>=1.e+30)
                                fprintf(fp,"\nThe number of repetitions to failure from the
                                bin values is infinite.");
                        else
                                fprintf(fp,"\nThe number of repetitions to failure from the
                                bin data is: %3.0lf",euroBf);
                }
                if (n_euroBf>=1.e+30)
                        fprintf(fp,"\nThe number of repetitions to failure from the exact
                        values is infinite.");
                else
                        fprintf(fp,"\nThe number of repetitions to failure from the exact
                        values is: %3.0lf",n_euroBf);
        }
```

```
        if (aus=='y'||aus=='Y')
        {
                fprintf(fp,"\n\nREPETITIONS TO FAILURE FROM THE
                AUSTROADS CODE");
                if(bin=='y'||bin=='Y')
                {
                        if (ausBf>=1.e+30)
                                fprintf(fp,"\nThe number of repetitions to failure from the
                                bin values is infinite.");
                        else
                                fprintf(fp,"\nThe number of repetitions to failure from the
                                bin data is: %3.0lf",ausBf);
                }
                if (n_ausBf>=1.e+30)
                        fprintf(fp,"\nThe number of repetitions to failure from the exact
                        values is infinite.");
                else
                        fprintf(fp,"\nThe number of repetitions to failure from the exact
                        values is: %3.0lf",n_ausBf);
        }

        if (history=='y'||history=='Y')
        {
                fprintf(fp,"\n\n\nFILTERED STRESS HISTORY\n");
                for (i=0;i<k+1;i++)
                {
                        fprintf(fp,"\n   %3.3f",stress[i]);
                }
        }
        fclose(fp);
}
```

Please see print copy of thesis for Appendix F.

Appendix G - Dynamic Stress Data Recovery from Strand7 Beam Element Sensitivity Models

The available stress output from Strand7, for dynamic analysis using beam models, is listed in Table G.1.

Min Fibre Stress (MPa)	Max Fibre Stress (MPa)	Mean Shear 1 (MPa)	Mean Shear 2 (MPa)	Max Shear 1 (MPa)	Max Shear 2 (MPa)	Max Torsion Stress (MPa)

Table G.1. Strand7 dynamic beam model stress output options.

Maximum, minimum and mean stresses are given regardless of where they act on the section. The maximum fibre stress, for example, is presented for a particular beam element, without consideration to where the position of maximum stress lies on the section. Conceivably, the loading may be reversed or varied during transient application and as a result the location of the maximum fibre stress may vary considerably. This is, of course, significant in fatigue assessment, where the stress history of a fixed location is required.

An alternative method for finding the stress history of a structure at a particular point on its section, is to derive stresses from applied forces, knowing the section details and choosing critical points on the section for assessment. The Strand7 force / moment output is listed in Table G.2.

Shear Force 1 (N)	Bending Moment 1 (N.mm)	Shear Force 2 (N)	Bending Moment 2 (N.mm)	Axial Force (N)	Torque (N.mm)

Table G.2. Strand7 dynamic beam model force / moment output options.

Using these internal forces for a beam section and knowing the section properties, standard engineering formulae have been employed, in this research, to find the transient stress history at critical locations on the section.

For this project, critical locations on the three main sections of the approach spans were considered. The broad flange beams, channel and equal angle sections of the approach span elements and the locations of assumed critical locations are shown below in Figure G.1. Critical locations are lettered and the axis of planes numbered.

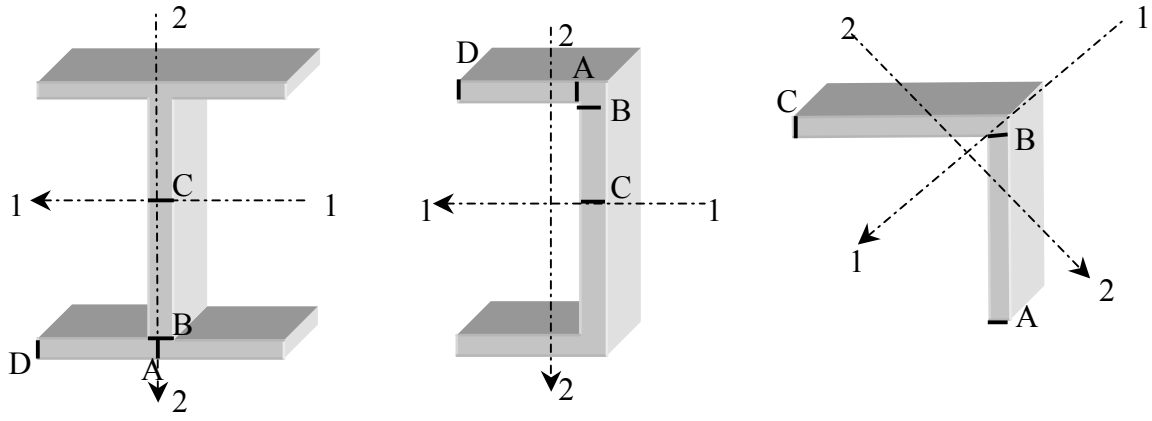

Figure G.1. Main section types of Mullet Creek approach spans and assumed critical locations.

Strand7 is native to the Microsoft Windows environment therefore output data is easily transferable to other windows programs. Taking advantage of this fact, spreadsheets have been set up with formulae for finding various components of stress at each of the critical locations of the sections noted above. The force output of Strand7 is simply

exported to spreadsheets and the stress history of each of the critical locations immediately computed and graphically presented.

In order to derive stresses in this way various assumptions have been made. These are listed below.

- **NORMAL STRESSES** Stresses derived are intended for use in coded fatigue assessment. Therefore, the general assumptions used in standard fatigue codes are assumed. For example, in fatigue assessment it is generally assumed that the through thickness component of stress is rarely relevant and can usually be ignored. This reduces the stress state to one of plane stress. Where the location of measured stresses is sufficiently far away from bearings and applied loads, it may also be assumed that vertical normal stresses may be ignored. This simplifies the stress state still further to plane stress with only one non-zero normal stress. The non-zero normal stress component, Equation (G.1), is made up of the summation of axial normal stress and normal stress due to bending in both planes.

$$\sigma_x = \frac{P}{A} + \frac{M_1 y_1}{I_{22}} + \frac{M_2 y_2}{I_{11}} \qquad \text{(G.1)}$$

- **SHEAR STRESSES** Through-thickness shear stress is assumed insignificant for thin-walled open cross sections. Where through-thickness shear stress is insignificant, the assumed stress state, at any location on the thin-walled open section, is plane stress acting on a plane parallel to the face of each plate.

  The assumed distribution of shear stress due to bending for each section is presented in Figure G.2.

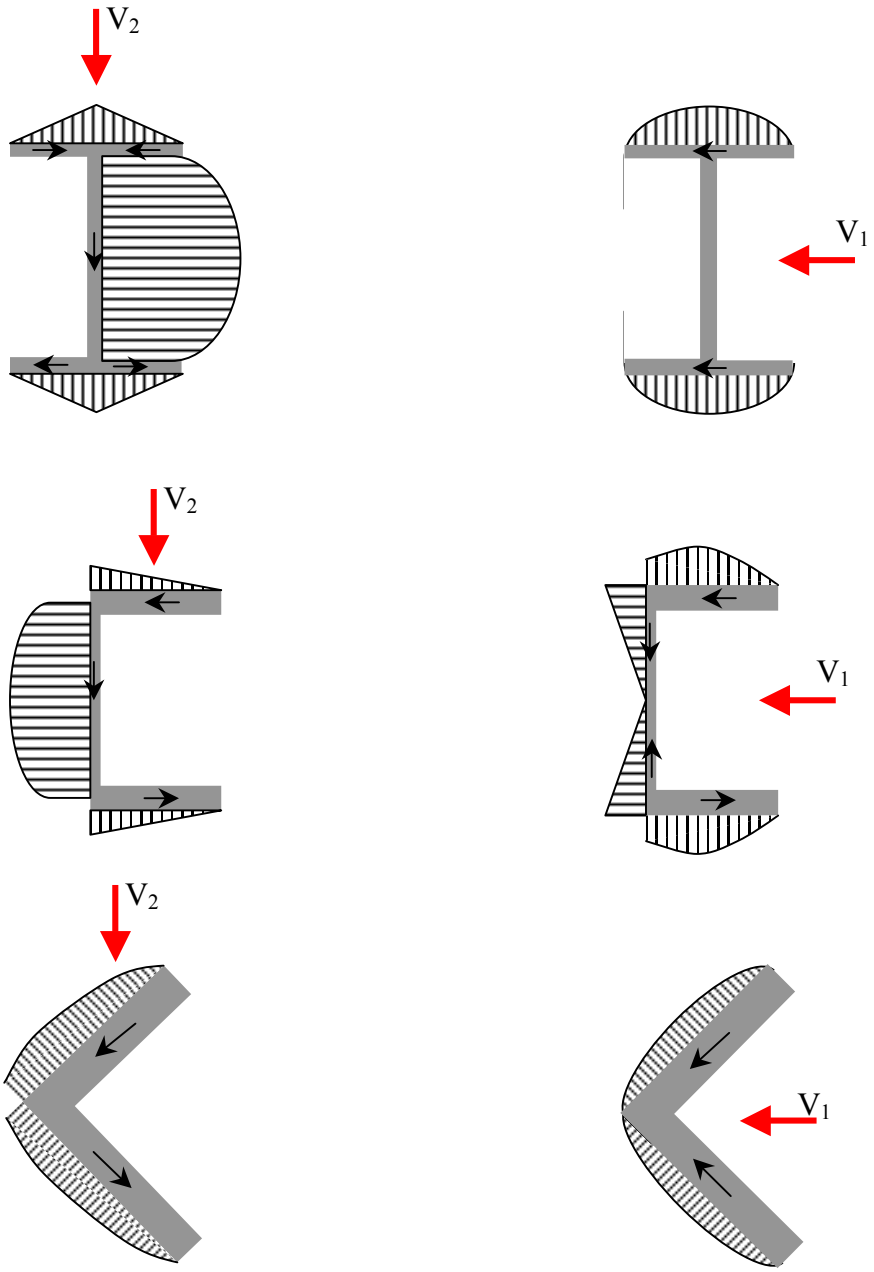

Figure G.2. Distribution of shear stresses and direction of shear flow in mullet creek sections.

Shear stress due to torsion has been accounted for according to Equation (G.2),

$$\tau = \frac{Tt}{J} \qquad \text{(G.2)}$$

where T is torque (constant for the section), t is plate thickness (constant for each plate) and J is the equivalent torsional constant of the section. Shear stress due to

torsion is assumed constant for constant thickness. The direction of shear stress due to torsion is assumed along the long axis of the plate, i.e. perpendicular to the thickness of the section, according to Prandtl's soap film analogy for thin walled sections. The plane of shear stress is the same for shear stress due to bending. Shear stresses may therefore be summed directly after taking account of the sign of the shear stress, Equation (G.3).

$$\tau = \frac{Tt}{J} + \frac{V_1 Q_{22}}{I_{22} t} + \frac{V_2 Q_{11}}{I_{11} t} \tag{G.3}$$

PRINCIPAL STRESSES Principal stresses and the angle of the plane of principal stress are calculated in the normal way, noting that there is only one non-zero normal stress.

$$\sigma_{1,2} = \frac{\sigma_x}{2} \pm \sqrt{\left(\frac{\sigma_x}{2}\right)^2 + \tau^2} \tag{G.4}$$

$$\theta_p = \frac{1}{2} \tan^{-1}\left(\frac{2\tau}{\sigma_x}\right) \tag{G.5}$$

The direction of the principal plane is significant for fatigue assessment. Many fatigue codes state that principal stress should only be used where shear and normal stress vary simultaneously and the angle of the principal plane of recorded stresses does not vary significantly.

Other finite element packages such as ABAQUS have a much more thorough treatment of stresses in beam elements and may be more appropriate for assessment using the method presented in this thesis.

Appendix H - Catalogue of Field Test Results

Tape	Event	Train Type	Direction	Time	Notes	July 3, 2000 WTT	km/hr
(Note: Italics indicate assumptions based on WTT or testing data)							
1	1	Freight	*up*	10:30			*68.6*
2 (Day 2)	18	National Rail	up	10:04	RHAF, RHBF, RHGF locos. These have been assumed to be 81 class locos.		*54.9*
2 (Day 2)	19	RSA Ballast	up		3 x 48 locos, NDFF wagons		*67*
2 (Day 2)	26	BHP	down	12:09	101 & 102 locos, wheels flats at third last carriage perhaps. 101 and 102 locos are 442 class according to railpage.com.au		*49.4*
2 (Day 1)	7	BHP	down	12:30	BXLA wagons, *2 x 442 locos*		*47.1*
1	10	BHP	down	12:58	*2 x 442 locos*		*27*
1	7	BHP	up		101 & 102 locos, static load test		-
2 (Day 2)	24	BHP	up	11:39	D47 & D49 locos. These are D46 class according to railpage.com.au		*17*
2 (Day 1)	14	BHP	up	1:48	103 & 102 locos. 103 locos are 45 class according to railpage.com.au		*29.3*
2 (Day 2)	31	BHP	up	2:00	101 & 102 locos, BXLA wagons		*22.2*
1	6	Manildra	*down*	12:01	2 x 81 locos		*81.6*
2 (Day 1)	10	Manildra	down	12:55	2 x 81 & 1 x 48 locos		*82.6*
2 (Day 1)	8	City Rail	down	12:30	electric	C435, 4DD IC	*90.6*
1	8	City Rail	down	12:32	missed it, *electric*	C435, 4DD IC	-
2 (Day 2)	27	City Rail	down	12:33	electric	C435, 4DD IC	*90.6*
2 (Day 1)	12	City Rail	down	1:16	electric, end of	C437, 4DD IC	-
2 (Day 1)	17	City Rail	down		electric	C445, 4DD G-Set	*89.7*
2 (Day 2)	23	City Rail	up	11:28	electric	C436, 4DD IC	*97.6*
2 (Day 1)	9	City Rail	up	12:43	electric	C440, 4DD IC	*96.5*
1	9	City Rail	up	12:46	*electric*	C440, 4DD IC	*96.5*
2 (Day 2)	28	City Rail	up	12:47	electric	C440, 4DD IC	*99.8*
2 (Day 1)	13	City Rail	up	1:36	electric	C442, 4DD IC	-
2 (Day 2)	30	City Rail	up	1:36	electric	C442, 4DD IC	*95.5*
1	2b	City Rail	down	10:57	*electric*	C429, 6DD IC	*96.5*
2 (Day 1)	2	City Rail	down	10:57	electric	C429, 6DD IC	*92.3*
2 (Day 2)	32	City Rail	down	2:25	electric	C441, 6DD IC	-
2 (Day 1)	15	City Rail	down	2:26	electric	C441, 6DD IC	*79*
2 (Day 1)	1	City Rail	up	10:42	electric	C434, 6DD IC	*97.6*
2 (Day 2)	20	City Rail	up	10:45	electric	C434, 6DD IC	*86.4*
1	2a	City Rail	up	10:48	*electric*	C434, 6DD IC	*95.5*
1	3	City Rail	up	11:05	*electric*	K434, 6DD IC	*92.3*
2 (Day 1)	3	City Rail	up	11:07	electric	K434, 6DD IC	*79.9*
2 (Day 1)	16	City Rail	up	2:35	electric	C444, 6DD IC	-
2 (Day 2)	33	City Rail	up	2:44	electric	C444, 6DD IC	*78*

Table H.1. Catalogued train data grouped in train types (page 1 of 1).

Tape	Event	Train Type	Direction	Time	Notes	July 3, 2000 WTT	km/hr
(Note: Italics indicate assumptions based on WTT or testing data)							
2 (Day 2)	22	City Rail	up		Tangara	K434, 6DD IC	*99.3*
2 (Day 1)	4	City Rail	down	11:23	diesel	C433, 4DD IC	*80.3*
2 (Day 2)	29	City Rail	down	1:12	diesel	KR37, 2 Car Endeavour	*95.5*
2 (Day 1)	11	City Rail	down	1:13	diesel, missed it	KR37, 2 Car Endeavour	-
1	4	City Rail	*up*	11:18	*diesel*	C433, 4DD IC	*67.1*
2 (Day 1)	5	City Rail	up	11:33	diesel	C436, 4DD IC	*87.3*
2 (Day 1)	6	City Rail	up	11:48	diesel	KR38, 2 Car Endeavour	*88.2*
1	5	City Rail	*up*				-
2 (Day 2)	25						-
This lot of testing carried out after transom change.							
4	1	BHP	down	2:15	1 x 81 loco, BXLA wagons		
5 (Day 2)	11	BHP	down	1:50	1 x 81 loco, BXLA wagons		
4	7	BHP	up	3:25	1 x 81 loco, BXLA wagons		
5 (Day 1)	4	BHP	up	1:45	1 x 81 loco, BXLA wagons, travelling at a speed of aprox. 10 km/hr for crawl calibration		
5 (Day 1)	7	BHP	up	2:45	1 x 81 loco, BXLA wagons		
5 (Day 2)	14	BHP	up	2:45	1 x 81 loco, BXLA wagons		
5 (Day 1)	1	Manildra	down		2 x 81 locos		
4	2	City Rail	down	2:27	electric		
5 (Day 1)	2	City Rail	down	1:15	electric, 4 carriages		
5 (Day 1)	5	City Rail	down	2:25	electric		
5 (Day 2)	9	City Rail	down	1:20	electric, 4 carriages		
5 (Day 2)	12	City Rail	down	2:25	electric		
3	1	City Rail	up	11:41	electric, 6 carriages		
3	2	City Rail	up	12:27	electric, 4 carriages		
4	3	City Rail	up	2:45	electric		
5 (Day 1)	3	City Rail	up	1:30	electric, 4 carriages		
5 (Day 1)	6	City Rail	up	2:32	electric		
5 (Day 2)	10	City Rail	up	1:35	electric, 4 carriages		
5 (Day 2)	13	City Rail	up	2:36	electric		
3	3	City Rail	up		diesel		
4	4	City Rail	up	2:55	diesel		
5 (Day 1)	8	City Rail	up	2:50	diesel		
4	5	City Rail	down	3:10	plant services vehicle		
4	6	City Rail	down	3:10	plant services vehicle		

Table H.2. Catalogued train data grouped in train types (page 2 of 2).

Tape	Event	Train Type	Dir'n	Time	Notes	July 3, 2000 WTT	Channel Input							
(Note: Italics indicate assumptions based on WTT or testing data)							1	2	3	4	5	6	7	8
1	1	Freight	up	10:30			SG - SE BFB	SG - E BFB	SG - NE BFB	SG - SW BFB	SG - W BFB	SG - NW BFB	Above SE web stiffener	Rail Bridge
	2a	City Rail	up	10:48	*electric*	C434, 6DD IC	(see photos of orginal set up)							
	2b	City Rail	down	10:57	*electric*	C429, 6DD IC								
	3	City Rail	up	11:05	*electric*	K434, 6DD IC								
	4	City Rail	up	11:18	*diesel*	C433, 4DD IC								
	5	City Rail	up											
	6	Manildra	down	12:01	2 x 81 locos									
	7	BHP	up		101 & 102 locos, static load test									
	8	City Rail	down	12:32	missed it, *electric*	C435, 6DD IC	Acc - NE Brg, z-axis	Acc - NW Brg, z-axis	Acc - W BFB, z-axis					
	9	City Rail	up	12:46	*electric*	C440, 4DD IC	(see photos of orginal set up)							
	10	BHP	down	12:58										
2 (Day 1)	1	City Rail	up	10:42	electric	C434, 6DD IC	Acc - NW Brg, x-axis	Acc - NW Brg, y-axis	Acc - NW Brg, z-axis					
	2	City Rail	down	10:57	electric	C429, 6DD IC	(see photos, gauges 1 & 2 approx. 115 mm up from top of base plate, all other dimension approax.							
	3	City Rail	up	11:07	electric	K434, 6DD IC	mid sections)							
	4	City Rail	down	11:23	diesel	C433, 4DD IC								
	5	City Rail	up	11:33	diesel	C436, 4DD IC	Acc - PFC, x-axis	Acc - PFC, y-axis	Acc - PFC, z-axis					
	6	City Rail	up	11:48	diesel	KR38, 2 Car Endeavour	(see photos, accelerometers at 2nd diaphram from northern end)							
	7	BHP	down	12:30	BKLA wagons									
	8	City Rail	down	12:30	electric	C435, 4DD IC								
	9	City Rail	up	12:43	electric	C440, 4DD IC								
	10	Manildra	down	12:55	2 x 81 & 1 x 48 locos		Acc - EA, x-axis	Acc - EA, y-axis	Acc - EA, z-axis					
	11	City Rail	down	1:13	diesel, missed it	KR37, 2 Car Endeavour	(axis notes above are for EA local co-ordinate system)							
	12	City Rail	down	1:16	electric, end of	C437, 4DD IC								
	13	City Rail	up	1:36	electric	C442, 4DD IC								
	14	BHP	up	1:48	103 & 102 locos									
	15	City Rail	down	2:26	electric	C441, 6DD IC								
	16	City Rail	up	2:35	electric	C444, 6DD IC								
	17	City Rail	down		electric	C445, 4DD G-Set	Acc - SW Brg, x-axis	Acc - SW Brg, y-axis	Acc - SW Brg, z-axis					

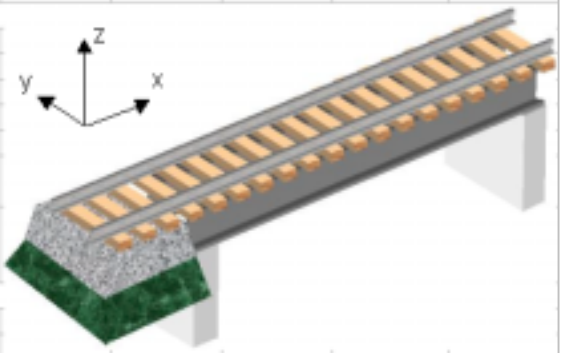

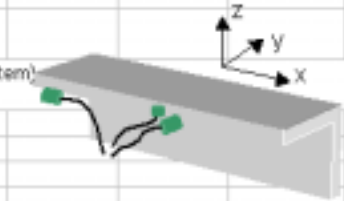

Table H.3. Catalogued train data grouped in order of events (page 1 of 3).

Tape	Event	Train Type	Dir'n	Time	Notes	July 3, 2000 WTT	Channel Input							
(Note: Italics indicate assumptions based on WTT or testing data)							1	2	3	4	5	6	7	8
2 (Day 2)	18	National Rail	up	10:04	RHAF, RHBF, RHGF locos		(see photos)							
	19	RSA Ballast	up		3 x 48 locos, NDFF wagons									
	20	City Rail	up	10:45	electric	C434, 6DD IC								
	21	City Rail	down	10:55	Tangara	C429, 6DD IC								
	22	City Rail	up		Tangara	K434, 6DD IC	Acc - SW Pier, z-axis							
	23	City Rail	up	11:28	electric	C436, 4DD IC		Acc - SW Pier, y-axis						
	24	BHP	up	11:39	D47 & D49 locos									
	25						Acc - NE Brg, x-axis (span 2)	Acc - NE Brg, y-axis (span 2)	Acc - NE Brg, z-axis (span 2)					
	26	BHP	down	12:09	101 & 102 locos, wheels flats at third last carriage perhaps		(see photos)							
	27	City Rail	down	12:33	electric	C435, 4DD IC								
	28	City Rail	up	12:47	electric	C440, 4DD IC	Acc - SW Brg, x-axis (span 1)	Acc - SW Brg, y-axis (span 1)	Acc - SW Brg, z-axis (span 1)					
	29	City Rail	down	1:12	diesel	KR37, 2 Car Endeavour	(see photos)							
	30	City Rail	up	1:36	electric	C442, 4DD IC								
	31	BHP	up	2:00	101 & 102 locos, BXLA wagons		Acc - E rail	Acc - E rail @ N PFC	None					
	32	City Rail	down	2:25	electric	C441, 6DD IC	(see photos, Acc 1 on rail at rail gauges (mid-span), Acc 2 on rail above diaphram to the north of rail							
	33	City Rail	up	2:44	electric	C444, 6DD IC	gauges, Acc 3 broken)							

Table H.4. Catalogued train data grouped in order of events (page 2 of 3).

Tape	Event	Train Type	Dir'n	Time	Notes	July 3, 2080 WTT	Channel Input							
							1	2	3	4	5	6	7	8
(Note: Italics indicate assumptions based on WTT or testing data)							SG - 1/4 span of BFB, SW	SG - 1/2 (mid)span of BFB, W	SG - 1/4 span of BFB, NW	Acc - 1/4 span of BFB, NW	Acc - 1/2 (mid)span of BFB, W	Acc - 1/4 span of BFB, SW		
3	1	City Rail	up	11:41	electric, 6 carriages									
	2	City Rail	up	12:27	electric, 4 carriages									
	3	City Rail	up		diesel									
4	1	BHP	down	2:15	1 x 81 loco, BXLA wagons									
	2	City Rail	down	2:27	electric									
	3	City Rail	up	2:45	electric									
	4	City Rail	up	2:55	diesel									
	5	City Rail	down	3:10	plant services vehicle									
	6	City Rail	down	3:10	plant services vehicle									
	7	BHP	up	3:25	1 x 81 loco, BXLA wagons									
							SG - 1/4 span of BFB, NW	Acc - 1/4 span of BFB, NW	Acc - 1/2 (mid)span of BFB, W	Acc - 1/4 span of BFB, SW				
5 (Day 1)	1	Manildra	down		2 x 81 locos									
	2	City Rail	down	1:15	electric, 4 carriages									
	3	City Rail	up	1:30	electric, 4 carriages									
	4	BHP	up	1:45	1 x 81 loco, BXLA wagons, travelling at a speed of approx. 10 km/hr for crawl calibration									
	5	City Rail	down	2:25	electric									
	6	City Rail	up	2:32	electric									
	7	BHP	up	2:45	1 x 81 loco, BXLA wagons									
	8	City Rail	up	2:50	diesel									
5 (Day 2)	9	City Rail	down	1:20	electric, 4 carriages									
	10	City Rail	up	1:35	electric, 4 carriages									
	11	BHP	down	1:50	1 x 81 loco, BXLA wagons									
	12	City Rail	down	2:25	electric									
	13	City Rail	up	2:36	electric									
	14	BHP	up	2:45	1 x 81 loco, BXLA wagons									

Table H.5. Catalogued train data grouped in order of events (page 3 of 3).

Appendix I - Analogue to Digital Conversion Software Source Code

```
/*****************************************************************
*
* Simple software for digitising analogue tape data
*
*****************************************************************/

/*
 * Includes:
 */

#include "nidaqex.h"

/*
 * Main:
 */

void main(void)
{
   /*
    * Local Variable Declarations:
    */


   /* File declaration. */
        FILE *fp;

        int i,Period,Rate;
        char outfile[20],strFilename[20];

        i16 iStatus = 0;
        i16 iRetVal = 0;
        i16 iDevice = 1;

        /* Number of seconds multiplied by 18 for timeout. */
        i32 lTimeout;

        /* Number of AMUX-64 T devices used. */
        i16 iNumMUXBrds = 0;

        /* Number of channels to be scanned. */
        i16 iNumChans = 8;

        /* Sampling rate. */
        f64 dSampRate;
```

```
/* Scanning rate (same as sampling rate when 0.0). */
f64 dScanRate = 0.0;

/* Number of data points to be counted. */
u32 ulCount;

/* Multplying factor to adjust gain when converting from binary. */
f64 dGainAdjust = 1.0;

/* Binary offset present in reading. */
f64 dOffset = 0.0;

/* Channels numbers to be digitised. */
static i16 piChanVect[8] = {0, 1, 2, 3, 4, 5, 6, 7};

/* Gain for digitised channels. */
static i16 piGainVect[8] = {1, 1, 1, 1, 1, 1, 1, 1};

/* Buffer to which digitised data is sent in binary form */
static i16 piBuffer[10000000] = {0};

/* Buffer to which data is sent to after converting from binary. */
static f64 pdVoltBuffer[10000000] = {0.0};

i16 iIgnoreWarning = 0;

/* On screen intrduction to the software. */
printf("SIMPLE SOFTWARE FOR DIGITISING ANALOGUE TAPE
DATA");
printf("\n\nThis simple software digitises data from an 8 channel analogue
tape.");
printf("\nThe software assumes all 8 channels are to be digitised and
recorded.");
printf("\n\nThe user will be required to enter:");
printf("\n1) the sampling rate per channel,");
printf("\n2) the period of data to be digitised, &");
printf("\n3) the name of the file the data is to be written to.");
printf("\n\nOnce the file name is entered, digitising begins.");

/* Parameter requests */
printf("\n\nEnter the sampling rate per channel (Hertz): ");
scanf("%d",&Rate);

printf("\nEnter the period of data to be recorded (seconds): ");
scanf("%d",&Period);

printf("\nEnter the name of the data file you would like to write the output to:
");
scanf("%s",&outfile);
sprintf(strFilename,"%s.dat",outfile);
```

```
        /* Conversions. */
        dSampRate = Rate * 8;

        ulCount = dSampRate * Period;

        lTimeout = Period * 18;

        /* This sets a timeout limit (#Sec * 18ticks/Sec) so that if there
        is something wrong, the program won't hang on the SCAN_Op call. */
        iStatus = Timeout_Config(iDevice, lTimeout);

        iRetVal = NIDAQErrorHandler(iStatus, "Timeout_Config",
        iIgnoreWarning);

        /* Acquire data from multiple channels. */
        iStatus = SCAN_Op(iDevice, iNumChans, piChanVect, piGainVect,
        piBuffer, ulCount, dSampRate, dScanRate);

        iRetVal = NIDAQErrorHandler(iStatus, "SCAN_Op", iIgnoreWarning);

        /* Rearrange data into rows. */
        iStatus = SCAN_Demux(piBuffer, ulCount, iNumChans, iNumMUXBrds);
        iRetVal = NIDAQErrorHandler(iStatus, "SCAN_Demux",iIgnoreWarning);

        /* Convert from binary to actual voltages. */
        iStatus = DAQ_VScale(iDevice, piChanVect[0], piGainVect[0], dGainAdjust,
        dOffset,
        ulCount, piBuffer, pdVoltBuffer);

        iRetVal = NIDAQErrorHandler(iStatus, "DAQ_VScale",iIgnoreWarning);

//              Open the created text file for writing only
        if ((fp=fopen(strFilename,"w"))==NULL)
        {
                printf("\nCannot open file %s",strFilename);
                getch();
                exit(1);
        }

        for(i=0;i<(ulCount/8);i=i++)
        {
                fprintf(fp,"%lf %lf %lf %lf %lf %lf %lf %lf\n", pdVoltBuffer[i],
                 pdVoltBuffer[i+1*ulCount/8], pdVoltBuffer[i+2*ulCount/8],
                 pdVoltBuffer[i+3*ulCount/8], pdVoltBuffer[i+4*ulCount/8],
                 pdVoltBuffer[i+5*ulCount/8], pdVoltBuffer[i+6*ulCount/8],
                 pdVoltBuffer[i+7*ulCount/8]);
        }

        fclose(fp);
```

```
        /* Disable timeouts. */
        iStatus = Timeout_Config(iDevice, -1);


}

/* End of program */
```

Appendix J - Simplified Traffic Data

Train Type	Frequency (/wk)	Type of Loco	Type of Carriage	Number of Carriages	Tonnes (/train)	Other Information
1968 Working Time Table (Assume 1965 - 1975)						
Diesel / Electric Freight						
	88	48			750	max length = 45 x 4 wheeled vehicles
Diesel / Electric Passenger						
	22	44	620 Class	6	300	
	46	48	620 Class	4	200	
						For BHP trains to Wongawilli see page 102
1979 Working Time Table (Assume 1975 - 1985)						
Frieght	86	48			590	single branch line, 45 x 4 wheeled carriages
BUDD	40		BUDD	5		
Diesel / Electric	40		V-Set IC	5	150	
Diesel	10	48	620 Class	4		
	26	48	620 Class	2		
1985 Working Time Table (Assume 1985 - 1995)						
Loco Hauled	95	48	620 Class	6		assumed average
2 Car Diesel	186		V-Set IC	2		
2000 Working Time Table (Assume 1995 - 2000)						
G-Set	64		G-Set	4		
V-Set IC	140		V-Set IC	4		
	78		V-Set IC	6		
Endeavour	137		TE / LE	2		

Table J.1. Simplified passenger traffic data.

Train Type	Freq. (/wk)	Passes	Type of Loco	No. of Locos	Type of Wagons	No. of Wagons	Tonnes (/train)	Other Information
1968 Working Time Table								
Diesel / Electric Freight								
	88	45760	48				750	max length = 45 x 4 wheeled vehicles
1979 Working Time Table								
Frieght	86	44720					590	single branch line
BHP- Wongawilli: (1965 - 2000)								
Up - Loaded	5	7800	D34		67	15		
Down - Loaded	5	7800	D34		67	15		
Up - Loaded	5	1300	45 & 442		67	15		assume D34 til 95, then 45 and 442 Class
Down - Loaded	5	1300	45 & 442		67	15		
Boral- Dunmore Quarry: (1965 - 1993, 2000 -)								
Up - Loaded	3 / mth	1008	48	1	41	25		assume same wagons as Bombo Quarry - 1000t
Down - Unloaded	3 / mth	1008	48	1	10	25		assumed loco
RSA- Bombo Quarry: (1965 - 2000)								
Up - Loaded		4821	48	2	41	48		assume 2000t as per Freight Corp.
Down - Unloaded		4821			10	48		assume wagons as per Bombo information
		340			54	42		
		340			15	42		
Australian Paper- Bomaderry: (1965 - 1987)								
Up - Loaded		1320	48	1	41	25		assume same configuration as Bombo Quarry - 1000t
Down - Unloaded		1320	48	1	10	25		assumed 48 Classloco
Manildra - Bomaderry: (1973 - 2000)								
Up - Loaded	6	8424	81	2	100	20		although 81 class locos were introduced until 1984
Down - Loaded	6	8424	81	2	100	20		assumed loaded in both directions

Table J.2. Simplified freight traffic data.

Appendix K - Remaining Life Calculations

Duty Cycle Train	BHP D34	BHP 442 Class	Dunmore etc. Loaded	Dunmore etc. UnLoaded	Manildra	44 Class Loco & 6 620 Class Carriages	44 Class Loco & 4 620 Class Carriages	48 Class Loco & 2 620 Class Carriages	BU00 Passenger	2 Carriage Electric Passenger	4 Carriage Electric Passenger	6 Carriage Electric Passenger	2 Carriage Diesel Passenger	4 Carriage Tangara Passenger	
SN Curve Cycles to Failure for each Duty Cycle Train															
Noisy Trains	40268356	36964764	266114600	465264128	34995956	44002686	76321440	1.48E+09	9.06E+09	3.47E+09	2.68E+09	2.36E+09	8.15E+09	6.42E+09	
Quiet Trains	55746084	56703264	490035488	6.21E+09	33773684	56669000	1.36E+09	2.92E+09	1.78E+10	1.05E+10	7.6E+09	6.61E+09	1.61E+10	1.01E+10	
Total Passes (1965 - 2000)	15600	2600	57690	57690	16848	60840	29120	13520	20800	96720	62400	20280	35620	116540	
% Noisy (1965 - 2000)	30	30	20	20	50	50	50	50	50	50	50	50	50	75	
Current Traffic Volume (/yr)		520	156	156	624						7384	4004	7124	3328	
% Noisy (Current /yr)	30	30	20	20	50	50	50	50	50	50	50	50	50	75	
Ni / Nfi (1965 - 2000)															Total
% Noisy Trains	0.0001162	2.001E-05	4.351E-05	2.48E-05	0.0002408	6.901E-05	1.90E-05	4.563E-06	1.145E-06	1.392E-05	1.164E-05	4.293E-06	2.185E-06	1.361E-05	0.000585
% Quiet Trains	0.0001959	3.21E-05	9.451E-05	7.45E-06	0.0002494	5.09E-05	1.06E-05	2.315E-06	5.829E-07	4.569E-06	4.105E-06	1.532E-06	1.101E-06	2.86E-06	0.000698
															0.001243
Nj / Nfj (Current /yr)															
% Noisy Trains	0	4.002E-06	1.172E-07	6.70E-08	8.918E-06	0	0	0	0	0	1.378E-06	8.477E-07	4.369E-07	3.883E-07	1.62E-05
% Quiet Trains	0	6.419E-06	2.547E-07	2.00E-08	9.238E-06	0	0	0	0	0	4.658E-07	3.024E-07	2.203E-07	8.216E-08	1.7E-05
															3.32E-05
Assumed Non Welded														**Bf =**	**30103.89**
No Correction Factors															
														% Noisy	
														Measured	**30103.89**
														100	**26326.06**
														0	**32923.62**

Table K.1. Remaining life calculations for BFB at mid span from BS7608.

Duty Cycle Train	BHP D34 & 442 Class	Dunmore etc. Loaded	Dunmore etc. UnLoaded	Manildra	44 Class Loco & 6 620 Class Carriages	44 Class Loco & 4 620 Class Carriages	48 Class Loco & 2 620 Class Carriages	BUDD Passenger	2 Carriage Elecrtic Passenger	4 Carriage Elecrtic Passenger	6 Carriage Elecrtic Passenger	2 Carriage Diesel Passenger	4 Carriage Tangara Passenger		
SN Curve Cycles to Failure for each Duty Cycle Train															
2nd Brg Test Results	122627	361231	117505912	75607	338457	692345	1094426	76180	747552	444595	354732	97861	61465		
Global FEA Results	176228	492994	317568992	73121	432024	692345	1586366	219732	1810997	1149126	874280	244722	163783		
Total Passes (1965 - 2000)	18200	57890	57890	16848	60840	29120	13520	20800	96720	62400	20280	35620	116640		
Current Traffic Volume (/yr)	520	156	156	624						7384	4004	7124	3328		
Ni / Nfi (1965 - 2000)														Total	
2nd Brg Test Results	0.1484176	0.1602576	0.0004927	0.2228365	0.179757	0.04206	0.0123535	0.2730375	0.1293823	0.1403525	0.0571699	0.3639857	1.8976653	3.627768	Failed
Global FEA Results	0.1021164	0.1174254	0.0001823	0.2304126	0.1408255	0.04206	0.0085226	0.0946608	0.053407	0.0543021	0.0231962	0.1455529	0.7121618	1.724826	Failed
Nj / Nfj (Current /yr)															
2nd Brg Test Results	0.0042405	0.0004319	1.328E-06	0.0082532	0	0	0	0	0	0.0166084	0.0112874	0.0727971	0.0641446	0.167764	
Global FEA Results	0.0029176	0.0003164	4.912E-07	0.0085338	0	0	0	0	0	0.0064258	0.0045798	0.0291106	0.0203196	0.072204	

Thickness Effect for 34mm
Assumed Welded and not stress relieved
No other Correction Factors

Table K.2. Remaining life calculations for Web Stiffener Connection from BS7608.

Duty Cycle Train	BHP D34 & 442 Class	Dunmore etc. Loaded	Dunmore etc. UnLoaded	Manildra	44 Class Loco & 6 620 Class Carriages	44 Class Loco & 4 620 Class Carriages	48 Class Loco & 2 620 Class Carriages	BUDD Passenger	2 Carriage Elecrtic Passenger	4 Carriage Elecrtic Passenger	6 Carriage Elecrtic Passenger	2 Carriage Diesel Passenger	4 Carriage Tangara Passenger	
SN Curve Cycles to Failure for each Duty Cycle Train														
2nd Brg Test Results	369823	2262644	infinite	190618	1012505	1526533	3449265	196711	3043095	2014020	1690125	246134	156685	
Global FEA Results	506418	3753814	infinite	174805	1246717	1921831	4879683	556660	8039197	5474378	4198358	592432	406225	
Total Passes (1965 - 2000)	18200	57890	57890	16848	60840	29120	13520	20800	96720	62400	20280	35620	116640	
Current Traffic Volume (/yr)	520	156	156	624						7384	4004	7124	3328	
Ni / Nfi (1965 - 2000)														Total
2nd Brg Test Results	0.0492127	0.0255851	0	0.0883862	0.0600886	0.0190759	0.0039197	0.1046746	0.0317834	0.0309828	0.0119991	0.1447179	0.7444235	1.3148496
Global FEA Results	0.0359387	0.0154216	0	0.0963817	0.0488002	0.0151522	0.0027707	0.0373657	0.0120311	0.0113986	0.0048305	0.060125	0.2871315	0.6273474
Nj / Nfj (Current /yr)														
2nd Brg Test Results	0.0014061	6.895E-05	0	0.0032736	0	0	0	0	0	0.0036663	0.0023691	0.0289436	0.0212401	0.0609676
Global FEA Results	0.0010268	4.156E-05	0	0.0035697	0	0	0	0	0	0.0013488	0.0009537	0.012025	0.0081925	0.0271581
Thickness Effect for 34mm														

Table K.3. Remaining life calculations for Web Stiffener Connection from Austroads.

Duty Cycle Train	BHP D34 & 442 Class	Dunmore etc. Loaded	Dunmore etc. UnLoaded	Manildra	44 Class Loco & 6 620 Class Carriages	44 Class Loco & 4 620 Class Carriages	48 Class Loco & 2 620 Class Carriages	BUDD Passenger	2 Carriage Elecrtic Passenger	4 Carriage Elecrtic Passenger	6 Carriage Elecrtic Passenger	2 Carriage Diesel Passenger	4 Carriage Tangara Passenger		
SN Curve Cycles to Failure for each Duty Cycle Train															
2nd Brg Test Results	587097	3484723	5.547E+10	328470	1598780	2440405	6041452	466258	5173595	4125250	3599125	569228	384942		
Global FEA Results	1247047	4.833E+09	6.24E+11	513026	3040199	4873854	11416553	1671822	14691755	10615911	7951734	1703685	1139062		
Total Passes (1965 - 2000)	18200	57890	57890	16848	60840	29120	13520	20800	96720	62400	20280	35620	116640		
Current Traffic Volume (/yr)	520	156	156	624						7384	4004	7124	3328		
Ni / Nfi (1965 - 2000)														Total	
2nd Brg Test Results	0.031	0.0166125	0	0.0512924	0.038054	0.0119324	0.0022379	0.0446105	0.0186949	0.0151264	0.0056347	0.062576	0.3030067	0.600778	
Global FEA Results	0.0145945	1.198E-05	0	0.0328404	0.0200118	0.0059747	0.0011842	0.0124415	0.0065833	0.005878	0.0025504	0.0209076	0.1024	0.225379	
Nj / Nfj (Current /yr)															
2nd Brg Test Results	0.0006857	4.477E-05	0	0.0018997	0	0	0	0	0	0.00179	0.0011125	0.0125152	0.0086455	0.026893	
Global FEA Results	0.000417	3.228E-08	0	0.0012163	0	0	0	0	0	0.0006956	0.0005035	0.0041815	0.0029217	0.009936	
												Bf (2nd Brg Test Results) =			14.84465
												Bf (Global FEA Results) =			40.18071
Thickness Effect for 34mm															
No other Correction Factors															

Table K.4. Remaining life calculations for Web Stiffener Connection from Japanese.